MULTIPHASE, MULTISCALE SIMULATION OF FRACTURED RESERVOIRS

by

Huabing Wang

A dissertation submitted to the faculty of
The University of Utah
in partial fulfillment of the requirements for the degree of

Doctor of Philosophy

Department of Chemical Engineering

The University of Utah

December 2008

THE UNIVERSITY OF UTAH GRADUATE SCHOOL

SUPERVISORY COMMITTEE APPROVAL

of a dissertation submitted by

Huabing Wang

This dissertation has been read by each member of the following supervisory committee and by majority vote has been found to be satisfactory.

21 July 2008 — Chair: Milind D. Deo

1 Aug 2008 — Craig B. Forster

31 July 2008 — Edward M. Trujillo

21 July 2008 — Jules J. Magda

21 JULY 2008 — Paul Borgmeier

THE UNIVERSITY OF UTAH GRADUATE SCHOOL

FINAL READING APPROVAL

To the Graduate Council of the University of Utah:

I have read the dissertation of Huabing Wang in its final form and have found that (1) its format, citations, and bibliographic style are consistent and acceptable; (2) its illustrative materials including figures, tables, and charts are in place; and (3) the final manuscript is satisfactory to the supervisory committee and is ready for submission to The Graduate School.

08/08/08
Date

Milind D. Deo
Chair: Supervisory Committee

Approved for the Major Department

JoAnn S. Lighty
Chair/Dean

Approved for the Graduate Council

David S. Chapman
Dean of The Graduate School

ABSTRACT

Numerical simulation of the geometrically complex fractured reservoirs has been a major engineering challenge. The deficiencies of continuum models are often addressed using the discrete fracture network (DFN) models which represent the complex fracture geometry explicitly. The primary goal in this dissertation is to explore ways of applying the DFN methodology to solve a variety of multiphase problems in oil reservoir simulation. Three-dimensional, three-phase simulators using the control-volume finite-element scheme were used. After completing validation and fracture-property sensitivity studies, the limitation of employing the often-used Oda homogenization method was shown followed by the development of a simpler geometric scheme.

The important question of oil recovery from basement reservoirs (Type I) composed of fractures of various sizes was examined in detail. Oil recovery and breakthrough behavior of this system comprised of seismic and subseismic features were investigated for different oil distributions, permeability values, levels of heterogeneity and rate. In general having more oil distributed in smaller systems led to lower recovery and quicker breakthrough. Lower permeabilities in the subseismic features also led to lower recovery. The recovery at given pore volume of water injected was rate dependent in all of the scenarios explored, with the lower rate production leading to about 5% higher oil in place recovery. This phenomenon was consistent when viewed from the point of view of gravity number for each displacement. The mechanism of gravity-dominated oil

recovery in two-phase applications was explored, and a "critical rate" concept for obtaining higher recoveries in gravity-dominated flow was developed

A multiscale upscaling exercise was performed to match the oil recovery performance from a structured fault zone using a single feature with different sets of relative permeability curves. The effectiveness of using DFN simulations for reservoirs containing matrix and fractures (Type II) was shown using two different systems. It was shown that placing wells either in the fault zone or in the matrix can have significant impact on recovery and breakthrough behavior. It was also demonstrated that fracture networks bring apparent anisotropy, and water-flooding from one direction or the other may affect oil recovery. Fractured reservoir simulation is high-performance computing – data and file management, computation, visualization, etc. are integral components of this exercise. A workflow to facilitate creation of fracture networks, gridding and simulation, and visualization was developed. A fully integrated two-dimensional graphical user interface (java-based) was also built.

CONTENTS

LIST OF TABLES

LIST OF FIGURES

ACKNOWLEDGMENTS

First and foremost, I would like to thank my advisor, Dr. Milind Deo, for his support, encouragement and guidance during this work. I want to thank him for being so supportive and for always giving insightful advice. This dissertation would not have been possible without his guidance.

I would also like to thank Dr. Craig Forster and the rest of my dissertation committee members, Dr. Edward Trujillo, Dr. Jules Magda and Dr. Paul Borgmeier for their valuable comments and suggestions on my proposal and dissertation. I especially thank Craig for all his geological support during this work.

I also wish to thank Dr. Tom Doe, and I appreciate his effort and time in characterizing DFN modeled fracture networks.

I would also like to thank Golder Associates, Schlumberger, Altair, Sandia National Lab and Argon National Lab for their academic license of various software packages being applied in this research.

I have received a lot of help and encouragement directly or indirectly from all members of the Petroleum Research Center and Chemical Engineering Department at the University of Utah. I am truly grateful to everyone who helped me in the past five years.

This research was generously supported by the United States Department of Energy through contract number DE-FC26-04NT15531 and CuuLong JOC. This support is greatly appreciated.

Finally, special thanks to my wife, Ning Zhuo, for her support and for giving me the joy of life, our son Jayden. I would also like to thank my parents-in-law for helping with the care of Jayden when he was born. My parents and brother also deserve my gratitude for supporting and encouraging my education from the very beginning.

CHAPTER 1

INTRODUCTION

Naturally fractured reservoirs occur worldwide and constitute an important reservoir type. About 60% of the world's remaining resources reside in such formations. The main feature that distinguishes naturally fractured reservoirs from conventional reservoirs is the presence of fractures. In naturally fractured reservoirs fluids exist in two interconnected systems: the rock matrix, which usually provides the bulk of the reservoir volume, and the highly permeable rock fractures. These types of reservoirs are well known as being both highly heterogeneous and complex and therefore may affect the oil and gas production in many ways. The fracture can enhance production if utilized properly, as in gas-induced gravity drainage of oil; or they can adversely affect oil production when the channeling paths of water or free gas break through early. A reduction in risk and an improvement in understanding of reservoir behavior will lead to enhanced profitability from under-exploited fractured fields.

Improving the recovery from fractured reservoirs is an increasingly important task for many oil companies. The recovery from reservoirs where fractures dominate permeability is often a fraction of the resource recovered from conventional reservoirs in which matrix permeability dominates. The lower recovery and higher risks associated with recovery from a fractured reservoir and a result of the uncertainty in forecasting how various completion placements, water flood patterns, and tertiary recovery processes will actually perform in fractured reservoirs. Fractures do more than simply increase

reservoir permeability; they fundamentally alter reservoir connectivity and heterogeneity. To improve oil and gas recovery in naturally fractured reservoirs, the reservoir model must be characterized correctly. Identifying, characterizing, and mapping the fracture network in terms of the fracture's properties will result in optimal reservoir management.

The fractured reservoirs are usually classified based on what positive effects the fracture system provides to the reservoir's overall quality. Nelson's (2001) classification is well respected and useful to the exploring community because it presents a classification system which provides geologists/engineers with a fractured model standard. Below are the four types of Nelson's fractured reservoirs classification:

Type I: Fractures provide the essential reservoir porosity and permeability.

Type II: Fractures provide the essential reservoir permeability.

Type III: Fractures enhance permeability in an already producible reservoir.

Type IV: Fractures provide no additional porosity or permeability but create significant reservoir anisotropy (barriers).

The first three types describe positive reservoir attributes of the fracture system. The fourth type describes those reservoirs in which fractures are important for both reservoir quality that they impart, and the inherent flow anisotropy and reservoir partitioning that they create.

Three main methods have been applied to model the fractured reservoirs: single porosity model, dual porosity model and discrete fracture network model. Comparing with the other two models, the Discrete Fracture Network approach (DFN) models the geometry of the fracture network explicitly and provides a realistic way of modeling

fractured reservoir performance (Dershowitz, et al., 1998). The approach consists of three general steps:

1) Fracture Data Analysis
2) Generation of Discrete Fracture Networks
3) Discrete Fracture Network Analysis

Step one involves analyzing the information from a variety of data sources to derive the parameters needed for step two. These parameters include fracture locations (spatial model), size, shape, orientation, flow properties, and number of distinct fracture sets. Step two involves generating multiple discrete fracture networks based on the results of the data analysis. Some geo-statistical models will be applied during this process. In step three, these networks are analyzed to derive engineering information. These include simple geometric analysis such as the computation of fracture densities, and the computation of complex multiwell flow simulations.

Typically, geologists use a forward modeling approach to iterate between steps two and three during the model calibration process. For example, the calculated fracture density or the calculated response from a transient well test is compared to field measurements. If there is not an acceptable match, the input parameters for the fracture network are changed and the network analysis task is repeated with the updated model.

Based on the analysis of the fracture reservoir data, two types of probability distributions can be applied to generate the DFN model. These two types are scalar data probability distribution and directional data probability distributions. Examples of scalar distributions are uniform distribution, exponential distribution, normal distribution, lognormal distribution, normal of log distribution and power law distribution. There are

four popular types of probability distribution directional vaiables: the univariate Fisher, the bivariate Fisher, the bivariate normal and the bivariate Bingham distribution.

Questions often being asked by reservoir management regarding DFN modeled fractured reservoirs are:

1) Are DFN model appropriate representations of fractured reservoirs? How does oil recovery and other recovery parameters (water cut, etc.) compare to results from conventional approach?
2) Fractures appear at various scales. There are several methods of representations of these fractures' existence. What are fundamental displacements in these multiscale environments?
3) How does rock matrix interact with fracture networks so created?

Some answers to the above questions could be discovered by the objectives of this research program as:

1) Benchmark the CVFE reservoir simulator with commercial finite difference reservoir simulator such as ECLIPSE (A Schlumberger product) by considering fracture networks of varying density; the idea is to highlight the physical mechanisms that can be represented more accurately using the DFN approach. Explore the similarities and differences in modeling fractured reservoirs using DFN, dual porosity and single porosity methods.
2) Study the impact of geometric aspects of fracture networks on the oil production from a basement reservoir.

3) Perform multiphase, multidimensional CVFE simulations on basement DFN models section to assess how best to represent fractures and fracture zones in basement reservoirs.
4) Study the Type II fractured reservoir by CVFE method; explore the impact of oil/gas production due to the presence of fracture networks.
5) Create a workflow for CVFE reservoir simulation that includes preprocessing and postprocessing utilities. Create an operating system free interface to make the simulation run locally and/or remotely.

Details to achieve the above goals are discussed below.

1.1 Discrete Fracture Network Modeling of Basement Reservoirs

Different types of fractured reservoirs may need different simulation approaches. Simulation of Type I reservoirs in detail is considered in this project task. Geologically, Type I reservoirs are granitic/basalt formations. Practically all of the oil in these reservoirs resides in fractures or fault zones. Since the geometry of the fracture network is critical in understanding recovery from these reservoirs, these lend themselves well for treatment by using the DFN approach. The primary questions to be answered are:

1) Are DFN models accurate in modeling physics of displacement in these reservoirs?
2) How do geometric aspects of fractured networks and other fracture characteristic affect displacements in these systems?

To answer the first question posed, we constructed a regularized fracture network that is amenable to gridding with the ECLIPSE program. The ECLIPSE program is the conventional finite-difference based reservoir simulator that allows a comparison to be

drawn with our CVFE simulation results thereby validating the CVFE simulator. In Chapter 3, this indexing verification will be discussed in greater detail.

Once the accuracy of the DFN approach is ascertained, and its effectiveness compared with the conventional single-porosity approach, detailed sensitivity studies of the impact of fracture characteristics on production from basement reservoirs can be conducted. In Chapter 3 of this dissertation, this sensitivity is outlined in great detail. Permeability distributions in the fracture zone, dip orientation and aperture variations, etc. are included in this sensitivity study to help quantify fractured networks uncertainties.

A typical fracture network is highly heterogeneous. In order to understand the impact of permeability heterogeneity between fractures, and within fractures, presence of preferred high permeability pathways between injectors and producers was examined in Chapter 3 of this dissertation. The extent to which the preferred pathway network leads to early breakthrough will be quantified to ascertain the risk of preferred flow pathway existence. The impact of shutting off the high permeability fractures using gel treatments on improving oil recovery is also studied to compare with the fracture networks without such treatments.

For irregular networks, DFN approach will be used directly to obtain simulation results. It will also be possible to "homogenize" the irregular fracture domain and create "equivalent" Eclipse input files. This entails creating porosity and permeability fields, using one of the methods outlined in the review of upscaling methods in Chapter 4. This study helps to evaluate the effectiveness of the upscaling techniques, and also to compare the DFN approach to what can be considered "single-porosity" simulation method.

This research program compared the performance of the DFN simulator to the dual porosity representation of the basement domain. These questions will be discussed and answered in Chapter 3 and 4.

1.2 Modeling Basement Reservoirs on a Variety of Scales

Seismic measurements are used to map the locations of major features in basement reservoirs. These features can be brought into a DFN model and the multiphase flow process can be simulated. However, it is recognized that the seismic mapping technique is identify features larger than a certain size. The smaller subseismic features are not represented in a model based only on seismic measurements. Smaller subseismic features do exist in basement reservoirs. The important questions are:

1) What is the relative importance of the subseismic features in oil storage and displacement?
2) How does the production rate affect of the final recoveries?

To answer the questions posed above, a conceptual multiscale basement model containing seismic and subseismic features is created and simulated. Greater details are discussed in Chapter 5.

1.3 Upscaling Relative Permeabilities in Basement Reservoirs

In basement reservoirs, FMI logs and cores may provide additional details regarding individual fracture zones (seismic features). This information can be used in a fracture characterization environment (such as FRED) to create models of fractures within the fault zone. In this project, these types of models are titled "embedded zone" models. To improve oil recovery in fractured network it becomes necessary to ask how

oil-water displacements behave in the embedded zone environment. Once that information has been ascertained, it becomes necessary to compare to its single feature representations adopted in full-field seismic and subseismic model. In Chapter 6, the answer to this question will be explored in greater detail by creating and simulating a number of embedded features. The upscaled representations are simulated using regular polynomial relative permeabilities, while the embedded zone itself is simulated using straight line relative permeabilities. The functionalities that give the "best-match" for oil recovery and/or water cut can be observed through this exercise. These relative permeability functionalities are considered "upscaled" relative permeabilities.

1.4 Simulation of Reservoirs with Fractures and Matrix

In most practical fractured reservoir simulation studies, fractures act as conduits while the matrix contains most of the fluids. The geometric aspects of fracture networks in the context of these Type II reservoirs are studied in greater detail in Chapter 7. The detailed Type II reservoirs case studies in Chapter 7 include:

1) Understanding the importance of a "dip-slip fault" that separates and connects two lobes of a fractured reservoir.
2) Understanding the oil production impacts from "strike-slip fault zone" type II reservoirs.
3) Analysis of preferred pathways in fracture networks on production performance.

1.5 Workflow

Simulating fractured reservoirs and predicting oil recovery requires integration workflows. The integration workflow should include geologic knowledge, petrophysical properties representation, well modeling and well history input. Most times, required data are scattered in geologic models, production histories and petrophysical property generation programs. One of the main project tasks is to bring about the integration of the geologic model and reservoir simulation input file. "FracMan Reservoir Edition" (FRED) is a sophisticated general program for importing a number of geologic inputs into a geologic model. The program can create fracture sets with characteristics of all of the measured data. FRED is used in this project as the primary fracture generation tool. These fracture sets may be operational in a Type I reservoir environment or a Type II reservoir situation. In Type II fractured reservoirs, the fracture sets are embedded into a reservoir matrix. When creating reservoir simulation input files using the sophisticated fracture network, both these aspects need consideration. A workflow tool will be discussed in Chapter 9 with the following features:

1) Treatment of fracture only reservoir or reservoirs with fractures and matrix.
2) Meshing the domain created.
3) Assigning properties to the control volumes and/or elements created during the meshing exercise.
4) Creating a simulation input file.
5) Assigning wells and well operational parameters.
6) Describing well production histories.
7) Executing the simulator with the given input file.

8) Generating output data for production analysis and for visualization.

9) Visualizing the data.

It may also be necessary to develop a geologist vision of what a fractured reservoir would look like. A modularized java tool which draws the fractured reservoir and most of its features is discussed in greater detail in Chapter 8.

CHAPTER 2

FUNDAMENTALS OF FRACTURED RESERVOIR MODELING

In this chapter, some fundamentals of fractured reservoir modeling are introduced. At the beginning, some basic concepts of black-oil reservoir model are presented. Then other concepts of fractured reservoir modeling are described from both geological and fluid flow aspects. At the end of the chapter, some background of control-volume finite-element (CVFE) reservoir simulator are presented. This CVFE formulation was used to study DFN characterized fractured reservoir throughout this research program.

2.1 Fundamentals of Oil Reservoir Modeling

2.1.1 Black-Oil Model

Crude oil may contain over thousand components which makes modeling all components neither possible nor meaningful. The black-oil model is the most widely adapted method in the reservoir simulation world. The assumptions of the black-oil model can be summarized as:

- At most three phases: oil (hydrocarbon liquid), water, hydrocarbon gas;
- Oil phase consists of only oil and solution gas;
- Gas phase consists of only free hydrocarbon gas;
- Isothermal system;
- Oil and gas phases can reach equilibrium instantaneous;

The black-oil model was used throughout this research work

2.1.2 Porosity

The porosity of a rock is a measure of the storage capacity (pore volume) that is capable of holding fluids. Quantitatively, the porosity is the ratio of the pore volume to the total volume (bulk volume). This important rock property is defined in Equation (2-1) as:

$$\Phi = (\text{pore volume}) / (\text{bulk volume}) \tag{2-1}$$

where Φ is the porosity.

2.1.3 Permeability

Permeability is a property of the porous medium that measures the capacity and ability of the formation to transmit fluids. The rock permeability, k, is a very important rock property because it controls the directional movement and the flow rate of the reservoir fluids. It is used in Darcy's law to calculate fluid flux. For a single-phase flow, Darcy's law is written in Equation (2-2) as

$$\mathbf{u} = -\frac{\mathbf{k}}{\mu}\nabla\varphi \tag{2-2}$$

where $\mathbf{u}$ is the Darcy's velocity, φ is the fluid potential, and μ is the fluid viscosity. The symmetric and positive-define permeability tensor k in three-dimensional space is given by Equation (2-3) as

$$\mathbf{k} = \begin{bmatrix} k_{xx} & k_{xy} & k_{xz} \\ k_{xy} & k_{yy} & k_{yz} \\ k_{xz} & k_{yz} & k_{zz} \end{bmatrix} \tag{2-3}$$

2.1.4 Phase Saturation and Potential

In multiphase flow problems, multiple types of fluids (at most oil, gas and water for black-oil model) can exist in any one pore. Phase saturation S_l describes the fracture of pore volume occupied by phase l and is defined in Equation (2-4) as

$$S_l = \frac{V_l}{V_{pore}} \tag{2-4}$$

where V_l is the pore volume occupied by phase l. To satisfy volume conservation, the summation of all phases' saturation should be equals to 1.

As shown in Equation (2-5), phase potential is defined by

$$\varphi_l = P_l + \rho_l \frac{g}{g_c} z \tag{2-5}$$

where P_l is the phase pressure, ρ_l is the phase density, g is the gravitational constant, g_c is a universal gravitational conversion constant, and z is the elevation of the fluid phase in consideration.

2.1.5 Relative Permeability

For multiphase flow problem, Darcy's law can be extended to Equation (2-6) as

$$\mathbf{u}_l = -\frac{\mathbf{k}k_{rl}}{\mu_l} \nabla \varphi_l \tag{2-6}$$

where the subscript l denotes an individual phases, k_{rl} is the phase relative permeability.

As shown in Figure 2.1, the relative permeability is considered as a rock property and is a function of the phase saturation S_l. For an oil-water system, the oil phase cannot move when the oil saturation is lower than the residual oil concentration (S_{ro}). The water phase becomes mobile only when water saturation is higher than the connate water saturation (S_{iw}).

2.1.6 Capillary Pressure

Capillary pressure P_c is defined as the pressure difference between the nonwetting phase and the wetting phase as a function of the (wetting phase) saturation. For oil/water systems in porous rock, oil is in general considered to be the least wetting phase. Therefore, the capillary pressure is defined in the Equation (2-7) as:

$$P_c(S_w) = P_o(S_w) - P_w(S_w) \tag{2-7}$$

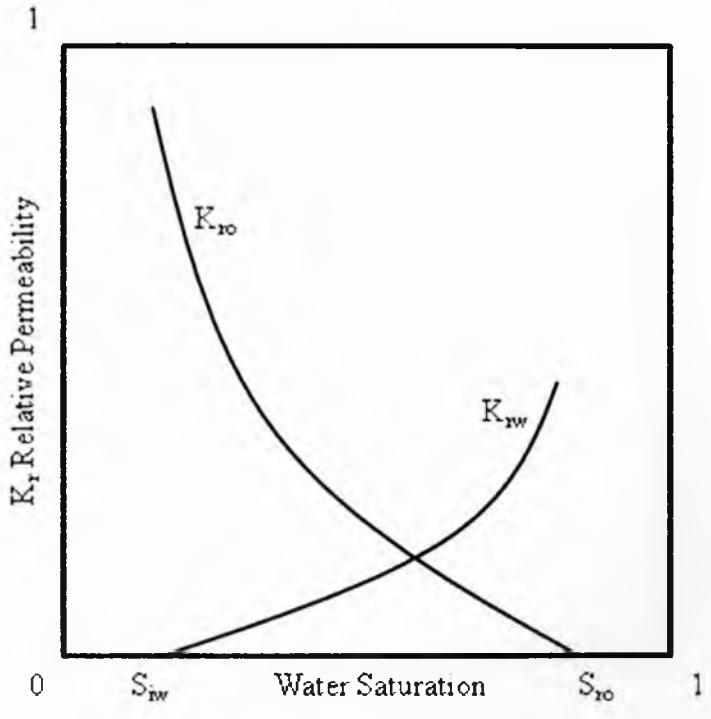

Figure 2.1 A relative permeability curve for oil-water system.

where subscript o and w represent oil and water phases. In reservoir engineering, P_c is an important parameter for simulation studies (in particular for heterogeneous systems).

2.1.7 Formulation Volume Factor

As shown in Equation (2-8), the reservoir fluid formation volume factor, B_l, is defined as the ratio of the volume of each reservoir fluid at the prevailing reservoir temperature and pressure to the volume of that fluid at the standard conditions.

$$B_l = \frac{V_{l,RC}}{V_{l,STC}} \tag{2-8}$$

where subscript l denotes an individual phase, RC and STC denote reservoir conditions and stock tank conditions.

2.2 Fractured Reservoir Classification

Based on what positive effects the fracture system provides to overall reservoir quality, Nelson's (2001) classified fractured reservoirs as the following four types:

Type I: Fractures provide the essential reservoir porosity and permeability.

Type II: Fractures provide the essential reservoir permeability.

Type III: Fractures enhance permeability in an already producible reservoir.

Type IV: Fractures provide no additional porosity or permeability but create significant reservoir anisotropy (barriers).

Nelson's fractured reservoir classification is demonstrated in Figure 2.2. The first three types describe positive reservoir attributes of the fracture system. The fourth type describes those reservoirs in which fractures are important not only for reservoir quality, but also the inherent flow anisotropy and reservoir partitioning that they create.

2.3 Modeling Fractures in Reservoir Simulation

Three types of main models formulations are popular for modeling and simulating flow through naturally fractured reservoirs: The single porosity model, dual porosity model, and DFN model.

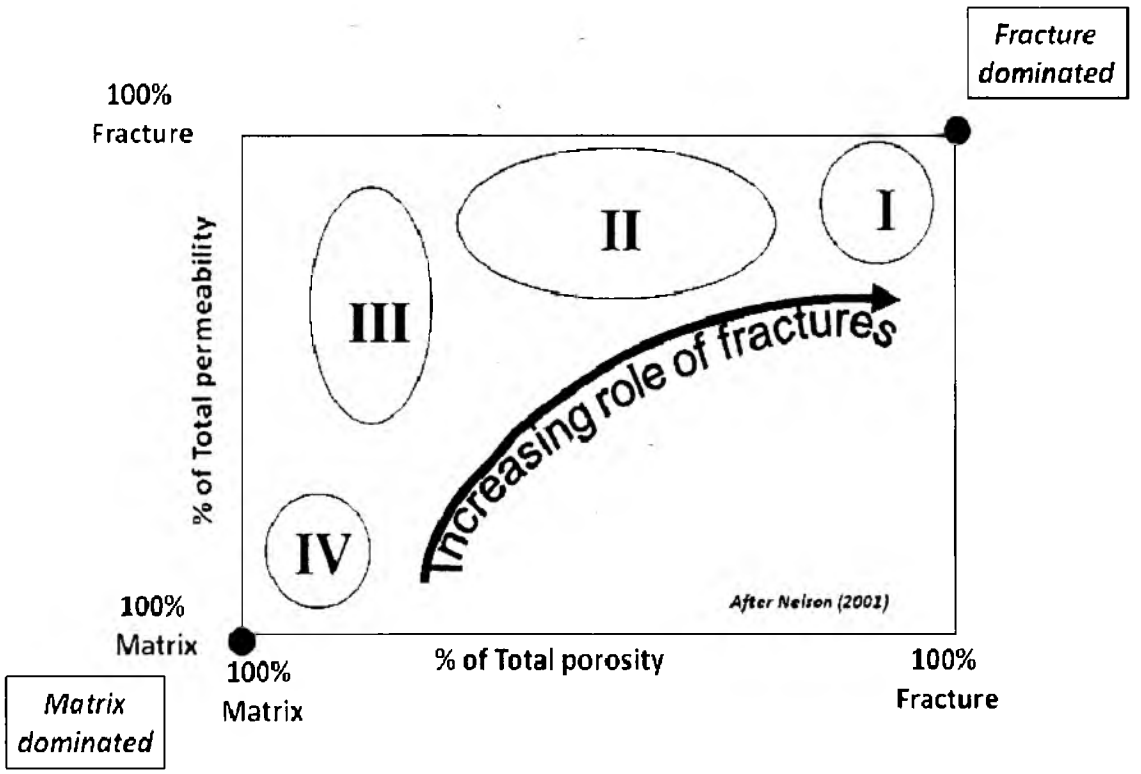

Figure 2.2 Schematic cross plot of percent reservoir porosity versus percent reservoir permeability (percent due to matrix versus percent due to fractures)

2.3.1 Single Porosity Model

The single porosity model is a straightforward application, as shown in Figure 2.3, fractures are represented explicitly by a fine-scale mesh.

The single porosity approach provides accuracy, but it is not practical due to a very large member of grids when considering even a few fractures. This is because of the big mesh size contrast ratios generated by the fractures and the matrix. This contrast ratio can reach over tens or hundreds of magnitudes which create numerical instabilities in multiphase flow simulation.

2.3.2 Dual Porosity Model

The dual porosity models are most widely used in large-scale fractured reservoir simulation. The dual-porosity system is represented by two different continua, one representing the porous matrix and the other representing the fractures. Fluid flow is primarily through the high permeability, low porosity fractures surrounding individual

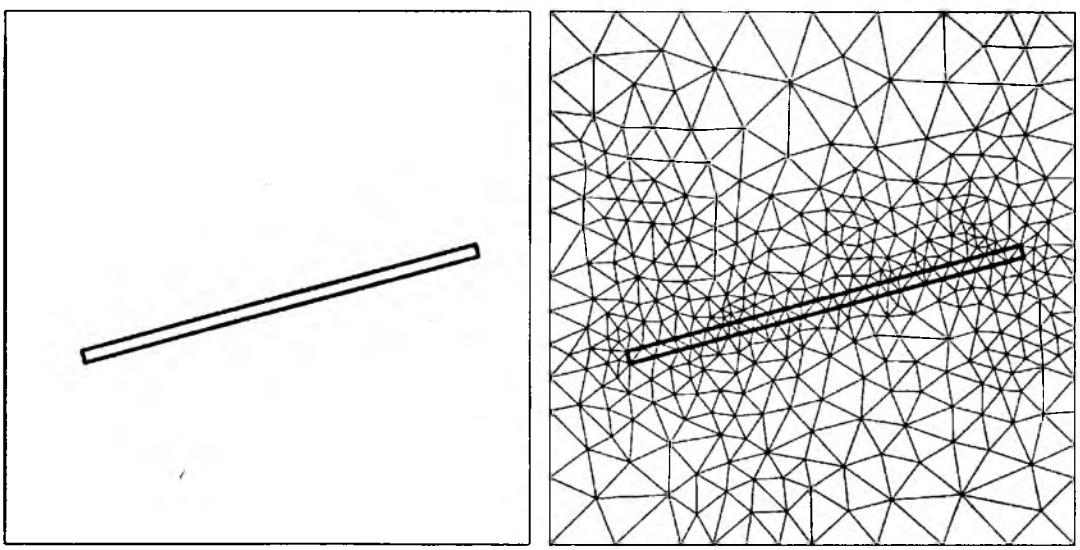

Figure 2.3 Single porosity model in finite element mesh

matrix elements. The matrix blocks contain a majority of the reservoir volume and act as sources or sinks to the fractures.

A shape factor represent transfer function describes the mass transfer between the matrix and fractures. The shape factor σ is defined in Equation (2-9) as

$$\sigma = 4\left(\frac{1}{L_x^2} + \frac{1}{L_y^2} + \frac{1}{L_z^2}\right) \tag{2-9}$$

where L_x, L_y and L_z are described in the dual porosity model illustration of Figure 2.4.

Despite the numerical efficiency, the dual porosity models have some drawbacks. The model is limited to sugar cube representation of fractured media. The shape factor is too simple to describe the fluid flow when gravity and viscous effects are involved. This approach also assumes that the medium to have dense closely connected fractured network and may not be very accurate when treating only a few fractures.

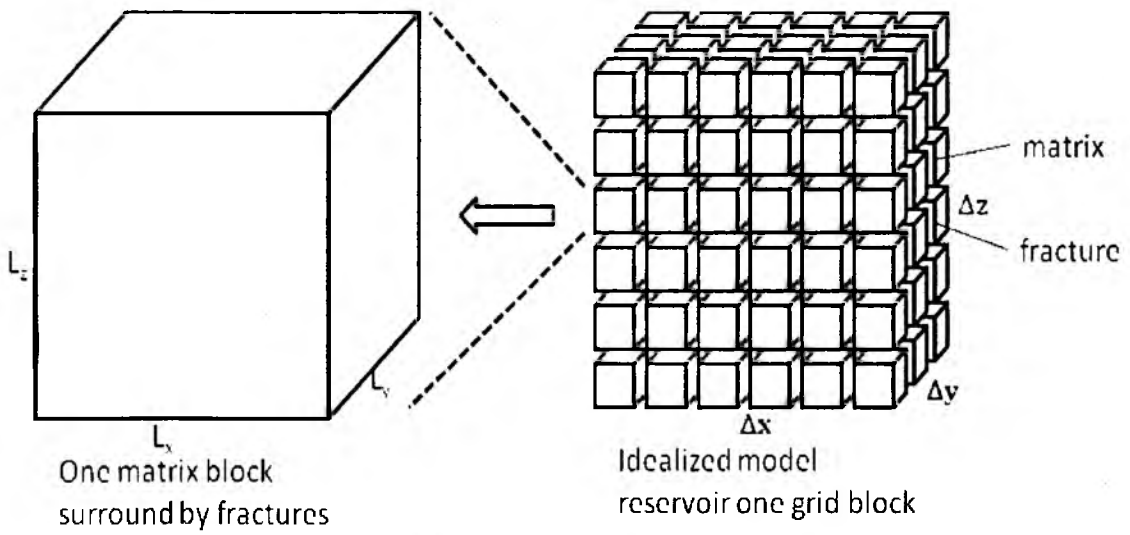

Figure 2.4 Dual porosity model illustrations (after Warren & Root, 1963)

2.3.3 DFN Model

Some deficiencies regarding conventional continuum model (dual-porosity) was discussed above. As a remedy, the DFN model provides relatively new mythologies for addressing some important needs.

The discrete-fracture model is an alternative to the single porosity model. In the discrete fracture model, the dimensionality of fractures is reduced from n to (n-1). This reduction greatly decreases the computational time. Compared to the continuum models, there are many advantages of the DFN model: it accounts for the heterogeneity in fractures accurately; the performance of the method is not affected by very thin fractures; it can account explicitly for the effect of even a single fracture on fluid flow; there is no need to compute transfer functions. The DFN model is illustrated by Figure 2.5. Comparing with the single porosity model (Figure 2.3), the DFN model could be treated as a simplified single porosity model.

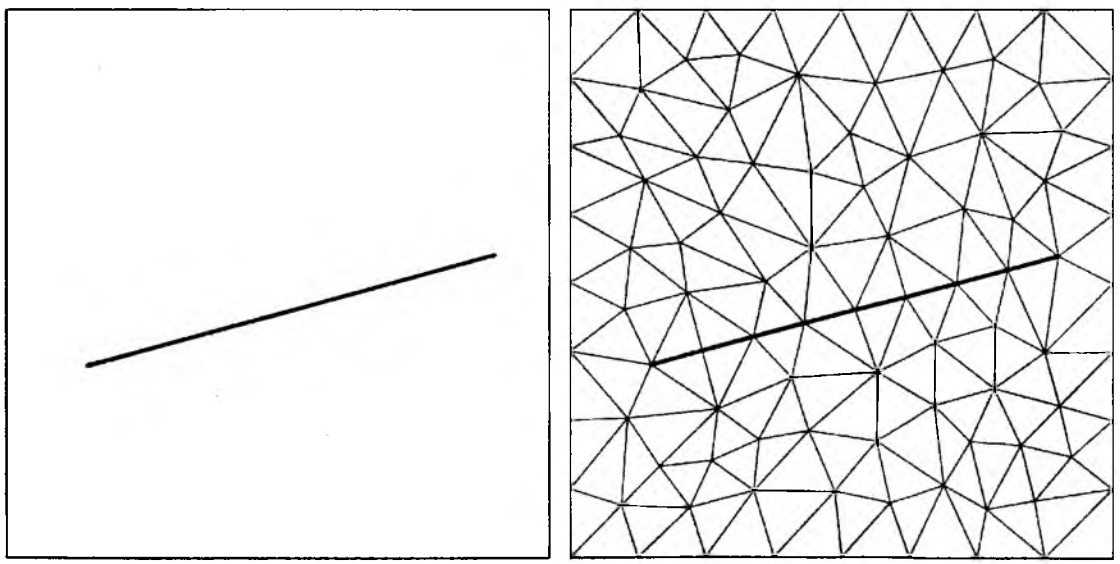

Figure 2.5 DFN model illustrations

However, there are a number of unresolved challenges with the DFN model based flow simulations. The bottle neck of simulating DFN characterized fractured reservoir is the unstructured domain meshing. Low quality mesh will result in a significant mathematical problem during the flow simulation.

2.4 Geological DFN Characterization

Throughout this research work, DFN characterized fracture networks were studied in various aspects. In this section, the methods of generating DFN models are discussed with extent details.

2.4.1 DFN Modeling Approach

The DFN (Dershowitz et al., 1984) approach models the geometry of the fracture network explicitly and provides a realistic way of modeling fractured reservoir performance. The DFN approach consists of three general steps:

- Fracture data analysis
- Generation of discrete fracture networks
- Discrete fracture network analysis

Step one involves analyzing the information from a variety of data sources to derive the parameters needed for step two. These parameters are fracture locations (spatial model), size, shape, orientation, flow properties, and number of distinct fracture sets. Step two involves generating multiple discrete fracture networks from the results of the data analysis in step one. In step three, these networks are analyzed to derive engineering information. These include simple geometric analysis like the computation of fracture densities, as well as complex multiwell flow simulations.

Typically, a forward modeling approach is applied to iterate between steps two and three during the model calibration process. For example, the calculated fracture density or the calculated response from a transient well test is compared to field measurements. If there is not an acceptable match, the input parameters for the fracture network are changed and the network analysis task is repeated with the updated model.

Most DFN models being studied in this work were characterized by FracMan Reservoir Edition (FRED) which is a product of Golder Associates.

2.4.2 Methods to Create DFN Model

After the fracture reservoir data analysis, two types of probability distributions are usually applied to generate the DFN domain: scalar data probability distribution and directional data probability distributions. Examples of scalar distributions are uniform distribution, exponential distribution, normal distribution, lognormal distribution, normal of log distribution and power law distribution.

For the directional data probability distributions, four types of major models are available in FRED: univariate Fisher distribution, bivariate Fisher distribution, bivariate normal distribution and bivariate Bingham distribution. These distributions are stated in terms of their probability density functions, for a variation about the mean direction. The actual direction chosen from a directional distribution is the composite of directional variation and mean directions.

All scalar and directional data probability distribution equations discussed here refer to FRED Manual (Golder Associates, 2007).

2.5 Background of Control-Volume Finite-Element (CVFE) Simulator

2.5.1 Governing Equations

As shown in Eq (2-10) to (2-12), in the three-phase black-oil model, the governing equations for each phase can be derived from the general continuity equations (Bird et al., 1960) by including porosity $\emptyset$ in the cumulative term (Aziz and Serrai, 1979; Peaceman, 1977)

OIL: $$-\nabla \cdot \mathbf{u}_o = \frac{\partial}{\partial t}\left(\emptyset \frac{S_o}{B_o}\right) + q_o \tag{2-10}$$

WATER: $$-\nabla \cdot \mathbf{u}_w = \frac{\partial}{\partial t}\left(\emptyset \frac{S_w}{B_w}\right) + q_w \tag{2-11}$$

GAS: $$-\nabla \cdot \left(R_s \mathbf{u}_o + \mathbf{u}_g\right) = \frac{\partial}{\partial t}\left(\emptyset \frac{R_s S_o}{B_o} + \emptyset \frac{S_g}{B_g}\right) + R_s q_o + q_{fg} \tag{2-12}$$

where subscript *o*, *w*, and *g* represent oil, water and gas phases, q is the source term, R_s is the gas-oil ratio, S is the saturation, B is the formation volume factor. The LHS in above equations represent the flux term, and **u** denotes to Darcy phase velocity (by combining Equation (2-5) and (2-6)).

In this three-phase black-oil model, capillary pressures coupling phase pressures are listed in Equation (2-13) and (2-14) as

$$P_c(S_w) = P_o - P_w \tag{2-13}$$

$$P_c(S_g) = P_g - P_o \tag{2-14}$$

and the volume conservation is defined in Equation in (2-15) as

$$S_o + S_w + S_g = 1 \tag{2-15}$$

All equations shown above make the three-phase black-oil problem description complete. For nonfractured reservoirs or continuum modeled fractured reservoirs, this type of problem is usually solved by finite-difference (FD) discretization of the partial differential equations. However, for DFN modeled complex fractured systems, finite-element discretization is required to solve the flow problem. A multiphase, multidimensional, upstream flux-weighted CVFE simulator is introduced in the rest of this chapter.

2.5.2 CVFE Formulations

The CVFE formulation applied in this research is derived from a finite-element point of view with a focus on the explicit expression for local flux. This discretization method has the advantage of easy handling unstructured geometry and higher order of accuracy (Young, 1978; Fung et al., 1991; Sukirman and Lewis, 1994; Yang, 2003; Fu, 2005; Matthäi et al., 2005). In three-dimensional spaces, the fractures are modeled as two-dimensional surfaces, and the matrix is modeled as three-dimensional solid tetrahedrons in three-dimensional space. The basic concept of upstream flux-weighted CVFE is to use the fluid potential values for flux calculation; the flux so obtained is then used for mass balance calculations.

To illustrate the concept of CVFE formulation, taking the example of the two-phase (water, oil), two-dimensional flow problem, governing equations derived above could be rewrote in Equation (2-16) as

$$\mathbf{0} = -\nabla \cdot \rho_l \mathbf{u}_l + \frac{\partial(\emptyset \rho_l S_l)}{\partial t} + \tilde{q}_l \tag{2-16}$$

where *l* represents phases.

Figure 2.6 shows that the residual function for a control volume $b_i \in \mathcal{B}$ with boundary T^i could be wrote by integrating Equation (2-16) to get Equation (2-17):

$$F^i = 0 = \int_{b_i} \nabla \cdot \rho \mathbf{u} + \frac{\partial(\phi\rho S)}{\partial t} dx = \int_{T^i} \rho \mathbf{u} \cdot \hat{\mathbf{n}}\, ds + \int_{b_i} \frac{\partial(\phi\rho S)}{\partial t} dx \qquad (2\text{-}17)$$

where $\hat{\mathbf{n}}$ represent the unit outward normal on T^i. For clarity, the phase term and source term in Equation (2-16) are omitted.

As shown in Figure 2.7, a control volume is usually distributed across several triangular elements. During the computation, this distribution makes it difficult to evaluate the residual equation (Equation (2-17)). To solve this problem, an element-by-element add up method is applied to calculate the contributions from subvolumes (as Figure 2.8 shows).

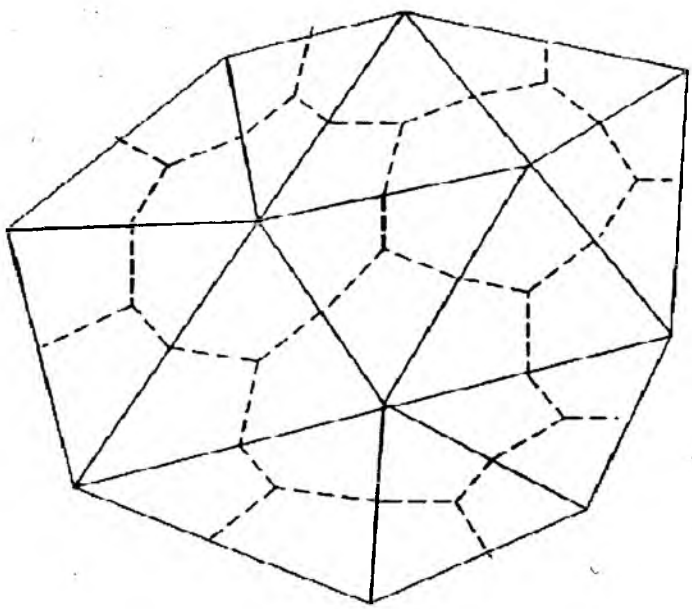

Figure 2.6 An example control volume mesh. The solid lines represent the triangulation T and the dashed lines represent the control volume $\mathcal{B}$

Mathematically, the residual equation for the control volume b_i in Figure 2.7 could be calculated by

$$F^i = \sum_{m=1}^{6} F_m^i \tag{2-18}$$

where subscript m denotes the subvolume of control volume b_i in Figure 2.8, F_m^i represents the subvolume residual function (shown in Equation (2-19)) which is contributed by $b_{i,m}$ and could be derived from Equation (2-17) as

$$F_m^i = \int_{T_{i,m}} \rho \mathbf{u} \cdot \hat{\mathbf{n}}\, ds + \int_{b_{i,m}} \frac{\partial(\emptyset \rho S)}{\partial t} dx \tag{2-19}$$

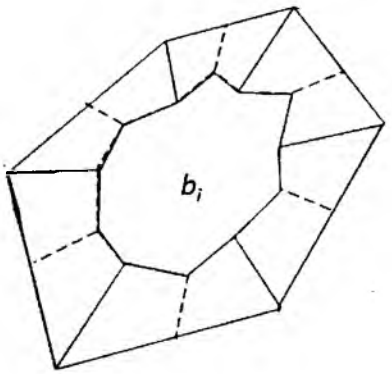

Figure 2.7 A control volume with its boundaries across several triangular elements

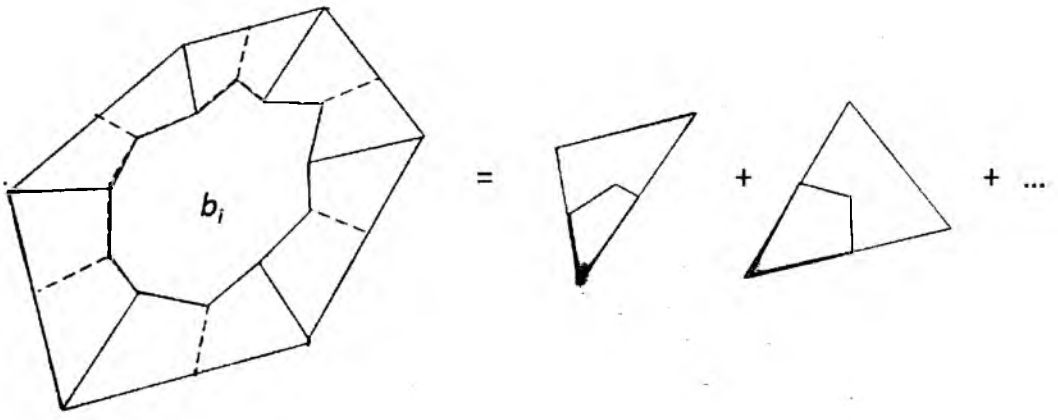

Figure 2.8 Decomposition of a control volume into several subvolumes

As shown in Figure 2.9, for a subvolume b_i in a triangle t_m, the subvolume residual function (Equation (2-19)) is rewritten for $b_{i,m}$ to Equation (2-20)

$$F_m^i = \int_{\overline{cij}} \rho \mathbf{u} \cdot \hat{\mathbf{n}}\, ds + \int_{\overline{cki}} \rho \mathbf{u} \cdot \hat{\mathbf{n}}\, ds + \int_{b_{i,m}} \frac{\partial(\theta \rho S)}{\partial t} dx \qquad (2\text{-}20)$$

where $\hat{\mathbf{n}}$ is the unit outward normal of the corresponding boundary as shown in Figure 2.9.

The first two terms in RHS of Equation (2-20) represent the flux flowing out of $b_{i,m}$ through the boundary $\overline{cij}$ and $\overline{cki}$. These two flux terms can also be defined in Equation (2-21) as

$$f_{i,\overline{cij}} = \int_{\overline{cij}} \rho \mathbf{u} \cdot \hat{\mathbf{n}}\, ds \text{ and } f_{i,\overline{cki}} = \int_{\overline{cki}} \rho \mathbf{u} \cdot \hat{\mathbf{n}}\, ds \qquad (2\text{-}21)$$

The flux-based upstream-weighting scheme (Yang, 2003) was applied in the CVFE formulation in this research program. The concept of this flux-based upstream weighting in CVFE is explained in the in the following.

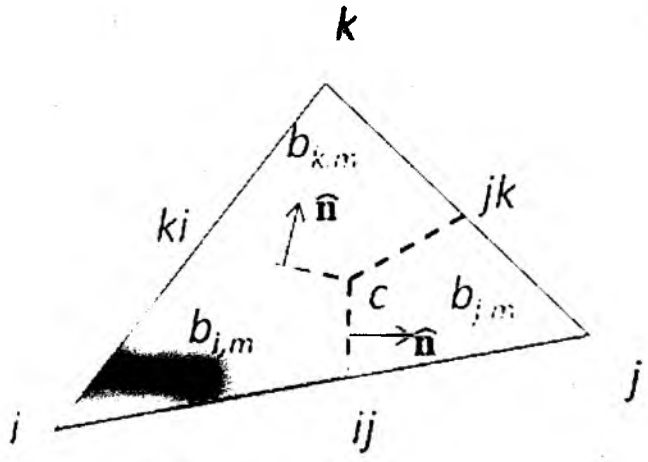

Figure 2.9 Unit outward normals of subvolume $b_{i,m}$ in triangle t_m

Figure 2.10 demonstrates a triangle with constant flux across the three control volume boundaries. The upstream direction is determined by the sign of the each flux. From the flux definition in Equation (2-21), while flux $f_i > 0$, the flux is flowing out of the control volume *i*. Therefore, for a control volume, the flux-based upstream operator up*(ij)* is defined in Equation (2-22) as

$$\mathrm{up}(ij) = \begin{cases} i & \text{if } f_{i,\overline{cij}} > 0 \\ j & \text{if } f_{j,\overline{cij}} > 0 \end{cases} \tag{2-22}$$

The above flux-based upstream-weighting scheme in CVFE formulation was validated and verified for mass balances both global and locally by Yang (2003).

2.5.3 CVFE Simulator

Discretization of PDE in the last section results in lots of nonlinear equations. To solve the flow problem, global residual functions need to be linearized for the system. A nonlinear solver is required to generate the Jacobian matrix and assembly the multiphase residual vector. The simulator needs a linear solver to solve the optimized sparse system. Some concepts regarding CVFE reservoir simulator implementation are discussed below.

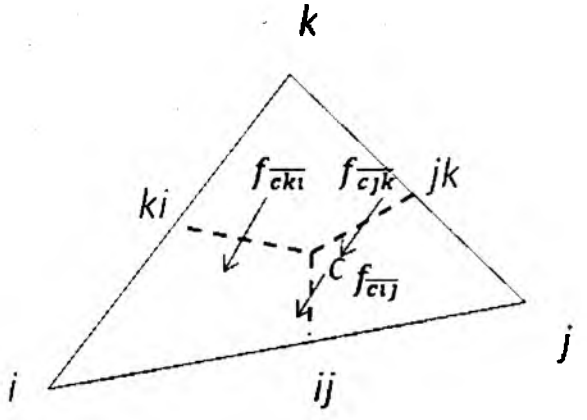

Figure 2.10 Illustration of upstream nodes and flux directions

2.5.3.1 Assembly of Global Residual Functions

As discussed in Section 2.5.2, partial residual functions need to be added up by the method of element-by-element. This element-by-element process utilizes local numbers of element for the computation convenience. However, for a reservoir simulation study, every node in the domain is assigned a unique ID. Compared with the local element-by-element number, this unique ID is called a global number. Therefore, a mapping between the local and global numbering system becomes necessary during the simulation study. This mapping system is normally accomplished by the local-to-global (LTG) array (Yang, 2003). By this LTG array, the global residual vector and Jacobian matrix can be assembled practically.

2.5.3.2 Nolinear Solver

To solve the set of highly nonlinear global residual functions (Equation (2-18)) by CVFE discretization, the quasi-Newton framework is adopted in the reservoir simulator which was applied in this research program. In numerical analysis, Newton's method is a well-known iterative type of method for solving nonlinear equations. If the initial guess value is close to the root, Newton's method can often converge remarkably quickly. However, far from the desired root, Newton's method can easily lead an unwary user astray with little warning. Thus, good implementations of the method embed it in a routine that also detects and perhaps overcomes possible convergence failures. For the quasi-Newton framework in the CVFE simulator, Newton's method is always applied first. If the full Newton step improves the approximation, it is accepted. If not, a global line search is applied. Detailed information regarding quasi-Newton framework refers to Yang's work (2003). After this nonlinear process, the derivative of residual functions will

be assembled in a Jacobian matrix. The analytical form of the derivative should be used whenever possible for the best performance. In the reservoir simulation, most of the time the functions of relative permeability k_r, formation factor B and viscosity μ are available, and their analytical form can be easily obtained. Compared to numerical derivatives, analytical derivatives are remarkable quickly. However, the problem associated with the analytical derivatives is that its derivation process is prone to human error. Simulators used in this research program have the capability of calculating derivatives both numerically and analytically.

2.5.3.3 Linear Solver

After the process of linearization, obtained set of linear equations need to be solved using an appropriate conjugate-gradient type of method. For the CVFE simulator used in this research program, the linear solver from Portable, Extensible Toolkit for Scientific Computation (PETSc) is adopted to solve the set of linearized equations obtained from the last section. PETSc was developed at Argonne National Laboratory in the Mathematics and Computer Science Division as a general purpose suite of tools for the scalable solution of PDEs and related problems. PETSc provides a rich set of Krylov subspace methods as the linear solvers, for example, generalized minimal residual (GMRES), conjugate gradient (CG), conjugate gradient squared (CGS), and so on. The GMRES method is used in this research. Furthermore, PETSc offers several preconditioners to help optimize the matrix. Those preconditioners include Additive Schwartz, Block Jacobi, Jacobi, ILU, ICC, and so on. The ILU preconditioner is adopted by the CVFE simulator in this research work. The robustness and efficiency of PETSc have been widely tested and recognized. There are several features from PETSc that

make it very convenient for the application programmer. For example, users can create complete application programs for the parallel solution of nonlinear PDEs without writing much explicit message-passing code themselves. Furthermore, PETSc enables a great deal of runtime control for the user without any additional coding cost. The runtime options include control over the choice of solvers, preconditioners and problem parameters as well as the generation of performance logs.

Some basic PETSc functions used in the CVFE simulator are briefly introduced below. Detailed information refers to PETSc Users Manual (2007).

VecSetValues(...): insert residual function values into a PETSc vector;

VecNorm(...): calculate the norm of a vector;

MatSetValues(...): insert gradients into the Jacobian matrix;

SLESCreate(...): create a PETSc linear solver;

KSPSetType(...): set method to solve the linear system;

SLESSolve(...): solve the set of linear equations

2.5.3.4 Modular Reservoir Simulator

Due to its complexity, modern reservoir simulator developing work usually requires team effort which makes the object orientated concepts widely adopted. Supported by the U.S. Department of Energy (DOE), the Utah Finite Element Simulator (UFES) is a framework that has been developed during the past decade. The CVFE simulators applied in this research were developed from this UFES modular framework.

Figure 2.11 shows that the main structure of the framework consists of three major modules: discretization method (DM), physical model (PM), and Utility. The selection of discrete scheme (for example, CVFE in this research) and physical model (black-oil model for this research) determines how DM and PM are implemented. The Utility module provides "in-house" libraries and some special routes for interfacing the external libraries and the framework.

The examples of the implementation layer in DM, the Interface policy provides driving forces between control volumes; the LineSouce policy provides the drive forces between control-volume and wells; the ControlVolume policy provides the size of the control-volume; the DiscretizationMethod policy provides the list of control-volume, line

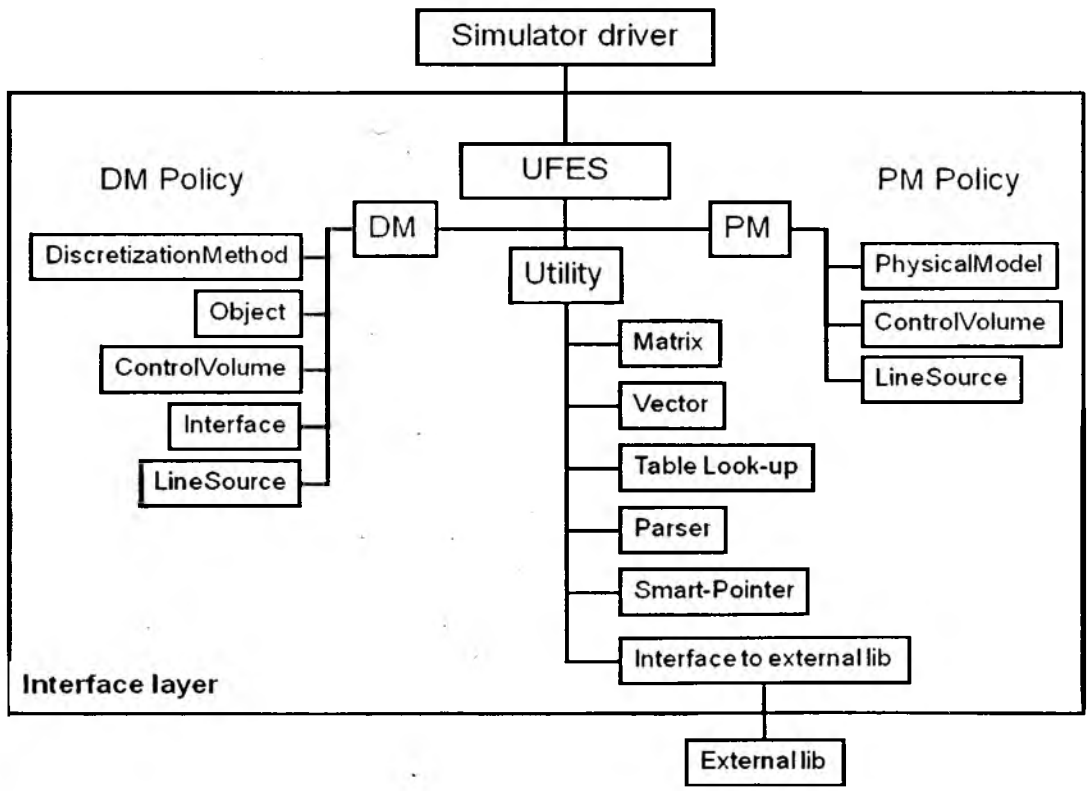

Figure 2.11 Illustrations of modular reservoir simulator framework

source, and the connectivity map; the Object policy provides the control-volume and line source lists.

On the implementation layer of PM, the PhysicalModel policy requires an implementation to decide how to get the solution of each time step and time step control; the ControlVolume policy requires the implementations to compute residual functions of each conservation equation, constraint equation and their derivatives; the LineSource policy requires the implementations of how the flows and their derivatives being computed between control-volumes and wells. Numerous submodules are included in the PM such as rock, fluid, rock-fluid modules, etc. The rock module provides information such as density, porosity, and permeability. In summary, during the simulation, all physical related behaviors will be provided by PM, and all numerical issues are governed by DM.

Based on this modular framework, several reservoir simulators were developed at the Petroleum Research Center (PERC) at the University of Utah. From the DM aspect, these simulators include CVFE, mixed finite-element (MFE), and finite-difference (FD). From the PM aspect, simulators include the black-oil model, thermal model, and compositional models. As mentioned above, the simulators applied in this research work are black-oil modeled simulators implementing CVFE discretization method.

2.5.4 Simulator Input and Output

Reservoir simulation can be described as using computer system to study fluid flow in a reservoir. For a simulation job, various disciplines contribute to the preparation of the input data set. These contributions need to be integrated during the reservoir modeling process. The contribution from different disciplines make to reservoir modeling

is illustrated by Figure 2.12. The simulator is the contact point among disciplines. The integrated data set (reservoir domain information, properties of rock and fluid, well trajectories and operating conditions, production data and observation, reservoir initial conditions and boundary conditions) is sent into the simulator as the input file and the results will be output with the information of phase saturations, pressures, rates and even some visualization files.

For the CVFE reservoir simulators used in this research program, the input file is a single Extensible Markup Language (*XML*) file. The *XML* is a general-purpose specification for creating custom markup languages. It is classified as an extensible language because it allows users to define their own elements. Its primary purpose of *XML* is to facilitate the sharing of structured data across different information systems. As shown in Figure 2.12, reservoir simulation input is a typical integrating information file from different resources which makes sense to adopt this format. Other reasons to

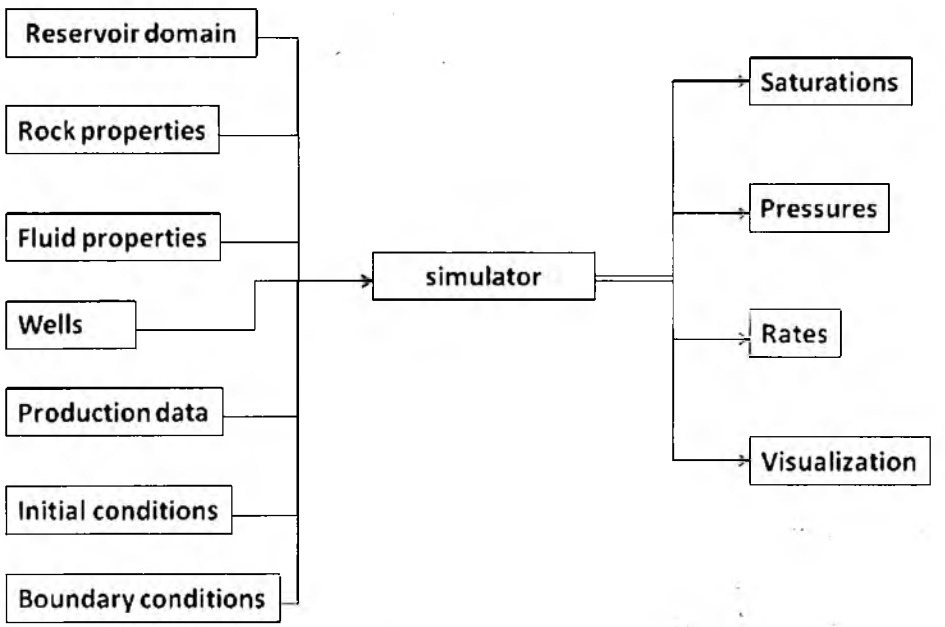

Figure 2.12 Illustrations of reservoir simulation input and output information

choose this format are its well-formed syntax and mature parsing capability supporting from other software packages possibly be used. To demonstrate the input file format, a simple two-phase basement example is shown below:

```
<?xml version="1.0"?>
<Simulation name="Example">
        <Partition name="Example-part"/>
        <Fluid name="PVT-10">
                <oil-density unit="API"> 45 </oil-density>
                <water-density unit="lbm/ft^3"> 63 </water-density>
                <oil type="function">
                  1130   1  1.e-6   0.90  0.0
                </oil>
                <water type="function">
                  14.7   1  3e-6   0.96   0.0
                </water>
        </Fluid>
        <Rock name="Rock-10">
                <oil-water>
                0.00 0.00 1.0000 14.0
                0.15 0.01 1.0000 13.0
                0.20 0.02 0.9600 7.0
                0.30 0.03 0.4300 4.0
                0.40 0.04 0.2000 3.0
                0.50 0.05 0.1000 2.5
                0.60 0.08 0.0600 2.0
                0.70 0.125 0.022 1.5
                0.80 0.25 0.0100 1.0
                </oil-water>
                <compressibility>
                 14.7 1.e-5
                </compressibility>
        </Rock>
        <PointSource name="Well1">
                <Point>
                        3874 9669
                </Point>
                  <PI>
                          1216
                  </PI>
        </PointSource>
        <Event time="0">
                <Element relay="true" action="set thickness">
```

```
                0 7.0
            </Element>
            <Element relay="true" action="set conductivity"
          name="permeability">
                0  F  1000 0 1000
            </Element>
            <ControlVolume relay="true"  action="set ControlVolume">
                0 PoSw 0.3 PVT-10 Rock-10 4300 0.15
            </ControlVolume>
            <PointSource relay="false" action="set PointSource">
                Well1 open BHP production 200
            </PointSource>
</Event>
<Event time="0.001">
            <ControlVolume action="write ControlVolume" property="S P"/>
           <PointSource action="write PointSource" property="Rate
          Cumulative"/>
</Event>
<Event time="1">
            <ControlVolume action="write ControlVolume" property="S P"/>
           <PointSource action="write PointSource" property="Rate
          Cumulative"/>
</Event>
<Event time="10">
            <ControlVolume action="write ControlVolume" property="S P"/>
           <PointSource action="write PointSource" property="Rate
          Cumulative"/>
</Event>
.....
<Event time="100">
            <ControlVolume action="write ControlVolume" property="S P"/>
           <PointSource action="write PointSource" property="Rate
          Cumulative"/>
 <PointSource relay="false" action="set PointSource">

          <!--
           example:
           well1 open BHP injection PVT-10 2600
           well2 open BHP production 1000
           well1 open LiquidRate injection PVT-10 26 0.8
           well2 open LiquidRate production 2.6
          -->
          Well1 open BHP injection PVT-10 3751

 </PointSource>
</Event>
```

```
.....
<Event time="900">
        <ControlVolume action="write ControlVolume" property="S P"/>
        <PointSource action="write PointSource" property="Rate
        Cumulative"/>
</Event>
<Vertex>
        <!-- CVID PN x y z -->
        0 2862371.612708016 3796320.6108746817 -15305.514648167276
        1 2862223.7030747165 3796258.2797346474 -15107.410070856731
        2 2862016.6404414456 3796419.2723770784 -15223.334613773755
        3 2861976.595561424 3796214.3124375804 -14872.203719736106
        ....
        9668 9668 2859619.1288819755 3792828.3183453325 -
        11757.863028030839
</Vertex>
<Element>
        <!-- ElementID Elementtype CVID0 CVID1 CVID2 (CVID3) -->
        0 F 0 1 2
        1 F 2 1 3
        2 F 4 5 6
        3 F 5 7 8
        .....
        19079 F 241 9668 9666
</Element>
</Simulation>
```

The data structure is clearly shown from the above example basement reservoir simulation input file. Every input file element is strictly defined by well-formed *XML* syntax with start-tag and end-tag. The above basement feature domain is described by meshed (domain mesh is separately discussed in the next section) 9669 nodes (under the Vertex tag from 0 to 9668) and 19080 triangles (under the Element tag from 0 to 19079). The double-precision Cartesian coordinates of each node is defined after its global ID with the order of x, y, and z. The basement features are composed of meshed triangles. Each triangle element is defined by the node global ID connections. The well in this basement reservoir is defined under the Point Source tag: the first number is the well

global ID in the Vertex tag, and the second number is assigned following last number of node global IDs. The well productivity index (PI) is calculated explicitly by Peaceman's (1977) well model:

$$\mathrm{PI} = \frac{2\pi kh}{\ln\left(\frac{r_e}{r_w}\right)+1} \tag{2-23}$$

In Equation (2-23), *kh* is the product of permeability and feature's aperture with the direction of well penetrating fractures, r_w is the well radius, and r_e is the equivalent control volume radius. r_e could be calculated by Equation (2-24)

$$r_e = \sqrt{\frac{A}{\pi}} \tag{2-24}$$

where A is the control-volume area being occupied by the well point-source.

The above example basement domain is a very simplified reservoir model with homogeneous thickness, porosity, permeability, initial saturation and pressures. As shown in the file, some fracture properties such as fracture thickness and transimissivity (*kh* value) are defined with triangular elements; other fracture properties such as rock type, porosity, initial pressure, initial saturation are defined with the control volumes (node centered). Properties such as density, viscosity relative permeability, capillary pressure, rock compressibility are defined at the beginning of the input file by their own start- and end- tags. These tag names are very straightforward to be found. The output time schedule and well control schedule are under the tag of "Event." For the real simulation cases with multiwells operations, "event" may need to be defined on a day-by-day schedule based on well operation/production data. If this situation happened, the input file might become big. As part of this research program, this situation was solved

by some preprocessing interfaces. Those preprocessing interfaces make the input file easy to assemble together.

Under the tag of "Fluid" in this example, oil and water's formation factor and viscosity are given by equations with the reference pressure and their compressibility. These equations are (2-25) and (2-26):

$$B_l = B_{ref,l} exp\left[-C_{B,l}\left(P - P_{ref}\right)\right] \tag{2.25}$$

$$\mu_l = \mu_{ref,l} exp\left[-C_{\mu,l}\left(P - P_{ref}\right)\right] \tag{2.26}$$

where subscript *l* denotes phases (oil, water), subscript *ref* denotes reference status.

Example of oil tag

```
<oil type="function">
  1130  1  1.e-6  0.90  0.0
</oil>
```

where reference pressure is 1130 psi, at this pressure, the oil's formation factor is 1.0, the oil formation factor compressibility is 10^{-6} in this case. Also, at this reference pressure (1130 psi), the oil's viscosity is 0.90 cp and it will not change with pressure (since its viscosity compressibility equals to zero).

For the output file from CVFE simulator, based on the "Event" setup on the input file, phase saturations, phase pressures are output by control-volume (node); well injection phase rate and production phase rate are output by well occupied point-source (node or control-volume). Phase saturations and phase pressures can be output as the visualization files which are in the format of *vtk*. Well injection/production performances are output by phase (oil, water, and gas) rates (STB/day) and cumulative amount to date (STB). Some reservoir behaviors can be analyzed through these well data, such as the oil

recovery (ratio of cumulative oil production over original oil in-place), water cut (ratio of water production rate and total fluid production rate), and so on.

2.6 Meshing

Domain meshing is an important concept for reservoir simulation. To calculate the fluid flow through the porous media, modeled reservoir domain must be meshed based on numerical discretization method adopted. Today, the trend in simulator development is to separate the meshing part from the flow calculation (simulator). The meshing part is normally done by the meshing software packages. The output from the meshing package is used as the input for the simulator (as shown in the example input file on last section). Through this approach, one simulator may couple with different meshing programs.

In a DFN modeled fractured reservoir, the fractures are modeled as two-dimensional surfaces in a three-dimensional space, and the matrix is modeled as three-dimensional solid in three-dimensional space. To get the fluid flow through fractures and matrix, at the beginning, the fractures have to be meshed into two-dimensional triangles. Then the matrix needs to be meshed as tetrahedrons in conformance with the meshed two-dimensional fracture triangles.

As mentioned in Section 2.3.3, the bottleneck of simulating DFN characterized fractured reservoir is unstructured domain meshing. Low quality mesh will result in a significant mathematical problem during the flow simulation. Several commercial three-dimensional finite-element mesh software packages were used in this research program. These packages include CUBIT from Sandia National Lab, HyperMesh from Altair Co., RoseMesh from Golder Associate, MeshMaster from Golder Associate. As part of this

research work, the above mesh software packages were integrated into the multiphase and multiscale fractured reservoir simulation workflow. Some interfaces were developed among DFN characterization, mesh software and simulators. Furthermore, some mesh postprocess schemes were developed by this research work to analyze mesh quality and even reconstruct/reorder meshes. These efforts normally can improve the reservoir simulation convergence. Taking the example of a basement reservoir, the meshed triangles aspect ratios and control volume ratios usually play an important role during the reservoir simulation. During the reservoir simulation, these mesh shape elements are used in flux calculation, which can directly change the condition number of the Jacobian matrix. Large flux contrast ratio results in a large Jacobian matrix condition number. A problem with a low condition number is said to be well-conditioned, while a problem with a high condition number is said to be ill-conditioned. Normally ill-conditioned matrix results in a convergence problem. Most commercial mesh software offers various mesh quality control options which can maximize assure desired mesh quality being obtained.

2.7 Chapter Summary

In this chapter, some fundamentals regarding fractured reservoir simulations were introduced. These fundamentals include basic concepts of black-oil reservoir models, fractured reservoir classifications, flow models to study fractured reservoir, background of the CVFE discretization method and the CVFE simulator development, simulation input/output files, and briefly introduction of unstructured domain geometry meshing.

2.8 Nomenclature

A	=	area, ft^2
B	=	formation volume factor
$\mathcal{B}$	=	control volume of T
b_i	=	control volume of node i
C	=	compressibility, psi^{-1}
F^i	=	residual function of node i,
F^i_m	=	partial residual function of $b_{i,m}$
f_i	=	total flux flowing out of b_i within a triangle,
h	=	fracture/fault aperture, ft
i	=	i^{th} discretized fracture elements
l	=	o, w, g, phases
L	=	side length matrix block in dual porosity model, ft
$\mathbf{k}$	=	permeability tensor, md
$k_{x,y,z}$	=	components of the permeability tensor **k**, md
k_r	=	relative permeability
n	=	number of discretized fracture elements
$\hat{\mathbf{n}}$	=	unit outward normal of a boundary
P	=	fluid pressure, psi
P_c	=	capillary pressure, psi
q	=	volume injected or produced, $ft^3/(ft^3 day)$
$\bar{q}$	=	mass injected or produced, $lbm/(ft^3 day)$
R_s	=	gas oil ratio, MSCF/STB

r	=	radius, ft
S_l	=	saturation of phase l
S_{iw}	=	connate water saturation
S_{ro}	=	residual oil sasturation
T	=	boundary of polygonal domain
T^i	=	control volume boundary b_i
t	=	time, day
t_m	=	triangle m
$\mathbf{u}$	=	Darcy's velocity, ft/day
up	=	upstream function
V	=	volume, ft^3
w	=	water phase
φ	=	fluid potential
$\emptyset$	=	porosity
ρ	=	density, lbm/ft^3
μ	=	viscosity, cp
σ	=	shape factor, ft^{-2}

2.9 Bibliography

Aziz, K., Settari, A., "Petroleum Reservoir Simulation," New York: Elsevier (1979)

Balay, S., Bushchelman, K., Eijkhout, V., Gropp, W., Kaushik, D., Knepley, M., McInnes L.C., Smith, B., Zhang, H., "PETSc Users Mannual," ANL-95/11 – Revision 2.3.3 (2007)

Dershowitz, W.S., "Rock Joint Systems," Ph.D Dissertation, Massachusetts Institute of Technology, Cambridge, MA (1984)

FracMan Reservoir Edition (FRED) User's Manual, Golder Associates (2007)

Fu, Y., Yang, Y.-K., Deo, M., "Three-Dimensional, Three-Phase Discrete-Fracture Reservoir Simulator Based on Control Volume Finite Element (CVFE) Formulation," paper SPE 93292, (2005)

Fung, L.S., Hiebert, A.D., and Nghiem, L.X., "Reservoir Simulation With a Control Volume Finite Element Method", paper SPE 21224 (1991)

Matthäi, S.K., Mezentsev, A., Belayneh, M., "Control-Volume Finite-Element Two-Phase Flow Experiments with Fractured Rock Represented by Unstructured 3D Hybrid Meshes", paper SPE 93341 (2005)

Peaceman, D.W., "Fundamentals of Numerical Reservoir Simulation," New York: Elsevier (1977)

Ronald A. Nelson, "Geologic Analysis of Naturally Fractured Reservoirs," Gulf Professional Publishing, second edition, (2001)

Sukirman, Y.B. and Lewis, R.W.: "Three-Dimensional Fully Coupled Flow: Consolidation Modeling Using Finite Element Method", paper SPE 28755, (1994)

Yang, Yi-kun, "Finite-element Multiphase Flow Simulation," Ph.D Dissertation, University of Utah, Salt Lake City, UT (2003)

Young, L.C.: "An Efficient Finite Element Method for Reservoir Simulation", paper SPE 7413, (1978)

CHAPTER 3

SENSITIVITY STUDY OF OIL PRODUCTION FROM FRACTURED/FAULTED BASEMENT RESERVOIRS

(A paper in preparation)

Huabing Wang, Craig Forster, Chung-Kan Huang, and Milind Deo

Department of Chemical Engineering

University of Utah

Salt Lake City, UT 84112

3.1 Abstract

A fully-implicit, three-dimensional (3D), three-phase, discrete fault/fracture, black oil CVFE simulator provides new insight and understanding of oil production from reservoirs in fractured, low-permeability basement rocks. In this chapter, two three-dimensional, naturally fractured reservoirs with different fracture orientations and intensities were characterized by a discrete fracture network (DFN) geological model. Performances of three-phase, black-oil reservoir simulators based on the single porosity finite difference and upstream flux weighted CVFE discretization method were then evaluated on an orthogonal basement fracture network. Benchmark work showed that the results were in close agreement, even under three-phase flow conditions. CVFE is then used to simulate a complex network of intersecting faults that mimic a more realistic basement reservoir. The CVFE simulator provides a method that allows for complex fracture/fault geometries and spatial variations in the internal properties of faults. CVFE simulations of the realistic network illustrate the possible consequences of uncertainty in knowing fracture/fault properties (e.g., porosity, permeability, thickness, dip orientation, connectivity and flow transmissibility). For example, one of the possible consequences is the introduction of spatial variability in permeability within the fault planes (using spatially randomized patterns of 10, 100 and 1000 md), while retaining a constant geometric mean permeability of 100 md. This enhanced oil production is due to the high-permeability pathways. A 50:50 mix of 10 and 1000 md elements yielded 36% OOIP recovery while a 33:33:33 mix of 10, 100 and 1000 md yielded 24% OOIP production. These results were 25% and 13% greater, respectively, than those obtained by the uniform 100 md case (11%OOIP). This inherent variability, combined with the

uncertainty of knowing the detailed connections between different regions of the fault network, impacts the pattern of sweep in ways that are important to understand when attempting to develop innovative approaches to reservoir management.

3.2 Introduction

Quantifying fractured reservoirs is much more difficult than quantifying nonfractured reservoirs due to the extreme complexity of the fractured reservoir. The complexity originates from the vast number of uncertain variables that dictate the final fractured reservoir response. Examples of these variables and their relatives in a fractured basement reservoir include the reservoir's storage from fracture thickness and porosity; fracture permeability/transimissivity distribution characterizations; and fracture geometry such as dip orientation, connectivity, area sizes etc. The single or combined effects of those fracture variables mentioned here can make the basement network act as both permeable pathways to fluid migration and also significant storage. This brings a wide range of uncertainties for basement fractured reservoir management.

At the beginning of this chapter, a regularized fracture network was constructed that was amenable to gridding using ECLIPSE, the conventional finite difference reservoir simulator. A three-dimensional, three-phase, black oil modeled control-volume finite element (CVFE) simulator was used in this study. In order to validate the CVFE simulator, the results of regularized DFN direct simulations were compared with the results from ECLIPSE. Once the accuracy of the DFN approach was ascertained, some sensitivity of "real" basement fracture network with the multiphase DFN modeled basement reservoir was directly simulated through the CVFE simulator.

Permeability distribution in the fracture/fault zone, dip orientation and thickness variations will be considered in this sensitivity study.

A typical fracture network is highly heterogeneous. To understand the impact of permeability heterogeneity between fractures, within fractures and the presence of preferred high permeability pathways between injectors and producers were quantitatively studied in this conceptual basement fractured network. The extent to which the preferred pathway network leads to early breakthroughs was also quantified by this chapter. The impact of shutting off the high permeability fracture using gel treatments on improving oil recovery will also be explored by this chapter.

3.3 Governing Equations and DFN Model

As shown in Equation (3-1) to (3-3), the equations describing compressible three-phase flow are obtained by combining Darcy's law and mass conservation for each phase:

OIL: $$-\nabla \cdot \mathbf{u}_o = \frac{\partial}{\partial t}\left(\emptyset \frac{S_O}{B_O}\right) + q_o \tag{3-1}$$

WATER: $$-\nabla \cdot \mathbf{u}_w = \frac{\partial}{\partial t}\left(\emptyset \frac{S_W}{B_W}\right) + q_w \tag{3-2}$$

GAS: $$-\nabla \cdot \left(R_s \mathbf{u}_o + \mathbf{u}_g\right) = \frac{\partial}{\partial t}\left(\emptyset \frac{R_s S_O}{B_o} + \emptyset \frac{S_g}{B_g}\right) + R_s q_o + q_{fg} \tag{3-3}$$

where subscript o, w, and g represent oil, water and gas phases, q is the source term, R_s is the gas-oil ratio, S is the saturation, B is the formation volume factor. The LHS in the above equations represent the flux term, and **u** denotes the Darcy phase velocity (by combining Equation (2-5) and (2-6)).

In this three-phase black-oil model, capillary pressures coupling phase pressures are listed in Equation (3-4) and (3-5) as

$$P_c(S_w) = P_o - P_w \tag{3-4}$$

$$P_c(S_g) = P_g - P_o \tag{3-5}$$

and the volume conservation equation is defined in Equation (3-6)

$$S_o + S_w + S_g = 1 \tag{3-6}$$

where the subscripts *o, w* and *g* refer to oil, water and gas phases, *u, ρ and μ* are the fluid velocity, density and viscosity. The rock is characterized by the porosity Φ and absolute permeability *k*. The multiphase properties are the relative permeability k_r and capillary p_c. R_s represents the gas-oil ratio which is the solubility of gas in oil as a function of pressure. *B* is the formation volume factor. Source terms are designated by *q*. The equations for three-phase flow are derived from the continuity equation: the left-hand side (LHS) is the flux term and the right-hand side (RHS) represents the cumulative term and the source term. For the basement reservoir study, all of the fluid flow through fractures is assumed to be governed by Darcy's law.

The discretization of these equations for modeling flow in basement reservoirs entails the use of the DFN approach and the CVFE scheme. In the DFN modeled three-dimensional basement domain, all of the single fractures are represented by two-dimensional surfaces and those two-dimensional surfaces will be meshed into triangle elements. These dimensional reductions greatly decrease the node numbers, resulting in reduced computational time. A control volume is usually distributed across several triangular elements and calculated by summing together its subvolumes, as shown in Figure 3.1.

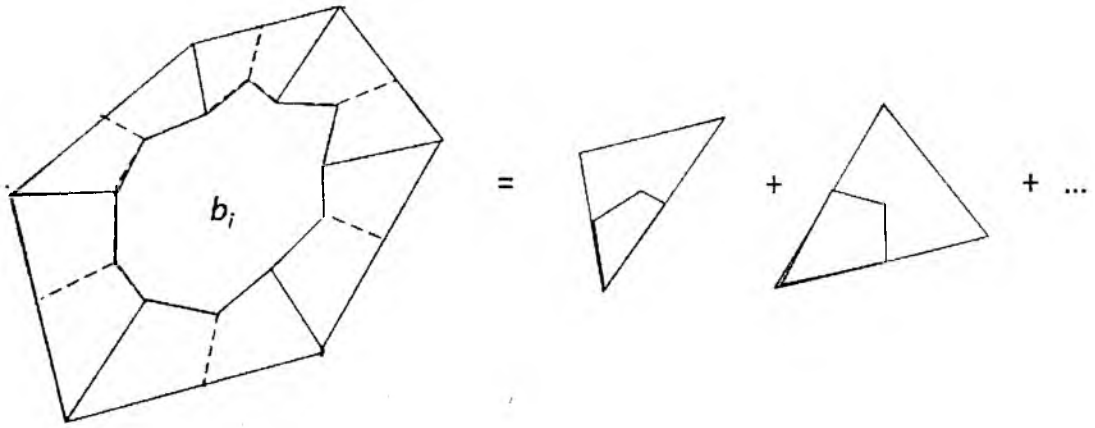

Figure 3.1 A control volume with its boundaries (dashed line) across several triangle elements and decomposition of a control volume into several subvolumes

Figure 3.1 shows an example of a control volume with its boundaries (dashed line) across several triangle elements and decomposition of a control volume into several subvolumes. Detailed background of CVFE discretization formulation and simulator development refer to Section 2.5, the fundamentals of fractured reservoir modeling.

3.4 Proposed Domain Characteristics

3.4.1 Regularized DFN Basement Domain

At the beginning of this study, a regularized well connected fracture network domain was generated for the purpose of verifying the CVFE simulator with the most popular commercial black oil simulator ECLIPSE. Since all of the features were connected orthogonally, the finite-difference based ECLIPSE simulator gave the most accurate solution. Two constraints were applied for the DFN regularized domain and its equivalent ECLIPSE single-porosity domain: the same OOIP and the same transmissivity (*kh* value). The regularized domain was characterized as a three-phase black oil model with initial solution gas in the oil phase. All simulations have the exact same fluid and

rock properties. Examples of these properties include fluid density, viscosity, compressibility, PVT table, formation factor, gas/oil ratio table, rock compressibilities, relative permeability curves, initial conditions, well operation conditions and schedules, etc. Common model properties in the basement model are shown in Figure 3.2:

- Impermeable matrix with $\Phi = 0$ (Type I, basement reservoir system)
- Domain = 1,000 ft by 1,000 ft by 200 feet deep
- Total feature length = 30,000 feet
- Feature property: k = 1,000 md, Φ = 14 %, width = 0.5 feet
- Original Oil In Place (OOIP) = 53,580 STB
- Injection Pressure = 4,300 psi

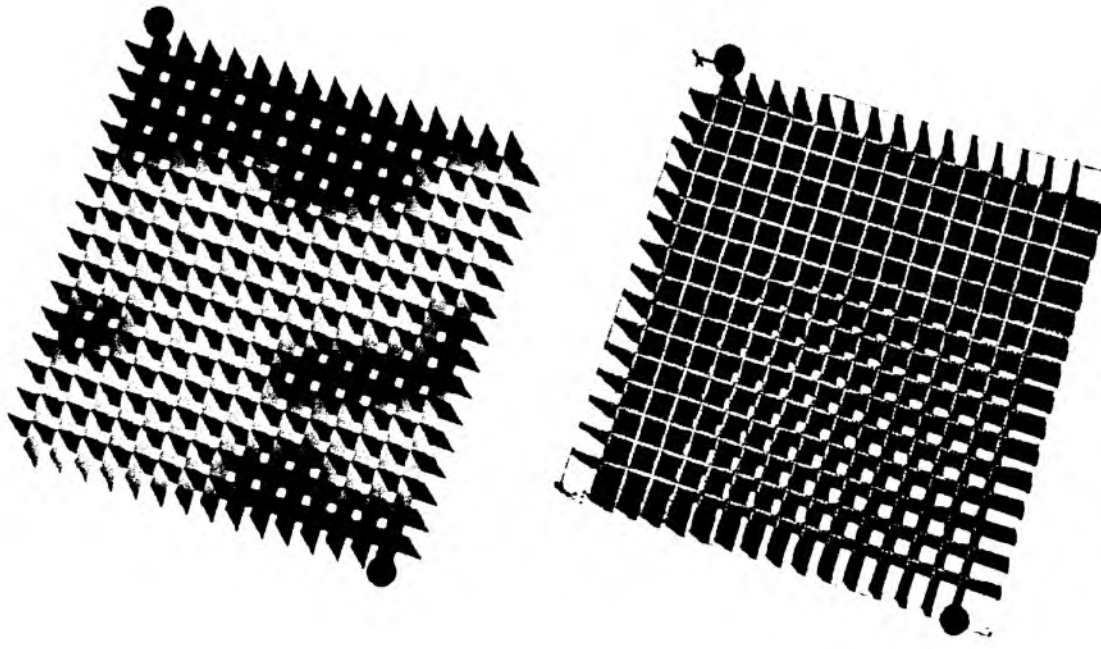

Figure 3.2 Regularized DFN basement model (left) and equivalent regularized ECLIPSE single porosity model

3.4.2 Irregularized (Hypothetical "Real") DFN Basement Domain

As shown in Figure 3.3, the properties in the irregularized DFN basement model were exactly the same as the regularized domain except for the feature orientation and connectivity. To distinguish the regular "ideal" basement model discussed in last section, this irregular domain was named the hypothetical "real" basement model. Two questions to be answered were: Can this hypothetical "real system" be easily represented by the equivalent "ideal system"? How could this domain be best represented by the traditional finite-difference based reservoir simulators such as ECLIPSE?

Figure 3.3 Irregularized DFN basement model with the same model properties as regularized DFN basement model but different orientation and connectivity

3.4.3 Geological Characteristics Comparisons Between Hypothetical "Real" System and Regular "Ideal" System

Certain fracture network geological characterization analyses were done on both "ideal" and "real" systems. Figure 3.4 shows that the regularized "ideal" system has only two orientations as (90, 0) and (180, 0); for the hypothetical "real" system, the main fracture pole orientations are distributed from (130, 0) to (350, 0). Figure 3.5 shows that the regularized "ideal" system has the uniform feature equivalent length (radius) of 252 feet, but the fracture sizes of hypothetical "real" system offered power law fitting of x_min = 252.1 feet and exponential term b = 5.2. Detailed fracture network analysis is shown in Table 3.1.

Fracture cluster analyses were performed on both "ideal" and "real" models. No isolated fracture was found in either system. The average fracture center was a little bit different:

1) Regularized "ideal system": (500.00, 500.00, 100)
2) Hypothetical "real system": (513.06, 488.70, 100)

3.5 CVFE Simulator Verification

The presence of fractures makes the reservoir domain geometrically complicated, particularly when the issue of connectivity dominates recovery. One of the key advantages of the DFN model, compared with conventionally fractured modeling, is to present the fracture orientation and connectivity explicitly. Obviously, the traditional finite-difference based simulator offered the option of the dual porosity model to simplify connectivity and heterogeneity issues that are modeled much more accurately by the DFN

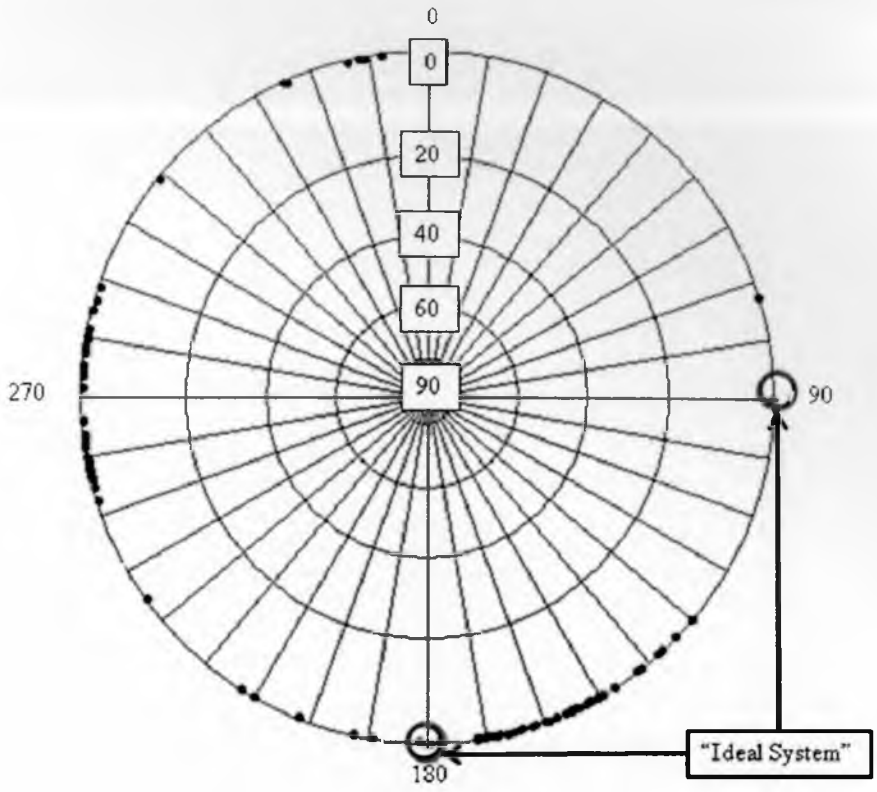

Figure 3.4 Fracture pole orientation (Wulff equal-angle projection, lower hemisphere) between hypothetical "real system" and "ideal system"

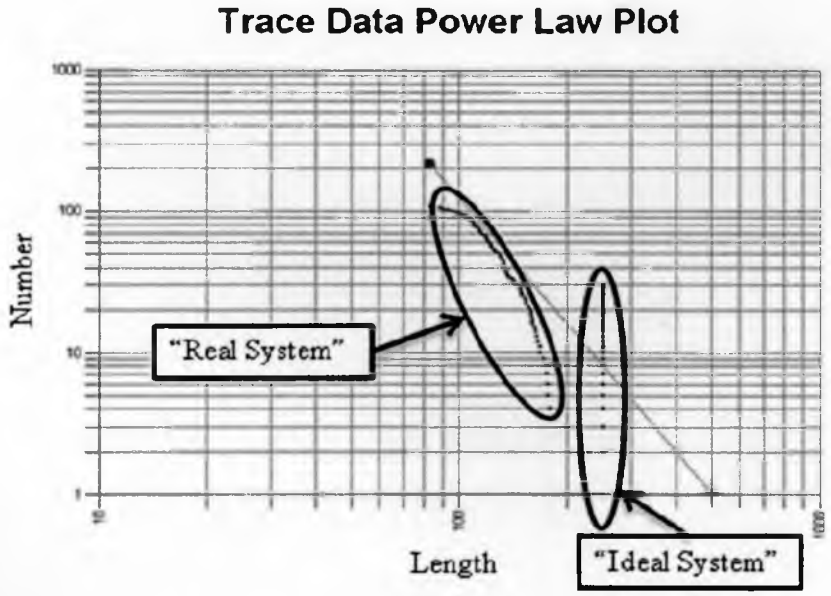

Figure 3.5 Comparisons of fracture size distribution (Power Law Plot) between the hypothetical "real system" and "ideal system"

Table 3.1 Fracture set statistics

	Regularized "Ideal System"	Hypothetical "Real System"
Number of fractures	30	107
Total fracture area	6000000	6000000
Total fracture volume	3000000	3000000
P32 (fracArea/volume)	0.02	0.02
P33 (fracVolume/volume)	0.01	0.01
Mean orientation	135, 0	197.2836, 0
Equivalent radius mean	252.13	130.59
Equivalent radius std dev	1.06	28.34
Equivalent radius min	252.13	83.40
Equivalent radius max	252.13	237.99
Area mean	200000	56075
Area std dev	0	26292
Area min	200000	21850
Area max	200000	177946
Thickness, mean	0.5	0.5
Thickness, std dev	0	0
Thickness, min	0.5	0.5
Thickness, max	0.5	0.5
Permeability, mean	1000	1000
Permeability, std dev	0	0
Permeability, min	1000	1000
Permeability, max	1000	1000
Compressibility, mean	5e-006	5e-006
Compressibility, std dev	0	0
Compressibility, min	5e-006	5e-006
Compressibility, max	5e-006	5e-006

approach. The characterization by the DFN model requires rotatable permeability tensor along fractures/faults, which the finite-element discretization formula achieves especially well. A three-dimensional, three-phase black oil reservoir simulator was developed using a new CVFE formulation (Yang, 2003; Fu et al., 2005; Fu, 2007). In this new CVFE approach, flux-based upstream weighting was applied to ensure flux continuity both locally and globally. This weighting function solved the local mass conservation problem from traditional finite-element or CVFE simulations.

Like all problems in the field of computation science and engineering, a new product needs to be "validated" and "verified" before it is actually implemented. The term validation means solving the right equation for a given problem and verification means solving the equations correctly. In the area of reservoir simulation, the same governing equations for a black-oil model have been widely used for the past few decades. Therefore, validation of a black-oil model is not considered for most new black-oil simulators. At the beginning, the focus of this study was to benchmark the CVFE simulator with the well-established commercial finite-difference based reservoir simulator ECLIPSE. This work could also be called as simulator verification by indexing method.

On this verification work, the regularized "ideal system" was tested with 15 by 15 feature/faults strictly orthogonal in the domain of 1000 by 1000 by 200 ft. The matrix was considered to contribute zero porosity and permeability. The detailed reservoir properties are described in Chapter 3.4. This is a three-phase (oil, water and gas) study. Initially the reservoir pressure was over the bubble point which ensures all of the gas solute in the oil phase. One injection well and one production well were positioned at the diagonal direction of the reservoir domain as Figure 3.2 showed. Both wells horizontally penetrated the top of features. Bottom-hole pressure (BHP) controls were applied for well operation. Since the DFN approach presents feature/faults as a two-dimensional plane in the three-dimensional space, the domain was meshed into triangles which shared the same side or node at the region of feature/faults interaction. For ECLIPSE simulator, the features were presented by the stack of grid blocks which have the actual width of the features (0.5 ft) or equivalent thickness by the constraint of constant *kh* value (500 md-ft).

To speed up calculations, the matrix blocks other than features in the ECLIPSE were set as nonactive. Another constraint for both the "ideal" and "real" systems was to set the constant total original oil in place (OOIP) as 53580 STB. The discretized domain for the DFN approach and conventional finite-difference are shown in Figure 3.6 and Figure 3.7.

Figure 3.6 and Figure 3.7 show that both the DFN triangular mesh and the ECLIPSE grid blocks have five element/grid layers in the z-direction. The simulations were run for 900 days with the first 300 days as the primary production period. Starting from day 301, simulation was considered to be secondary recovery with the water injector being introduced.

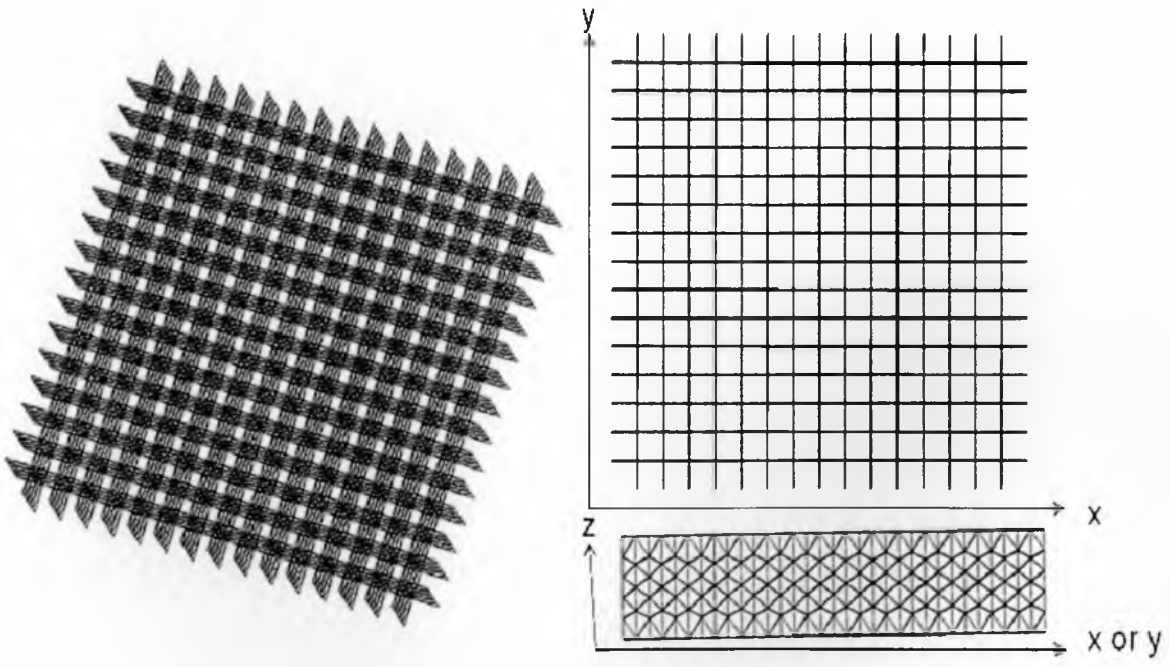

Figure 3.6 Three-dimensional view (left) and two-dimensional view (right) of discretized regularized, DFN modeled "ideal" basement reservoir domain for the CVFE simulator

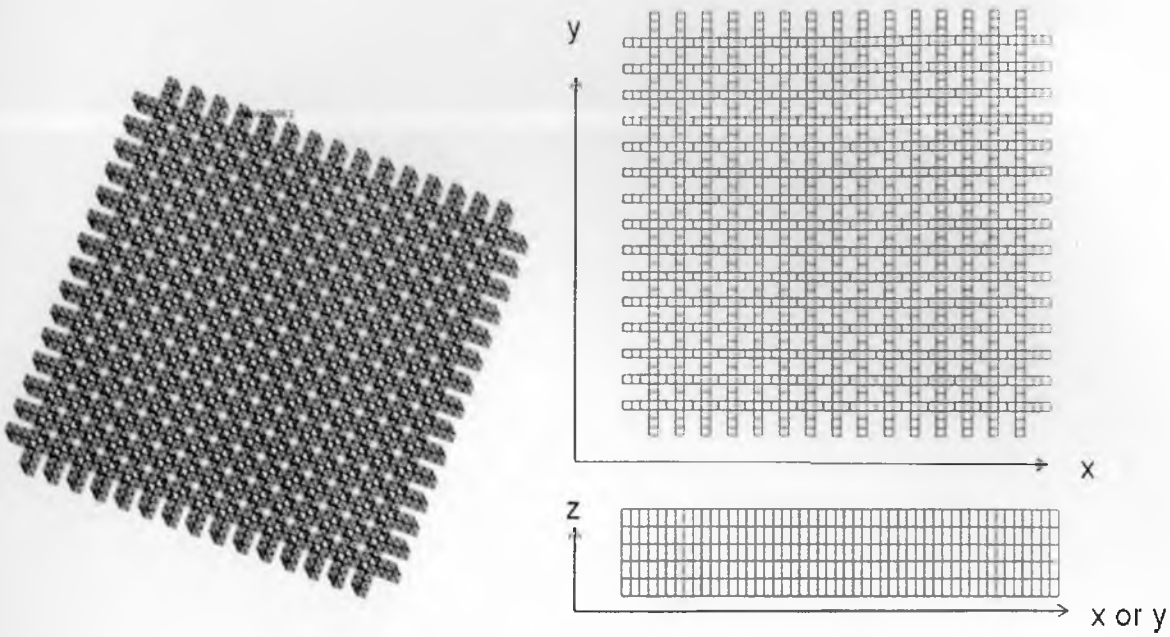

Figure 3.7 Three-dimensional view (left) and two-dimensional view (right) of discretized, regularized finite-difference modeled "ideal" basement reservoir domain for the ECLIPSE simulator

Simulation results from CVFE and ECLIPSE simulators such as oil production rates and oil recovery are compared in Figures 3.8 and 3.9. Figure 3.8 and Figure 3.9 show that results of both oil production rate and oil recovery from CVFE simulation are almost the same as the results from ECLIPSE. Since the regularized basement model is strictly orthogonal (which can be accurately calculated by ECLIPSE), this close agreement between results made a very positive conclusion about the CVFE simulator. Note that this case study was performed under the three-phase condition, and with the solution gas involved, the simulation results showed that CVFE simulator was benchmarked with ECLIPSE black-oil simulator remarkably well. This conclusion can also be observed from oil distribution snapshots shown in Figure 3.10.

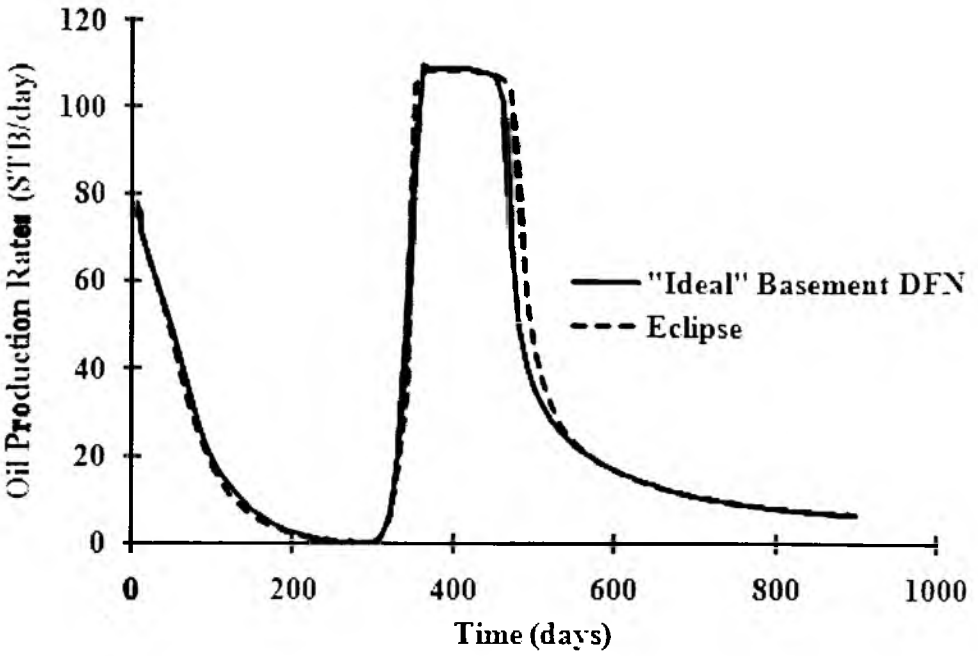

Figure 3.8 Comparisons of oil production rate between the DFN modeled CVFE simulator and the single porosity modeled ECLIPSE simulator for the regularized "ideal system"

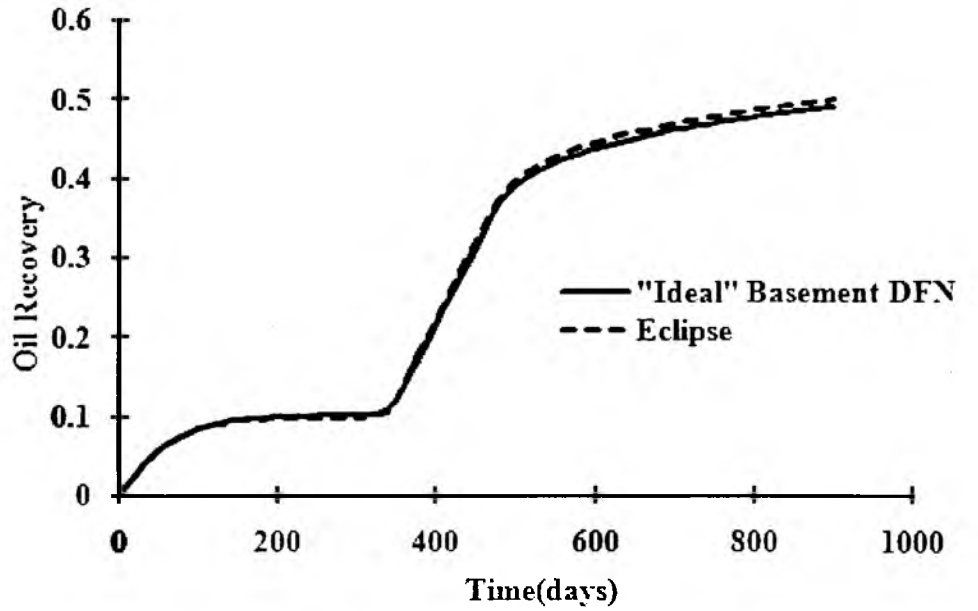

Figure 3.9 Comparisons of oil recovery between the DFN modeled CVFE simulator and the single porosity modeled ECLIPSE simulator for the regularized "ideal system"

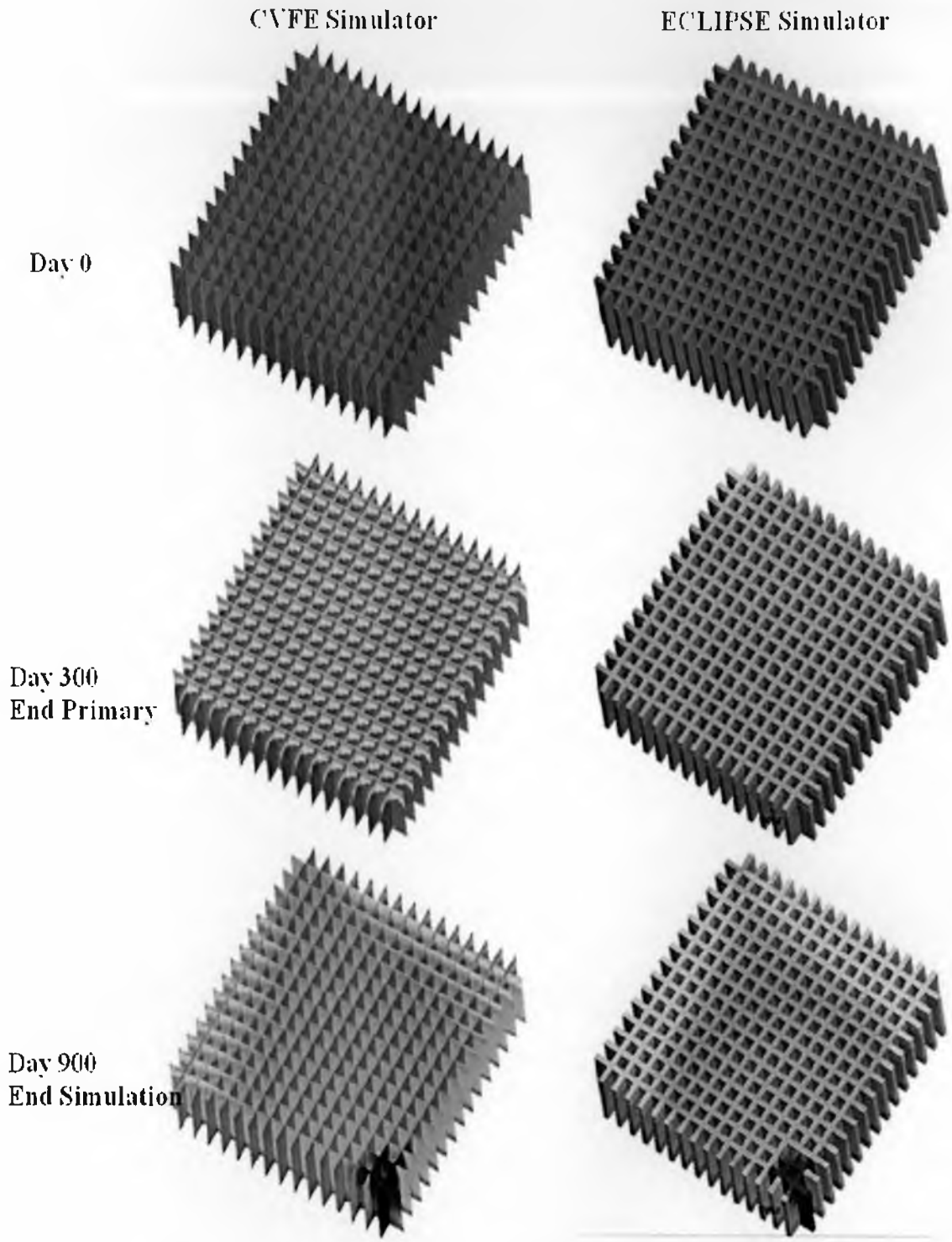

Figure 3.10 Snapshot of oil saturations for the regularized "ideal" basement domain from both CVFE simulator (left column) and ECLIPSE simulator (right column)

The verification of constraints (constant kh value and constant OOIP) are shown in Figure 3.11. At day 900 (end of simulation), simulations with 0.5 ft to 20 ft fracture thickness had reached the same the residual oil distributions from the ECLIPSE simulator.

The indexing verification methodology adopted by this study was commonly applied to verify a new reservoir simulator in the petroleum industry. Other more strict mathematical verification work has been done (Yang, 2003; Fu, 2007) on the CVFE formulation by implementing the manufactured solution method. In the manufactured solution approach, a solution function that satisfied both initial and boundary conditions was first synthesized or manufactured. That solution function was then substituted into the governing equation to find the corresponding source function. Mathematically, the solution obtained from the CVFE simulator showed an excellent order of convergence rate with the manufactured solution.

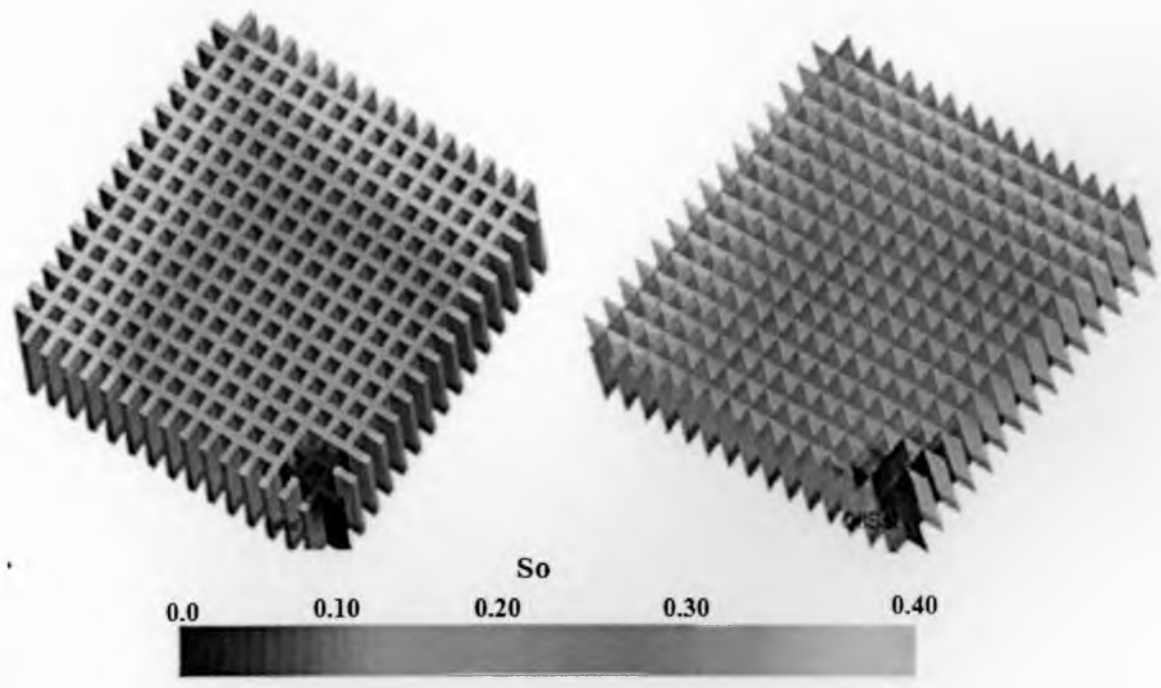

Figure 3.11 Comparisons between feature/fault grids block thickness (left 20ft; right 0.5ft) by applying two constraints: OOIP & kh value.

Through this indexing verification with the well-known ECLIPSE simulator, now the accuracy of the CVFE simulator is ascertained. Some sensitivities of DFN characteristics are discussed below.

3.6 Applications

Uncertainty exists around the fractured reservoir due to the fracture network's heterogeneous properties. These fracture network properties include connectivity, permeability distribution, dip orientation, and size distribution. To demonstrate the impact effects of uncertain elements on the multiphase oil recovery scheme, as shown in Figure 3.12, this study used a "real" fracture network generated by a network of intersecting faults that mimic a more realistic basement reservoir.

3.6.1 Permeability Variations Studies

Permeability is an important property of the porous medium and is a measure of the capacity of the medium to transmit fluids. Hydrocarbon reservoirs can have primary and secondary permeability.

Figure 3.12 Irregularized DFN basement model with the same model properties as regularized DFN basement model with different orientation and connectivity

Primary permeability is referred to as matrix permeability by reservoir engineers. Secondary permeability can be by either fractures or solution vugs. In this chapter, only the Type I (basement type) reservoirs are considered. Therefore, all the permeability discussed in this chapter is fracture permeability. Generally fracture permeability abides by cubit law of fracture thickness. Since the fracture is generated due to the stress and strain acting on the rock, the thickness of fractures cannot be homogeneous. This results in a highly heterogeneous permeability distribution within each fracture/fault. In this section, the hydrocarbon recovery scheme from three homogenous permeability models (1000 md, 100 md, 10 md) and two heterogeneous permeability models (with random geometric mean of 100 md) have been compared in order to demonstrate the fracture network uncertainty.

The homogenous permeability models are easily understood. The results of oil saturation distribution snapshots from various homogeneous permeability models are shown in Figure 3.13.

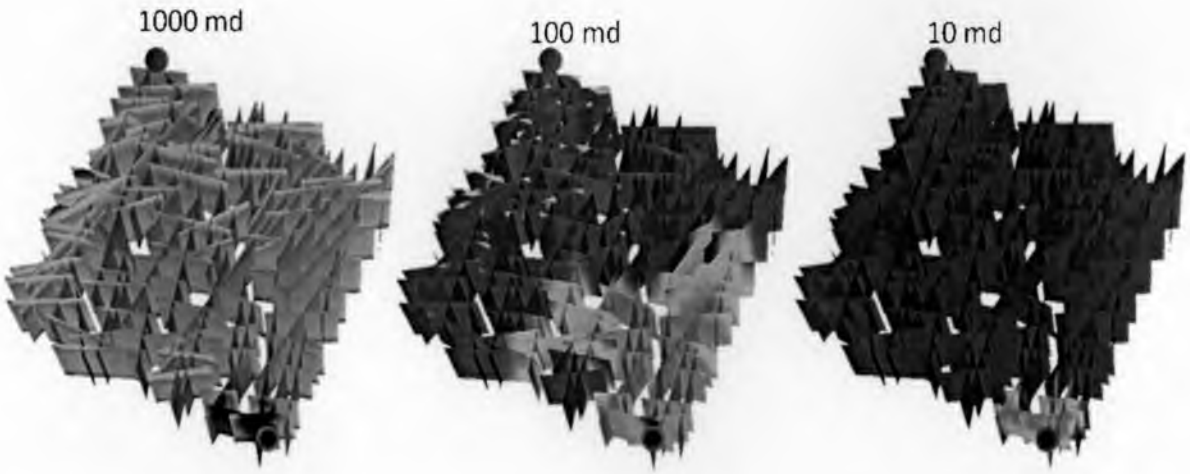

Figure 3.13 At day 900, oil saturation distribution snapshots from different homogenous permeability models

Figure 3.14 demonstrates that with lowering the homogeneous permeability by one or two magnitudes in the whole basement reservoir, water breakthrough times were delayed significantly. The simulated water breakthrough time, after the water injections, is 185 (1000 md), 3200 (100 md), and 14700 (10 md).

The calculation geometric mean of a permeability data set [k_1, k_2, …, k_n] could be described by the Equation (3-7):

$$(\prod_{i=1}^{n} k_i)^{1/n} = \sqrt[n]{k_1 \cdot k_2 \cdots k_n} \tag{3-7}$$

where k is the permeability, and n represents the numbers of discretized elements.

Mathematically, geometric mean is an average indicating the central tendency or typical value of a set of number. It can be understood in terms of geometry. The

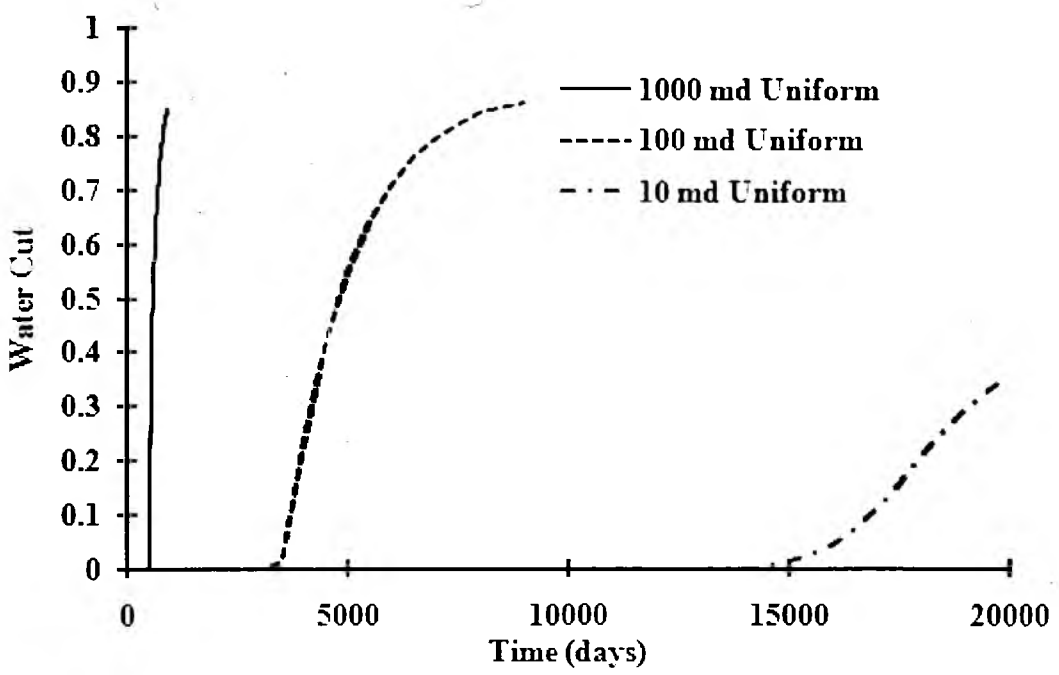

Figure 3.14 Comparisons of water breakthrough and water cut among different homogeneous permeability models

geometric mean of two numbers, *a* and *b*, is simply the side length of the square whose area is equal to that of a rectangle with side lengths *a* and *b*. that is what is n such that $n^2=axb$. Similarly, the geometric mean of three numbers, *a, b*, and *c*, is the side length of a cube whose volume is the same as that of a rectangular prism with side lengths equal to the three given numbers. This geometric interpretation of the mean is probably what gave it its name. It is important to note that the geometric mean applies only to positive values to prevent the result of imaginary numbers. For example, no negative fracture permeability exists physically. However, physically there might be some "zero" permeability existing inside the fault. In that case, other average methods might be applied instead of the geometric mean.

Figure 3.15 illustrates the geometric mean based intrafault permeability distributions. If the intrafault were composed of two types of permeability values: 10 and

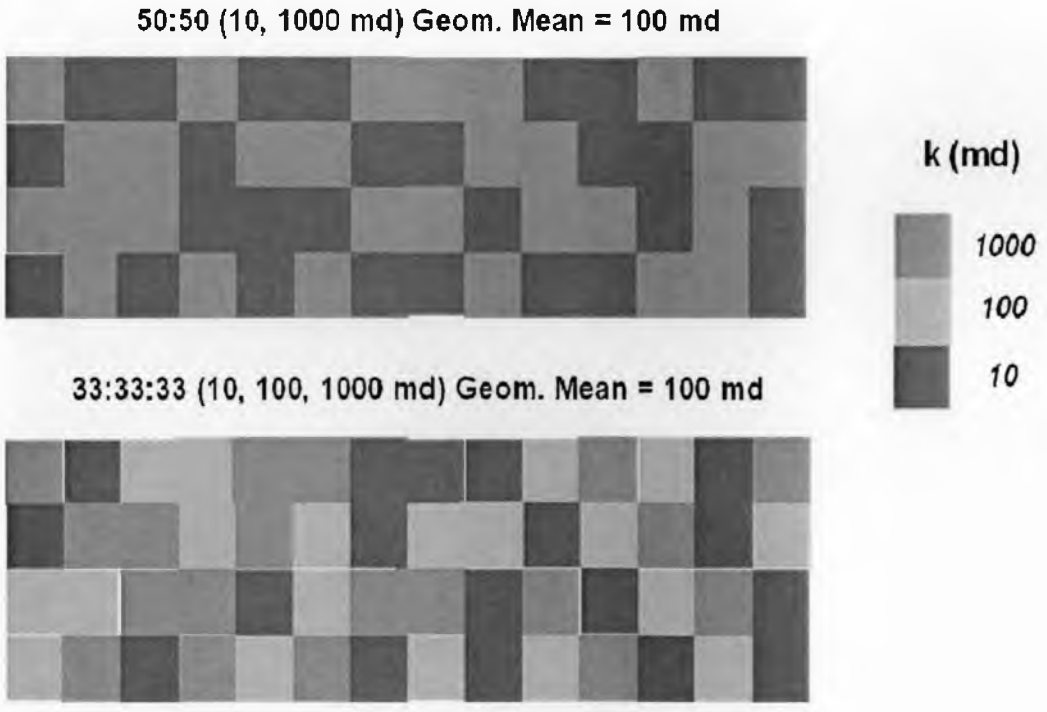

Figure 3.15 Illustrations of geometric mean based intrafault permeability distributions

1000 md, the 100 md geometric mean will give the half-half percentage of the two permeability values. Then the permeability of discretized elements can be characterized based on the percentage distribution. If the intrafault were composed of three types of permeability (10, 100 and 1000 md), the geometric mean of 100 md will result in one-third quantity distributions with each permeability value.

Figure 3.16 shows residual oil saturation of three basement fracture networks (one uniform 100 md case and two various 100md geometric mean domains). As previously shown in the simulation, all three cases passed primary production stage (first 300 days) and secondary production (from day 301 to 900). Obviously, the water flooding patterns are totally different by different fracture network characterizations: uniform 100md case study offers the medium performance between the two types of 100 md geometric mean permeability values, the one-third permeability distribution cases result in the best water flooding and the half-half case offers the worst water flooding scenario.

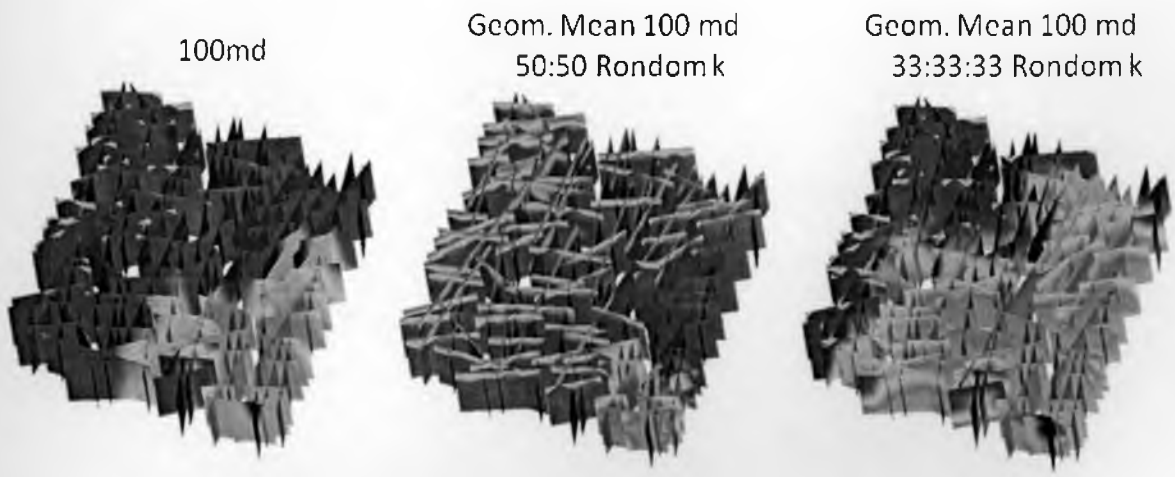

Figure 3.16 At day 900, oil saturation distribution snapshots from different homogenous permeability models

Figure 3.17 to 3.19 compared simulation results as the oil production rate, oil recovery and water cut. Obviously, the randomized intrafault permeability distributions brought totally different hydrocarbon recovery mechanisms to our proposed basement domain. The figures of the oil production rate, water breakthrough time, and water cut scales show possible large-range variations. In the random permeability distribution case, the oil production rate could be higher than in the uniform permeability case, due to possible high permeability channels (with those 1000 md characterized elements); the oil production rate also could be lower than in the uniform permeability case due to the low permeability in the main water flooding channel (with 10 md characterized elements). However, if a certain number of simulations were performed based on different random seeds, some uncertainty range might be identified. The more simulations performed, the more accurately the risk range might be described. Based on this hypothesis, a set of

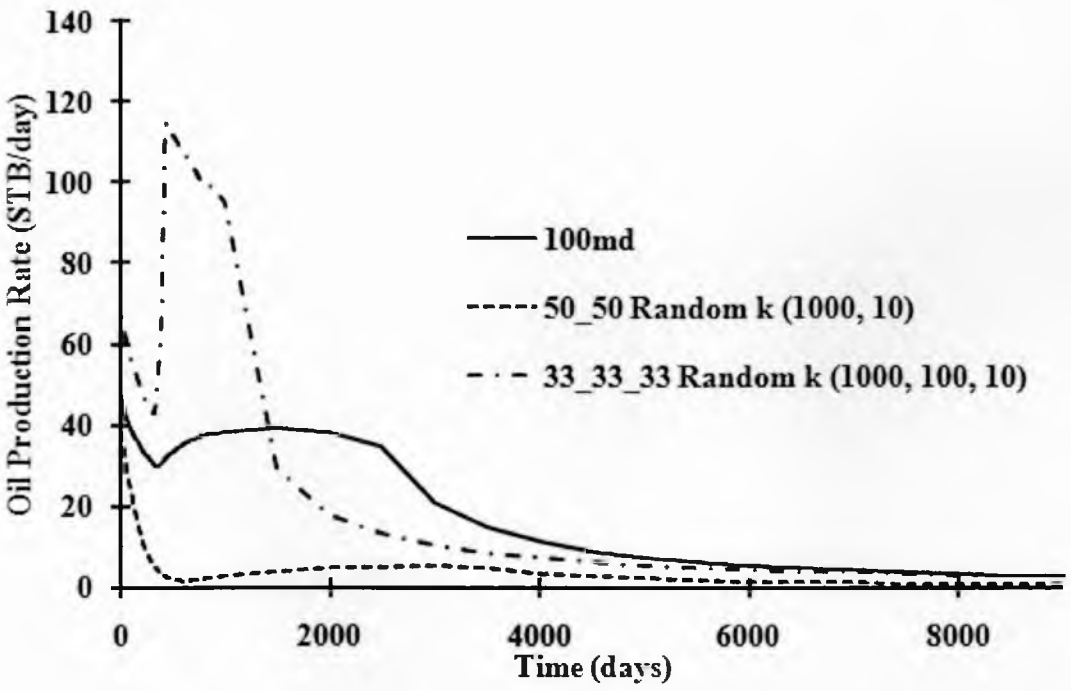

Figure 3.17 Oil production rate comparisons among uniform 100 md and geometric mean 100 md cases

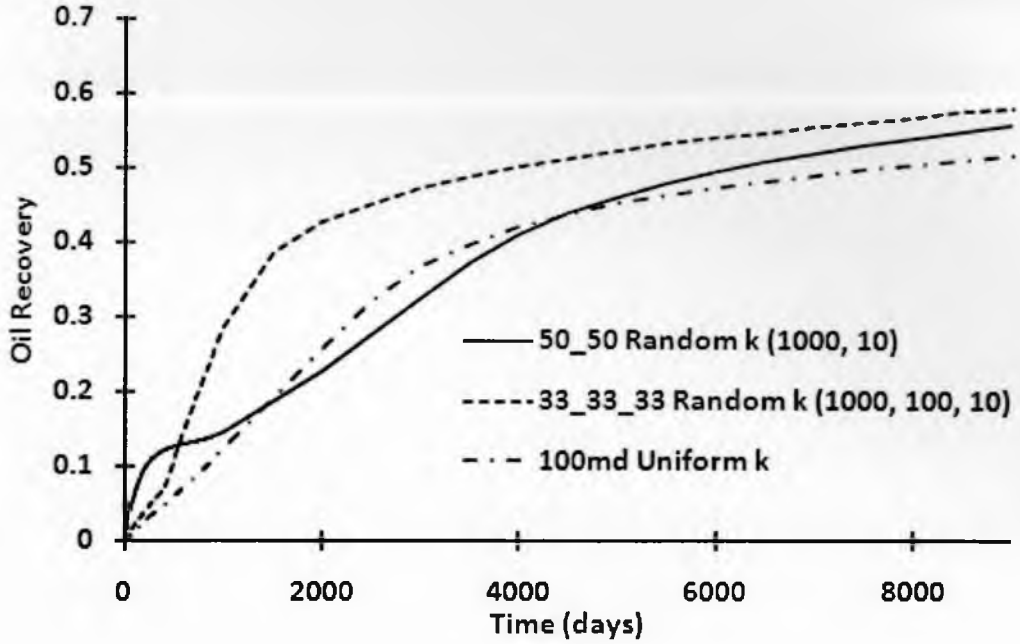

Figure 3.18 Cumulative oil production comparisons among uniform 100 md and geometric mean 100 md cases

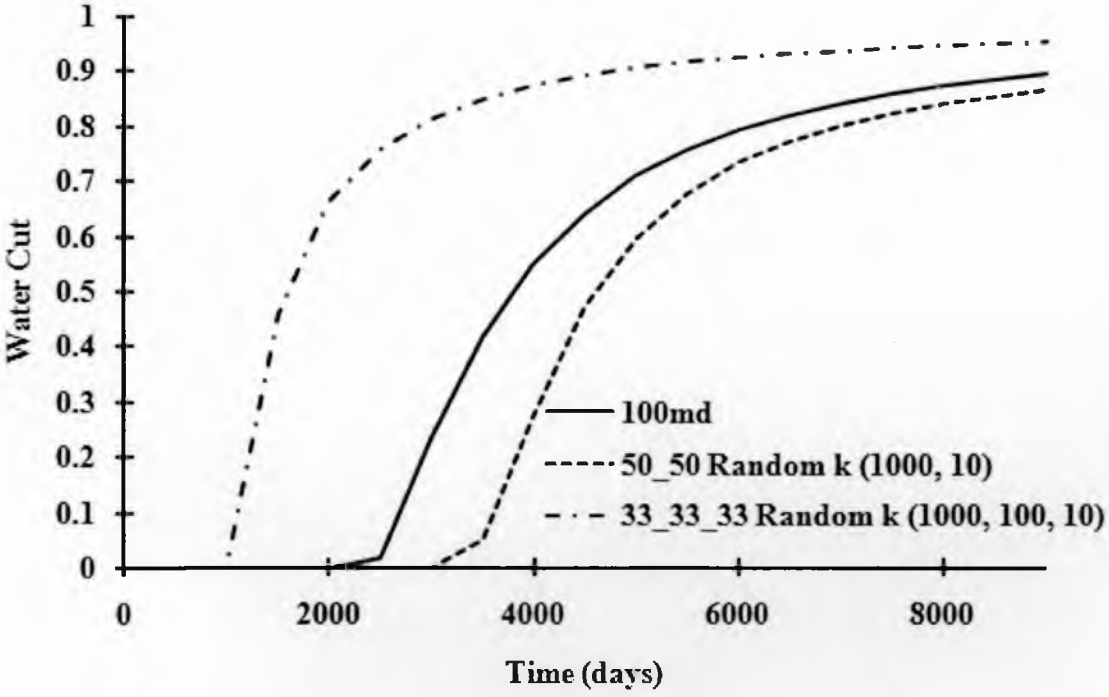

Figure 3.19 Water cut comparisons among uniform 100 md and geometric mean 100 md cases

geometric mean (33:33:33) 100 md simulations have been performed. The only difference among these simulations is the detailed element permeability distributions on each single feature. The water cut results of these simulations are shown in Figure 3.20.

In the water flood case studies, water cut and water breakthrough time are the principal ways of making reservoir management decisions. Figure 3.20 shows a large range of water breakthrough times. For the same domain with the exact same operating conditions, the water flooding patterns were totally different. This type of modeling mimics big impacts on the pattern of sweep, due to the uncertainty of the fracture/fault permeability distributions. In a way, this is important for understanding the fracture network uncertainty when attempting to develop innovative approaches to reservoir management.

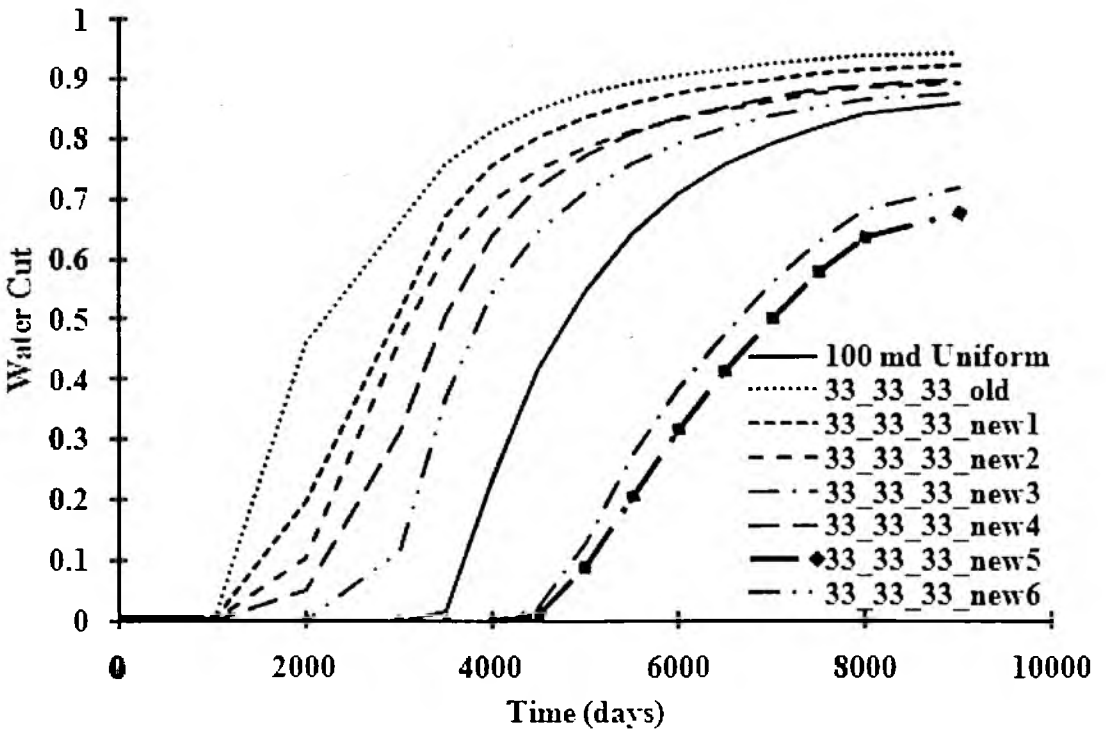

Figure 3.20 Water cut comparisons for 33_33_33 geometric mean with random seeds

Some conclusions can be drawn from the studies in this section:

1) The rock permeability is an important parameter of fluid flows inside the fracture networks. The variation of rock permeability distributions results in a huge uncertainty, particularly for the secondary production with water flooding.
2) Introducing spatial variability in permeability within the fault planes (using spatially randomized patterns of 10, 100 and 1000 md), while retaining a constant geometric mean permeability of 100 md, yields enhanced oil production due to the high-permeability pathways. And these kind of pathways result in different oil recovery factors for the long-term or short-term view, which might suggest totally different recovery plans for reservoir management.

3.6.2 Fracture Network Connectivity Studies

The connectivity of fracture/fault in subsurface rock formations is a key factor in understanding and predicting fluid flow in hydrocarbon reservoirs. This is especially true in Type I basement reservoirs, since in this type of reservoir all hydrocarbons exist inside the fractures, and the fractures provide essential permeability. This permeability then makes the connectivity problem fatal for the hydrocarbon production. Some impacts, due to the connectivity, were already shown in the simulations in the above two sections.

An example of residual oil resulting from the fracture network's connectivity is shown in Figure 3.21. In this figure, some oil traps (circled) result from the fracture connectivity. Obviously these main traps are limited in connection with the major water flooding way between the injector and the producer.

In this section, the critical fracture/fault connections between the injector and the producer are identified by the trace map in Figure 3.22.

Figure 3.22 demonstrates that the fracture networks were divided into two separate zones: west zone (left-side) and east zone (right-side). These two zones are connected by four east-west fractures/faults. The injector and the producer are located in different zones. The whole reservoir is assigned with uniform permeability at 1000 md.

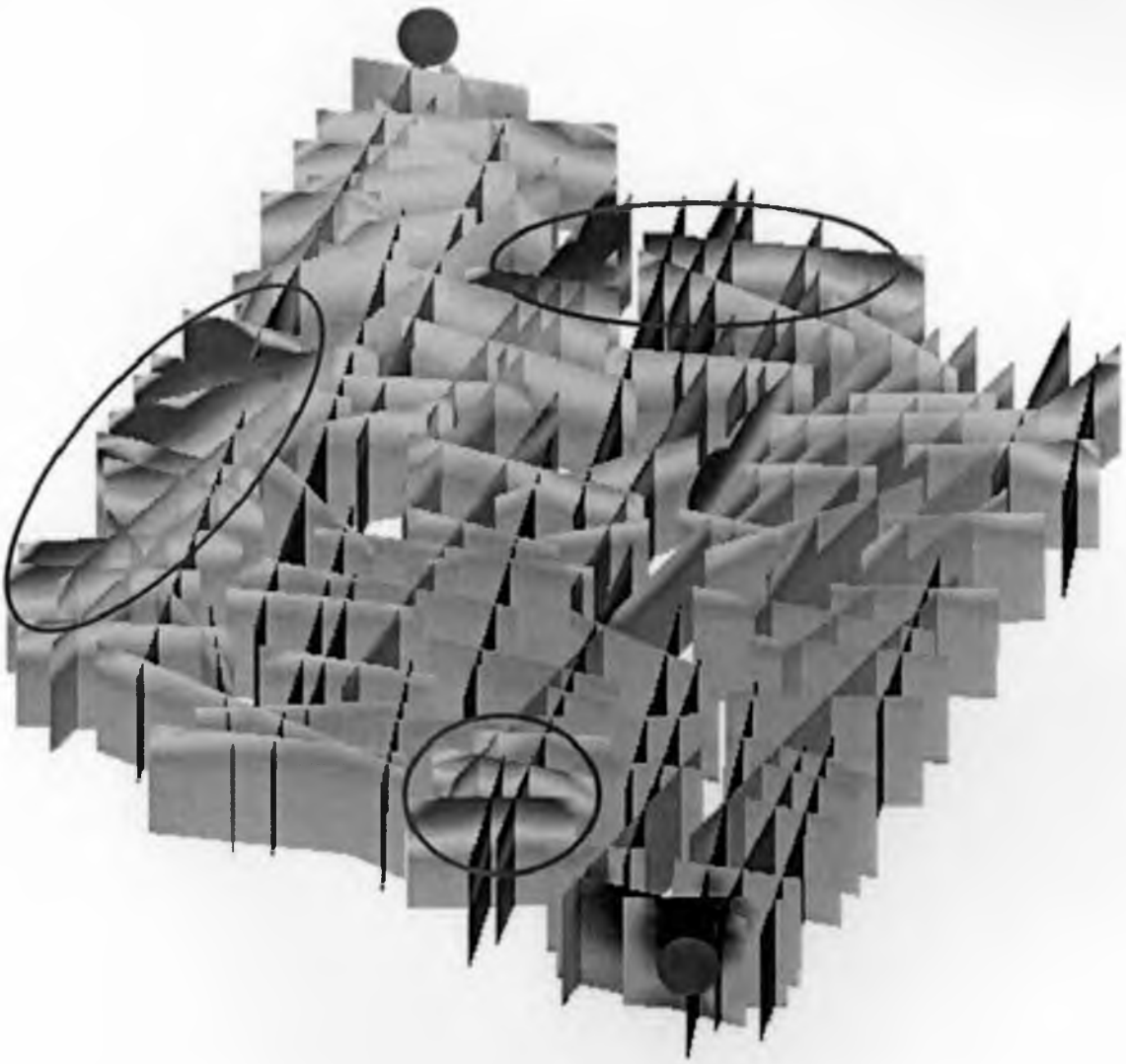

Figure 3.21 Residual oil saturation distribution snapshot due to the fracture network connectivity (Case 1000 md uniform k with day 600)

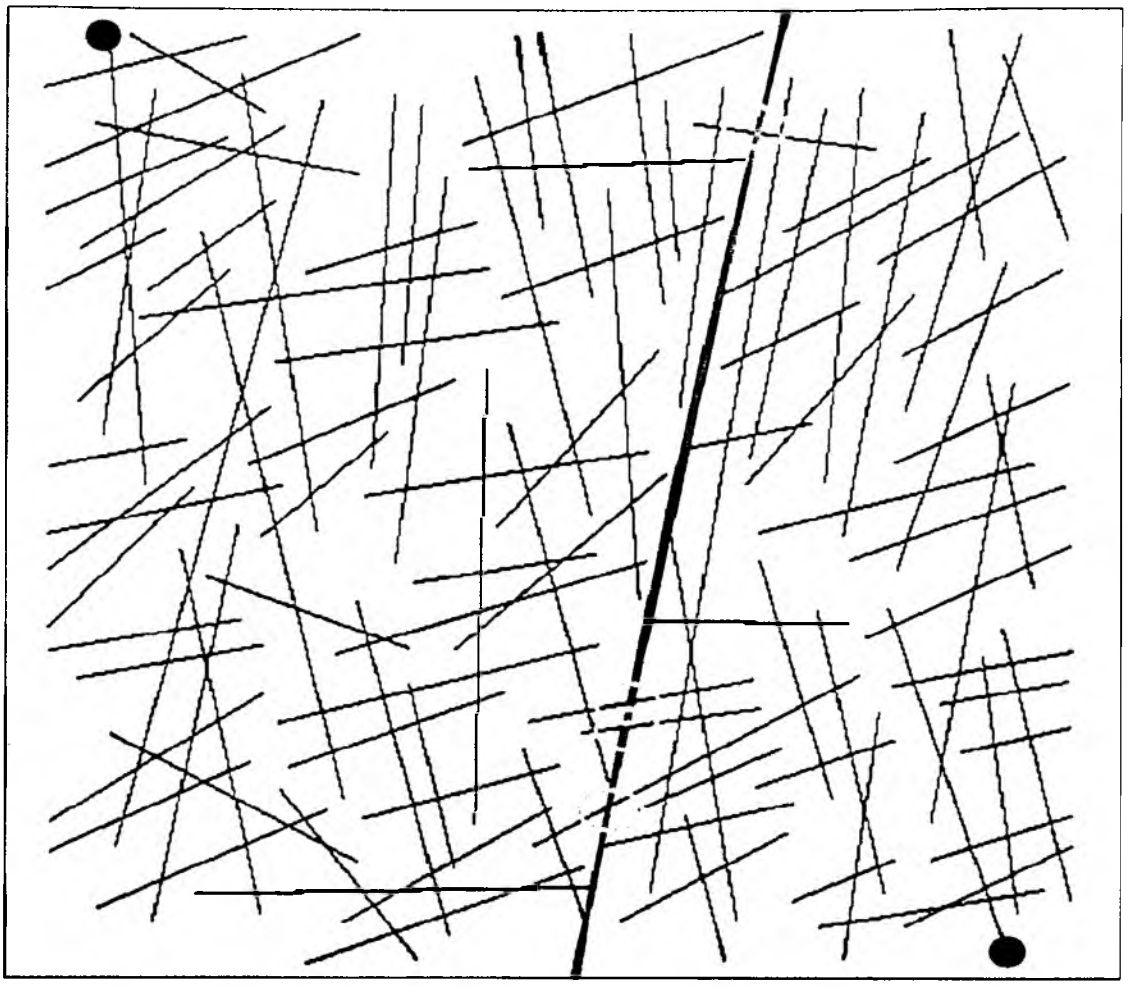

Figure 3.22 Illustration of two separate fracture zones (separated by the acclivitous line in the middle of trace map) connected by four fractures (circles)

The hypothesis for studying the fracture connectivity and how it impacts oil production was produced by comparing the productions from the original fracture network and the disconnected fractured network (disconnecting the bottom three connections).

Figure 3.23 presents the large difference in oil saturation distribution at the end of the simulation: obviously, since three main connections on the south were disconnected, the only bridge between the injector cluster and the producer cluster was on the north side of the fracture network. There are large amounts of oil on the south-west corner of the

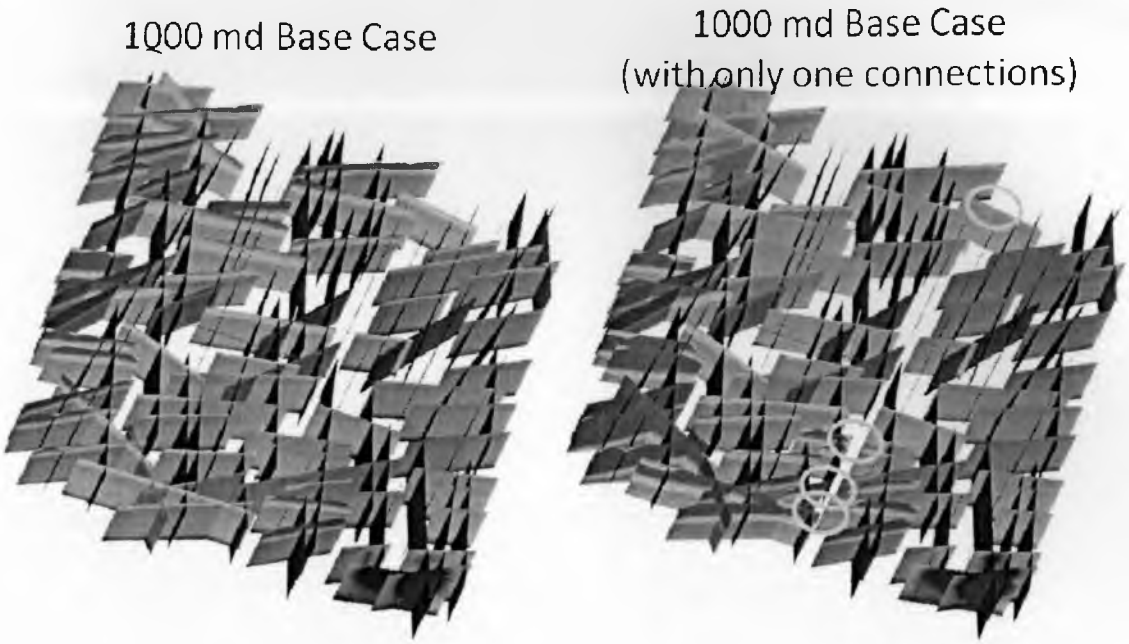

Figure 3.23 Comparisons of oil saturation distributions between the original fracture network and disconnected model at day 900

proposed basement domain that cannot be swept out. These differences are due to the connectivity of the fracture network.

To a large extent, the fracture network connectivity does not impact the primary productions. During the primary production stage, solution gas provides the main reservoir driving force. Since the gas mobility is large, and as long as the whole fracture network is connected (even if it has only one connection), the oil production rates from both simulations are almost identical. However, on the secondary production stage, the fracture network connectivity plays an important role.

Figure 3.24 shows that the peak oil production rate was reduced about 65.1% by disconnecting the lower three connections. Figure 3.25 shows that there is 12.6% cumulative oil production reduction on the disconnected model.

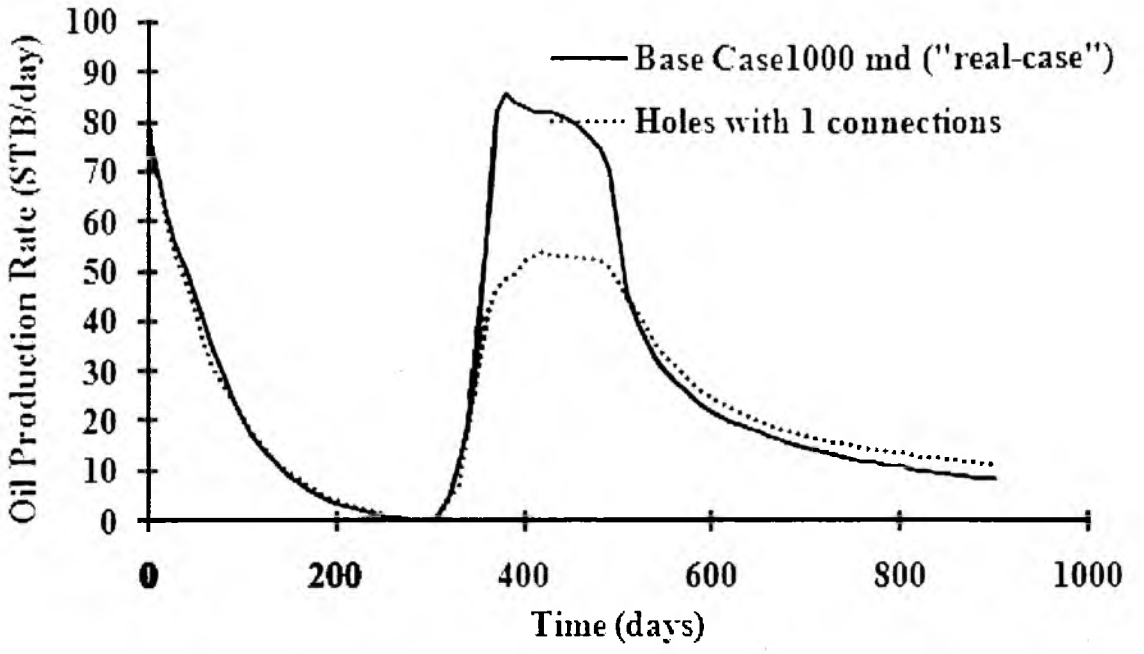

Figure 3.24 Oil production rate comparisons between base case and reduced connections case

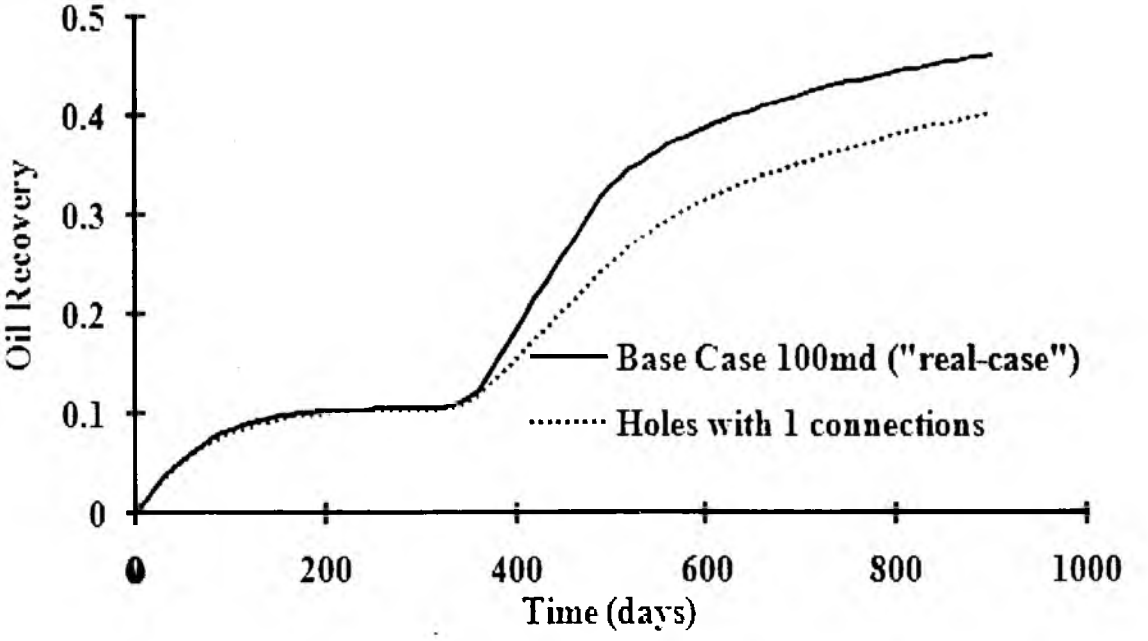

Figure 3.25 Oil recovery factor comparisons between base case and reduced connections case

This connectivity case study simply shows the large impact of fracture network connectivity on hydrocarbon recovery, particularly for the Type I basement reservoir. When basement reservoirs are compared with other types of fractured reservoirs such as Type II or III, the matrix does not contribute any permeability to fluid flow. Therefore, in the basement type reservoirs, fluid cannot bypass discontinued fractures through the matrix. This makes it essential to study the connectivity risk model in order to understand the reservoir behavior. As addressed before, this conceptual model also shows the importance of reservoir characterization. The correct fracture network connectivity characterization will be the key to understanding the basement reservoirs.

3.6.3 Fracture Orientation Impacts

As classified above, for the basement type reservoir, all the reservoir fluids exist only inside of fracture/fault. Since the orientation has always been an important characteristic for the fracture existence, it is instructive to quantify the impacts on hydrocarbon productions due to the fracture/fault orientations in the basement reservoir.

Before studying fracture orientation impacts on the oil/gas recovery, it is useful to know some fracture terms. Generally, pole and dip vectors are terms used to define the orientation of a plane in space. Fractures in the DFN modeled basement reservoir are planar polygons and use poles or dips to describe their orientation. The pole is a vector normal to the fracture plane and usually points downward. The dip vector is a vector normal to the pole and lies in the plane pointing in the direction of the maximum slope gradient. The angle between the dip vector and the horizontal is called the dip angle. The direction of the horizontal trace left by a fracture/fault intersecting a horizontal plane is called its strike. The concepts of dip and strike are shown in Figure 3.26 and Figure 3.27.

Figure 3.26 Illustration of single DFN modeled fracture orientation (pole and dip vector)

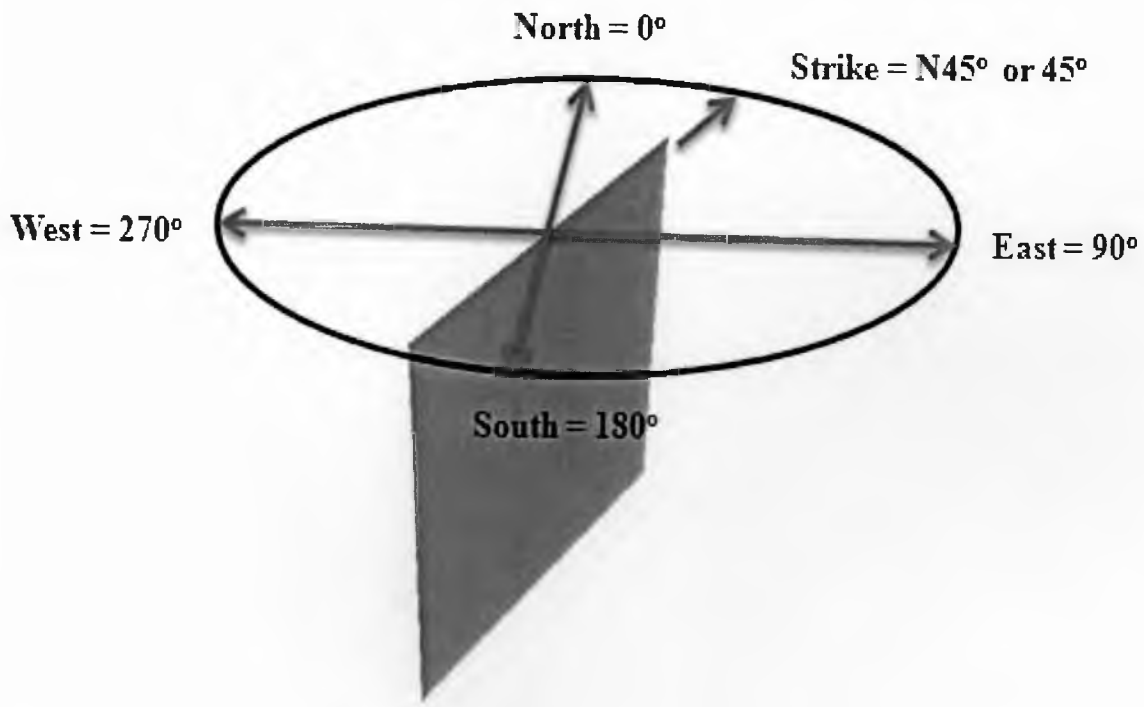

Figure 3.27 Illustration of fracture strike orientations

The "real" basement model discussed above was characterized with the dip angle of 90°. In this section, the fractures/faults in the "real" basement reservoir model were identified as two sets of fractures based on their strike. The strikes from 0 to 45° were identified as fracture/fault set 1 and the rest were marked as fracture/fault set 2. For fractures/faults in set 1, the dip angles were kept the same as before (90°), and the fractures/faults in set 2 were tuned into 45° as their dip angles. Both the injector and the producer were located in the fracture/fault set 1, and there was no change in their operating conditions and the fracture condition they located. This gave the smallest effects on the wells. For fractures/faults in set 2, their upper edges were exact as before but the bottom edges were in different locations based on their strike angle. The areas and shapes for all of the fractures/faults in this basement domain were kept the same which resulted in the same hydrocarbon in place as before. The hypothesis of this study was conceptually tested by the impacts of fracture orientations on the hydrocarbon recovery.

The populations of the fracture's orientation distribution could be visualized by stereo-plots. In the stereo-plots, the orientations are plotted in terms of the locations of poles. Horizontal fractures are demonstrated in the center of the stereo-plot; vertical fractures are represented on the circumference.

The stereo-plots in Figure 3.28 describe orientation differences between the base case and the tilted orientation distributions case. It clearly shows that in the tilted basement domain, there are two sets of fractures with two different pole/dip orientations (set 1 with 0° of pole which is 90° dip orientation and another set with 45° dip/pole orientation).

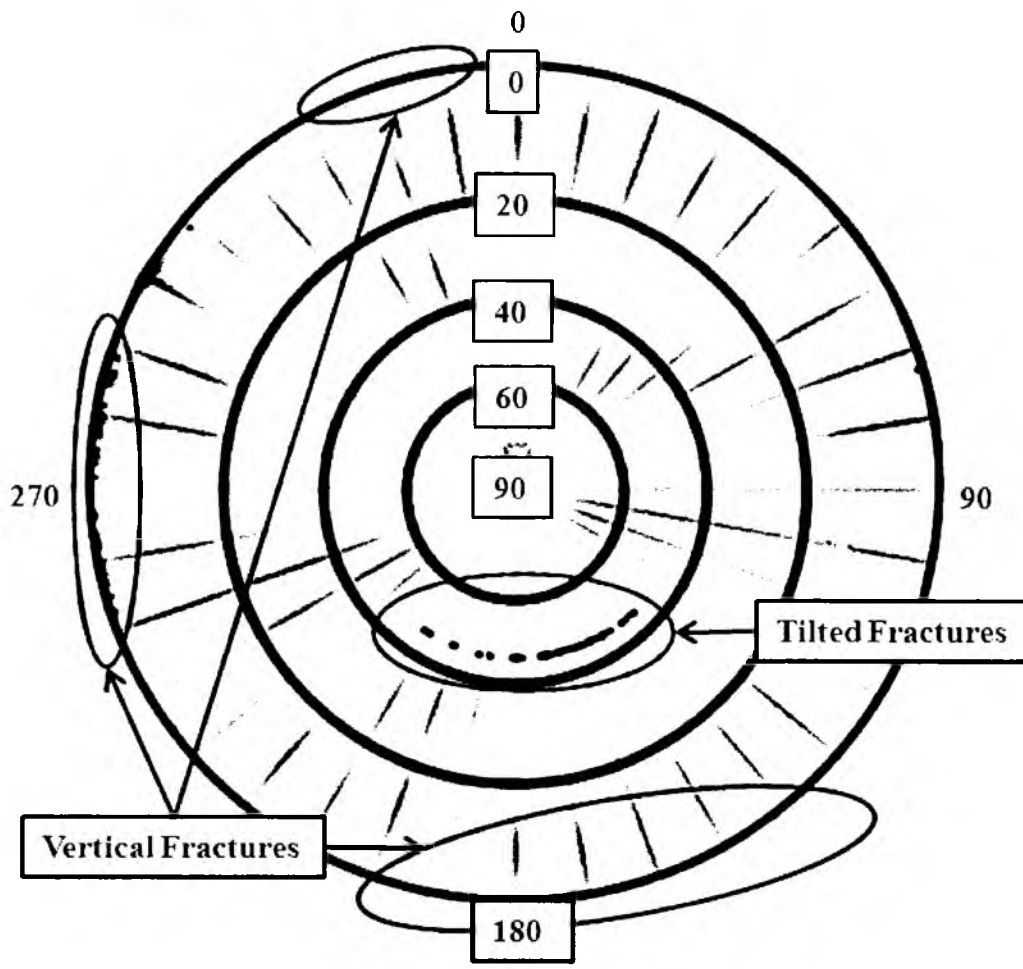

Figure 3.28 Comparisons of fracture orientation distribution between base case and titled case by stereo-plots

Figure 3.29 and Figure 3.30 show that the fracture orientation impacts the hydrocarbon production rates but not the overall recovery. The peak oil production rate in the tilted domain was about 12% higher than the base case. However, after 900 days which include primary and secondary production stages in this study, the overall oil recoveries were very close (less than 2% difference) between the all vertical fracture case and the tilted domain case.

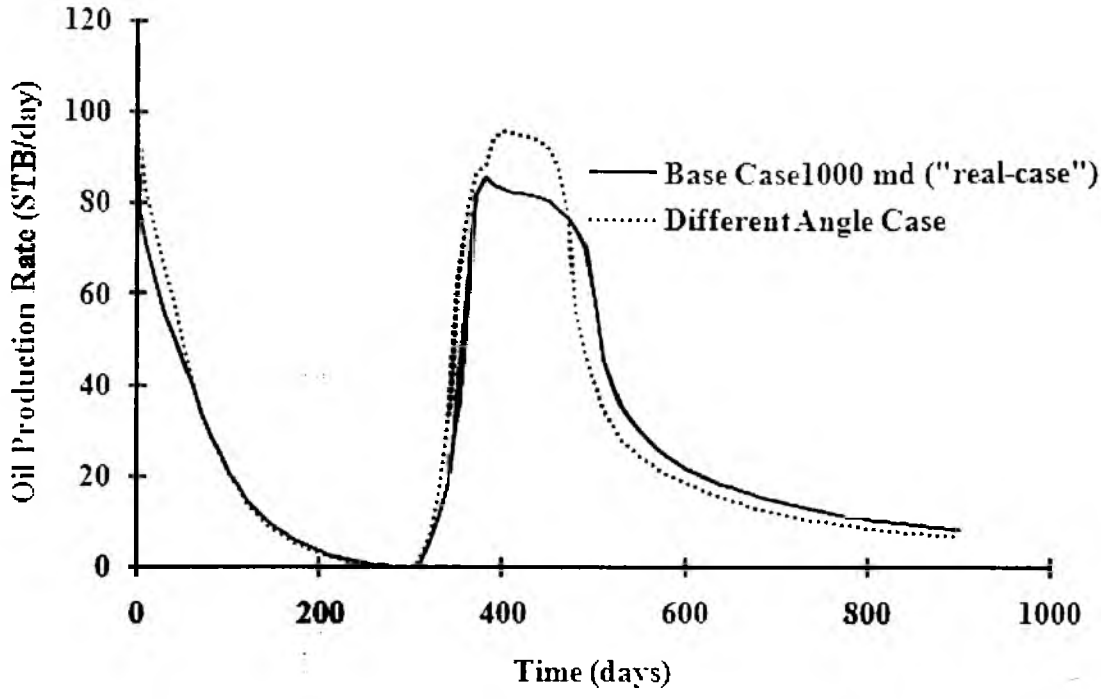

Figure 3.29 Oil production rate comparisons between the base case and the dip angle case

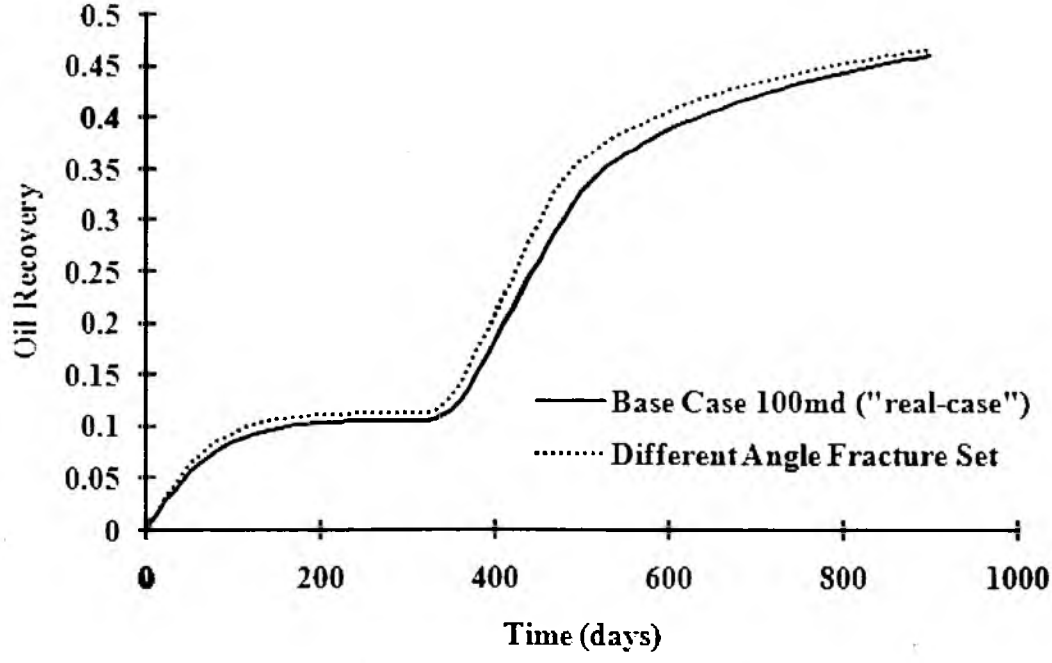

Figure 3.30 Recovery comparisons between the base case and the dip angle case

Figure 3.31 shows that the residual oil distributions are slightly different at the end of simulation between the base case and tilted domain case study. The reason for obtaining this result might be related to tilted fracture set characterization. In this case study, fracture orientation variations result in fractures' contacts being increased slightly and making more reservoir fluid exist on slightly higher locations. This study qualitatively demonstrates that the fracture orientation can impact on oil productions.

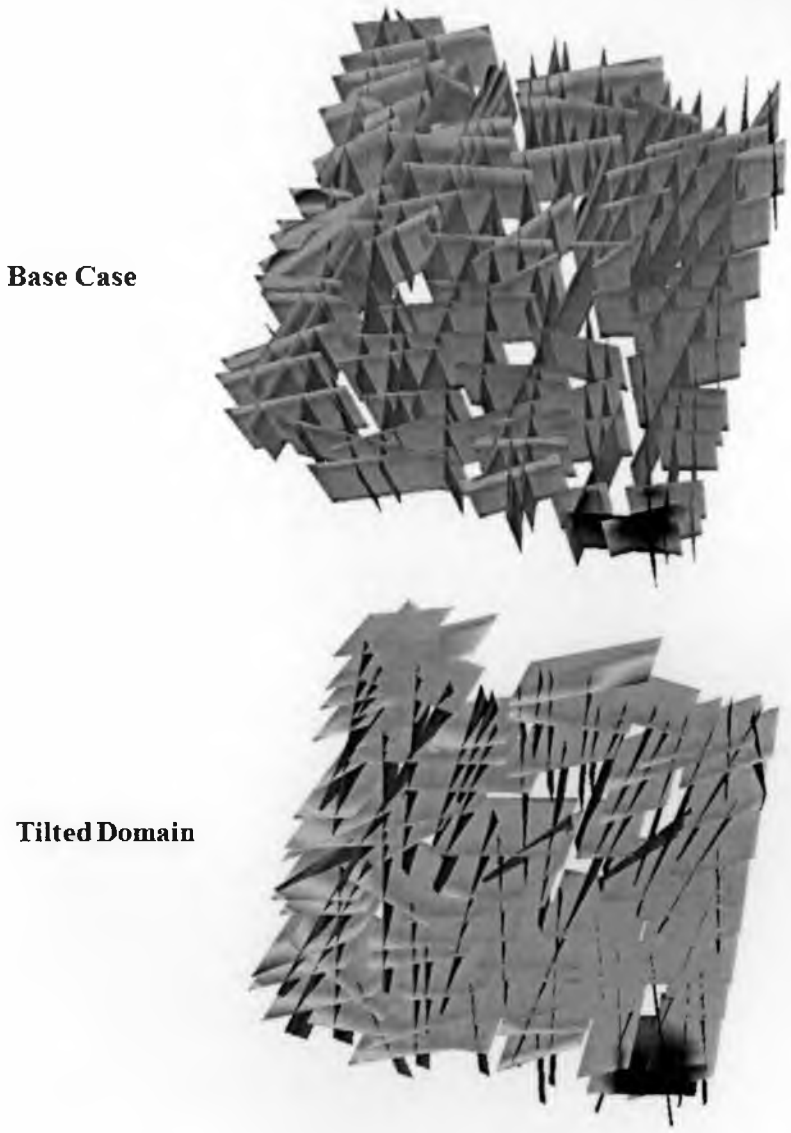

Figure 3.31 Oil concentration distribution comparisons between base case (top) and the tilted domain case (bottom)

3.6.4 Fracture Height Variations Studies

Like fracture properties discussed in this chapter (connectivity, permeability), the fracture size is also an important parameter in the fracture reservoir modeling. Limited information was acquired from normal exploring results in poorly defined fracture network modeling. Thus, quantifying the uncertainty on the fracture size information becomes essential in understanding fractured reservoir behavior.

In this section, a sensitivity study of fracture length in the z-direction (vertical) was proposed on the basement reservoir. The 1000x1000x200 ft base case domain with 1000 md k being studied before was still treated as the base case in this section. On the same trace map domain, two sets of fracture/fault clusters were identified by their strike angles. The strikes from 0 to 45° were characterized as fracture/fault set 1 and the rest were marked as fracture set 2. For fractures/faults in set 1, all fractures were kept the same height as originally (200 ft); the heights of fracture in set 2 were shrunk to a half of the original size (100 ft). Two simulations were performed in this study: fracture set 2 on the top and on the bottom. As mentioned in the last application, the producer and injector were located on fractures set 1. Therefore, nothing was changed for the fractures related to wells. To keep the same oil in place, the porosity in fracture set 2 was doubled (since the height of fracture set 2 is half as the base case).

These two simulations were performed with the same reservoir fluid properties and operating conditions.

Figures 3.32 and 3.33 show that comparisons of oil production rates and oil recoveries among the studies of the base case (full fracture height), the half-top case and

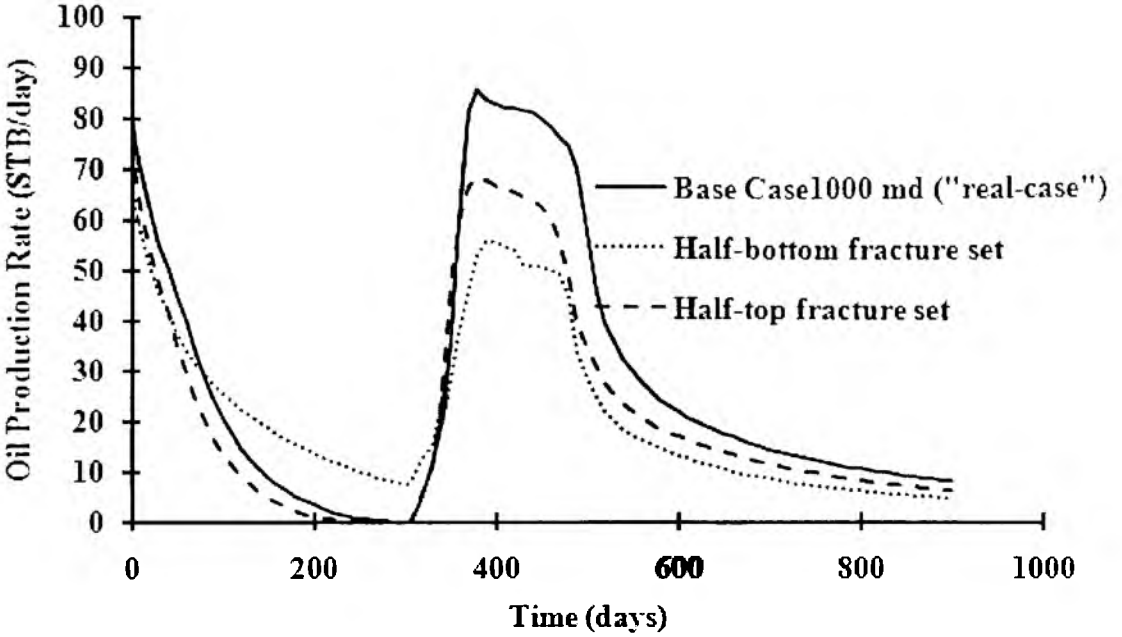

Figure 3.32 Oil production rate comparisons among base case (full fracture height), half-top case and half-bottom case with same oil in place and well properties

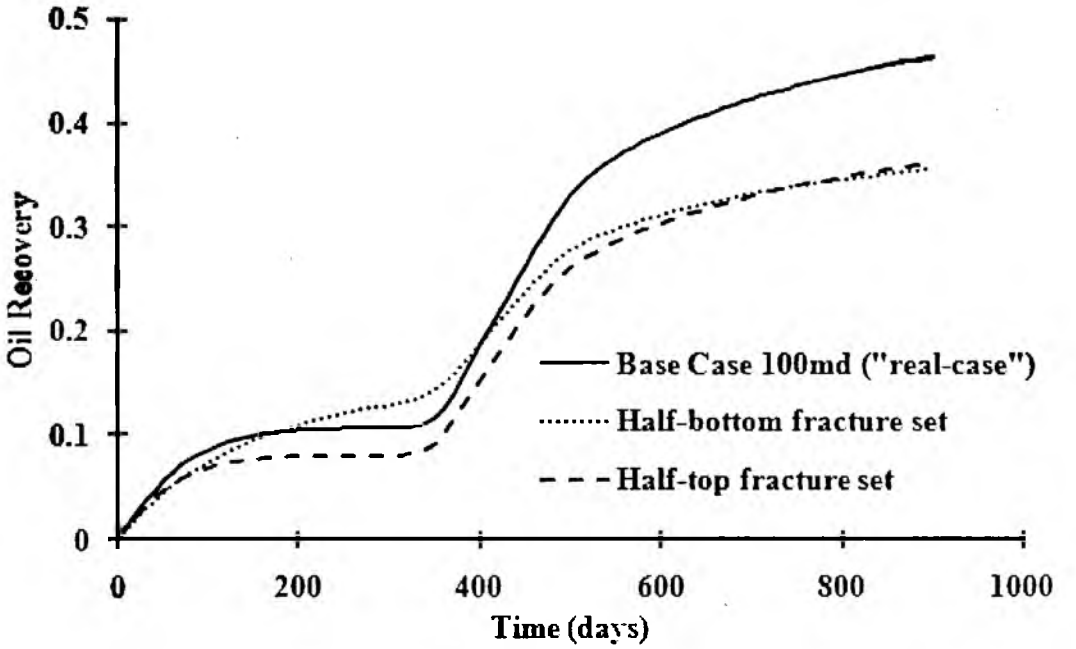

Figure 3.33 Oil recovery comparisons among base case (full fracture height), half-top case and half-bottom case with same oil in place and well properties

the half-bottom case. The comparison results are interesting: during the stage of primary production, the half-bottom case shows significantly higher rates than the other two; after the water injection since day 300, the best oil production rate came from the base case, then second-best came from the half-top case, and the lowest rate came from the half-bottom case. Figure 3.33 shows similar trends as shown in the rate figure. However, at the end of simulation (day 900), both "half-" case studies almost reached the same hydrocarbon total production (1.40% difference). The base case with full fracture/fault heights offered 30.66% higher oil production than the half-bottom case.

Figures 3.34 and 3.35 deomonstrate the reason for higher oil production rate from the half-bottom case: during the primary oil production stage, reservoir energy (pressure) is the only driving force producing hydrocarbons. For this three-phase black oil model, the production well was located on the corner of the upper-left fractures and operated with bottom-hole pressure (BHP) control, which was higher than the bubble point pressure. The reservoir pressure decreased as oil was produced. The gas-phase was gathered on the top of the reservoir. At the end of primary production, the oil saturation from the base case and the half-top case showed close, even distributions. However, only half of the fractures in the half-bottom case were characterized on the top of the reservoir; the gas-phase moves to the top through fractures with full-height fracture set (set 1) in this case. Since the original oil in place was the same for all three cases, the fracture vertical size difference resulted in higher concentration with lower fracture numbers on the top of the reservoirs. Figure 3.35 shows at the day 300 (end of primary production), no oil is produced from the base case and the half-top case. The half-bottom case still has enough reservoir energy to produce at that time. This explains the significantly higher

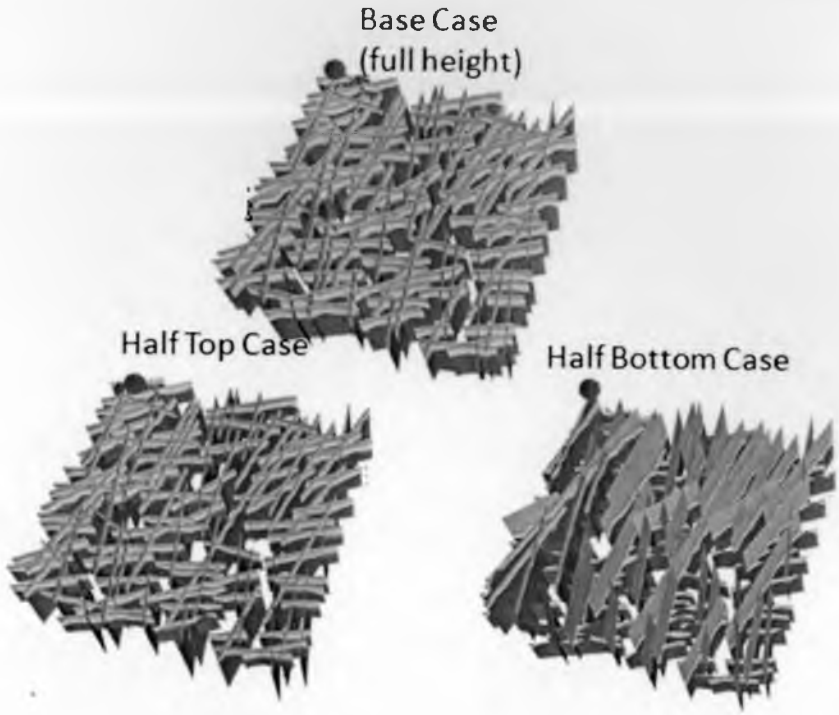

Figure 3.34 Oil saturation distribution comparisons at the end of the primary production (day 300)

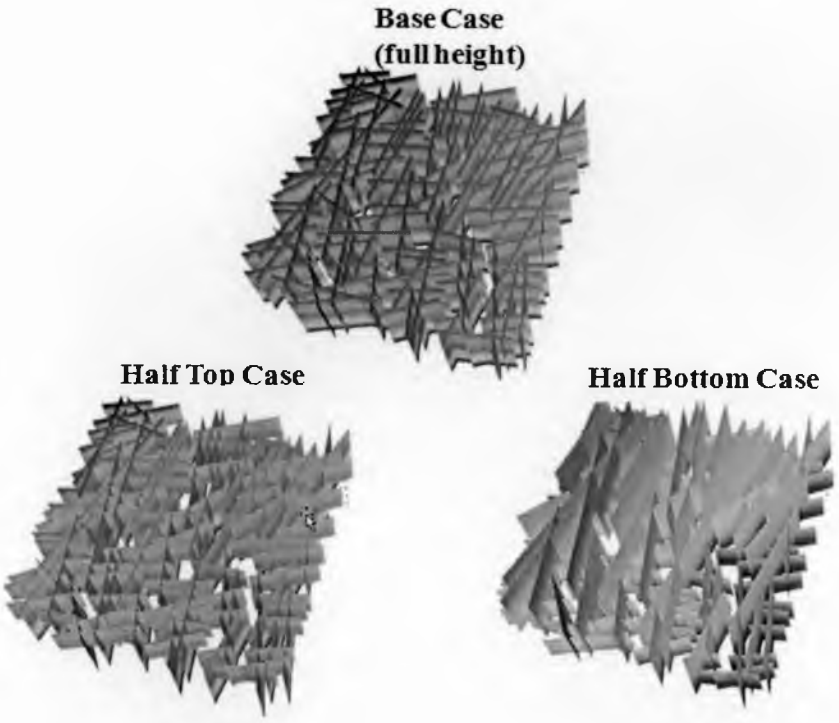

Figure 3.35 Pressure distribution comparisons at the end of the primary production (day 300)

rates from the half-bottom case study at the end of primary production. The rate difference between the other two cases (the half-top and the base cases) during the primary production could be explained as the result of more fracture connection areas in the base case: when pressure decreases, gas-phase in the oil phase goes to the reservoir top, and full height fractures offer more connection areas and thus more potential to make fluid flow.

The secondary productions were started from day 301 and lasted until the end of simulation (day 900). The water cut comparisons are shown in Figure 3.36.

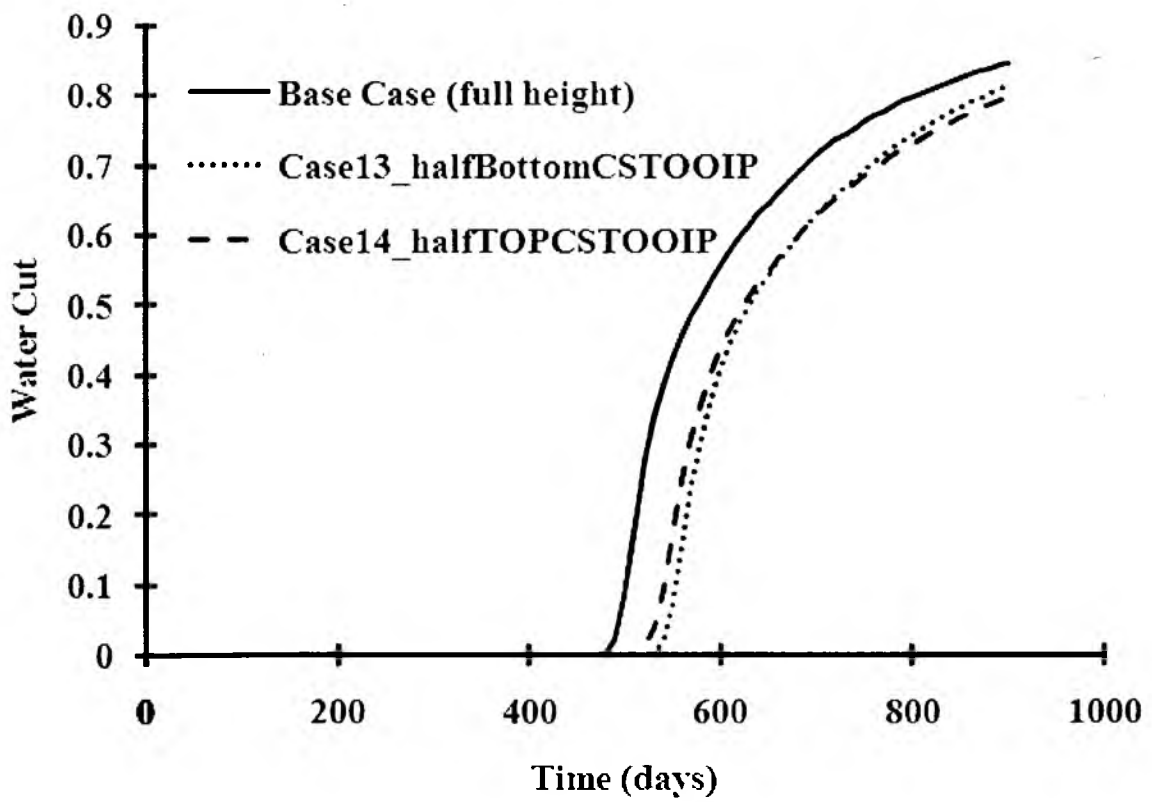

Figure 3.36 Water cut comparisons among base case (full fracture height), half-top case and half-bottom case with same oil in place and well properties

Figure 3.36 shows that the base case had the earliest breakthrough, and the other two cases had the similar breakthrough. At the end of simulation (day 900), the water cut values in three simulations were: base case (0.85); half-top case (0.81) and half-bottom case (0.80).

Figure 3.37 show that the injected water sweeps the fracture network from the bottom first due to gravity effects. The residual oil (red) remained in the fracture set 2 (with strike larger than 45°) on the west side of the fracture networks. The base case has moderate residual concentrations, the half-top case has the strongest residuals, and the half-bottom case almost gets those residuals swept out. This could be explained as the better connectivity (more connection areas) for the base case with full fracture heights.

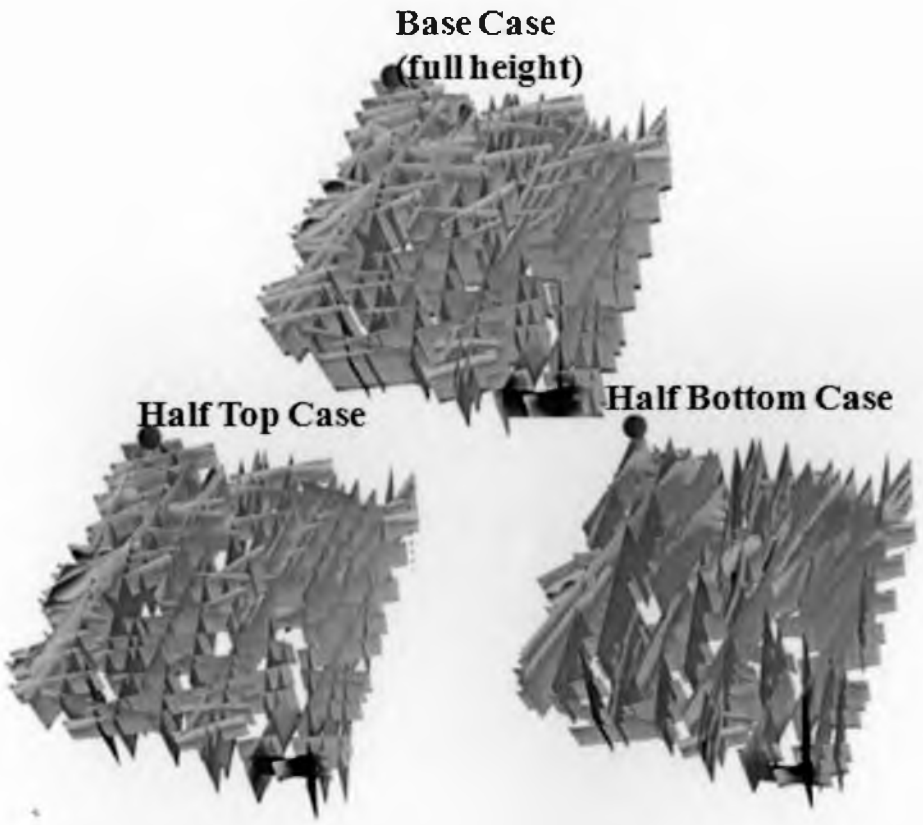

Figure 3.37 Oil saturation distributions at the end of simulation (day 900)

Some conclusions can be drawn through the studies in this section:

1) Fracture size does play an important role in the hydrocarbon recovery process, at least in the size variations in vertical fractures/faults. It impacts the water flooding patterns and residual hydrocarbon distributions.
2) Lower vertical fracture height resulted in higher hydrocarbon production rate during the primary production and lower hydrocarbon production rates (if producers are located on the top of reservoir fractures) during secondary production.
3) Connectivity is still a big issue for fractured reservoirs. In the studies in this section, the fracture connection area shows clear differences during the hydrocarbon recovery.

3.6.6 Preferred Pathway Studies

It is known that a typical fracture network is highly heterogeneous. If the production and injection wells happen to be set up with the connection of short-circuit fracture networks (with much higher permeability than the rest of the fractures in the basement case), unexpected early breakthroughs will be revealed. This could make the most of the hydrocarbon residence inside of the reservoir and cannot be swept out or it takes a much longer time and more water to produce the hydrocarbon. This phenomenon can also be called the "preferred pathway" in the process of oil production. The preferred pathway can lower oil recovery efficiency dramatically. From the point of view of reservoir management, this is not preferable in any sense. Generally, if this preferred pathway existed, some techniques need to be taken to improve the oil recoveries. One typical solution is to use gel treatments to shut off the high permeability features.

In this section, to understand the impact of the preferred high permeability pathways phenomenon and the impact of shutting it off, three new simulations are characterized below:

1) Base case study: all permeability equals 100 md
2) Preferred pathway study (as shown in Figure 3.38):
    a. Permeability on preferred pathway: 100,000 md
    b. Permeability on the rest of the reservoir: 100 md
3) Preferred pathway with cut-off zones:
    a. Permeability on preferred pathway: 100,000 md
    b. Permeability on preferred pathway cut-off zones: 0.1 md

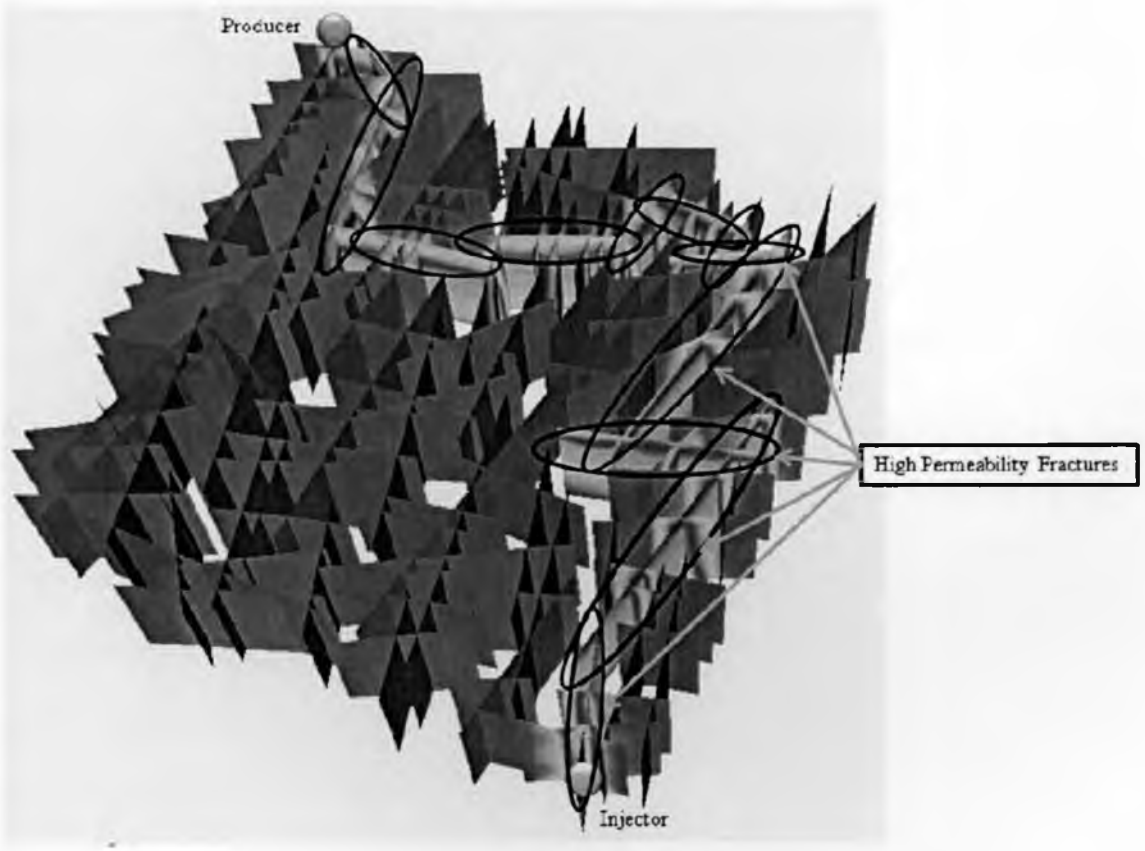

Figure 3.38 Illustration of preferred pathway characterization (other than circled area) and preferred pathway with cut-off zone (circled).

c. Permeability on the rest of the reservoir: 100 md

4) Other reservoir information:

a. Pore volume: 67287 STB

b. OOIP: 52830 STB

c. Phase: two phases (oil and water)

In this two-phase preferred pathway study, injection was started from day 1. The base case fracture permeability was characterized as 100 md. Both the injector and the producer were controlled by bottom-hole pressure control. Other than the permeability variations, all conditions in three models were the same. The results of oil saturation distribution on different times (day 10, 100, 1000 and 8000) are shown in Figure 3.39.

Figure 3.39 shows totally different water flooding patterns from three models. As shown in the figure, the results from different simulations vary by columns and the output times vary by rows. The first row demonstrates the oil saturation distributions at the 10^{th} day. At that time, the preferred pathway simulation in the middle of the row shows a clear water breakthrough path between the producer and the injector. The base case has only a small area affected near the injector; the cut-off zone case shows stronger water effect than the base case but not as much as the preferred pathway case. This is from a couple of short, high permeability features which still exist near the injector. At day 100, Figure 3.39 shows a much clearer effect among different cases: the water flooding path is equally distributed on the base case, but there is a high water cut on the preferred pathway case. The cut-off zone study still shows the greatest water-affected areas, but the feature with gel treatment shows a stronger barrier effect. On day 1000, the oil in this basement reservoir model had been recovered as base case (0.45); the preferred pathway

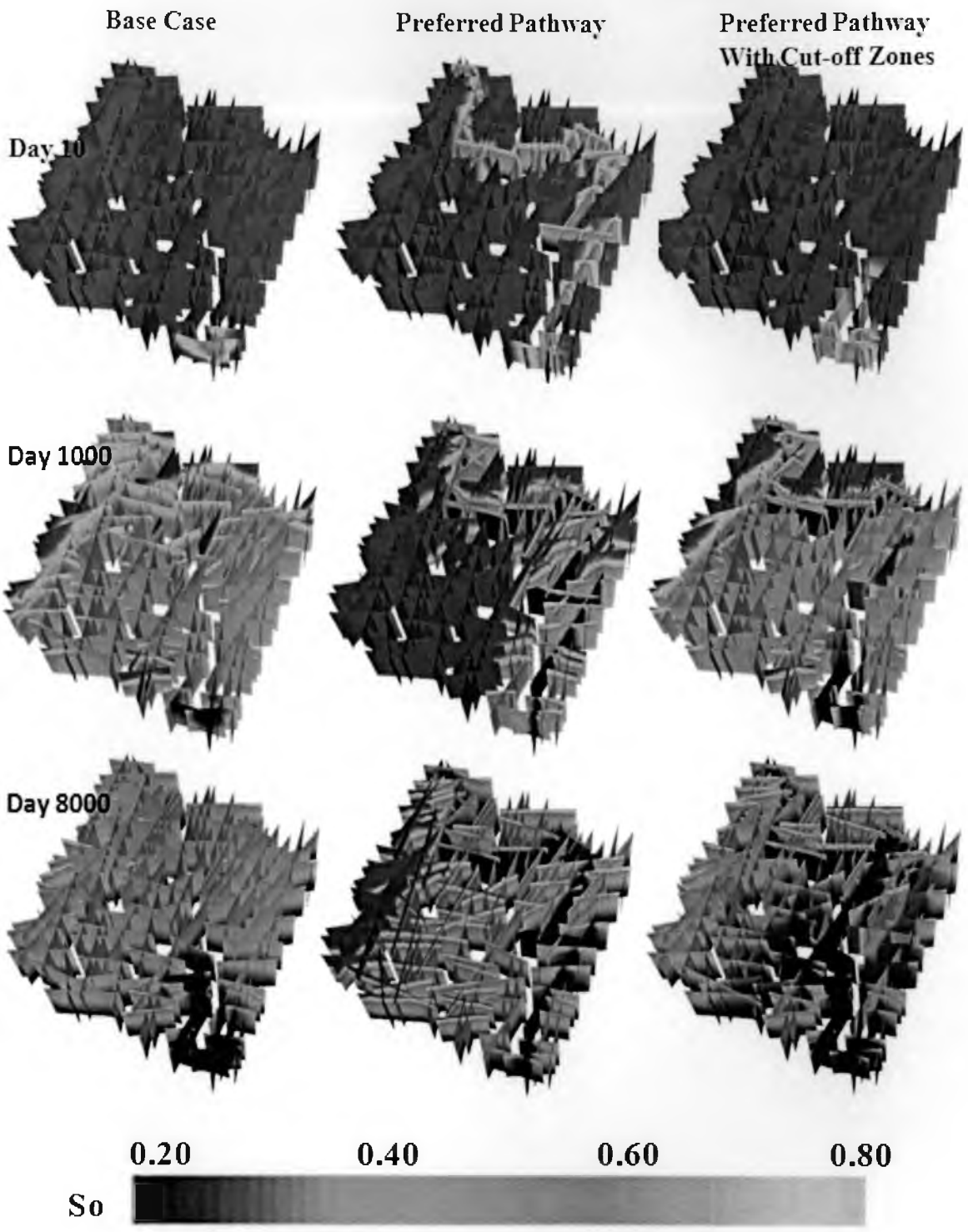

Figure 3.39 (continued) Oil saturation distribution comparisons among different fracture permeabilities (base case, preferred pathway, and preferred pathway with "cut-off zone")

case (0.27), which is 40% lower than base case; and preferred pathway with cut-off zone (0.51), which is 13% higher than base case. At the end of the simulation runs (day 8,000), results of oil recovery rates are base case (0.63); preferred pathway case (0.58), which is 8% lower than base case; and cut-off zone case (0.70), which is 11% higher than base case. The residual oil saturation distribution at the end of the simulations has totally different patterns. Base case has the most even water flooding between injector and producer, preferred pathway simulations gives large amounts of higher concentration residual oils on the southwest part of the reservoir; and cut-off zone simulation offers the smallest amount of residual oil left in the reservoir with the highest residual oil remaining in the gel-treated cut-off features. Comparisons of oil recoveries for preferred pathway study are shown in Figure 3.40.

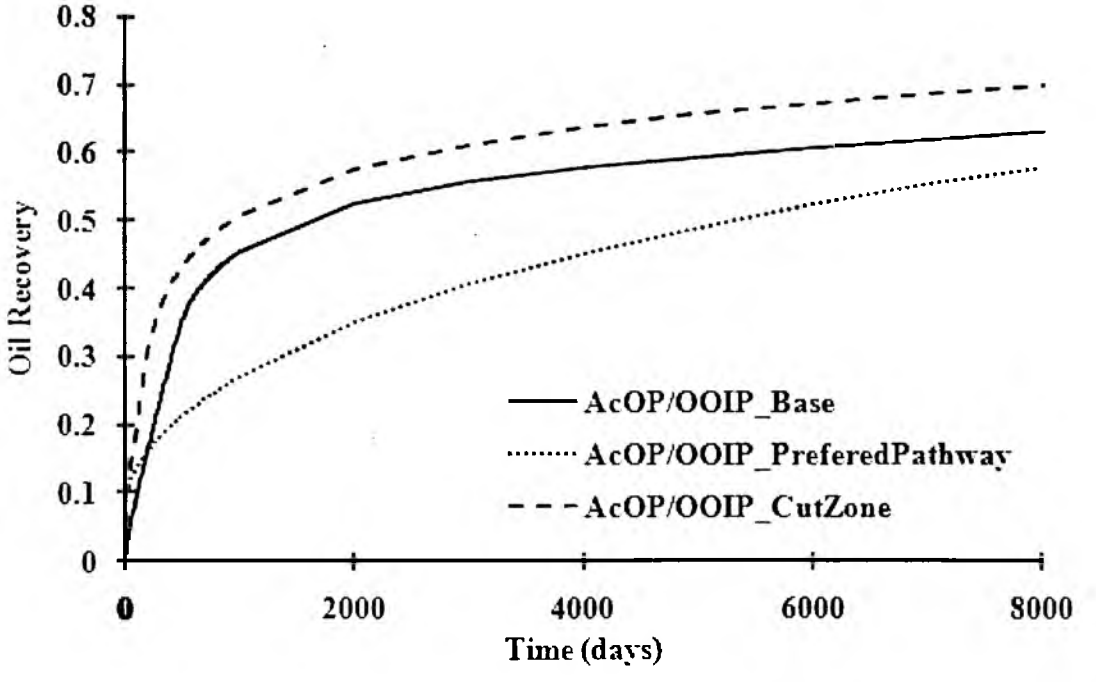

Figure 3.40 Comparisons of oil recoveries for preferred pathway study

Figure 3.40 shows that at the beginning of the simulations, for a short period, both the preferred pathway and the cut-off zone cases have identical oil recovery rates, which are higher than base case. This is due to the existence of higher permeability fractures near the injector. Then the trend of oil recoveries in Figure 3.40 displays the recovery with the order from high to low as: cut-off zone case, base case and preferred pathway case. This result is encouraging for the idea of treating higher permeability fractures with special techniques such as gels in order to lower or block the water breakthrough. The treatments can dramatically increase the oil recovery. For example, to reach 40% oil recovery, the homogeneous permeability base case required 660 days, the preferred pathway case required about 2900 days, and cut-off zone case required only 382 days. There is nearly one magnitude difference before and after the treatment.

To analyze the relationship between recovered oil and injected/produced water, some dimensionless analysis is demonstrated in Figure 3.41.

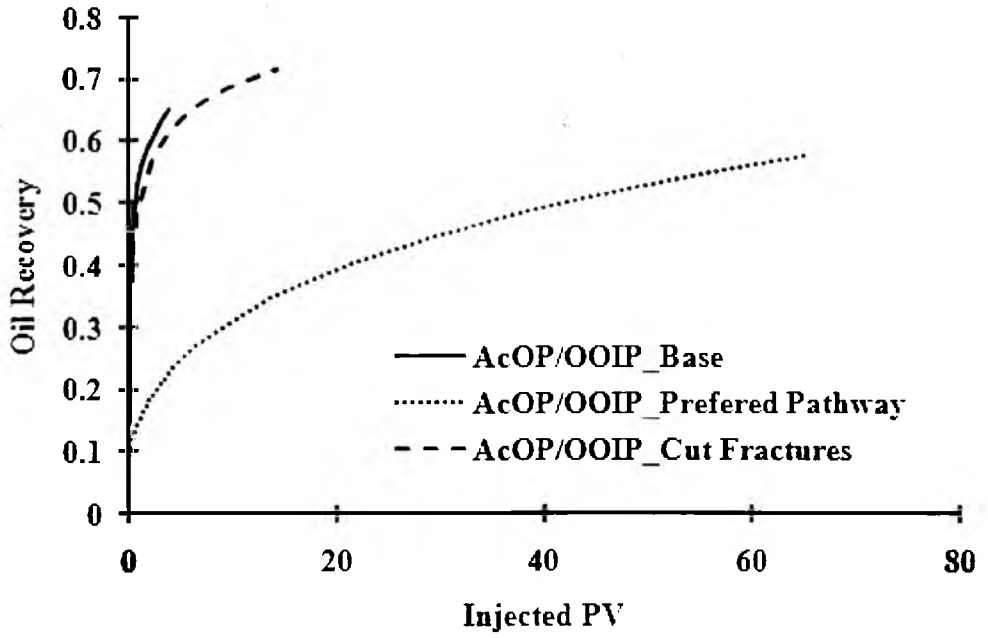

Figure 3.41 Dimensionless analysis of oil recovery vs. injected pore volume

The correlations between recovered oil and injected/produced water in Figure 3.41 is interesting: to reach 40% oil recovery, the base case required 0.32 volume of PV (reservoir pore volume) water injected, the preferred pathway case needed 21.68 PV water; and the cut-off zone case needed 0.40 PV water. The difference between injection water required for the preferred pathway and the cut-off zone (for 40% recovery) is more than 54 times of PV. From another point of view, with equal PV water being injected, the base case gave 54% recovery, the preferred pathway case offered 15% oil recovery; and the cut-off zone case resulted in 50% oil recovery. The recovery difference between the preferred pathway and the cut-off zone models is 35% of OOIP.

The recovery-produced water correlations are shown in Figure 3.42. For 40% target oil recovery, the base case produced 0.017 PV water, the preferred pathway case

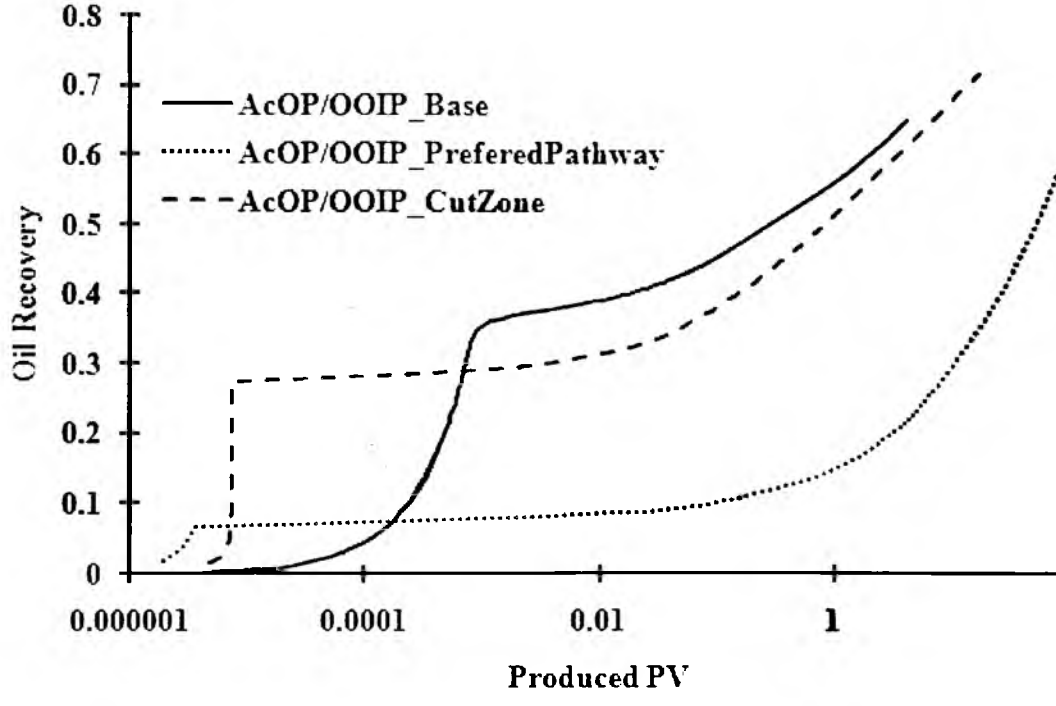

Figure 3.42 Dimensionless analysis of oil recovery vs. produced water

produced 26.3 PV water, and the cut-off zone model produced 0.146 PV water. The produced water volume between the preferred pathway model and the cut-off zone model gave more than 26 PV difference in this scenario. The preferred pathway model produced more than 180 times more water than the cut-off zone model. If the reservoir produced one time of PV water cumulatively, then the base case had 57% oil flooded, the preferred pathway model had 15% oil recovered, and the cut-off zone model had a 51% oil recovery rate. Therefore, one time of PV cumulative water production between the preferred pathway model and the cut-off zone model results in a 36% difference in original oil recovery.

The following points from this section could be highlighted:

1) If injectors and producers are linked by ultra high permeability fracture networks, limited water flooding efficiency can be expected.
2) The method of using gel or blocking the main preferred pathway fracture/faults can dramatically eliminate the negative effects caused by the ultra high preferred pathway. The advantages include higher recovery rate, lower injection-water demand, lower produced water-treatment cost (can reach two magnitude difference or more), etc.

3.7 Chapter Summary

At the beginning of the chapter, a regularized fracture network was simulated with ECLIPSE (a well-established commercial reservoir simulator) and CVFE (an in-house DFN simulator developed by the University of Utah). The results of the two simulations were compared, and they showed that both simulators were in close agreement, even under the three-phase conditions.

Sensitivity case studies in this chapter demonstrated the importance of fractured reservoir characterization work. A precisely characterized fracture network could reduce the reservoir production uncertainty risk significantly. Quantitatively, this chapter discussed the effect of different fracture properties on multiphase flow performance in a "real" basement fracture model. This "real" fracture network was difficult to simulate by conventional finite-difference simulators such as ECLIPSE. The following conclusions can be drawn from this study:

1) When a random permeability distribution was characterized for the network, the flow performance was dominated by the presence of the low permeability features. The permeability distribution also impacts oil recovery and water cut.
2) The DFN approach allows us to cut off main connections in the flood pathway (between injector and producer) and evaluate those cut-off impacts. It was shown that primary production was not impacted significantly by the disturbance in connectivity, but water flood performance was.
3) Changing the fracture's dip orientations resulted in production rate variations but did not impact the overall recovery significantly.
4) When the fracture height was reduced in one of the two intersecting networks, the oil recovery was significantly lowered.
5) The DFN approach also allowed us to evaluate "what-if" scenarios. If one of the main pathways between the injector and the producer has inherently higher permeability (or an induced high permeability), then water channels through this pathway lower recovery by as much as 10-15%. By blocking the

preferred pathway, water can be diverted into other parts of the reservoir, increasing oil recovery.

3.8 Nomenclature

B	=	formation volume factor
e	=	fracture/fault storage aperture, ft
g	=	gas phase
i	=	i^{th} discretized fracture elements
k	=	permeability tensor, md
k_r	=	relative permeability
n	=	number of discretized fracture elements
o	=	oil phase
p	=	fluid pressure, psi
q	=	flux vector
R_s	=	gas-oil ratio, MSCF/STB
S	=	phase saturation
u	=	velocity, ft/day
w	=	water phase
Φ	=	porosity
ρ	=	density, lbm/ft^3
μ	=	viscosity, cp

3.9 Bibliography

Fu, Yao, "Multiphase Control Volume Finite Element Simulations of Fractured Reservoirs," Ph.D Dissertation, University of Utah, Salt Lake City (2007)

Fu, Y., Yang, Y-K., and Deo, M., "Three-Dimensional, Three-Phase Discrete-Fracture Reservoir Simulator Based on Control Volume Finite Element (CVFE) Formulation", paper SPE 93292, (2005)

Yang, Yi-kun, Finite-element Multiphase Flow Simulation, Ph.D Dissertation, University of Utah, Salt Lake City, UT (2003)

CHAPTER 4

SIMULATING FRACTURED BASEMENT RESERVOIRS: COMPARING DISCRETE FRACTURE NETWORK MODELS TO THE UPSCALED EQUIVALENTS

(A paper in preparation)

Huabing Wang, Craig Forster, and Milind Deo.

Department of Chemical Engineering

University of Utah

Salt Lake City, UT 84112

4.1 Abstract

Naturally fractured reservoirs are an important, but difficult-to-manage, worldwide reservoir type. Complex and difficult to define, fracture networks yield reservoir systems that can be important assets for oil companies, yet the ability to improve production in these reservoir systems is hampered by their complexity. Despite the key role of fracture networks in production performance, reservoir simulations typically use equivalent porous medium properties to represent the aggregate impact of fracture networks.

In Chapter 3, the indexing verification showed that the CVFE simulator can accurately represent displacement physics in DFN modeled fracture networks. In this chapter, an irregular basement reservoir model was adopted for upscaling studies. An absolute permeability upscaling technique (geometric Oda method) was examined for testing the transformation from the DFN fine-grid model to a coarse-grid flow model. A new, fine grid with a fracture intensity analysis-characterized fracture/nonfracture basement model was also tested by ECLIPSE for the convergence with the CVFE simulation results. The upscaling procedure enables creation of single-porosity input files. The single-porosity simulations were performed using ECLIPSE. The grid resolutions in the single porosity simulations were critical in capturing the geologic information from the DFN models; however, in all cases a prespecified resolution did not produce the same result as the DFN approach. Instead, the prespecified resolution depended on fractured network geometry and the physical problem at hand. The advantage of using upscaled property is to speed up the simulation process. A portfolio of comparative simulation results helped us to better understand the level of uncertainty that might be introduced

when using equivalent property and multiphase simulators to represent fractured reservoir systems.

4.2 Introduction

For many years now, the most popular method of constructing detailed geological models of oil/gas reservoir was the classical deterministic method, which is widely applied in the fractured reservoir characterization. Geologists use this approach to interpret the existing data allowing them to build target-fractured reservoir models. However, since the past decade or so, deterministic approaches have been complemented by more and more quantitative geo-statistical approaches, such as multipoint statistics (MPS) (Horne et al., 2004, Liu et al., 2004) and discrete fracture network (DFN) (Dershowitz et al., 1998) modeling. Compared to the MPS model, the DFN model has the advantage of presenting fracture orientation explicitly. This allows the geologists to model the flow units and fracture flow paths.

Experience in fractured reservoir with low permeability formations often produces fluids through open fractures. An extreme case of Type I (Nelson's, 2001) classified reservoir will be considered in this study. In Type I fractured reservoir, fractures provide the essential reservoir porosity and permeability. Geologically, Type I reservoirs are granitic/basalt formations. They are also called "Basement Reservoirs." Practically all of the oil in these reservoirs resides in fractures or fault zones. Since the geometry of the fracture network is critical in understanding recovery from these reservoirs, these lend themselves well for treatment by using the DFN approach. The primary questions to be answered are:

1) Are DFN models accurate in modeling physics of displacement in these reservoirs?
2) How could DFN properties be homogenized into the conventional finite-difference simulators for the multiphase flow calculations?
3) For the process of "homogenization," how accurate can they be and how can multiphase model impact it?

The first question was answered by indexing verification work in Chapter 3. The benchmark work showed that CVFE simulator can accurately represent the displacement physics of the fractured basement reservoirs.

Once the accuracy of the DFN approach was ascertained, an irregular basement network was constructed for the simulation purpose and the DFN approach was used directly to obtain simulation results. It was also possible to "homogenize" the irregular fracture domain and create "equivalent" ECLIPSE input files. This entails the creation of porosity and permeability fields, using one of the DFN upscaling methods (Oda method). The geometry-based Oda method was used to upscale permeability tensors initially defined in the discrete fracture network. Volumetric (P33) fracture intensity was calculated in each grid block to represent the upscaled porosity. Upscaling with a series of different grid block sizes (ranging from 10-ft to 200-ft cubes) in a 1000 by 1000 by 200 ft reservoir volume revealed that the upscaled results depend strongly on the relationship between grid block size, multiphase impact, fracture network geometry and simulator type. This study helped us evaluate the effectiveness of the upscaling techniques, and also compared the DFN approach to what can be considered a "single-porosity" simulation method toward the Type I basement reservoir.

4.3 Numerical Methods Overviews of Fracture Reservoir Simulation

Conventional reservoir simulators use finite-difference methods with two-point flux calculations. With the development of full tensor permeability (Lee et al., 1994) and nonorthogonal grid technique, multipoint flux calculations (Verma and Aziz, 1996; Gunasekera et al., 1998) are becoming more and more popular since the last decade. At the same time, control volume methods (Aavatsmark et al., 1997) have become the method of choice for today's simulator because of their capacity for handling complex geometric systems using unstructured grids. To achieve higher accuracy, limited work has also been done on advanced finite element methods (Young, 1978; Sukirman and Lewis, 1994). Yang (2003) developed an upstream transmissibility weighted control-volume finite-element discrete fracture network simulator.

Three types of main model formulations are popular for modeling and simulating flow through naturally fractured reservoirs: the single porosity model, the dual porosity model, and the DFN model. For detailed background regarding these three fracture simulation models refer to Section 2.3.

4.4 Proposed Domain Characteristics

Common model properties for both domains:

- Impermeable matrix with $\Phi = 0$ (Type I, basement reservoir system)
- Domain = 1,000 ft by 1,000 ft by 200 feet deep
- Total feature length = 30,000 feet
- Feature property: k = 1,000 md, Φ = 14 %, width = 0.5 feet
- Original Oil In Place (OOIP) = 53,580 STB
- Injection Pressure = 4,300 psi

- Lower dot = Injection Well, upper dot = Production Well

As shown in Figure 4.1, the regularized and irregularized fracture network domains were generated. Two constraints were applied for the DFN irregularized domain and its equivalent regularized domain: the same OOIP and the same transmissivity (kh value). Both domains were characterized as a three-phase black-oil model with initial solution gas in the oil phase and the exact same fluid and rock properties. Examples of

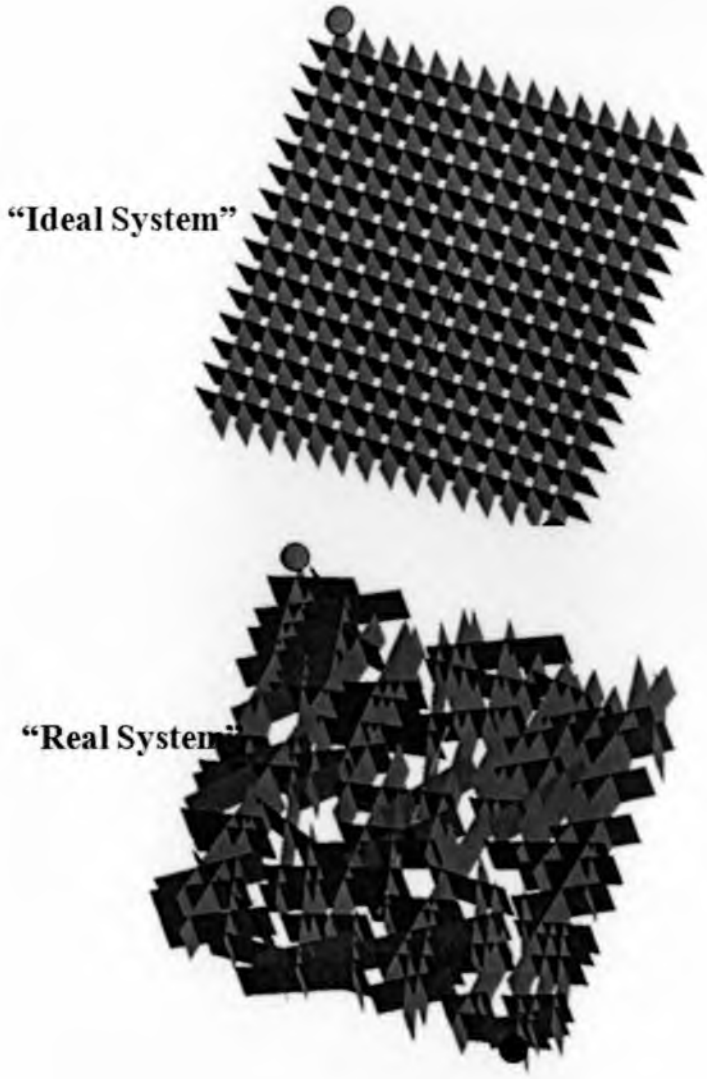

Figure 4.1 Irregular "real" DFN basement model (bottom) and equivalent regularized "ideal" DFN basement model (top)

these properties include fluid density, viscosity, compressibility, PVT table, formation factor, gas/oil ratio table, rock compressibilities, relative permeability curves, initial conditions, well operation conditions and schedules, etc. For detailed geological information, refer to Section 3.4.

4.5 CVFE Simulator Verification

As mentioned at the beginning of this chapter, the CVFE simulator has been indexed verified by with the well-known commercial reservoir simulator ECLIPSE in Chapter 3. Some other CVFE formulation verifications have been reported through the manufacture solution method (Yang, 2003; Fu, 2007).

4.6 Study of Hypothetical "Real" Basement Reservoir Model

In this section, the hypothetical "real" basement system was studied using the CVFE simulator as the base solution of series of upscaling/integrating approaches. For

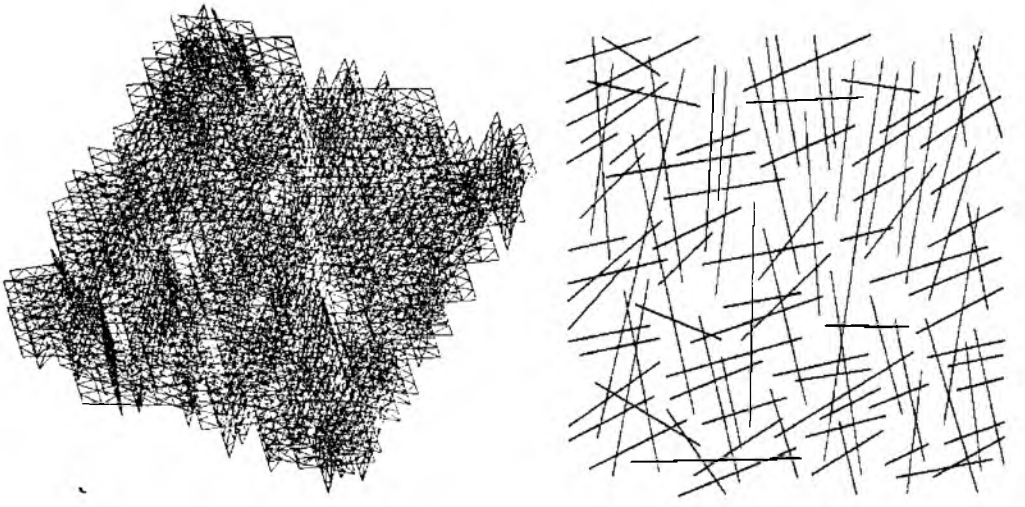

Figure 4.2 Three-dimensional view (left) and two-dimensional view (right) of discretized, irregularized DFN modeled "real" basement reservoir domain for the CVFE simulator

both "ideal" and "real" systems, the analyses of fracture/fault orientation and connectivity are discussed in Section 3.4. Other than that, "real" and "ideal" basement systems shared all of the remaining reservoir characteristics and operating information, including the well positions. From this point of view, this study is trying to answer the following questions:

- Can a "real" basement reservoir be presented by an "ideal" system regardless of fracture/fault orientation and connectivity? (Figure 4.2)
- Can a "real" basement system be represented (upscaled or integrated) by the conventional finite-difference black-oil simulator?
- If the basement system could be studied by ECLIPSE, will grid-block size impact the oil recovery results?

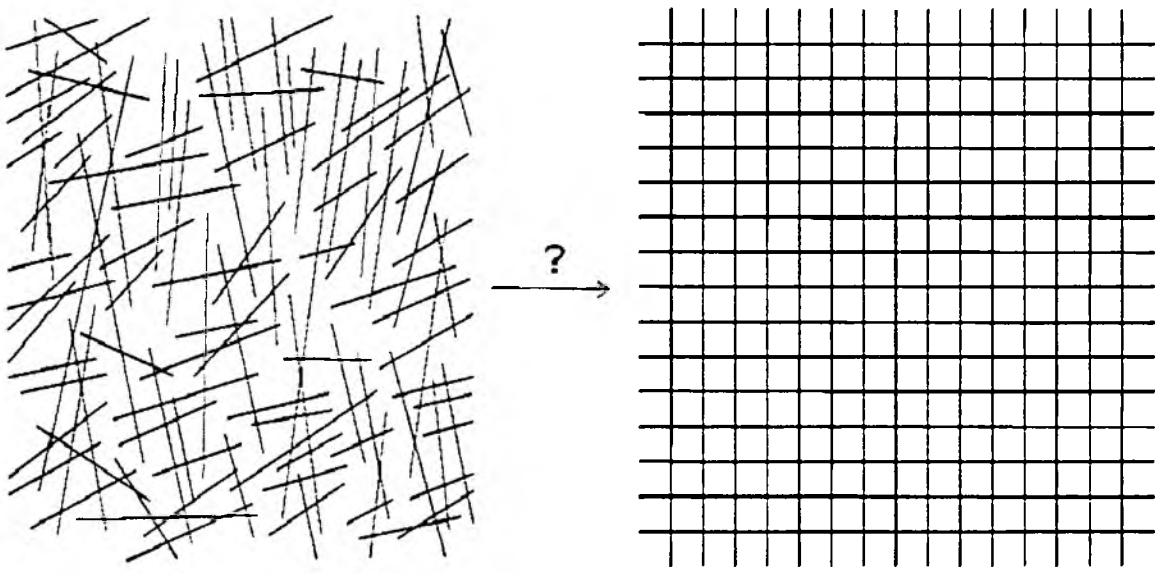

Figure 4.3 Simplification of "real" basement system (left) to "ideal" basement system (right)

4.6.1 Can a "Real" Basement Reservoir Be Presented By an "Ideal" System Regardless of Fracture/Fault Orientation and Connectivity?

From the fracture cluster analysis, the "real" basement fracture/fault system was considered the "well connected" system. One of the hypotheses regarding this "well connected" system was the question of whether this system could be simplified as the "ideal" system? (Figure 4.3) During this simplification process, 107 fractures are treated as 30 uni-sizes perfectly connected fracture network. Other than that everything stays the same except the connectivity and orientation. To answer this question, a simulation was performed on the "real" basement system.

Figures 4.4 through 4.6 show that on the stage of primary production, the "ideal" system and the "real" system are well matched. The only driving force on this production stage is the reservoir pressure. At the end of primary production, the reservoir pressure is dropped to 2370 psi which is lowered than the fluid model bubble point at 2700 psi.

Figure 4.7 shows the gas phase saturation distributions under these conditions. Since there is no isolated fracture in both "real" and "ideal" systems, much of the "mobilized" gas-phase is evenly distributed on the top of the reservoir. This even gas distribution made the system pressure evenly distributed and explained the excellent match during primary production.

In secondary production, the significant differences are shown between "real" and "ideal" systems. Quantitatively, the peak daily oil production rate from the "ideal" basement system was 27.13% higher than the "real" basement system, and the cumulative oil production from the "ideal" system was 6.77% higher than from the "real" system at the end of simulation. Instead of an even water flooding pattern from the "ideal" system,

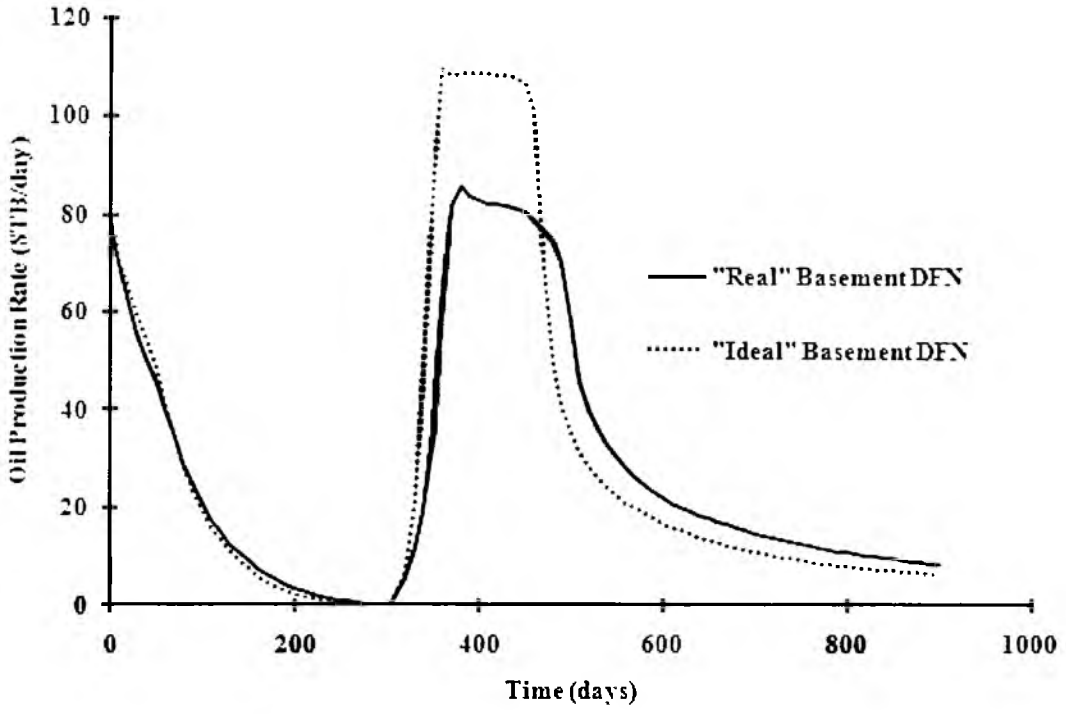

Figure 4.4 Comparisons of oil production rate between the "ideal" and "real" system

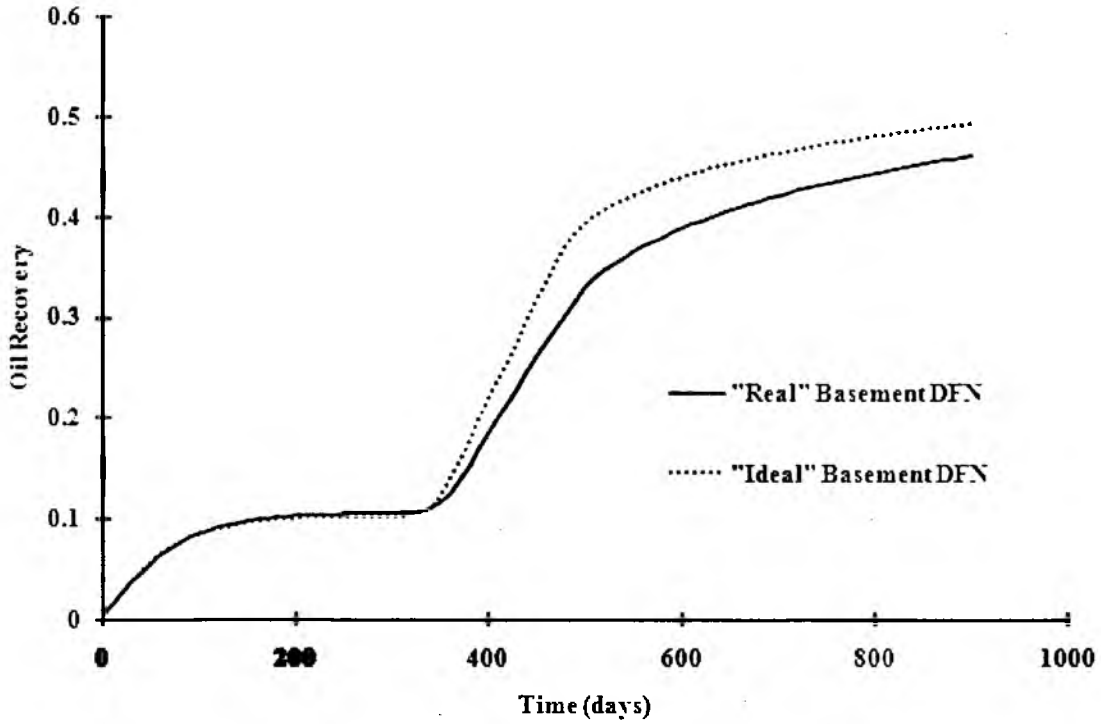

Figure 4.5 Dimensionless analysis of cumulative oil production rate between the "ideal" and "real" systems

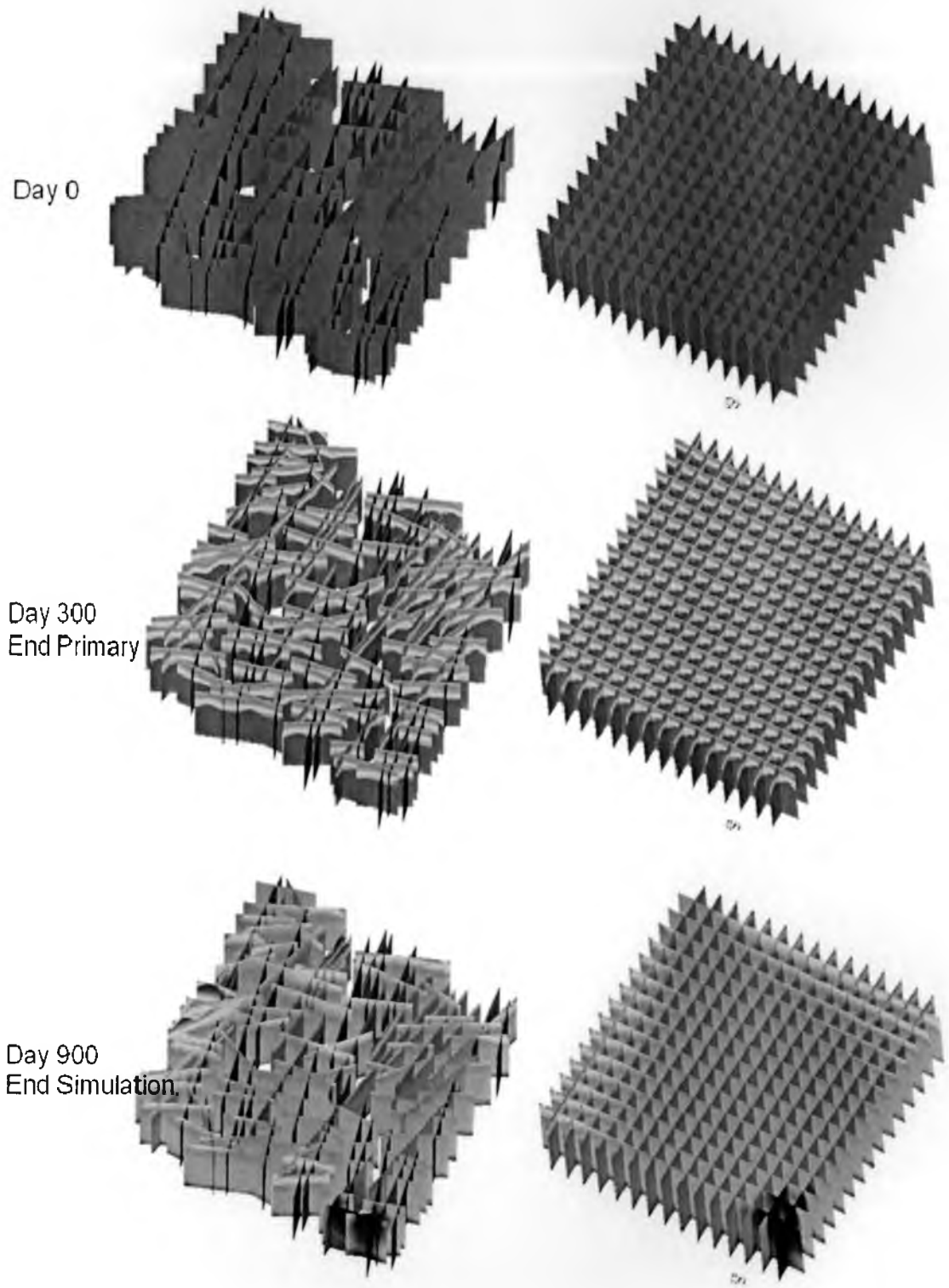

Figure 4.6 Snapshot of oil saturations for the "real" basement system and "ideal" basement system

the oil distribution snapshot in Figure 4.6 shows that the "real" system has more stranded oil spots than the "ideal" system. Obviously, these oil trappings are a result of the fracture/fault connectivity. An interesting observation found at the end of simulations is that the "ideal" oil production rate is only slightly higher than "real" production rate. This is due to the similar reservoir driving force at the day 900 ("real": 2870 ~ 4130 psi; "ideal": 2940 ~ 4100 psi). At the end of the simulations, the "ideal" system shows a little narrower pressure distribution than the "real" system due to the local fracture/fault cluster connectivity issue.

Figure 4.8 shows that the fracture/fault connectivity plays an important role in the basement reservoir study. In the "real" system, the pressure has a significant drawn-down near the main connections between the injector and the producer. This phenomenon can be found from the "ideal" system oil pressure distributions.

This study suggests the following conclusions:

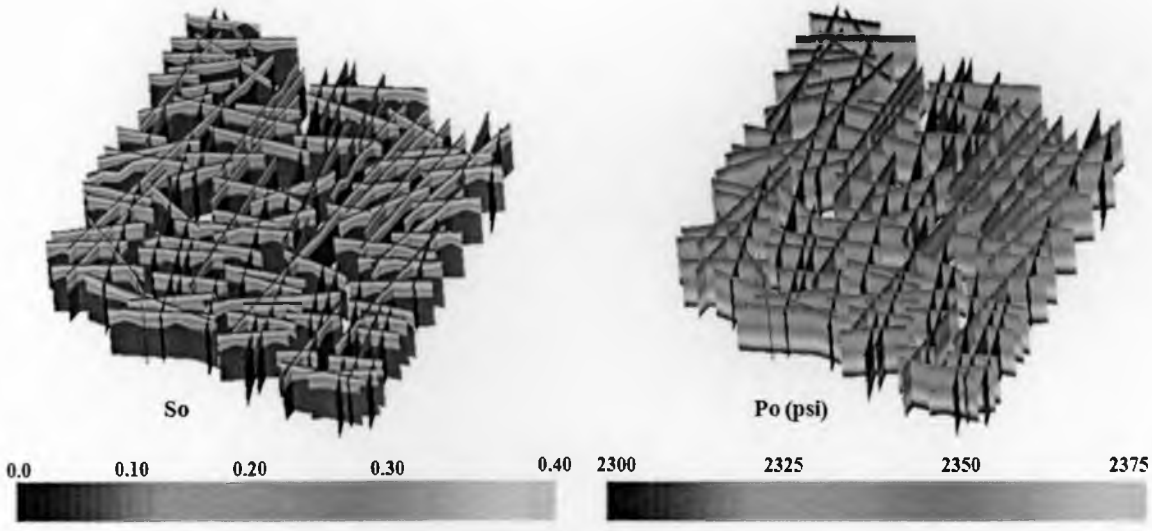

Figure 4.7 At day 300 (end of set primary production), the gas saturation (left) and the oil pressure distributions (right)

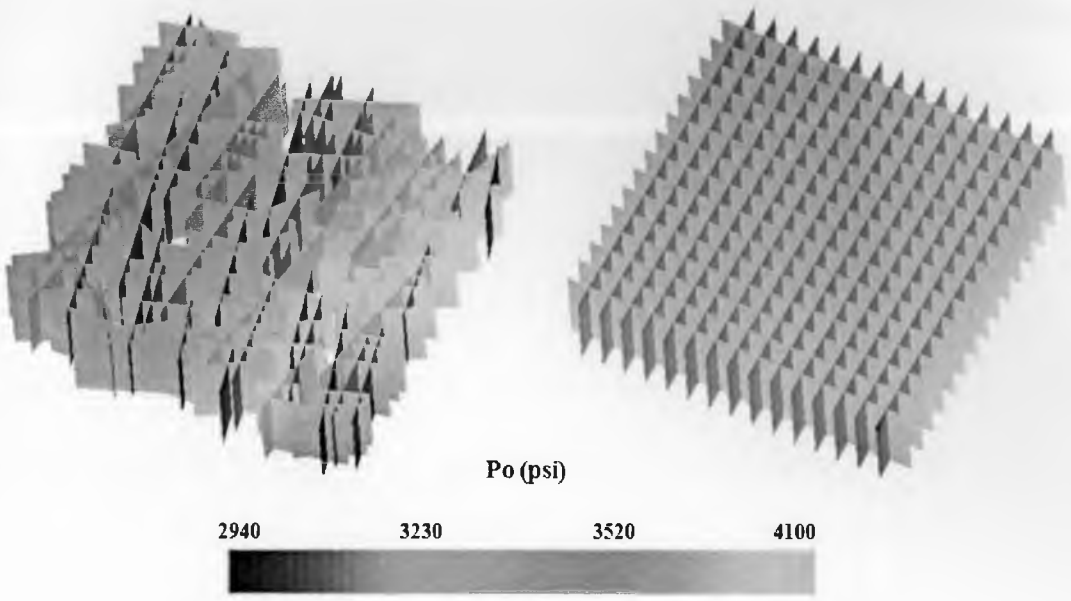

Figure 4.8 At the end of simulation (day 900), the pressure distributions on "real" (left) basement model and the "ideal" (right) basement model

1) The fracture/fault cluster connectivity plays an important role in fractured reservoir productions.
2) In primary production stage, the "real" system can be represented by the regularized "ideal" system.
3) In the secondary production scenario:
    a. Theoretically, the "real" system cannot be described precisely by the equivalent "ideal" system for the water flooding study.
    b. Practically, the "ideal" system can be used for the fast oil production forecast qualitatively. However, this might be too risky due to the existence of many uncertainties.
4) CVFE simulator is a powerful tool for studying DFN modeled fractured reservoirs. The "real" fracture/fault model is difficult to describe and calculate through conventional finite-difference based reservoir simulators.

4.6.2 Can a "Real" DFN Modeled Basement Fracture Network Be Represented by a Conventional Finite-Difference Simulator?

Reservoir simulation can be significantly more challenging for naturally fractured reservoirs than it is for conventional classic reservoirs. In the Type I basement reservoir, all hydrocarbons are stored and flow among the fractures/faults network. Since most modern reservoir simulators are based on finite-difference method, it becomes interesting to ask whether the DFN modeled fracture network can be simulated by a conventional finite-difference simulator such as ECLIPSE. If the answer were "yes," the accuracy and stability of this integration would need to be quantified.

Dershowitz et al. (2000) first presented the method of integration of DFN with conventional simulator approach. In their work, the DFN model was characterized as having the fracture continuum for a single-phase dual porosity simulation. No multiphase integration work has been reported since then.

In this study, a DFN modeled "real" basement fracture network was "homogenized" or "equivalent" as the single porosity continuum model. This concept consists of overlapping the fracture/fault network and a finite-difference orthogonal grid, by considering the fracture properties such as density, permeability, thickness and porosity in each grid and assigning equivalent values to each grid cell in the finite-difference grid. Figure 4.9 shows how this concept works.

As shown in Figure 4.9, the basement reservoir properties are "homogenized" by the DFN model into the finite-difference grid blocks. For flow simulations, homogenized grid porosity and permeability are discussed in the following sections.

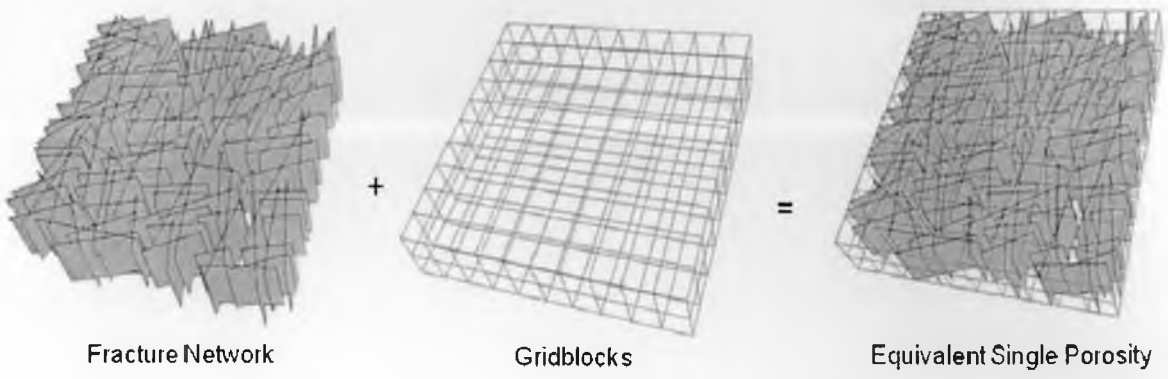

Figure 4.9 "Homogenized" or "Equivalent" single porosity modeled "real" basement reservoirs

4.6.2.1 Grid Block Porosity

The fracture-system porosity was calculated as the product of the fracture intensity expressed as fracture area per unit volume (P32) and the storage thickness of fracture/fault (Equation (4-1)):

$$\Phi_{GridBlock} = \frac{V_{DFN}}{V_{GridBlock}} = \frac{\sum (A_{DFN} \cdot e)}{V_{GridBlock}} = P_{32} \cdot e \qquad (4\text{-}1)$$

where:

$\Phi_{GridBlock}$ = basement fracture/fault porosity

V_{DFN} = basement fracture/fault volume

$V_{GridBlock}$ = finite-difference grid block volume

A_{DFN} = basement fracture/fault area

e = basement fracture/fault storage thickness

P_{32} = basement fracture/fault intensity as fracture area per unit volume

To calculate the "equivalent" porosity for each grid cell, the fracture/fault volume needs to be averaged by the volume of the grid blocks.

4.6.2.2 Grid Block Permeability

The approaches for calculating continuum grid block effective directional permeability can be achieved by two main methods: 1) the geometry-based Oda method (Oda, 1985), and 2) the flow-based "Block K" method. These two methods are reviewed below.

In a three-dimensional system, single-phase fluid flow through an isotropic porous media is described by the differential form of Darcy's law (Equation (4-2)):

$$\mathbf{q} = -\frac{\rho}{\mu} k \nabla \mathbf{P}(x, y, z) \tag{4-2}$$

where

$$\nabla \mathbf{P}(x, y, z) = \left(\frac{\partial P}{\partial x}, \frac{\partial P}{\partial y}, \frac{\partial P}{\partial z}\right) \tag{4-3}$$

is the pressure gradient at the point (x,y,z), and **q** is the resultant flux vector (mass per unit time per unit area) at the point. The isotropic permeability k is a local property of the medium, while the density, ρ, and viscosity, μ, are properties of the fluid.

A 3x3 symmetric permeability tensor of a fracture could be calculated by projecting its isotropic permeability, k, onto its plane (Oda's method). Let n denote the unit pole (normal) vector of the fracture. The components of the Oda tensor can be derived by subtracting the normal component of the flux, leaving a flux vector q_f in the plane of the fracture, as shown in Equation (4-4):

$$\mathbf{q_f} = \mathbf{q} - \mathbf{n}\mathbf{n}^T\mathbf{q} = (\mathbf{I} - \mathbf{n}\mathbf{n}^T) \cdot \mathbf{q} \tag{4-4}$$

where **I** is the 3x3 identity matrix, and $\mathbf{nn}^T$ is the matrix outer product given by Equation (4-5):

$$\mathbf{nn}^T = \begin{bmatrix} n_1^2 & n_1 n_2 & n_1 n_3 \\ n_1 n_2 & n_2^2 & n_2 n_3 \\ n_1 n_3 & n_2 n_3 & n_3^2 \end{bmatrix} \tag{4-5}$$

Substituting these expressions back into Darcy's equation, and accounting for the ratio between the fracture volume (thickness, e, multiplied by area, A) and the cell volume, V, Equation (4-6) is defined as:

$$\mathbf{q_f} = -\frac{\rho}{\mu}\frac{\mathbf{keA}}{\mathbf{V}}(\mathbf{I} - \mathbf{nn}^T)\nabla\mathbf{P} = -\frac{\rho}{\mu}\mathbf{k}\nabla\mathbf{P} \tag{4-6}$$

where the six unique entries of the symmetric Oda tensor **K** are simply represented by Equation (4-7):

$$\mathbf{k_{ij}} = \mathbf{k}\frac{\mathbf{eA}}{\mathbf{V}}(\delta_{ij} - \mathbf{n_i n_j}) \tag{4-7}$$

The indices I and j can be 1, 2, or 3 (for each coordinate direction), and the Kronecker delta function is given by Equation (4-8):

$$\delta_{ij} = \begin{cases} \mathbf{1, when\ i = j} \\ \mathbf{0, otherwise} \end{cases} \tag{4-8}$$

If the flux through each fracture within the cell is assumed to be additive, then these matrices can be summed together to get a net permeability tensor $\mathbf{K}_{net}$. The principal permeabilities and flow directions within this cell are given by the eigen values and eigenvectors of $\mathbf{K}_{net}$.

One drawback of Oda's method is that it does not take into account fracture network connectivity and therefore is limited to well-connected fracture networks. The "real" basement model is a well-connected fracture network.

The second approach of equivalent directional permeability tensor calculations could be done by the "block-K" method (Long, 1984; Doolin et al., 1995 and Clemo, 1998).

Figure 4.10 shows how x-directional permeability tensors are calculated. Starting with areal map of a "real" basement DFN model and overlapping with a 10x10x2 orthogonal finite-difference grid block, a single-phase (for example, water) steady-state flow along x-direction has been applied on the circled grid block cell. The only pressure gradient is in the x-direction (as shown in Equation (4-9).

$$\nabla P = \frac{\partial P}{\partial X}\hat{i} \tag{4-9}$$

The Darcy equation could be simplified in Equation (4-10) :

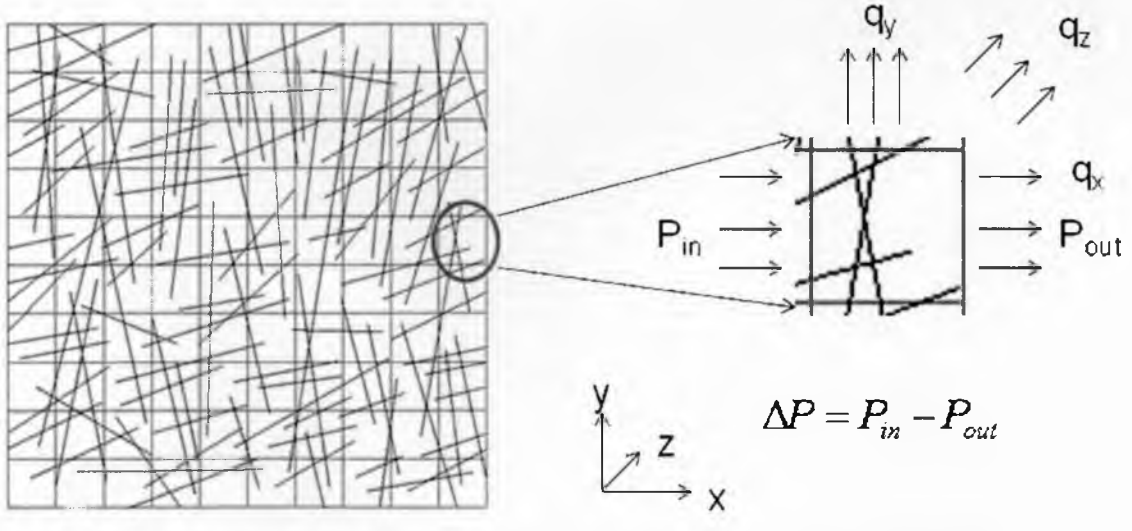

Figure 4.10 Illustration of the block-K method for calculating the x-directional permeability tensor

$$\begin{bmatrix} q_x \\ q_y \\ q_z \end{bmatrix} = \begin{bmatrix} k_{xx} & k_{xy} & k_{xz} \\ k_{yx} & k_{yy} & k_{yz} \\ k_{zx} & k_{zy} & k_{zz} \end{bmatrix} \begin{bmatrix} \frac{\partial P}{\partial x} \\ 0 \\ 0 \end{bmatrix} \tag{4-10}$$

The above equations could be represented by Equations (4-11) to (4-13)

$$q_x = k_{xx}\left(\frac{\partial P}{\partial x}\right) \tag{4-11}$$

$$q_y = k_{xy}\left(\frac{\partial P}{\partial x}\right) \tag{4-12}$$

$$q_z = k_{xz}\left(\frac{\partial P}{\partial x}\right) \tag{4-13}$$

The directional permeability tensor could be calculated by inverting above three equations to Equations (4-14) through (4-16):

$$k_{xx} = \frac{q_x}{\left(\frac{\partial P}{\partial x}\right)} \tag{4-14}$$

$$k_{xy} = \frac{q_y}{\left(\frac{\partial P}{\partial x}\right)} \tag{4-15}$$

$$k_{xz} = \frac{q_z}{\left(\frac{\partial P}{\partial x}\right)} \tag{4-16}$$

The block-K method is based on the steady-state flow simulation on each separated grid block cell. Compared with Oda's method, it has some drawbacks such as numerical tolerance of block cell face curvatures and the computation times. In the study, only Oda's method will be applied since the fractures/faults are well-connected.

4.6.3 Case Studies on Simulating a "Homogenized DFN Basement" Continuum Single Porosity Model by Conventional Finite-Difference Simulator ECLIPSE

The process of integrating a DFN modeled fracture network with conventional continuum grid blocks was discussed in the last section. This makes simulation of the DFN characterized fracture network possible through the conventional finite-difference simulator. In this section, various homogenized "real" DFN modeled fractured networks were simulated by ECLIPSE under multiphase conditions. Then the results from ECLIPSE were compared with the results from the CVFE simulator. These comparisons aided in understanding the accuracy and stability of this homogenization process if the results from CVFE simulator are presumed to be correct.

4.6.3.1 Grid Block Sensitivity Studies with Both Porosity and Permeability Homogenization

In this section, both porosity and permeability homogenization are studied regarding grid block size sensitivity.

A series of simulations are designed with different grid block sizes (from 10-ft cube to a 333x333x200-ft grid block cell), as shown in Figure 4.11. For different grid block sizes, the porosity of the homogenized grid blocks are calculated and visualized as shown in Figure 4.12.

Figure 4.12 shows that with various resolutions of grid block sizes, the local fracture/fault porosity density distributions are better honored by finer grid blocks. Examples of 3x3x1 grid block resolution resulted in close porosities being calculated other than 50x50x1 resolution which had distinguished porosities in each grid block.

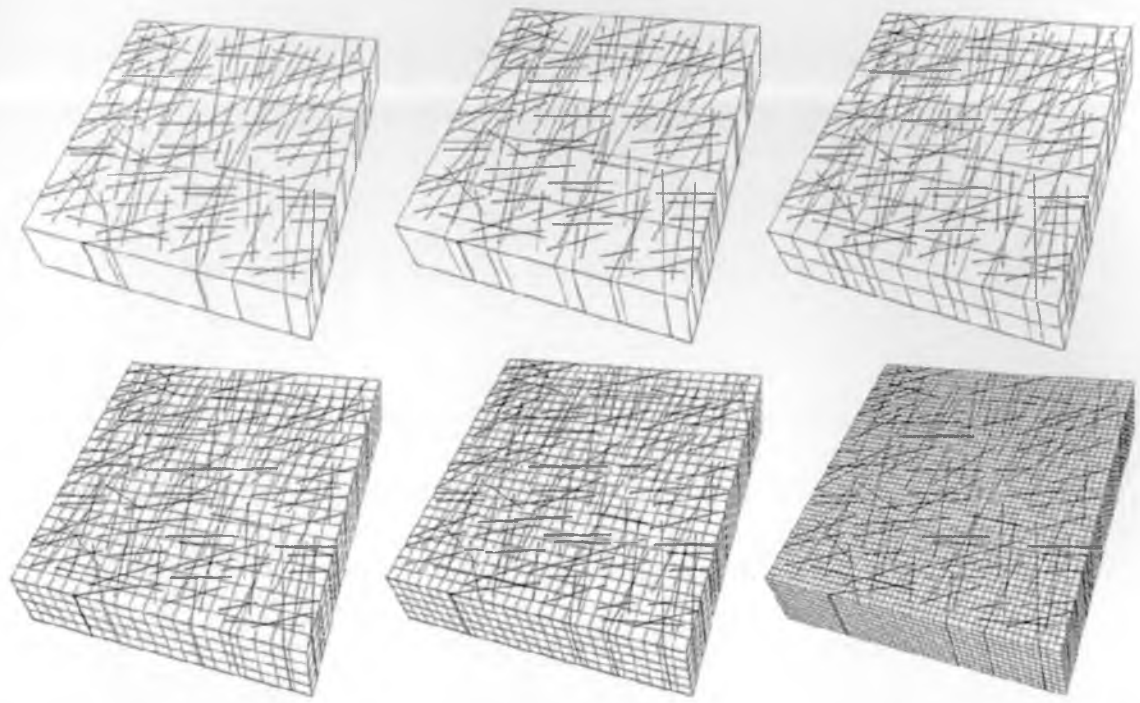

Figure 4.11 Illustrations of homogenized DFN grid with different cell sizes

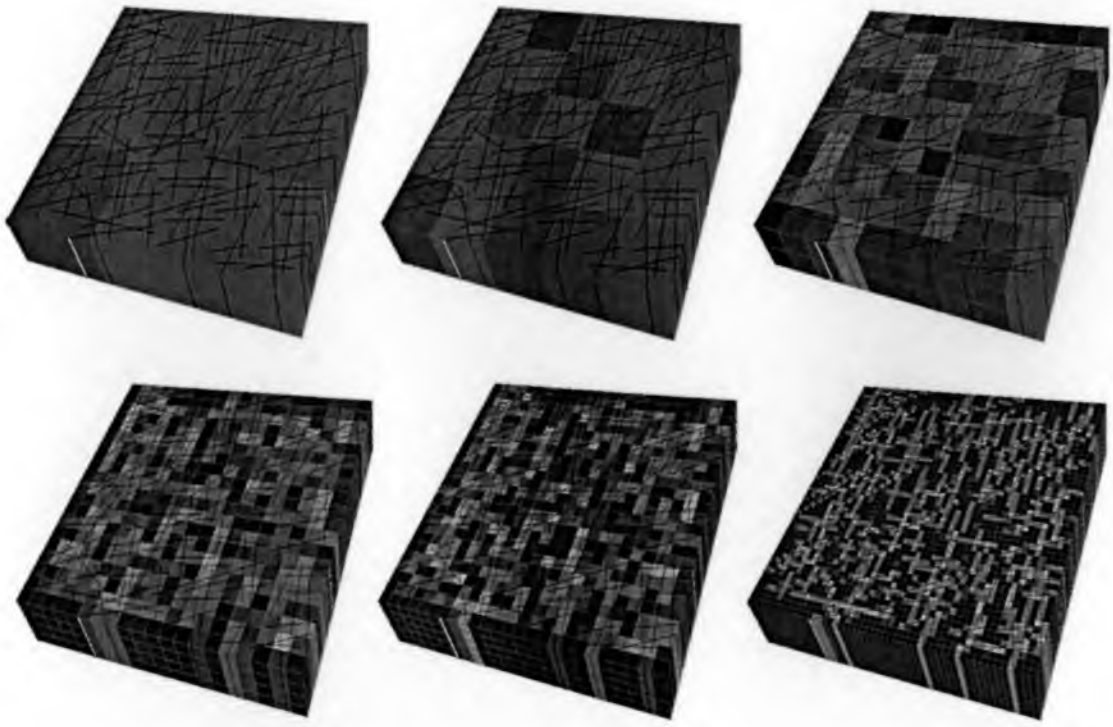

Figure 4.12 Visualization of porosity on homogenized DFN grids

An example of permeability homogenization with the grid block size of 40-ft cubes (25x25x5 grid blocks) is shown in Figure 4.13. The equivalent permeability tensor being calculated from Oda's method are a symmetric tensor, which means $k_{xy} = k_{yx}$, $k_{xz} = k_{zx}$, *and* $k_{yz} = k_{zy}$. Since all fractures in the "real" basement domain are vertical, the cross permeability term related to z-direction is zero, as the last two pictures shown in Figure 4.13.

A series of three-phase simulations with the same operating conditions were performed on the ECLIPSE simulator. The simulation results are shown below.

Figure 4.14 shows that the solutions of oil production rates on the homogenized grid are sensitive to the grid block sizes. Starting from the coarsest grid (3x3x1) blocks, and then proceeding to the more refined grid blocks, at the stage of primary production

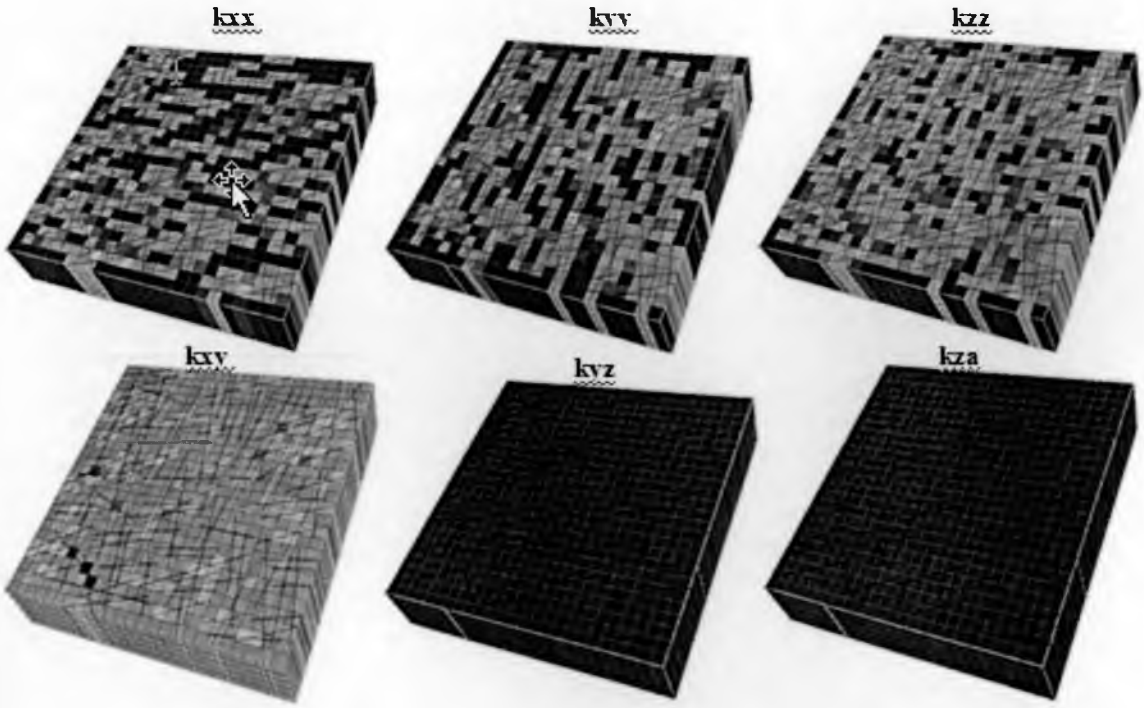

Figure 4.13 Visualization of the permeability tensors on homogenized DFN grids (The grid block sizes chosen are the 40-ft cube, 25x25x5 equal blocks on a 1000ft x 1000ft x 200ft domain.)

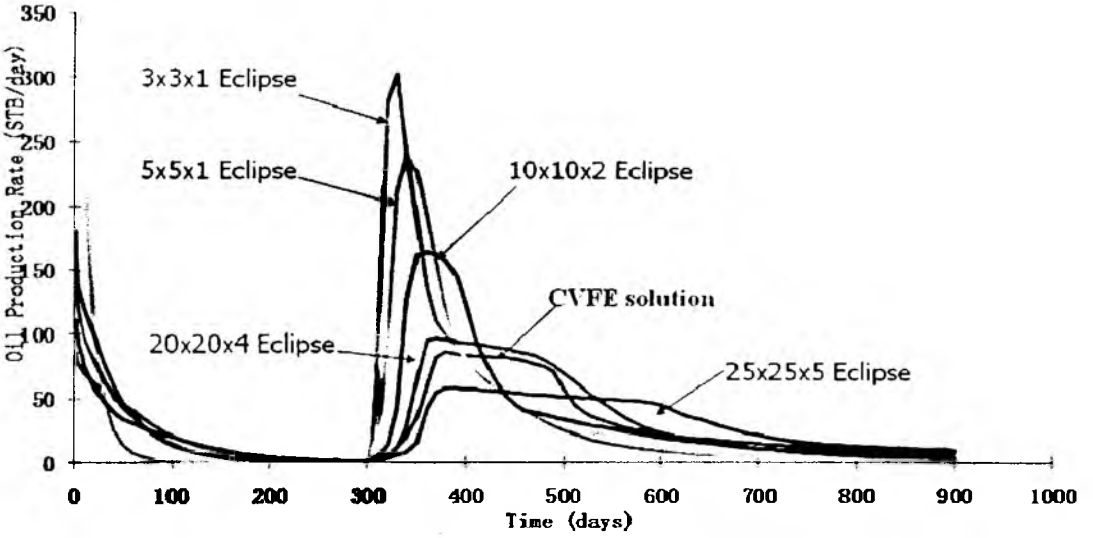

Figure 4.14 Oil production rate comparisons among homogenized ECLIPSE simulations and CVFE simulation

the finer grid presented better matches of CVFE solution. At the stage of secondary production, the reservoir oil production behavior is quite different from refined grid block sizes: Figure 4.13 shows that with refining grid block sizes, the oil production rate approaches the CVFE solution. Then the production rate passes the CVFE solution and gets further and further with the grid refinement. The finest grid in Figure 4.14 is the 40-ft cube; some finer grids such as 20-ft and 10-ft cubes were also studied but they cannot be converged.

Since the secondary production is the water flooding study, the water cut curve comparisons are shown in Figure 4.15.

The same trends are discovered on the water cut curves among the various homogenized grid block sizes as compared to the CVFE solution. Meanwhile, in the case of presenting the "real" basement system, the homogenized 20x20x4 (50-ft cube)

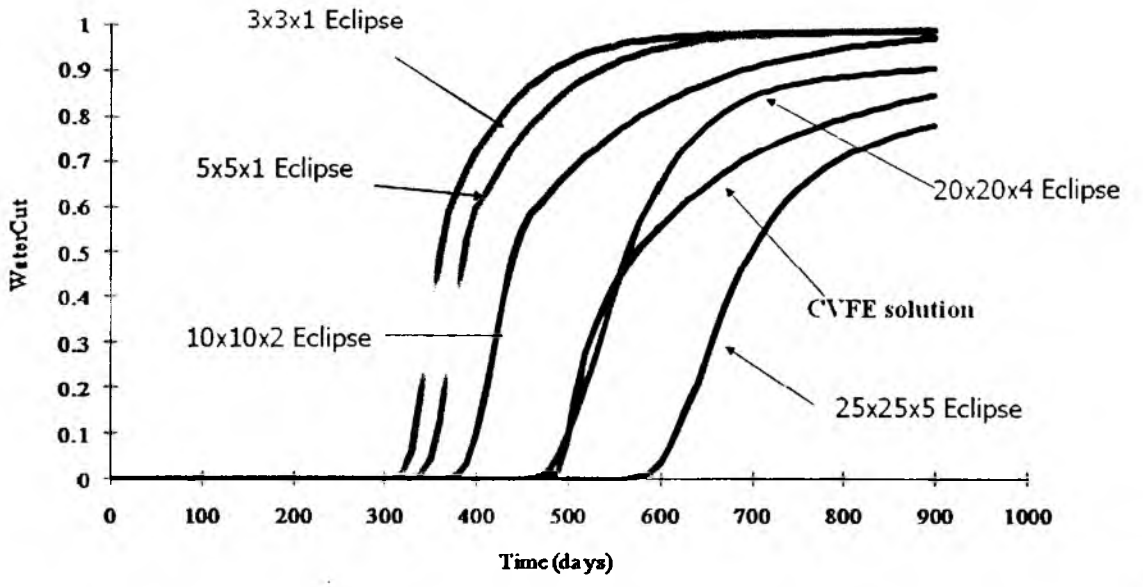

Figure 4.15 Water cut comparisons among homogenized ECLIPSE simulations and CVFE simulation

ECLIPSE simulation shows the best water breakthrough time match but still has certain errors after the middle of injection. The same phenomenon from the water cut figure is observed as from the oil production rates figure: the finer grids with both porosity and permeability homogenized are difficult to converge. The reason is discussed below.

Figure 4.16 qualitatively demonstrates the limitation of Oda's method in fine grid blocks. If a fracture only penetrates a small section of a grid block, the grid block permeability tensor calculated from Oda's method is very small. Under this small permeability, fluid cannot flow through that grid block. This explains the reason for nonconvergence phenomena observed in finer grid block cells. Therefore, during this type of homogenization process, it becomes essential to choose the right grid-block sizes. CVFE simulator is one option for helping to choose grid block sizes. Another method is discussed in the next section on the conventional FD simulator approach.

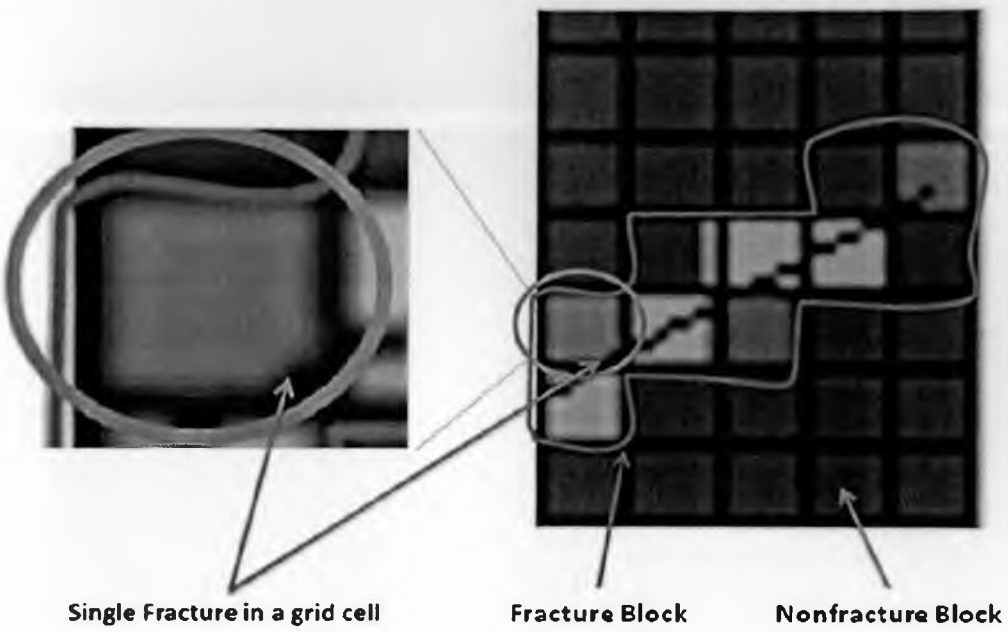

Figure 4.16 Limitation of Oda's permeability tensor calculation with fine grid cells

4.6.3.2 Fine Grid for Conventional Finite-Difference Simulator of ECLIPSE

Fracture density/intensity analysis is a popular method for studying fractured reservoir flow behaviors by conventional reservoir simulators such as ECLIPSE. The case study proposed here is to make very fine grid blocks (100x100x20, 10-ft cube, as shown in Figure 4.17) to separate fracture-occupied grid and nonfracture-occupied grid blocks for the "real" basement system. Then based on the intensity of fracture weighting in the fracture-occupied grid, the porosity of that grid will be calculated for a single porosity model. Assuming that the transmissivity (kh value) of that grid block were the same as the DFN characterized fracture value. This fine-grid characterized, single porosity basement model helps elucidate the maximum accuracy of conventional fractured reservoir flow simulation achieved by ECLIPSE. Results from this study were compared with the CVFE simulation results.

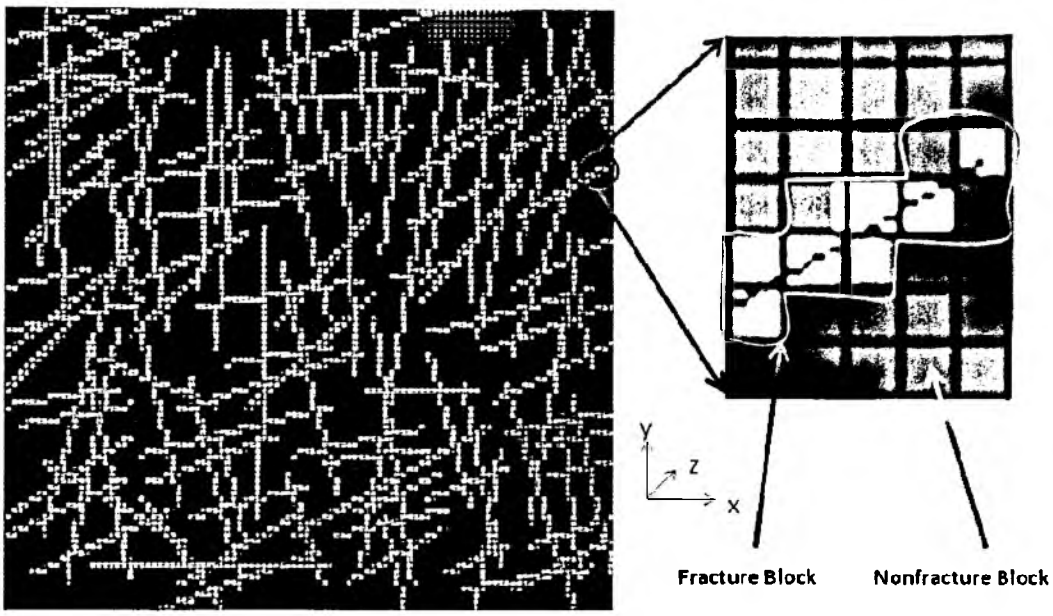

Figure 4.17 Illustration of simplified permeability constrain calculations

$$\Phi_{GridBlock} = \frac{V_{DFN}}{V_{GridBlock}} = \frac{\sum (A_{DFN} \cdot e)}{V_{GridBlock}} = P_{32} \cdot e \tag{4-17}$$

Figures 4.18 to Figure 4.20 show the comparisons between results from the case of fine grid (100x100x20) porosity homogenization and CVFE. Figure 4.20 shows that each single fracture/fault in the basement reservoir model is clearly represented by the single grid block row/column in this finer grid ECLIPSE model. The oil saturation distribution fronts/residuals are basically identical with the CVFE results (from Figure 4.18 and 4.19). Furthermore, the oil production rate and water cut are basically matched with the solution from CVFE results in a reasonable range. The difference is possibly caused by uncorrected permeability tensor and the flow path in the fracture/fault grid. For example, the single fracture/fault is not parallel to the grid block row/column in the conventional finite-difference approach.

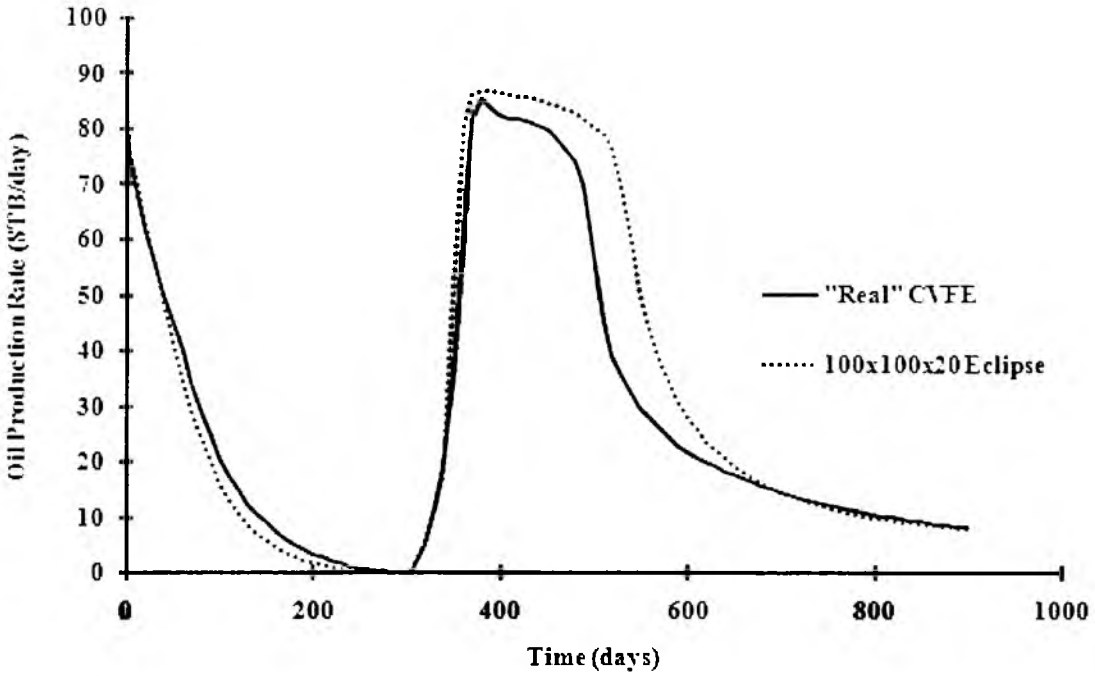

Figure 4.18 Oil production rate comparisons among homogenized (simplified) ECLIPSE simulation and CVFE simulation

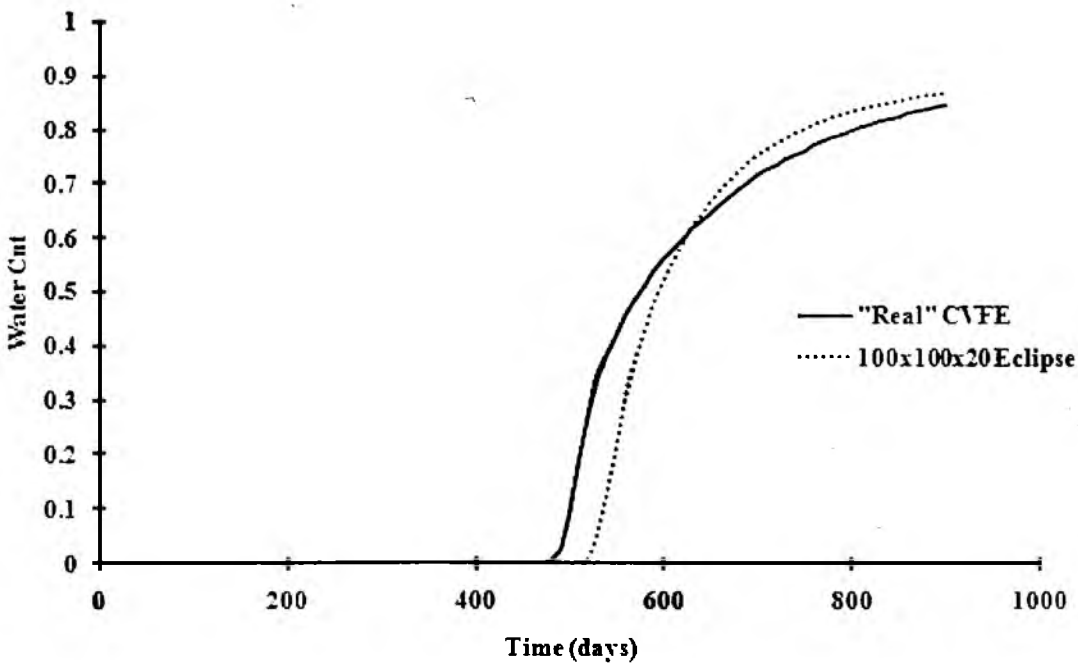

Figure 4.19 Water cut comparisons among homogenized (porosity only) ECLIPSE simulations and CVFE simulation

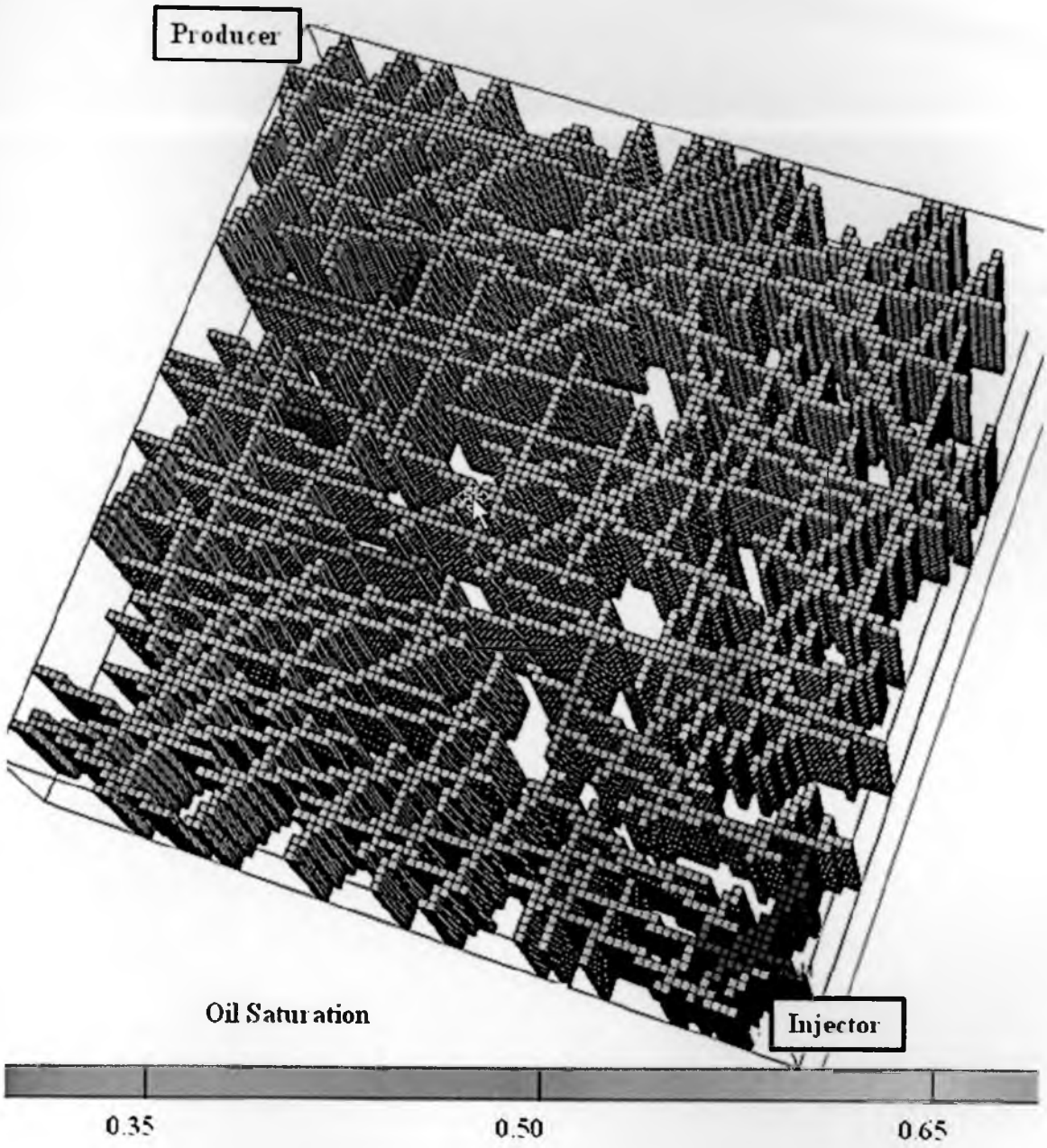

Figure 4.20 Oil saturation distributions for simplified fracture homogenization simulation (at day 900) by ECLIPSE

Figure 4.21 shows that the flow path through the homogenized grid block is longer than the DFN modeled fluid flow path. Compared to the CVFE results, this longer flow path partly explained the later water breakthrough by homogenized grid simulation. Since the only reservoir driving force was coming from the decreased pressure at the primary production stage, the oil production rate was almost identical for both the CVFE and the ECLIPSE simulations. During secondary production, water flooding becomes the major reservoir driving force. Figure 4.18 shows that both simulations reached a similar highest production rate, but the rate from the homogenized simulation is a little higher than the rate from the CVFE simulation. In this study, the homogenized grid-block permeabilities are just simply implied by constraining constant *kh* value from the fracture permeability. Mathematically, this simplified permeability is somewhat higher than its true value. This explains why the oil production rate in homogenized finite-difference simulation is higher than the rate from CVFE simulation.

Study in this section helped in understanding the basement reservoir in the following ways:

1) Running the fine-grid, porosity-homogenized, DFN-modeled basement reservoir through a conventional finite-difference simulator achieved reasonable accuracy as compared to the CVFE direct-DFN simulation results.

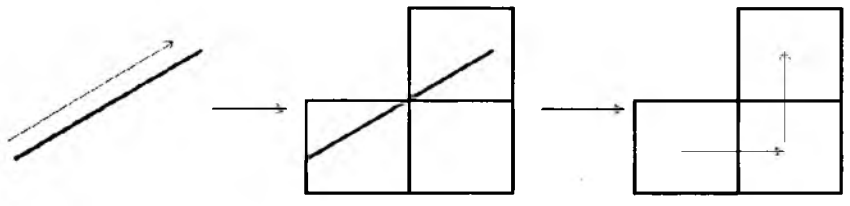

Figure 4.21 Fluid flow through fracture/fault represented by the equivalent grid blocks (DFN → homogenized DFN → homogenized grid blocks)

2) From the aspect of simulation efficiency, the CVFE simulator revealed its advantage over the homogenized ECLIPSE simulator: in the case of three-phase black-oil basement reservoir with 900 days simulation time, the CVFE simulator requires 28 minutes cluster time rather than 3259 minutes required by the ECLIPSE simulator.

4.7 Chapter Summary

This chapter was focused on upscaling the DFN-characterized fracture network model to its equivalent model. While the basement fracture network was made more irregular, results from DFN simulations differed considerably from the regularized ECLIPSE equivalent simulations. The ECLIPSE simulator cannot precisely simulate highly irregular basement fracture networks. However, the irregular fracture networks can be homogenized using a variety of approaches for the ECLIPSE simulator. These approaches include the geometric-based Oda method and the flow-based "Block K" method. The Oda method was applied to all of the homogenization studies in chapter. If the results from DFN simulation are correct, the results from the Oda homogenization show great sensitivity to grid-block size. Surprisingly, convergence was not achieved with finer grid-block size. This is due to the Oda method of permeability upscaling, and homogenization is more accurate when the single fracture penetrates the entire block diagonally (maximum penetration). A simple geometric homogenization scheme involved with fine mesh is achieved by assigning the permeability of the fracture to the block that it penetrated. This approach led to the homogenized results matching the DFN simulation results reasonably well but with high computing cost.

4.8 Nomenclature

A_{DFN}	=	fracture area, ft^2
b	=	exponential term in the power law relations
e	=	fracture/fault storage thickness, ft
e_i	=	i^{th} fracture storage thickness inside of certain grid cell, ft
h_x, h_y, h_z	=	grid block thickness, ft
$\mathbf{K}$	=	permeability tensor, md
k_{xx}, k_{yy}, k_{zz}	=	principal permeability, md
l_i	=	i^{th} fracture length inside of certain grid cell, ft
p	=	fluid pressure, psi
P_{32}	=	fracture intensity as fracture area per unit volume, ft^2/ft^3
P_{33}	=	fracture intensity,fracture volume per unit volume, ft^3/ft^3
$\mathbf{q}$	=	flux vector
V_{DFN}	=	fracture/fault volume, ft^3
$V_{GridBlock}$	=	grid block volume, ft^3
x_min	=	minimum x value in the power law relations, ft
Φ	=	porosity
$\Phi_{GridBlock}$	=	grid block porosity
σ	=	shape factor in the dual porosity model
ρ	=	density, lbm/ft^3
μ	=	viscosity, cp
δ_{ij}	=	Kronecker coefficient

4.9 Acknowledgments

The research described in this paper was supported by the U.S. Dept. of Energy through the National Energy Technology Laboratory Contract No. **DE-FC26-04NT15531.** The authors would also like to thank Golder Associates, Schlumberger for their academic software license support.

4.10 Bibliography

Aavatsmark, I., Barkve, T. and Mannseth, T.: "Control Volume Discretization Methods for 3D Quadrilateral Grids in Inhomogeneous, Anisotropic Reservoirs", paper SPE 38000, (1997)

Dershowitz, B., LaPointe, P., Eiben, T., Wei, L., "Integration of Discrete Feature Network Methods with Conventional Simulator Approaches", paper SPE 49069 (1998)

FRED User's Mannual, Golder Associate (2007)

Fu, Yao, "Multiphase Control Volume Finite Element Simulations of Fractured Reservoirs," Ph.D Dissertation, University of Utah, Salt Lake City (2007)

Fu, Y., Yang, Y.-K., Deo, M., "Three-Dimensional, Three-Phase Discrete-Fracture Reservoir Simulator Based on Control Volume Finite Element (CVFE) Formulation," paper SPE 93292, (2005)

Fung, L.S., Hiebert, A.D., and Nghiem, L.X., "Reservoir Simulation with a Control Volume Finite Element Method", paper SPE 21224 (1991)

Horne, R., and Raghavan, R., "Reservoir Description and Dynamics", *JPT* (Match 2004) 32-33

Lee, J., Kasap, E., and Kelkar, M.G., "Analytical Upscaling of Permeability for 3D Gridblocks", paper SPE 27875 (1994)
Liu, Y., Harding, A., Abriel, W., Strebelle, S., "Multiple-point Simulation Integrating Wells, Three-Dimensional Seismic Data and Geology", *AAPG Bulletin* (July 2004) v.88, No. 7, 905-921

Matthäi, S.K., Mezentsev, A., Belayneh, M., "Control-Volume Finite-Element Two-Phase Flow Experiments with Fractured Rock Represented by Unstructured 3D Hybrid Meshes", paper SPE 93341 (2005)

Ronald A. Nelson, "Geologic Analysis of Naturally Fractured Reservoirs", Gulf Professional Publishing, second edition (2001)

Sukirman, Y.B. and Lewis, R.W.: "Three-Dimensional Fully Coupled Flow: Consolidation Modeling Using Finite Element Method", paper SPE 28755, (1994)

Verma, S. and Aziz, K.: "A Control Volume Scheme for Flexible Grids in Reservoir Simulation", paper SPE 37999, (1997)

Yang, Yi-kun, "Finite-element Multiphase Flow Simulation," Ph.D Dissertation, University of Utah, Salt Lake City, UT (2003)

Young, L.C.: "An Efficient Finite Element Method for Reservoir Simulation", paper SPE 7413, (1978)

CHAPTER 5

MULTIPHASE SIMULATIONS OF FRACTURED BASEMENT RESERVOIR COMPOSED WITH SEISMIC AND SUBSEISMIC SCALE FEATURES

(A paper in preparation)

Huabing Wang[1], Tom Doe[2], a+nd Milind Deo[1]

1. Department of Chemical Engineering

University of Utah

Salt Lake City, UT 84112

2. FracMan Technology Group

Golder Associates Inc.

18300 NE Union Hill Road

Redmond, WA 98052 USA

5.1 Abstract

Due to the presence of highly heterogeneous, complex fracture networks, low permeability/porosity matrix with high permeability fractures, naturally fractured basement reservoirs have been known within the oil and gas industry for many years but were generally regarded as having "no economical potential." These reservoirs have now become legitimate targets due to an ability to better characterize the fracture networks, and understand the mechanics of flow. Since almost all the oil resides in fracture networks, discrete fracture network (DFN) model is one of the best ways to characterize the basement type reservoir. However, there are still some open questions about how to simulate the DFN modeled basement reservoir.

Basement reservoirs are often modeled using maps of faults imaged using the seismic method. Only large features are imaged and the reservoir is constructed using these trace maps. In discrete fracture network modeling, we are representing the significant fractures and faults as discrete features rather than as equivalent continua. Among the basic questions that we are addressing are:

1) How does fracture geometry and particularly fracture heterogeneity affect water oil displacement in the reservoir, and
2) Does rate affect recovery?

Given the influence of heterogeneity on water-oil displacement we are also looking at the influence of different heterogeneity types. In particular we are interested in identifying the influences of fractures that are not detected by seismic exploration. We refer to the fractures and fractures zones that are detected by seismic exploration as "seismic" fractures. However, we know that there are more fractures within the reservoir

that may contribute to both storage and connections. These undetected, but potentially significant fractures are the "subseismic" fractures.

In this study, a DFN based conceptual seismic and subseismic basement reservoir model was constructed with two vertical parallel seismic scale features and 117 uniform area subseismic scale features with different orientations. The seismic features were 1489 feet X 1489 feet. The area of each subseismic feature is about 3.86% of the seismic feature. All seismic and subseismic features are well connected. The distance between the two seismic features is 1000 ft. This conceptual model could be treated as a portion of a giant basement reservoir model with granite/basalt formations. Five sets of simulations have been performed in order to study water oil displacement mechanisms for such a reservoir to address the following central questions.

1) What influence does the subseismic feature permeability have on displacement? In this set, simulations with different subseismic feature permeabilities were compared.
2) How does oil distribution in seismic/subseismic features affect recovery and water cut behavior? This is one of the most pertinent questions in the recovery of oil from basement reservoirs. In these sets of simulations, the distribution of oil in the seismic and subseismic features was varied.
3) How does the system behave when porosities and permeabilities are depth dependent? Often, in basement systems, porosities and subsequently permeabilities are lower at increasing depths. What are the characteristics of recovery under these realistic conditions?

4) How does rate influence recovery? This is another important question that relates to the operational aspects and reservoir management.

Constant seismic feature bottom water support is applied in all simulations.

5.2 Introduction

Seismic measurements are used to map the locations of the major features in basement reservoirs. These features can be brought into a DFN model for the multiphase flow simulations purpose. Will et al. (2005) reported a method of integration of seismic anisotropy attributes with reservoir-performance data for characterization of naturally fractured reservoir using DFN approach. However, it is recognized that the seismic mapping technique is able to pick out features larger than a certain size. Since most of the basement reservoirs exist in the deep formations (over 2000 meters), most high frequency seismic waves will be lost during the seismic reflecting survey and cannot reach the objective basement formation. In most cases, low frequency seismic method is adopted as the method to do basement reservoir seismic survey. The low frequency seismic waves usually result in limited detection and resolution scale and during interpretation only large size faults in the basement reservoirs are observed. Due to this, the smaller subseismic scale features cannot be represented in conventional deterministic modeling (Araujo et al., 2004). But subseismic scale features do exist in the basement reservoirs. One of the primary questions is: what is the relative importance of the subseismic features in oil storage and displacement?

Other than the seismic and subseismic issues, characterization of the petrophysical properties of fractured basement reservoirs is challenging. Behrenbruch et al. (1995) report large variations in oil properties of basement reservoirs offshore of

Vietnam with depth varied from 1750 to 2440 meters. Sibbit (1995) quantified porosity from well logs in fractured basement reservoir and estimated permeability from that field. Li et al. (2004) describes that permeability is one of the most difficult parameters to assess in a reservoir and it is even more challenging when it is the basement reservoir. They also report on a method to quantitatively evaluate basement reservoir's permeability based on image logs with the integration of other open-hole logs, mud gas data, drilling data, dynamic well testing and production logging data.

In the DFN (Dershowitz et al., 1998; Basquet et al, 2005; Araujo et al., 2004) approach, the geometry of the fracture network is explicitly modeled and a realistic way of modeling basement reservoir performance is provided. However, these DFN descriptions are generally too detailed and geometrically complex to be simulated by conventional reservoir simulators. Some research has been done by connecting DFN with a dual-porosity model for the case of single-phase flow by Dershowitz (1998). This approach is limited to single-phase flow and no multiphase flow study has been reported.

One serious consideration for the production of oil from basement reservoirs is excess water production which not only reduces the artificial lift efficiency, but also damages the oil zones (Chan et al., 2006). A detailed study of multiphase flow in basement reservoirs has not been reported.

In this study, an upstream flux weighted three-dimensional, two-phase (oil, water) black oil CVFE simulator is developed and employed (Yang, 2003; Fu et al., 2005). This CVFE formulation has been validated and verified through various methods: indexing method (Chapter 3); manufactured solution method (Yang, 2003; Fu et al., 2005); core-scale verifications with Pooladi-Davish and Firoozabadi's (2000) fracture water level

experiment (Chapter 7). The flux-based upstream-weighting function on CVFE discretization formulation is good at handling rotatable permeability tensor. This makes the direct accurate simulation of DFN modeled fractured basement reservoir possible.

With the same fluid-rock data set and boundary conditions, five sets of multiphase simulations were performed on the same basement reservoir domain based on various assumptions related to the seismic and subseismic features' characteristics.

5.3 Governing Equations

The equations describing compressible two-phase flow are obtained by combining Darcy's law and mass conservation for each phase, and have been discussed in Section 3.3. The only difference between three-phase and two-phase systems is the existence of the gas phase. Since the dynamics of water injection was the subject of this study, two-phase, oil-water system was used.

5.4 Modeling the Fractured Basement Reservoir

5.4.1 The Seismic and Subseismic Basement Reservoir Geological Model

As Figure 5.1 shows, the conceptual seismic and subseismic scale basement reservoir model is composed of two vertical parallel seismic scale features and two sets of well-connected subseismic scale features. There are two seismic features and two sets of subseismic scale features. Detailed feature information is summarized in Table 5.1.

This domain was constructed under the FRED working environment. The isolated fractures were removed during the domain construction. HyperMesh was applied for the domain meshing. Adaptive meshing method was chosen to have the complex area fine meshed but have the simple area with the coarse meshed.

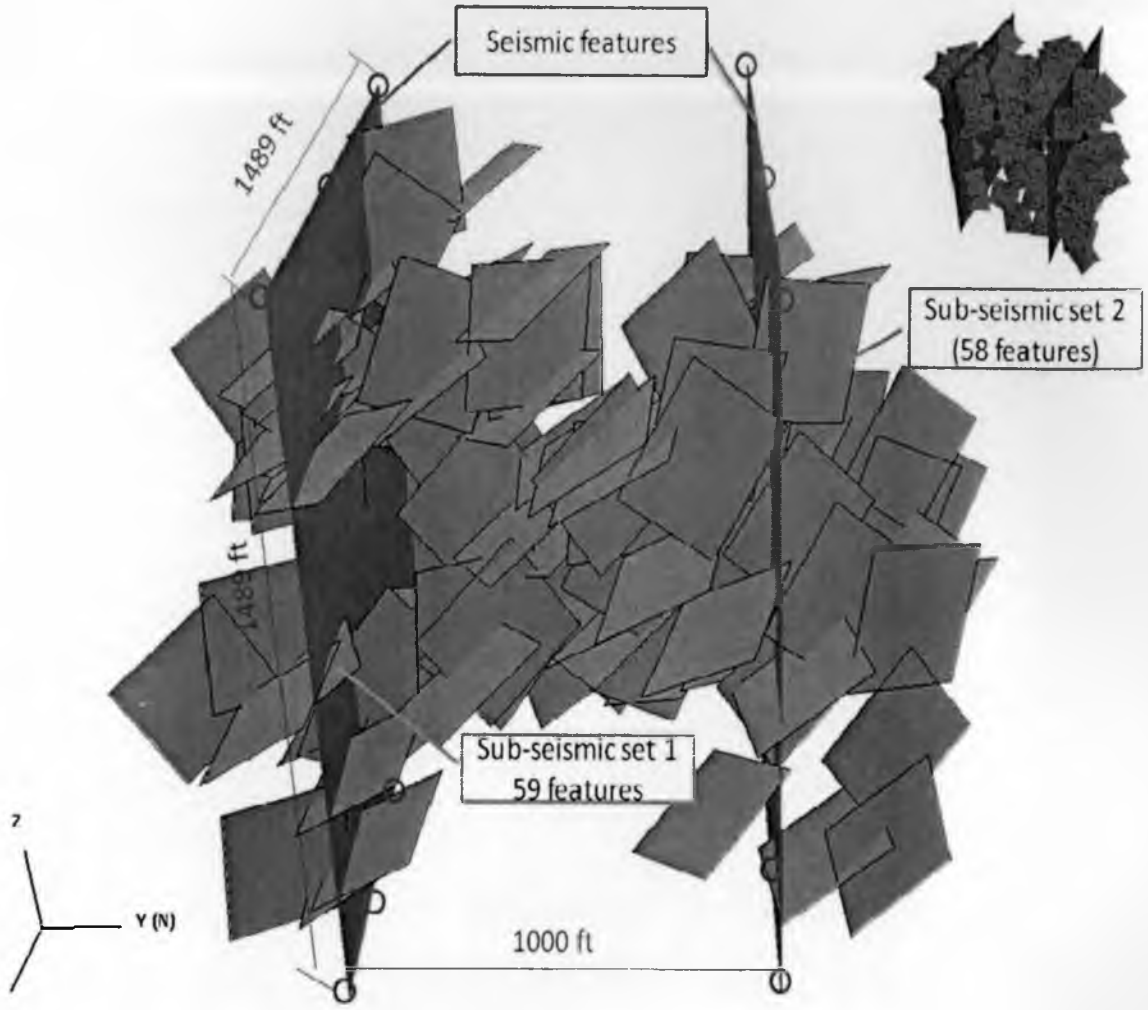

Figure 5.1 Illustration of the basement reservoir domain composed by seismic features and subseismic features

Table 5.1 Summary of seismic and subseismic features

	Seismic features	**Subseismic set 1**	**Subseismic set 2**
Number of features	2	59	58
Total feature area (ft^2)	4433290	5046262	4960732
Mean orientation	180, 0	0, 60	240, 0
Equivalent Radius mean (ft)	840	165	165
Equivalent radius std dev	1.5E-5	5.3E-6	3.5E-6
Area mean (ft^2)	2216645	85530	85230

Based on the above feature summary, the area of each subseismic feature is about 3.86% of each seismic feature. Seismic feature area occupied 30.7% of total area and the rest 69.3% belongs to subseismic features. The feature thicknesses are varied from case to case for the purpose of adjusting reservoir storage. It will be addressed in the separate case studies later. If the same thickness is used for all the features, the storage in the reservoir will be distributed in proportion to the area (which is about 30/70 from seismic to subseismic size features).

5.4.2 Other Model Parameters

Other than the geological model, there are several other factors that influence the behavior of a producing reservoir, which must be incorporated in the modeling effort to understand their relative importance. Several property sets are required in order to perform the multiphase flow simulations.

1) Reservoir property model: the key to DFN simulation is the assignment of reservoir properties (porosity, permeability, thickness, compressibility) to the features of the geologic model. These properties are either homogeneous or they are varied according to geologic expectations as discussed below.
2) Phase model: this includes two-phase (water and oil) properties such as end-points on the relative permeability curves and initial fluid saturations.
3) Fluid property model: fluid properties include fluid viscosity, compressibility, density, and formation volume factor.

Table 5.2 Summary of reservoir data for modeling seismic and subseismic featured basement reservoir

Simulator	**CVFE**			
Grid information				
Number if nodes	3690			
Number of triangular elements	6846			
Fluid property	Water			oil
γ (lbf/ft^3)	62			53
Fluid data				
	Water properties*			***Oil properties****
Reference pressure (p_{ref}, psi)	14.7			4850
formation volume factor B_r @ reference pressure (rb/stb)	**1.0**			1.17
Compressibility C_B (1/psi)	3 e-6			1e-6
Water viscosity (μ_r) @ reference pressure (cp)	**0.3**			1.0
C_μ (1/psi)	0.0			0.0
Rock-fluid data				
Oil-water system				
	S_w	k_{rw}	K_{ro}	p_{cow} (psi)
	0.20	0.00	1.00	7.0
	0.30	0.07	0.40	4.0
	0.40	0.15	0.125	3.0
	0.50	**0.24**	0.0649	2.5
	0.60	**0.33**	0.0048	2.0
	0.80	0.65	0.00	1.0
	0.90	0.81	0.00	0.2
Initial conditions				
P (psi)	4300			
S_w	0.2			
Boundary conditions	Constant seismic feature bottom water pressure support: 6 water injection wells on the bottom of two seismic features (3 on each) which are operated as 4500 psi bottom-hole pressure (BHP) control. Nonflow boundary conditions other than seismic feature bottoms			
Production wells	6 production wells are chosen on the top of seismic scale features (3 on each seismic feature, two on the corners and one on the middle, as shown on the geological model illustrations (red circled on the top))			

* Reservoir fluid properties (pressure related) are calculated by the following equations:

$$B = B_r \exp\left[-C_B(P - P_{ref})\right] \tag{5-1a}$$

$$\mu = \mu_r \exp\left[-C_\mu(P - P_{ref})\right] \tag{5-1b}$$

4) Boundary conditions: the behavior of the model may be strongly influenced by the boundary conditions that are assumed for the fractured basement. The boundaries are usually considered as nonflow or constant pressure features.
5) Discretized mesh: in the numerical simulation the DFN based reservoir domain has to be meshed into triangles along each feature. The conformal nodes and sides of intercrossed features have to be honored for the purpose of fluid flow computations.

Some reservoir properties are varied in different case studies and the details will be discussed later. Other reservoir parameters which were held constant throughout the simulations are summarized in Table 5.2.

As shown in Table 5.2, the bottom supporting water boundary conditions could either be treated as water injectors or the bottom aquifer support. Some type of water aquifer support is evidenced in a number of basement reservoirs world-wide.

5.5 Case Studies

5.5.1 Base Case Simulations to Choose the Production Well Operating Strategy

In this model, we assume both seismic and subseismic features have constant porosity (30%) and thickness. A set of simulations were carried out to pin down the operating conditions. The initial average reservoir pressure was set at 4300 psi with 4500 psi bottom water support on the seismic features. The vertical drop was about 1500 ft equivalent to a hydraulic head of about 675 psia. A 4500 psi bottom water support pressure will give about 3825 psi static pressure at the top of the reservoir. Under these conditions, the bottom-hole pressures at which the producers operate will have to be

determined. In these simulations, the reservoir has about 0.72 MMSTB (million stock tank barrels) oil in place. Three different production pressures, 3500/2500/1500 psi, were examined with two sets of fracture permeabilities. In set 1 seismic and subseismic feature have the same permeability – 100,000 md. and in set 2 the seismic features have 100,000 md permeability and the subseismic features have 1,000 md permeability). Therefore, there are six simulations in this base case study in total, which are identified in Table 5.3.

The following questions are being addressed in these simulations.

1) Do operating parameters significantly impact the production behavior?
2) Even when the properties are homogeneous, does a permeability contrast (between seismic and subseismic features) make a significant difference in performance?

The oil recovery comparisons, shown in Figure 5.2, depict two distinct sets of oil recovery results due to the difference in permeability of subseismic features. Obviously, higher subseismic feature permeability results in higher oil recovery at a given time.

Table 5.3 Summary of reservoir properties and operating conditions for case 1 set of simulations

	K1A	K1B	K1C	K3A	K3B	K3C
Porosity	0.3	0.3	0.3	0.3	0.3	0.3
Thickness (ft)	1.4	1.4	1.4	1.4	1.4	1.4
Permeaiblity (md) (seismic)	100,000	100,000	100,000	100,000	100,000	100,000
(subseismic)	100,000	100,000	100,000	1,000	1,000	1,000
Producer's pressure (psi)	3,500	2,500	1,500	3,500	2,500	1,500

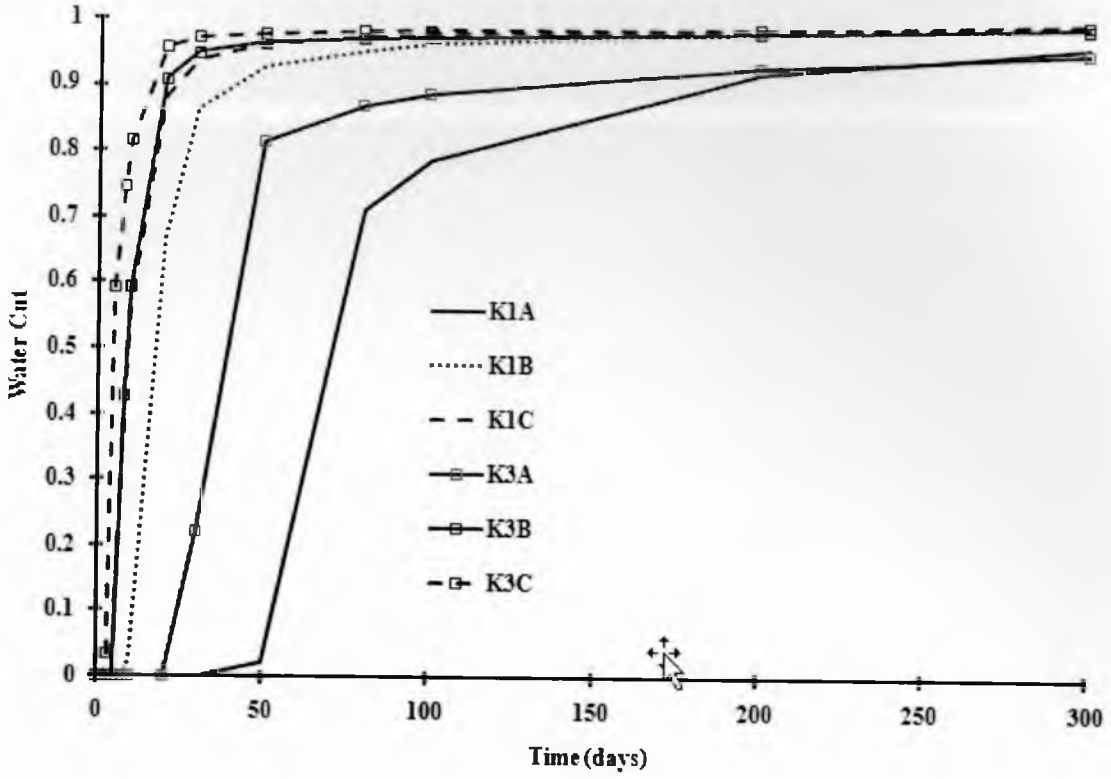

Figure 5.2 Comparison of oil recovery for case 1 set of simulations

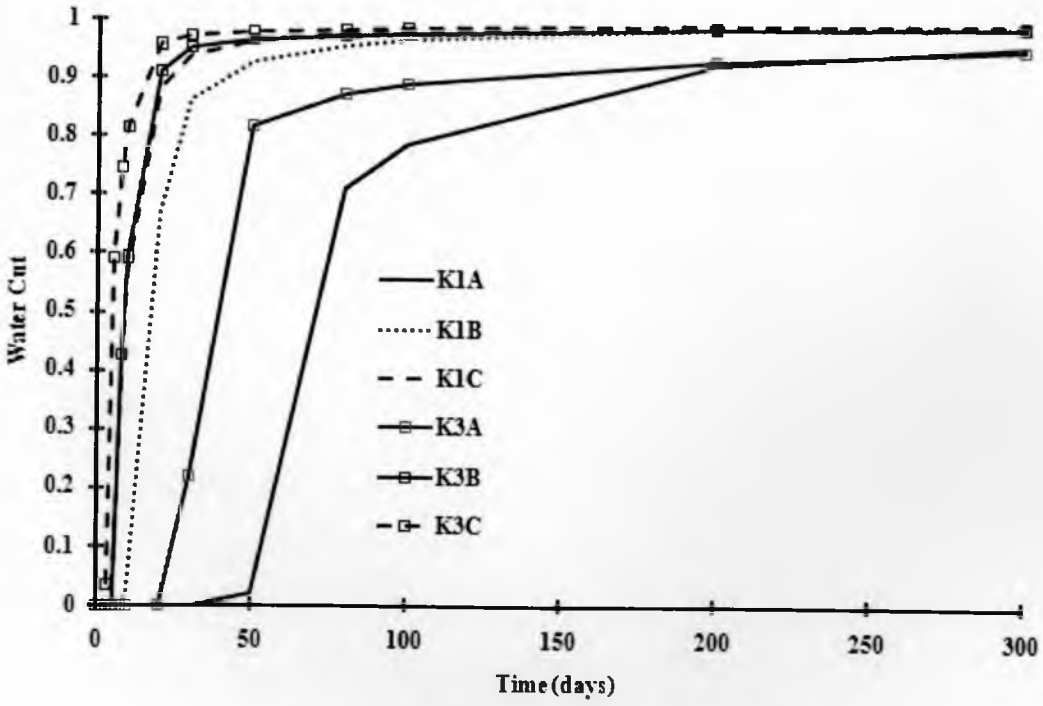

Figure 5.3 Comparison of water cut versus for case 1 set of simulations

The water cut picture is a bit more complex (Figure 5.3). The slowest breakthrough is obtained when the subseismic permeability and the producer BHP are the highest. The water arrives early in cases where the permeability and producer pressures are lower because a higher water drawdown is created and the water velocity through the system is higher. Since the water cut on day 2,000 is almost 1 in all the cases, the ultimate recoveries for the six simulations are can be summarized as in Table 5.4.

The high and the low permeability scenarios can be treated as extreme cases of permeability variation in the next sets of simulations. The highest producer pressure was chosen for further simulations to limit the impact of rate of water rise. The rate effect was studied separately by using explicit production rates in the producers.

In this multiscale system where the properties of each of the subsystems are homogeneous, some observations could be summarized as follows.

1) There is significant impact of the permeability of the subseismic features. Lower subseismic permeabilities result in lower recoveries and quicker breakthroughs for the same drawdown.
2) Recovery is not impacted by drawdown (lower producer pressures), but breakthrough is quicker with a steeper drawdown.

In reservoirs with significant vertical extent, the displacement of oil (the lighter fluid), with water (the heavier fluid) is gravity dominated. The relative magnitude of prevailing gravity forces to viscous forces is given by the gravity number (N_G) (Shook et al., 1992; Kulkarni et al., 2006).

Table 5.4 Case 1 simulation summaries at the end of simulations (day 2,000)

	K1A	K1B	K1C	K3A	K3B	K3C
Recovery factor, R	0.60	0.61	0.61	0.46	0.47	0.48

$$N_G = \frac{\Delta\rho.g.\mathbf{k}/\emptyset}{\mu_o.v} \tag{5-2}$$

It is known that as the gravity number increases, so does recovery in gravity dominated systems. Another way of looking at this is that sufficient time is made available for gravity to take effect. As the system permeability decreases, so do the gravity number and the recovery decreases. When the drawdown increases, the velocity increases, reducing the gravity number, but not sufficiently to lower recoveries significantly.

5.5.2 Case 2: OOIP Distribution Based on Thicknesses of Seismic and Subseismic Features

All the simulations were performed with a constant BHP of 3500 psi in the producers. The sets of simulations in this section were designed to address the central question of how different oil distributions in the two subsystems impacted recovery. Three different distributions of 80/20, 50/50 and 20/80 in the seismic and subseismic features were created. These proportional distributions were created by adjusting the thickness of seismic features and subseismic features, even with constant thicknesses for each of those systems.

Since the areas of total seismic and total subseismic are known, and with constant porosity (30%) the OOIP distribution is directly proportional to the pore volume or product of area and thickness. These relations could be described from Equation (5-3) to Equation (5-6):

$$\text{PV (pore volume)} = \text{S(Area)} \times \text{e (thickness)} \times \phi \text{ (porosity)} \tag{5-3}$$

$$\frac{PV_{seismic}}{PV_{subseismic}} = \frac{S_{seismic} \times e_{seismic}}{S_{subseismic} \times e_{subseismic}} \tag{5-4}$$

$$PV_{total} = PV_{seismic} + PV_{subseismic} \tag{5-5}$$

$$OOIP = PV \times S_{oil} \tag{5-6}$$

Based on the above relations and known parameters, six simulations were built in this case study as shown in Table 5.5.

More or less ultimate recoveries were reached by day 2000 and these are shown in Table 5.6. The ultimate oil recoveries have large variations from set to set as shown in Figure 5.4 and Table 5.6. The significant results are discussed below.

Table 5.5 Summary of reservoir properties and operating conditions on case 2 studies

	8020K1A	**8020K3A**	**5050K1A**	**5050K3A**	**2080K1A**	**2080K3A**
Porosity	0.3	0.3	0.3	0.3	0.3	0.3
Thickness (ft)						
(seismic	**3.6**	**3.6**	2.3	2.3	0.9	0.9
features)	**0.4**	**0.4**	1.0	1.00	1.6	1.6
(subseismic features)						
Permeaiblity						
(md)	100,000	100,000	100,000	100,000	100,000	100,000
(seismic)						
(subseismic)	100,000	1,000	100,000	1,000	100,000	1,000

Note: "8020" means 80% OOIP in seismic features and 20% OOIP in subseismic features

Table 5.6 Recovery comparisons from case 2 sets of simulations

	8020 K1A	**8020 K3A**	**5050 K1A**	**5050 K3A**	**2080 K1A**	**2080 K3A**
Recovery, R	0.70	0.68	0.64	0.55	0.57	0.41

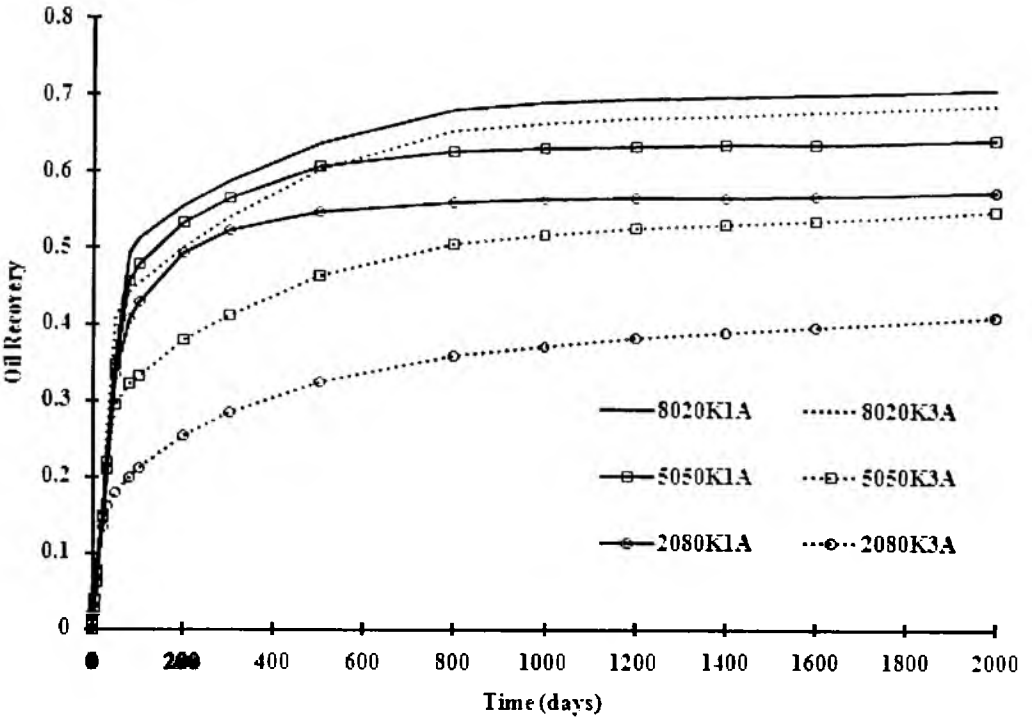

Figure 5.4 Comparisons of oil recovery versus simulation time for case 2 studies.

Comparing different OOIP distributions with same permeability in the seismic and subseismic features:

1) When the permeability is held high (100,000 md), the oil recovery decreases as more oil is distributed into the subseismic features. The gravity number analysis provided earlier was established for conventional matrix-dominated porous media. The gravity number is affected only to the extent to which the Darcy velocity in the system is impacted. As more oil is distributed into the seismic features, the vertical velocity through the system is lower (as indicated by later breakthroughs shown later). However, this decrease is not sufficient to explain the significant decline in recovery (from 71% at 80/20 to 54% at 20/80). What we are seeing here is the reduction in recovery related to the geometry and connectivity of the fracture system.

2) When the permeability in the subseismic features is reduced to 1000 md, the trend described above becomes even more exaggerated. The recovery decreases from 68% for the 80/20 distribution to 55% for the 50/50 distribution, and to 41% for the 20/80 distribution. Once again this is related the reduced gravity numbers as the velocity through the system increases. But superposed on this is the geometric effect of the fracture network, which becomes more of a factor, as the permeability in the more numerous subseismic features is reduced in comparison to the seismic features.

Comparing different permeability with same OOIP distributions in the seismic and subseismic features:

1) When the subseismic features have only 20% of the oil, reducing their permeability does not impact recovery significantly, as evidenced by 68% recovery for the 1000 md case compared to 70% for the 100,000 case. This should be compared to the previous case study where 70% of the oil was in the subseismic features and a difference in recovery of about 7% was observed. The gravity number in these comparisons is affected both by permeability and velocity, and it is surprising to see little change in recovery. This underscores the importance the characterization of fracture networks and their properties.
2) As more and more oil is distributed into the subseismic features the recovery difference between the two permeability cases widens (9% for 50/50 and 16% for 20/80). Thus not only knowledge of the hydrodynamic parameters of the

system is important (permeability, viscosity, velocity, etc.), but also the fracture characterization and connectivity.

As shown in Figure 5.5, the water breakthrough times are related directly to the average water advance velocity in the system. As more oil is distributed in the subseismic features or as the permeability of the subseismic feature is reduced, the water advance velocity increases (on the average, since this is a highly complex function of saturation, location and time) leading to earlier breakthroughs. These earlier breakthroughs are the cause of lower recoveries at a given time.

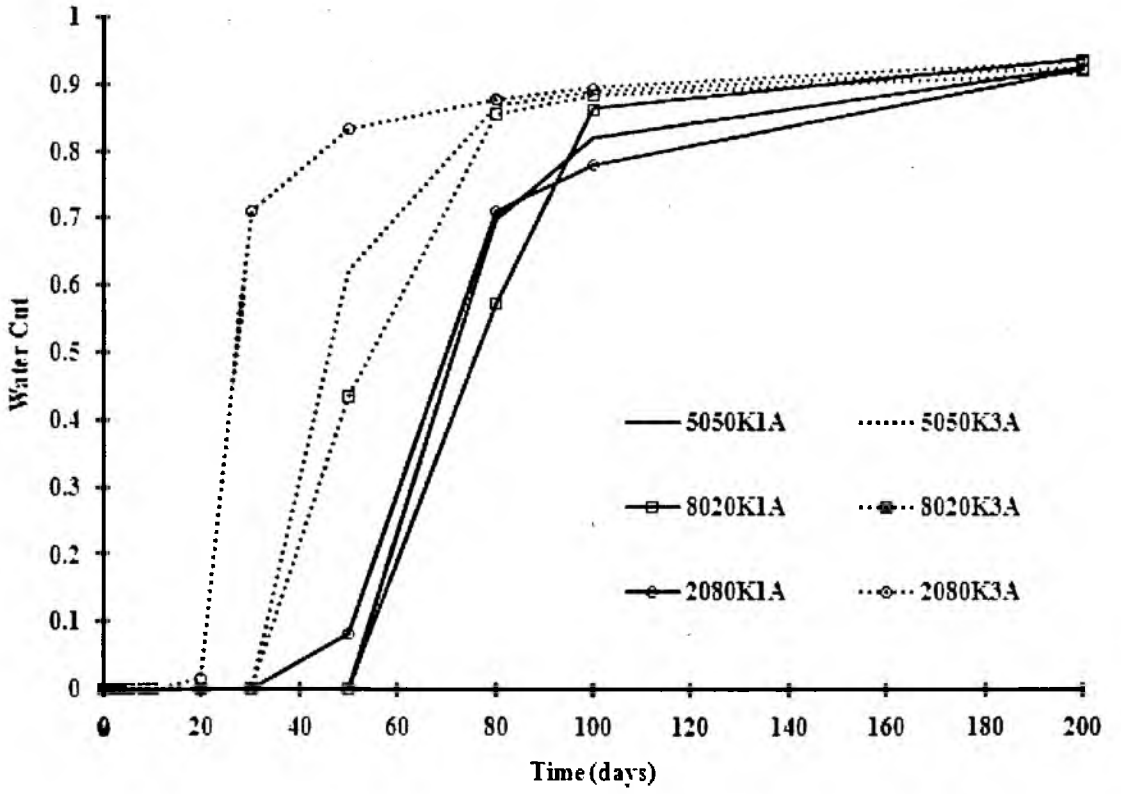

Figure 5.5 Comparisons of water cut versus simulation time for case 2 studies with different time scales.

5.5.3 Case 3: Depth Dependent Reservoir Porosity and Permeability Distributions

Both case studies discussed above have basic assumptions of constant porosity distributions and constant permeability distributions vertically either in seismic scale features or subseismic scale features. Basement reservoirs are highly complex structures, and with the vertical drop of 1,500 ft they are comprised of different formations and sedimentary layers geologically. The fracture/microfracture porosity changes very strongly with depth as reported by Chan et al. (2006). In this case study, two depth dependent basement porosity models are presented and the permeability is correlated with porosity distributions.

The depth dependent porosity and permeability correlations are shown in the Figure 5.6. For porosity, two models (linear and nonlinear) are presented in the range of 90 ~ 10% from the top reservoir surface to the bottom of reservoir. Based on the porosity value, permeability of both the seismic and the subseismic features is calculated by correlating with porosity values. An assumption here is the permeability only depends on porosity value no matter the size of the feature. The nonlinear porosity distribution function is defined in Equation (5-7):

$$\Phi = 0.511405 - 0.05625 \ln (D) \tag{5-7}$$

where Ø is the porosity and D is the depth from the top reservoir surface. This equation ensures that with total depth of 1500 ft, the porosity would be distributed from 90% to 10% vertically.

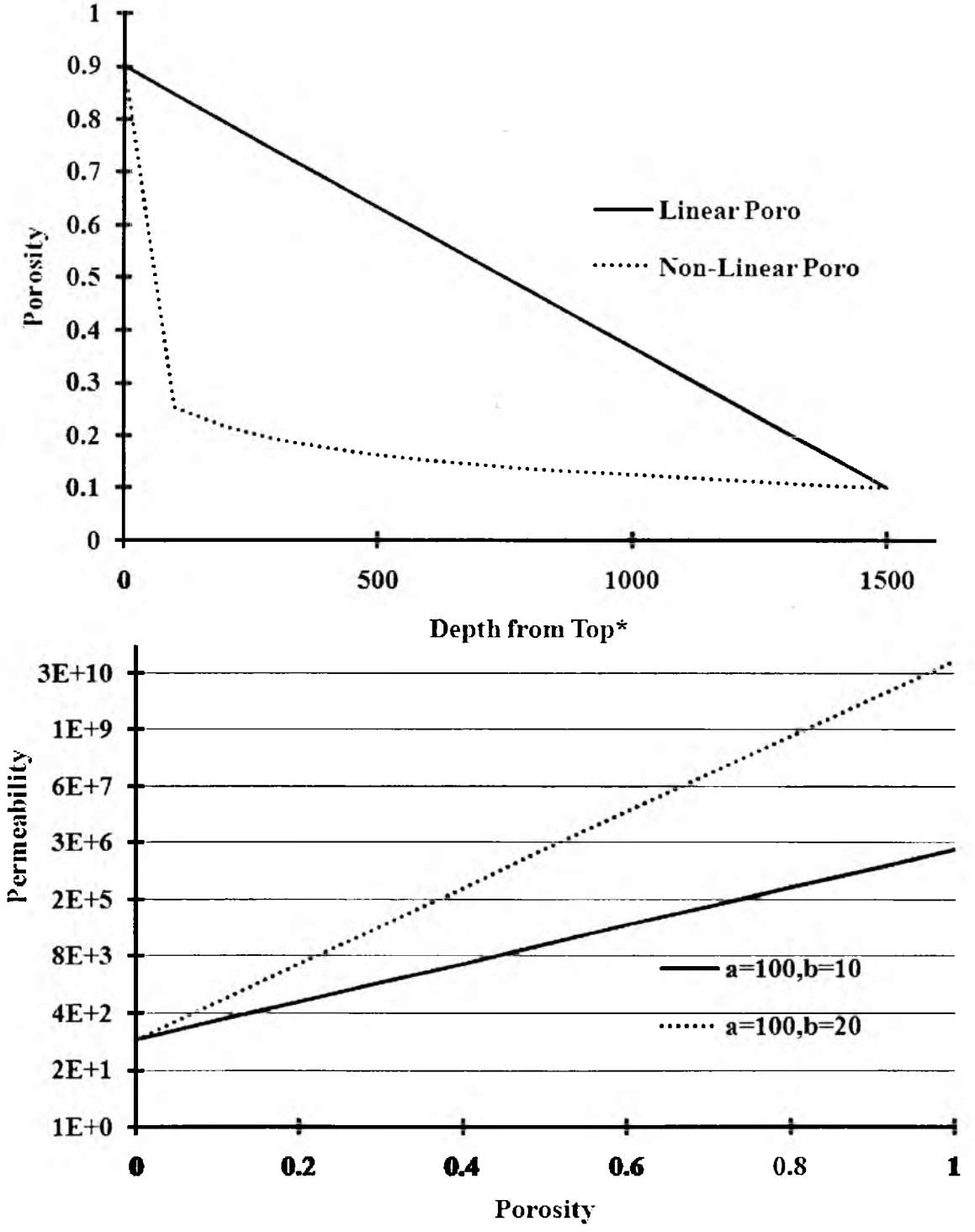

Figure 5.6 Depth dependent porosity and permeability.

The permeability correlation is defined in Equation (5-8):

$$K = a * \exp(b * \Phi) \tag{5-8}$$

where K is the permeability and a and b are the constants as shown in Figure 5.6.

Three different correlations were examined.

1) Linear porosity with permeability correlation 1 (a = 100, b = 10);

2) Nonlinear porosity with permeability correlation 1 (a = 100, b = 10);

3) Nonlinear porosity with permeability correlation 2 (a = 100, b = 20).

The resultant reservoir property distributions in these case studies are summarized in Table 5.7.

The figures of oil recovery and water cut versus time are shown in Figure 5.7 and 5.8. Some reservoir properties have also been shown in the above table. The difference of the upper porosity limit (0.9 (linear porosity) versus 0.46 (nonlinear porosity)) is due to the strong changes of in porosity due to the implementation of nonlinear porosity equation near the top surface. Since the meshed triangle element center coordinates have been used as depth data in those calculations, depth (from top surface) of 2.49 ft from the top surface could result in 46% porosity with nonlinear porosity distributions and 89% porosity on the linear case. This is the reason to choose the permeability correlation 2 as another option for nonlinear porosity correlated permeability. This makes simulation "*DepthNonLinearK2A*" have the same permeability magnitude with "*DepthLinearK1A*".

Table 5.7 Summary of reservoir properties and operating conditions on case 3 studies:

	DepthLinearK1A	**DepthNonLinearK1A**	**DepthNonLinearK2A**
Porosity	0.1 ~ 0.89	0.1 ~ 0.46	0.1 ~ 0.46
Permeability (md)	294 ~ 744759	273 ~ 3520	748 ~ 123884
Thickness (ft)	0.8	2.79	2.79
OOIP (MMSTB)	0.72	0.72	0.72

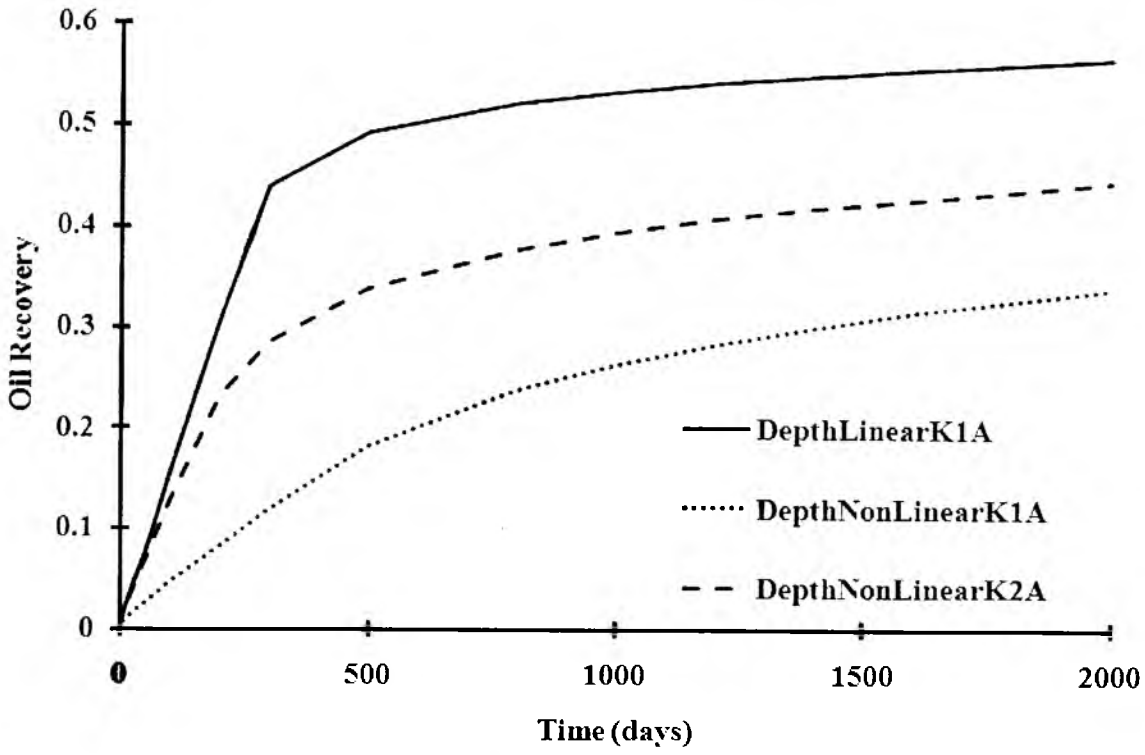

Figure 5.7 Comparisons of oil recovery versus simulation time for case 3 studies.

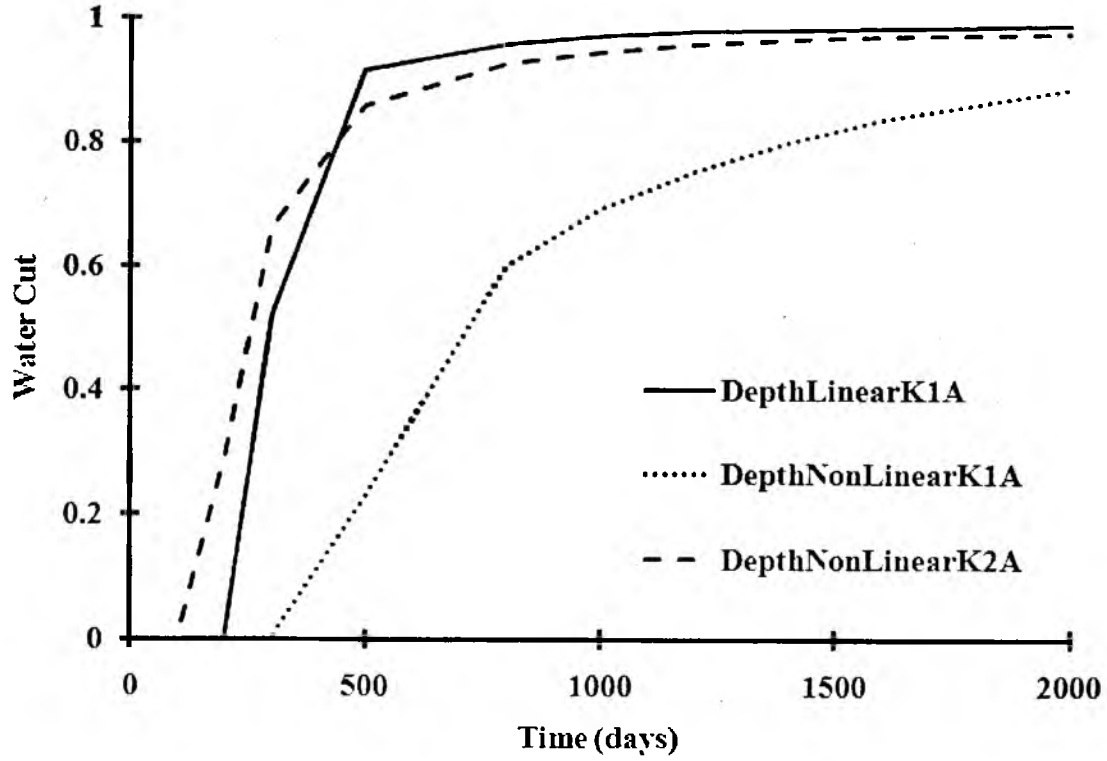

Figure 5.8 Comparisons of water cut versus simulation time for case 3 studies.

The *DepthNonLinearK1A* has a very narrow and low permeability distribution. As a result, it has the least recovery, but later breakthrough. It is difficult to characterize the gravity number for these displacements – some sort of permeability averaging will have to be employed. At the end of simulation (day 2,000), the oil recoveries were: *DepthLinearK1A* (56% of OOIP); *DepthNonLinearK1A* (33% of OOIP); *DepthNonLinearK2A* (44% of OOIP).

Figure 5.9 explained the observation of early breakthrough and lower recovery that happened in the case *DepthNonLinearK1A*. This phenomenon was caused by relative low permeability distributions in the case of *DepthNonLinearK1A* than in other cases.

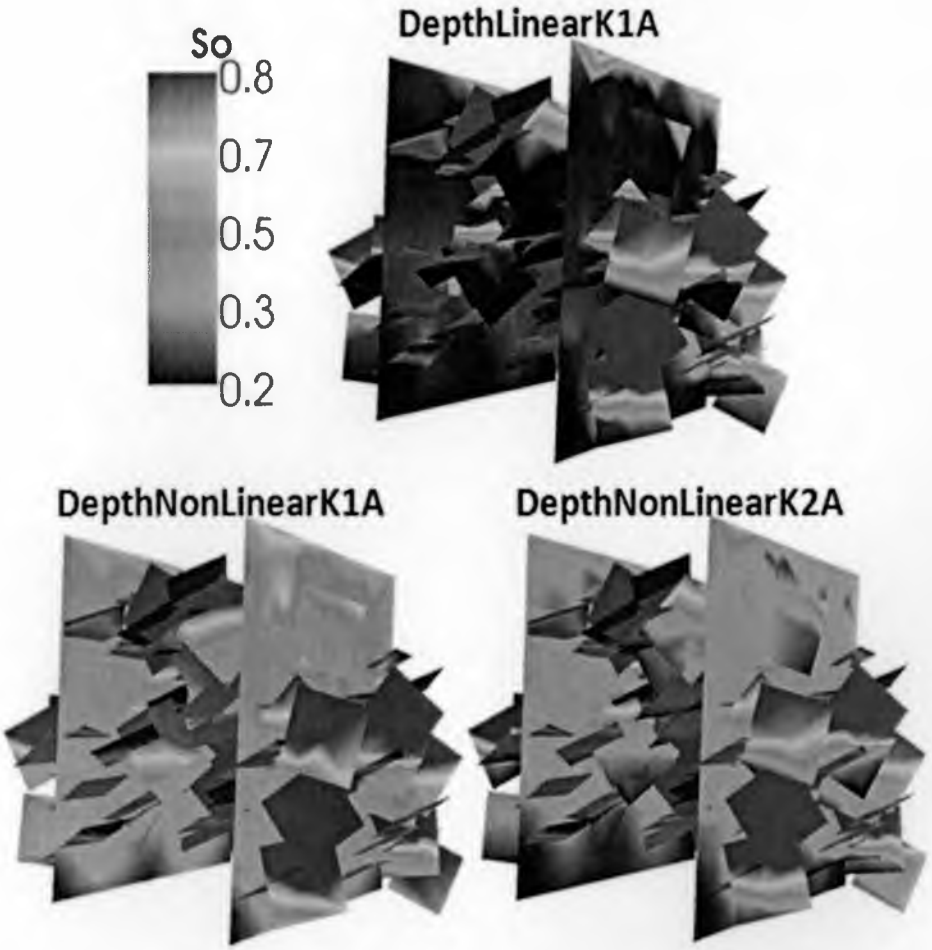

Figure 5.9 Oil saturations at the end of simulation

Some points could be highlighted from this case study:

1) Realistic depth dependent petro-physical properties can be employed in populating the basement domains created in the DFN models.
2) Increased heterogeneity, particularly with narrow tight distributions peaking at lower permeability values, results in lower recoveries, but later breakthroughs. It is difficult to pinpoint the reason for the later breakthrough with such low recoveries, but it may be related to the narrow, low permeability distribution, and geometric trapping due to this combination.

5.5.4 Case 4: Depth Dependent Reservoir Properties with Proportional OOIP Distributed in Seismic and Subseismic Features

Both oil distributions and heterogeneous property distributions had significant impact on oil production from basement systems. In this section, we combine the two effects to see the impact on oil recovery. Distributions are characterized using the relationships from Equation (5-9) to Equation (5-16).

$$OOIP = S_{oil} * PV \tag{5-9}$$

$$S_{oil} = 20\% = \text{constant} \tag{5-10}$$

$$PV = S * e * \phi \tag{5-11}$$

$$PV_{total} = PV_{seismic} + Pv_{subseismic} \tag{5-12}$$

$$PV_{seismic} = S_{seismic} * e_{seismic} * \emptyset_{seismic}$$

$$= \sum_i S_{seismic,i} * e_{seismic,i} * \emptyset_{seismic,i} \quad (5\text{-}13)$$

$$PV_{subseismic} = S_{subseismic} * e_{subseismic,i} * \emptyset_{subseismic}$$

$$= \sum_i S_{subseismic,i} * e_{subseismic,i} * \emptyset_{subseismic,i} \quad (5\text{-}14)$$

$$e_{seismic} = \text{const}; \quad (5\text{-}15)$$

$$e_{subseismic} = \text{const}; \quad (5\text{-}16)$$

where S is the area; e is the thickness; $\emptyset$ is the porosity, subscript i is the discretized finit-element i. Therefore, the ratio of original oil in place can be defined in Equation (5-17)

$$\frac{OOIP_{seismic}}{OOIP_{subseismic}} = \frac{PV_{seismic}}{PV_{subseismic}}$$

$$= \frac{\sum_i S_{seismic,i} * e_{subseismic} * \emptyset_{seismic,i}}{\sum_i S_{subseismic,i} * e_{subseismic} * \emptyset_{subseismic,i}} \quad (5\text{-}17)$$

From Equations (5-9) to (5-17), various OOIP distribution relations can be derived for proportional OOIP distributions between seismic and subseismic features, as shown in Equation (5-18) to Equation (5-20).

80/20 (80% OOIP in seismic features, 20% in subseismic features):

$$\frac{e_{seismic}}{e_{subseismic}} = \frac{4 * \sum_i A_{subseismic} \emptyset_{subseismic}}{\sum_i A_{seismic} \emptyset_{seismic}} \quad (5\text{-}18)$$

50/50 (50% OOIP in seismic feature, 50% in subseismic features):

$$\frac{e_{seismic}}{e_{subseismic}} = \frac{\sum_i A_{subseismic}\emptyset_{subseismic}}{\sum_i A_{seismic}\emptyset_{seismic}} \tag{5-19}$$

20/80 (20% OOIP in seismic feature, 80% in subseismic features):

$$\frac{e_{seismic}}{e_{subseismic}} = \frac{\sum_i A_{subseismic}\emptyset_{subseismic}}{4*\sum_i A_{seismic}\emptyset_{seismic}} \tag{5-20}$$

The same as in case study 3, two sets of depth dependent porosity and permeability distributions were chosen in this case study:

1) Linear porosity with permeability correlation 1 (a=100, b=10): *LPK1A*;
2) Nonlinear porosity depth dependent with permeability correlation 1 (a=100, b=10): *NLPK1A*;
3) Nonlinear porosity depth dependent with permeability correlation 1 (a=100, b=20): *NLPK2A*.

Three property models plus three OOIP distribution relations generate nine simulation sets and are summarized in Table 5.8.

Oil recovery and water cut with time are shown in Figures 5.10 and 5.11, and the comparisons are summarized in Table 5.9. Looking at oil recoveries, it appears that for a given property distribution (say NLPK1A), the three OOIP distributions fan out and provide a range of outcomes. At 80/20 in this case, the recovery is highest and breakthrough most delayed, while at 20/80 the recovery the least the breakthrough fastest. If we observe different property distributions at the same OOIP distribution, the tightest distribution with least permeability NLPK1A has the least recovery, but the late

Table 5.8 Summary of reservoir properties and operating conditions for case 4 sets of simulations

		80/20	50/50	20/80
LPK1A*	$\sum_i A_{seismic}\emptyset_{seismic}$	2213393	2213393	2213393
	$\sum_i A_{subseismic}\emptyset_{subseismic}$	4853008	4853008	4853008
	$e_{seismic}$ (ft)	2.2	1.4	0.5
	$e_{subseismic}$ (ft)	0.3	0.6	1.0
	$e_{seismic} / e_{subseismic}$	8.77	2.19	0.55
NLPK1A*	$\sum_i A_{seismic}\emptyset_{seismic}$	684844	684844	684844
	$\sum_i A_{subseismic}\emptyset_{subseismic}$	1433018	1433018	1433018
	$e_{seismic}$ (ft)	7.0	4.4	1.8
	$e_{subseismic}$ (ft)	0.8	2.1	3.4
	$e_{seismic} / e_{subseismic}$	8.37	2.09	0.52
NLPK2A*	$\sum_i A_{seismic}\emptyset_{seismic}$	684844	684844	684844
	$\sum_i A_{subseismic}\emptyset_{subseismic}$	1433018	1433018	1433018
	$e_{seismic}$ (ft)	7.0	4.4	1.8
	$e_{subseismic}$ (ft)	0.8	**2.1**	3.4
	$e_{seismic} / e_{subseismic}$	8.37	2.09	0.52

*Depth dependent porosity and permeability refer to data summary in case 3

Table 5.9 Case 4 simulation summary at the end of simulations (day 2,000)

	LPK1A *Recovery*	**NLPK1A** *Recovery*	**NLPK2A** *Recovery*
80/20*	0.66	0.45	0.54
50/50*	0.60	0.38	0.49
20/80*	0.54	0.31	0.42

* 80/20 means 80% of OOIP is distributed in seismic features and 20% of OOIP is in subseismic features

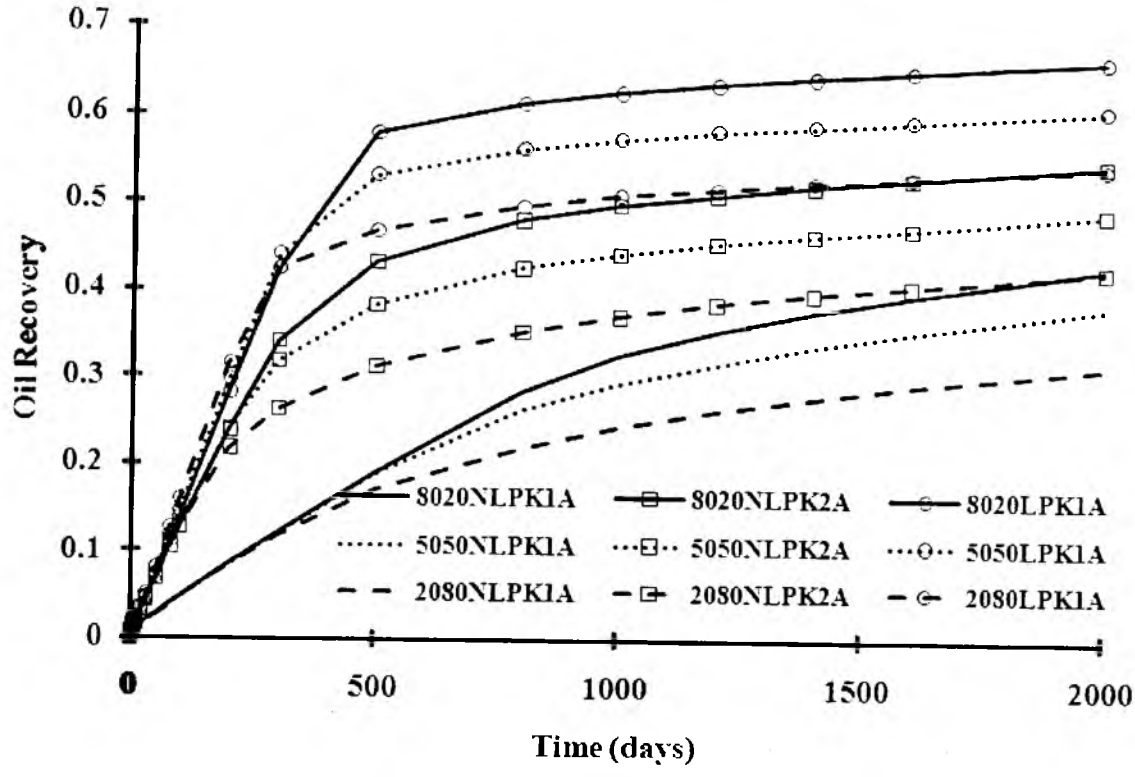

Figure 5.10 Comparisons of oil recovery versus simulation time for case 4 sets of simulations

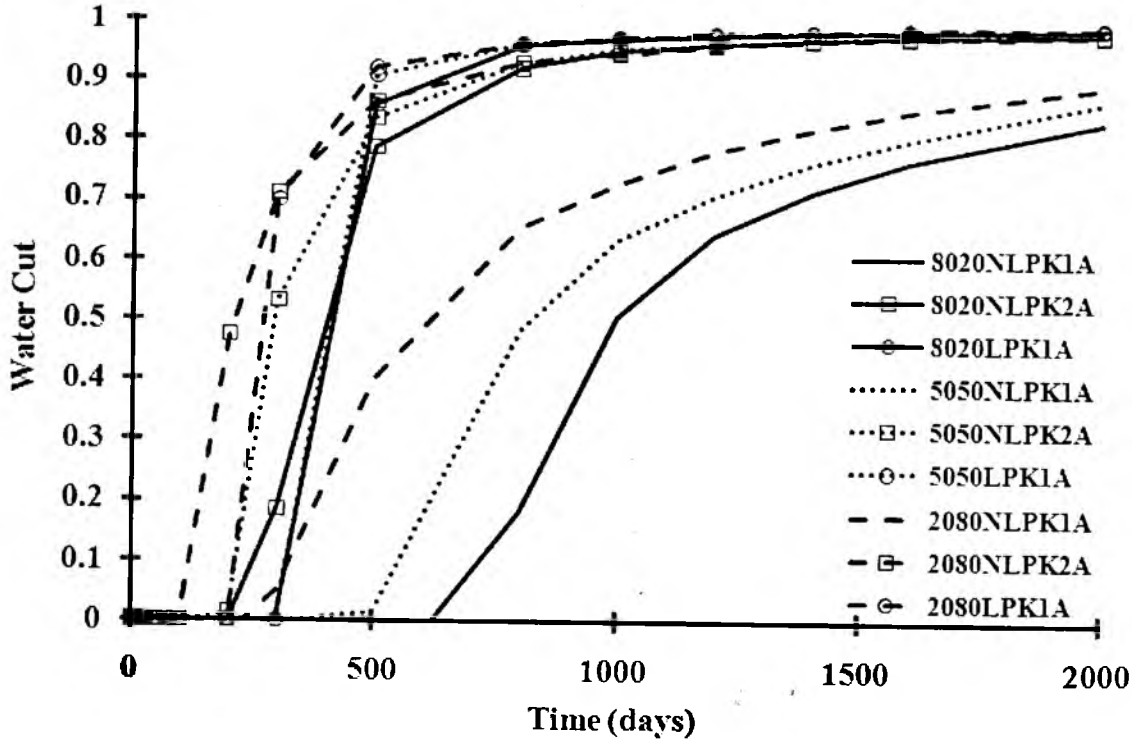

Figure 5.11 Comparisons of water cut versus simulation time for case 4 studies.

breakthrough. It should be noted that this is a reinforcement of the results of the previous section (30/70 distribution). Low recovery coupled with late breakthrough is an unexpected anomaly and is probably related to geometric trapping. It could also be due to the fact that under low permeability conditions, water influx is lower, leading to low water advance velocities. The spread between the linear distribution with a broader distribution and high median permeability and the tight nonlinear distribution increases as more oil is distributed in subseismic features.

5.5.5 Case 5: Production Rate Effects with Depth Dependent Reservoir Properties and Proportional OOIP Distributed in Seismic and Subseismic Features

Excessive water production is an often observed phenomenon from fractured basement reservoirs (Chan et al., 2006). Excess water reduces the artificial lift efficiency and sometimes is believed to cause irreversible damage to oil bearing zones. The postproduction treatment of water, required for environmental reasons, is also very expensive. The understanding of how production rate affects the displacement of oil by water in a basement reservoir system is essential to the operation of these reservoirs.

In this section, total flow rate control was imposed on all the six production wells on the top of two seismic features. Based on the case studies above, two rates were examined: high rate at 712.4 STB/day and low rate at 171.8 STB/day. One of the depth dependent reservoir property models (nonlinear porosity with porosity-permeability correlation 2, "*NLPK2A*") was chosen with three OOIP distribution scenarios in this work. Therefore, six simulations were performed, summarized in Table 5.10.

Figure 5.12 and 5.13 clearly show that simulations with higher total production rate control will result in earlier water breakthrough than the lower rate simulations. For the same controlling rate, simulations with more OOIP distributed in the seismic features offers delayed water breakthrough. This phenomenon makes sense since the supporting water is coming from the bottom of seismic features: more oil originally distributed in the seismic features requires more time to sweep it out. Oil recoveries in case 5 simulation are summarized in Table 5.11.

Two quantitative comparisons are listed below.

Comparing different OOIP distributions in subseismic features from 20%, to 50% to 80% with same operating rates at the injected PV of 1.0:

1) With the higher operating rate: Recovery decreases from 0.51, to 0.46, to 0.40.
2) With the lower operating rate: Recovery decreases from 0.55, to 0.49, to 0.44.

Table 5.10 Summary of reservoir properties and operating conditions for case 5 sets of simulations.

	8020* HighR	8020 LowR	5050 HighR	5050 LowR	2080 HighR	2080 LowR
Porosity				0.1~0.46		
Thickness (ft)						
(seismic)	7.01	7.01	4.38	4.38	1.75	1.75
(subseismic)	0.84	0.84	2.10	2.10	3.35	3.35
Permeaiblity (md)						
(seismic & subseismic)				748~123884		
Production well (STB/day)	712.4	178.1	712.4	178.1	712.4	178.1

* "8020" means 80% OOIP in seismic features and 20% OOIP in subseismic features, similar interpretation for "5050" and "2080"

Table 5.11 Case 5 simulation summaries

	8020 HighR	8020 LowR	5050 HighR	5050 LowR	2080 HighR	2080 LowR
Oil recovery (at injected PV of 1.0)	0.51	0.55	0.46	0.49	0.40	0.44

* Cumulative water production / pore volume

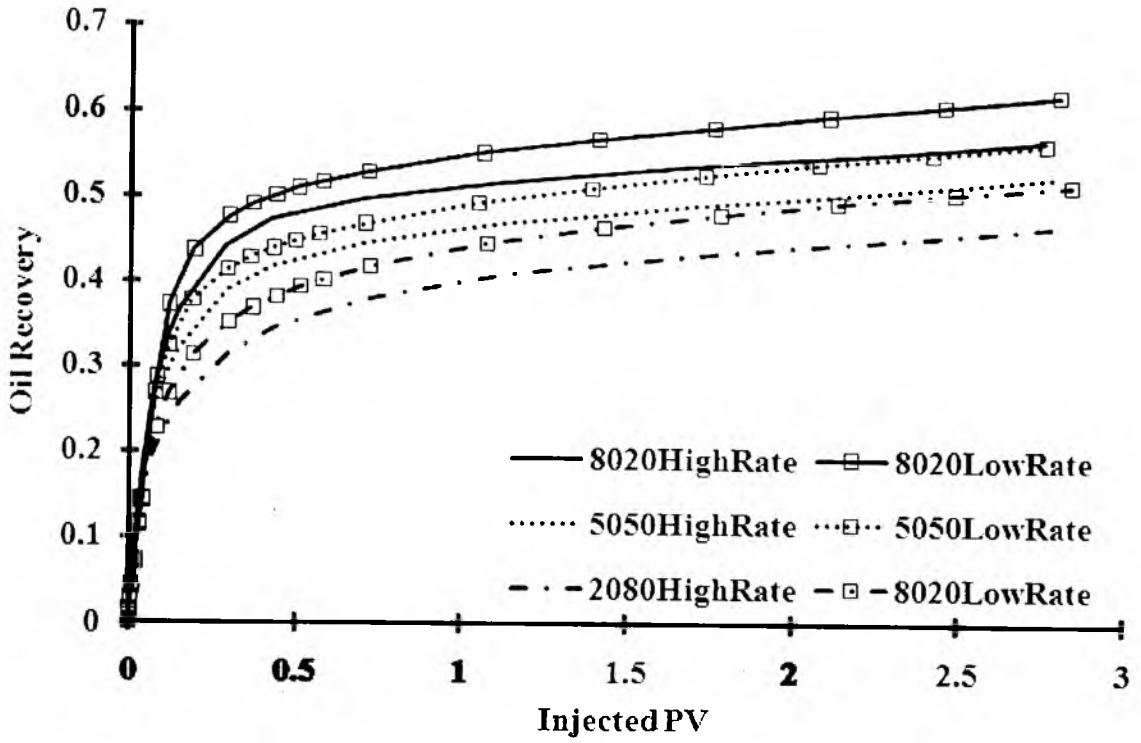

Figure 5.12 Comparisons of oil recoveries in case 5

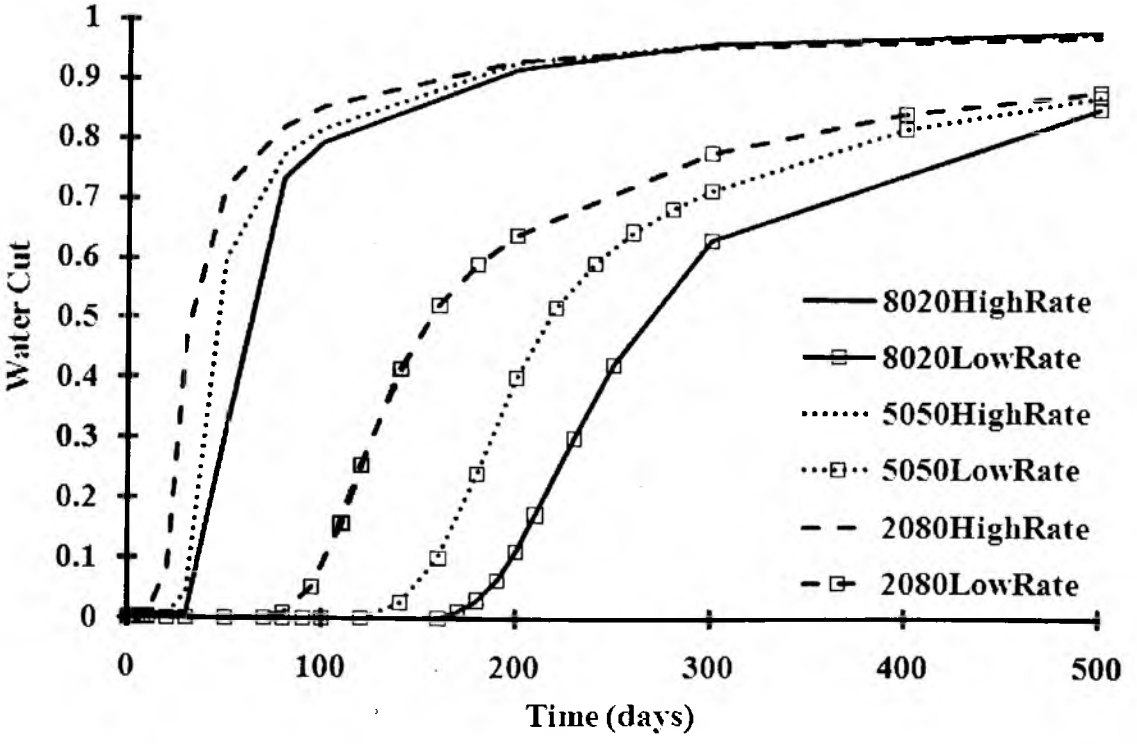

Figure 5.13 Comparisons of water cut in case 5

Comparing different operating rates with same OOIP distributions:

1) With 20% OOIP being distributed in subseismic features: Oil recoveries from high rate and low rate are: 0.51 and 0.55. There is 4% difference.
2) With 50% OOIP being distributed at subseismic features: Oil recoveries from high rate and low rate are: 0.46 and 0.49. There is 3% difference.
3) While 80% OOIP being distributed at subseismic features: Oil recoveries from high rate and low rate are: 0.40 and 0.44. There is 4% difference.

The above two comparisons show that higher production rate will result in higher recovery by the same time period but lower recovery by the same amount of water being injected. Lower operating rate always results in much delayed water breakthrough than higher operating rate.

Figure 5.14 shows the water cut with oil recovery. For a given recovery, the water cut is always lower when lower rate is used. The absolute values are different, but as more oil is distributed in the subseismic features, the relative recoveries with respect to low and high rates do not change significantly. Given the permeability distribution, K in the gravity number is fixed, no matter how it is calculated. The only variant appears to be the Darcy velocity which is most significantly impacted by the rate. Hence changing relative distribution of oil does not affect the differences between low and high rate.

Some residual oil saturation snapshots are presented at the end of simulations (day 2,000). As shown in Figure 5.15, the left column represents high production rate studies and the right column represents the low production rate studies; the first row is 20/80 OOIP distributions characterization, then the second and third rows are 50/50 and 80/20 OOIP distribution scenarios.

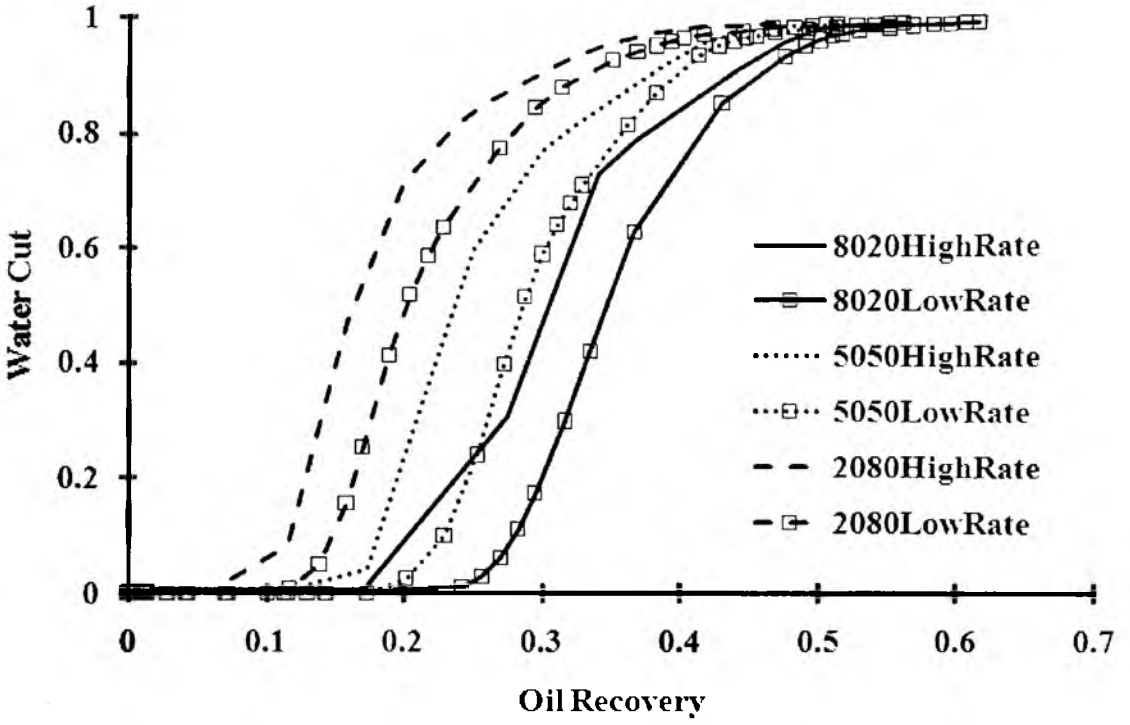

Figure 5.14 Dimensionless analyses of water and oil productions in case 5

Figure 5.15 shows that more residual oil is trapped in subseismic features than in seismic features. During the reservoir characterization, the more OOIP being assigned into subseismic features, the less oil can be flooded out. This explains why the lower subseismic OOIP distribution always has the highest oil recovery among various OOIP distributions.

Observed between columns on each row, high operating rate (left column) always get more oil swept than the low rate operating conditions. The water levels on both seismic and subseismic features are higher in the high operating rate cases. This phenomenon is more obvious in the picture of time dependent oil saturation snapshot comparisons.

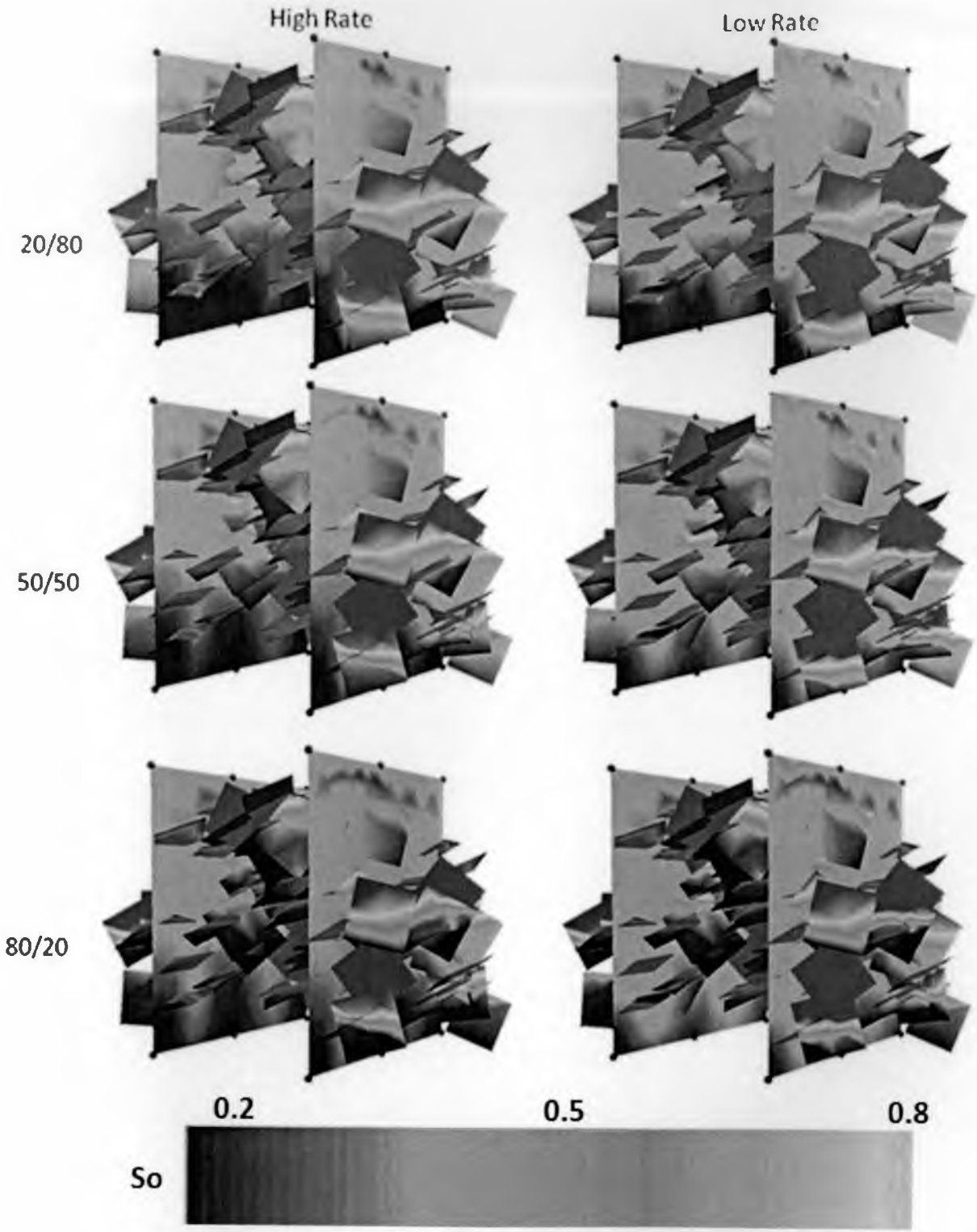

Figure 5.15 Oil saturation comparisons at the day 2,000 (end of simulation)

The water levels at different OOIP distributions are quite different: 80/20 offers the lowest water level on seismic feature and the highest water level on the subseismic features; 20/80 OOIP distributions has the reverse result compared to 80/20 cases and 50/50 OOIP distribution cases are in the middle between these two. This is due to the OOIP characterization: in order to keep the same OOIP, 80/20 cases have the largest seismic thickness and smallest subseismic thickness and this makes the above phenomenon happen. Another interesting thing that could be observed is by comparing two seismic features on each independent oil saturation file; even though both seismic features have exact boundary and operating conditions, their oil saturations vary considerably. This phenomenon is definitely caused by the existence of subseismic features.

The time dependent oil saturation comparisons are shown in Figure 5.16 for the case of 50/50 OOIP distributions. Under the operating condition and assumptions in this case study, two conclusions could be reached through this time dependent comparisons:

1) Seismic feature's oil will be flooded first, then subseismic feature's;
2) For the same time scale, high rate cases will produce more subseismic feature's oil than low rate cases.

5.6 Chapter Summary

This work quantitatively demonstrates hydrocarbons being recovered from a conceptual fractured basement reservoir model with bottom water supporting system on the major seismic features. Different percentages of OOIP were distributed between seismic and subseismic scale features in this reservoir model. Furthermore, various reservoir property models and operating conditions under the same boundary condition

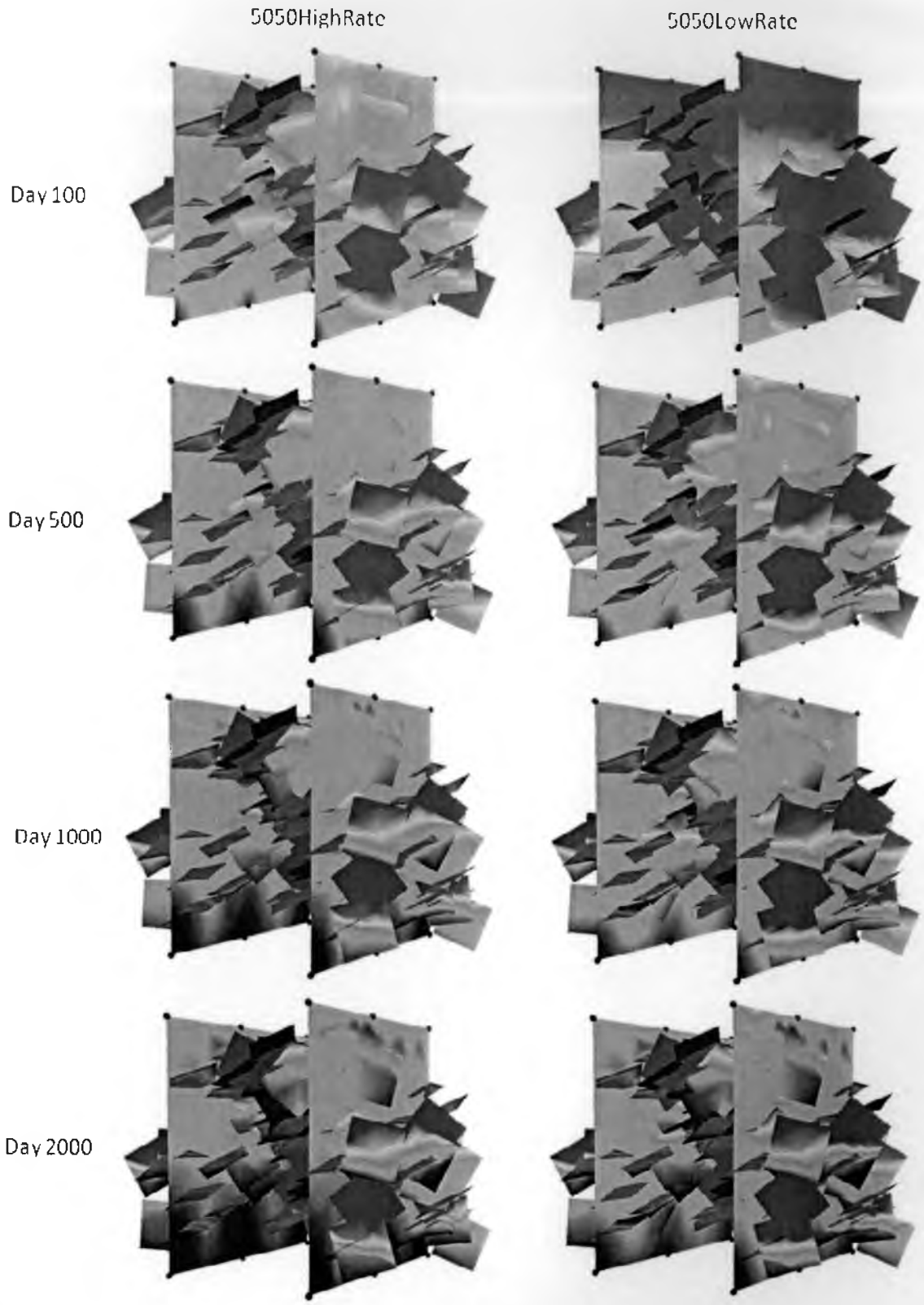

Figure 5.16 Oil saturation comparisons for OOIP characterization of 50/50 cases

were studied. A new three-dimensional, multiphase, upstream mobility weighted CVFE simulator was used in all simulations. Some conclusions could be reached from this study:

1) CVFE simulator is a very powerful tool to directly simulate multiphase flow in DFN characterized fractured basement reservoirs.
2) If the boundary conditions are ascertained, basement reservoir's recovery factor will be highly dependent on OOIP distributions and reservoir property distributions at both the seismic/subseismic scales. Hence characterization of the basement reservoir is of paramount importance.
3) Reservoir operating conditions will definitely affect basement reservoir behavior. To reach the same oil recovery, lower operating rate is preferred for decreasing water production and early breakthrough.
4) The existence of subseismic scale features does have a big impact on basement reservoir production behavior.
5) The connectivity, orientation, and size distribution of basement features will affect the basement reservoir production behavior. Boundary conditions are a very important consideration to affect oil productions from basement reservoir. Other than bottom water support, side water intrusion on the same reservoir model might lead us to different quantitative results. Qualitatively, the results are expected to be the same.

To understand the basement reservoir's water-oil displacement mechanism deeper, some work could be suggested for future study:

1) Boundary aspect: try different boundary conditions, either declining bottom pressure support or side aquifer support from either seismic features or subseismic scale features.
2) Geological aspect: try different subseismic feature DFN characterizations with variations of depth dependent sizes distributions, orientations and connectivity. This will expect the heterogeneity from the fracture network geometry may lead to preferred pathways (or oil traps) in the process of water sweeping.
3) Operating aspects: try different operating conditions such as production wells locations with rates or controlling pressures. Some special recovery method also could be studied such as gas injection, CO2 EOR, thermal recovery, etc.
4) Reservoir property aspect: try different fluid properties such as PVT, relative permeability, capillary pressure and three-phase (with solution gas involved) model. This is to study the fluid property impacts on the basement hydrocarbon recoveries.

To be considered a valid model of the basement reservoir, all heterogeneity uncertainties have to be evaluated to study the reservoir behavior practically.

5.7 Nomenclature

$\boldsymbol{A}$	=	area, ft^2
$\boldsymbol{B}$	=	formation volume factor
c	=	compressibility, 1/pisa
$\boldsymbol{e}$	=	fracture/fault storage thickness, ft
$\boldsymbol{g}$	=	acceleration of gravity, ft/sec^2
k	=	permeability tensor, md

k_r	=	relative permeability
n	=	number of discretized fracture elements
N_G	=	gravity number
o	=	oil phase
p	=	fluid pressure, psi
q	=	flux vector
R	=	oil recovery
S	=	phase saturation
u	=	velocity, ft/day
w	=	water phase
WC	=	water cut
WP	=	water production, pore volume
ϕ	=	porosity
ρ	=	density, lbm/ft^3
μ	=	viscosity, cp

5.8 Bibliography

Araujo, H., Lacentre, P., Zapata, T., Del Monte, A., Dzelalija, F., Repsol-YPF; Gilman, J., Meng, H., Kazemi, H., Ozkan, E., "Dynamic Behavoir of Discrete Fracture Network (DFN) Models," paper SPE 91940 (2004)

Basquet, R., Cohen, C.E. and Bourbiaux, B., "Fracture Flow Property Identification: An Optimized Implementation of Discrete Fracture Network Models," paper SPE 93748 (2005)

Behrenbruch, P., Du, P.Q., "The Significance of Large Variations in Oil Properties of the Dai Hung Field, Vietnam," SPE 29302, (1995)

Chan, K., Lam D.D., Ivanov, A., Apisitsareekul, K., Hai, L.V., Nghi, N.C., Hung, V.Q., and Lang. L.D, "Production Improvement Water Shutoff for White Tiger Field," SPE 103329 (2006)

Dershowitz, B., LaPointe, P., Eiben, T., Wei, L., "Integration of Discrete Feature Network Methods with Conventional Simulator Approaches," paper SPE 49069 (1998)

Fu, Yao, "Multiphase Control Volume Finite Element Simulations of Fractured Reservoirs," Ph.D Dissertation, University of Utah, Salt Lake City (2007)

Li, B., Guttormsen, J., Hoi, T.V., Duc, N.V., "Characterizing Permeability for the Fractured Basement Reservoirs," SPE 88478, (2004)

Pooladi-Darvish, M. and Firoozabadi, A., "Experiments and Modelling of Water Injection in Water-wet Fractured Porous Media," J. Can. Pet. Tech., vol. 39, no. 3 (2000)

Ronald A. Nelson, "Geologic Analysis of Naturally Fractured Reservoirs," Gulf Professional Publishing, second edition, (2001)

Sibbit, A.M., "Quantifying Porosity and Estimating Permeability from Well Logs in Fractured Basement Reservoirs," SPE 30157 (1995)

Will, R., Archer, R., Dershowitz, B., "Integration of Seismic Anisotropy and Reservoir-Performance Data for Characterization of Naturally Fractured Reservoirs Using Discrete-Feature-Network Models," SPE 84412 (2005)

Yang, Yi-kun, "Finite-element Multiphase Flow Simulation," Ph.D Dissertation, University of Utah, Salt Lake City, UT (2003)

CHAPTER 6

MULTIPHASE SIMULATIONS AND UPSCALING OF EMBEDDED FRACTURED/FAULTED ZONE MODEL ON BASEMENT RESERVOIR

(A paper in preparation)

Huabing Wang[1], Tom Doe[2], and Milind Deo[1]

1. Department of Chemical Engineering

University of Utah

Salt Lake City, UT 84112

2. FracMan Technology Group

Golder Associates Inc.

18300 NE Union Hill Road

Redmond, WA 98052 USA

6.1 Abstract

A certain amount of the world's proven oil reserve occurs in fractured basements. The basement reservoirs have been known within the hydrocarbon industry for many years but generally have been regarded as nonproductive. The high price of crude oil urges explorers to draw their attention to this type of reserves. Generally, basement reservoirs have the following main characteristics: fracture/faults provide essential porosity and permeability; fracture networks are highly heterogeneous; fluid and rock properties may vary through depth. Those characteristics present many of challenges for the exploration and the production management of this hidden resource. For example, the major features in this type of reservoirs are detected by 3-D seismic reflection survey but many limitations remain for seismic interpretation. The basement features are usually in the formation of granite/basalt but located very deeply, which makes for a large loss of high frequency seismic waves. Thus seismic reflection resolution can only show major faults, which are constructed by small fractures. The reservoir engineers faced with difficulties of modeling fluid flow on this type of reservoirs, since it is difficult to use the well-known finite-difference based commercial packages to simulate them.

In this chapter, with a single basement feature through the 3-D seismic reflecting survey, a local discrete fracture network (DFN) was constructed by using the combination of measured fractures from the field FMI logs along with insights from geologic studies of fault zones elsewhere. This embedded zone model reflects the reality that fracture zones and faults are themselves made up of a conducting fracture network. A question of significant importance is: how does oil-water displacement behave in the embedded zone environment in comparison to its single feature representations adopted in full-field seismic and subseismic models? The answer to this question will be explored

in detail by simulating a number of embedded features. The "upscaled" representation will be simulated using regular polynomial relative permeabilities, while the embedded zone will be simulated using the straight-line relative permeabilities. The functionalities that give the "best-match" for oil recovery and/or water cut are sought in this exercise. These relative permeability functionalities will be the "upscaled" relative permeabilities. Some speed sensitivity simulations regarding various boundary conditions were also studied a single basement feature by ECLIPSE. As an important dimensionless operational parameter dependent group, gravity number analysis is applied at the end of this chapter helping understand the oil-water displacement mechanism in the large vertical basement environment. This type of work has, to date, never been reported on the DFN modeled fracture networks.

6.2 Introduction

Multiphase fluid-flow simulations of oil reservoirs are computationally intensive. Normally, the geological reservoir models are built with a large number of grid blocks or elements in order to represent all of the available geologic information. It is often impossible to perform multiphase flow calculations using a large number of grid cells created in a geologic model. The fine-scale systems are often "upscale" into coarser scale meshes. "Upscaling" could be described as assigning "effective" properties to coarse scale cells from properties on the fine scale model to capture flow features of the fine scale model. For the computer simulation of fluid flow through porous media, permeability upscaling plays an important role, and this is particularly true for fractured reservoirs. Permeability upscaling technique is classified as absolute permeability and relative permeability upscaling.

It is sometimes suggested (Durlofsky et al., 1994; Muggeridge, 1991) that the scaling up of absolute permeability alone is not enough to capture the effects of highly heterogeneity on multiphase fluid-flow simulations. From this point, relative permeability upscaling techniques (also called pseudo-relative permeabilities) are suggested by many authors (Coats et al., 1971; Warren and Root, 1963; Jacks et al., 1973; Kyte and Berry, 1975; Stone, 1991; Hewett et al., 1997; and so on). The role of pseudo-relative permeabilities is to determine the flow rate of each phase out of a grid block. They relate the flow rate to the pressure gradient between the grid block and its neighbor, given the average saturation in the gridblock. Both the flow rate and the pressure gradient depend on the details of the saturation distribution within the grid block. It is necessary to determine the saturation distribution within the grid block for any given average saturation. Modern scholars classify the pseudo-relative permeabilities into two categories: static pseudo (also called "vertical equilibrium" pseudo) (Coats et al., 1971; Warren and Root, 1963; Jacks et al., 1973; and so on) and dynamic pseudo (Kyte and Berry, 1975; Stone, 1991; Thomas et al., 1975; Barker et al., 1994; Hewett et al., 1991; and so on). Dynamic pseudo-relative permeability has been chosen as the major reservoir upscaling technique. Tremendous reviews were done regarding the dynamic pseudo-relative permeability upscaling (Christle et al., 2001; Cao and Aziz, 1999; Barker et al., 1997; Okano et al., 2005; Ringrose, 2007; King, 2007).

Numerous studies have been performed applying pseudo relative permeabilities on fractured reservoir simulation (Warren and Root, 1963; Dean and Lo, 1988; Rossen and Shen, 1989; Talukdar et al. 2000; Ding et al., 2006; and so on). So far, almost all of these works are upscaling for conventional finite difference simulator. No relative

permeability upscaling technique has been reported for a DFN based finite element simulator, which is the goal of this study.

In this chapter, the idea behind the direct upscale DFN model is to use the straight-line relative permeabilities for the detailed structure of the seismic feature, and match the water flood performance using the regular polynomial relative permeabilities for the upscaled single feature. The straight-line relative permeability curves was published by Romm (1966) and quoted by numerous authors thereafter. This finding was based on experiments of flow between two parallel glass plates, showing a linear dependency between phase relative permeability and phase saturations. However, the experiment did not report the implications on the reservoir scale. In this work, assuming straight-line relative permeability represents all small fractures in the embedded zone model but it will not be true while the features size. Polynomial relative permeability will be used in the upscaled single feature in order to match recovery or water breakthrough time and scales in the embedded zone model. In addition to the relative permeability study, depth-dependant properties (porosity and absolute permeability) are also studied with the embedded zone model in this work. The water breakthrough time and water cut rate are quantified by comparing cases with or without depth-dependent reservoir properties. This will aid in understanding oil/water displacement mechanisms on the fractured basements.

6.3 Governing Equations, Discrete Fracture Network (DFN) Model and CVFE Simulator

The equations describing compressible two-phase flow were obtained by combining Darcy's law, and mass conservation for each phase was discussed in Chapter 2. In this study, a flux-based upstream-weighting three-dimensional, two-phase (oil, water) black-oil CVFE simulator being developed in the University of Utah (Yang, 2003; Fu et al., 2005) was employed. This CVFE formulation was validated and verified through various methods: indexing method (Chapter 3); manufactured solution method (Yang, 2003; Fu, 2007); and lab core (Pooladi-Davish et al., 2000) verification (Chapter 7). The CVFE simulator applied in this research gives an accurate solution for fluid flow on fractures and this is especially ascertained for the DFN modeled basement reservoir type.

6.4 Model Descriptions

There are several factors that influence the behavior of a producing reservoir and which must be incorporated in the modeling effort to understand their relative importance to reservoir performance. The fracture basement modeling must consider the factors:

- Geologic model: the static model of reservoir geometry, especially the fracture zones detected by seismic reflection and fracture zones that may lie undetected but nonetheless influence reservoir storage and fluid movements.
- Reservoir property model: the key to DFN simulation is the assignment of reservoir properties (porosity, permeability, thickness, compressibility) to the features of the geologic model. These properties are either homogeneous or they are vary according to geologic expectations as discussed below.

- Phase model: this will enclose two-phase (water and oil) properties such as n-points on the relative permeability curve and initial saturations.
- Fluid property model: fluid properties are very important during the multiphase simulations and this will include fluid viscosity, compressibility, density, and formation volume factor.
- Boundary conditions: the behavior of the model may be strongly influenced by the boundary conditions that are assumed for the fractured basement. The boundaries are usually considered as nonflow and constant-pressure features.

6.4.1 Geological Models

There are two geological models in use: a single seismic feature model and an embedded fracture zone model. The seismic model was identified by 3-D seismic reflection surveys. To simplify the question, this seismic feature is approximated as having four-sided, planar features with the approximate corner location and correct average orientation.

The embedded fracture model tests the influence of fracture network within a major seismic feature. The model takes one seismic feature and replaces it with a local fracture network. This model reflects the reality that fracture zones and faults are themselves made up of conducting fracture networks. The embedded zone model uses a combination of the measured fractures from the field FMI logs along with insights from geologic studies of fault zones elsewhere. The embedded zone model in this study is built by three sets of small features: in-plane features, pseudo-horizontal features, and pseudo-vertical features. All features have the same size distributions but the orientations vary by sets as described in Table 6.1.

Table 6.1 Summary of constructed embedded zone model

	In plane set	Pseudo horizontal set	Pseudo vertical set
Number of features	83	55	112
Total feature area (ft^2)	2686364	1772403	3726334
Mean orientation	293.8, 30.6	167.3, 44.1	43.3, 30.3
Equivalent Radius mean (ft)	101.7	101.2	101.9
Equivalent radius std dev	7.96	7.84	8.37
Area mean (ft^2)	32740.4	32365.8	32225.5
Area std dev	5056.2	4964.0	5291.7

Specifically, as shown in Figure 6.1, the embedded model starts with the main fracture zone surface and is defined by two subsidiary surfaces that are offset with one on each side of the master surface. The amount of offset varies with depth, so the embedded zone thickness as it approaches upward to the basement surface. Geometrically this is very meaningful for representing basement faults/fractures for the modeling purpose. The emphasis of this study is going to be on the oil/water displacement mechanisms and the basic upscaling from the reservoir engineering point of view. Therefore, only one embedded zone model is presented in this work.

6.4.2 Reservoir Property Models

The reservoir properties model describes the way properties are assigned to the individual features in the DFN model. There are four models of reservoir properties being used:

1) Homogenous models: the homogenous model uses homogenous properties for all fractures throughout the model. The properties include the porosity, the permeability, the thickness, and the compressibility on the fractures. The DFN defined fluid-transmission properties of fractures as product of the thickness and the permeability, which is equivalent of *kh* for a porous reservoir.

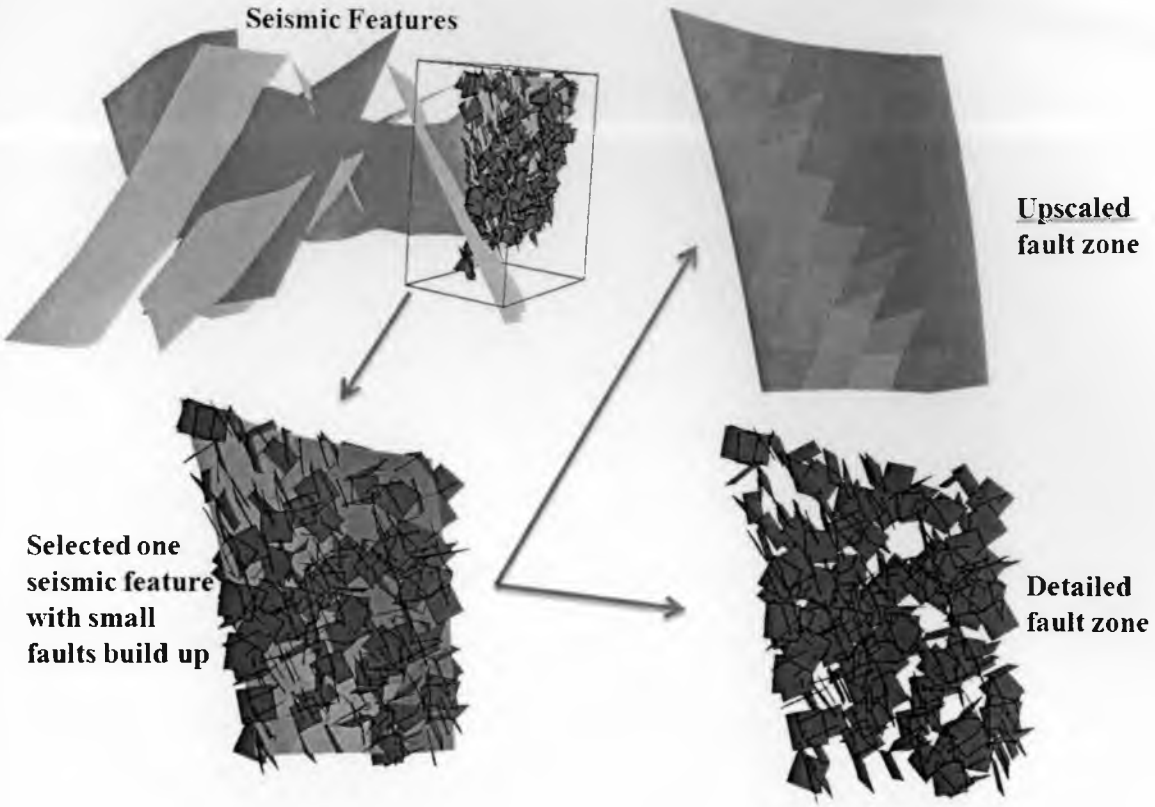

Figure 6.1 Illustration of seismic features and the fault zone model

And the pore volume of the fracture is controlled by product of the thickness and the area. The fracture also has a compressibility, which reflects the elastic properties of the fracture itself. This storativity of the fracture is given by the combination of aperture, fracture compressibility and the compressibility of the fluid in the fracture.

2) Depth-dependent heterogeneous models: this depth-dependent model is the key for fractured basement reservoirs. For each discretized triangle element, both porosity and permeability are varied from depth to the surface of the basement.

6.4.3 Phase Model

The DFN modeling work on this study used the 2-phase model which contains only the water and the dead-oil phase. Certain assumptions were applied on this two-phase black-oil model: no free gas phase, constant temperature, and insoluble water and oil phase.

6.4.4 Fluid Properties Model

There was no expectation of varying fluid properties as part of the simulation program in this work. The initial condition for the saturations on the embedded zone model was 100% oil. Water viscosity was set at 1 cP and oil viscosity was set as 0.7 cP. Water compressibility was 3E-6 and oil compressibility was 9E-6 1/psi.

6.4.5 Boundary Condition Models and Initial Conditions

Boundary conditions are key controlling influences on both reservoir and numerical simulation behaviors. There are four essentially sides to the embedded zone and upscale single seismic feature – top, sides and bottom. Each must have a specified boundary over its surface. For the DFN models in this study the following boundary condition variations were applied:

1) No flow boundary: the no flow boundary condition was applied to the top of all simulations, and it was assumed that the sediments at the top of the basement surface act as seals. Unless otherwise specified, all other model boundaries were nonflow boundaries.
2) Lateral aquifer support: this type of boundary condition supplies a water source of either constant rate of pressure.

3) Restricted aquifer support: this aquifer condition recognizes that although the aquifer may be effectively infinite in volume, it may have either a limited conductivity due to the properties of the sediments, or the aquifer may have decreased pressure to support the embedded zone/seismic fault.

6.4.6 General Embedded Fault Zone and Upscaled Single Fracture Flow Model Parameters Summary

Parameters of embedded fault zone model and single feature model regarding flow simulations are summarized in Table 6.2.

6.5 Case Studies

6.5.1 Can Embedded Fault Zone Be Represented by Single Seismic Feature?

If the DFN modeled embedded fault zone presumably represents the real existence of basement fracture network underground instead of single seismic reflecting resulting feature, the first question to be asked in this study is: can this embedded fault zone be represented by that single seismic feature? (Figure 6.2) On a practical level, this is a meaningful upscaling question in basement reservoir management: if these kinds of embedded fault zone models could be simplified into the single seismic feature model, not only is computational time largely reduced, but also this type of reservoir study flow simulation is made possible (finite-difference reservoir simulators are still dominating the market today).

Table 6.2 Summary of critical data for modeling embedded zone and upscaled single fracture basement model

Simulator	**CVFE**	
Grid information	Embedded zone model	Single feature model
Node number	7702	1053
Fracture triangle elements	14040	1980
Fluid property	Water	oil
γ (lbf/ft^3)	62.4	52.9
Fluid data		
	Water properties*	***Oil properties****
Reference pressure (p_{ref}, psia)	14.7	4850
Water formation factor B_r @ reference pressure (rb/stb)	1.0	1.17
B_r's compressibility (1/psia)	3.25e-6	0.9e-5
Water viscosity (μ_r) @ reference pressure (cp)	0.3	1.0
μ_r's compressibility (1/psia)	0.0	0.0

Rock-fluid data (straight-line relative perm curve with "zero" capillary pressure)

Oil-water system

S_w	k_{row}	K_{rw}	p_{cow} (psia) (fracture & fault)
0.00	0.00	1.00	0.0
0.10	0.10	0.90	0.0
0.30	0.30	0.70	0.0
0.50	0.50	0.50	0.0
0.70	0.70	0.30	0.0
0.90	0.90	0.10	0.0
1.00	1.00	0.00	0.0

Initial conditions	
P (psia)	3300
S_w	1.0

Boundary conditions

Unless otherwise specified, all other model boundaries are nonflow boundaries.

* Reservoir fluid properties (pressure related) were calculated by the following equations:

$$B = B_r * exp\,[-C_B * ((P - P_{ref})] \tag{6-1}$$

$$\mu = \mu_r * exp\,[-C\mu * (P - P_{ref})] \tag{6-2}$$

In this study, simulations were performed on embedded zone and single fracture basement models with the exact same reservoir conditions (including the same straight-line relative permeability and "zero" capillary pressure). Two injection wells were on the bottom with constant bottom hole pressure control (6,000 psi); two other injectors on the middle two sides of domain with constant injection rate control (89 STB/day). Four production wells were on the top of the reservoirs with constant rate control (89 STB/day). The oil recovery and water cut figures are shown in Figure 6.3 and 6.4.

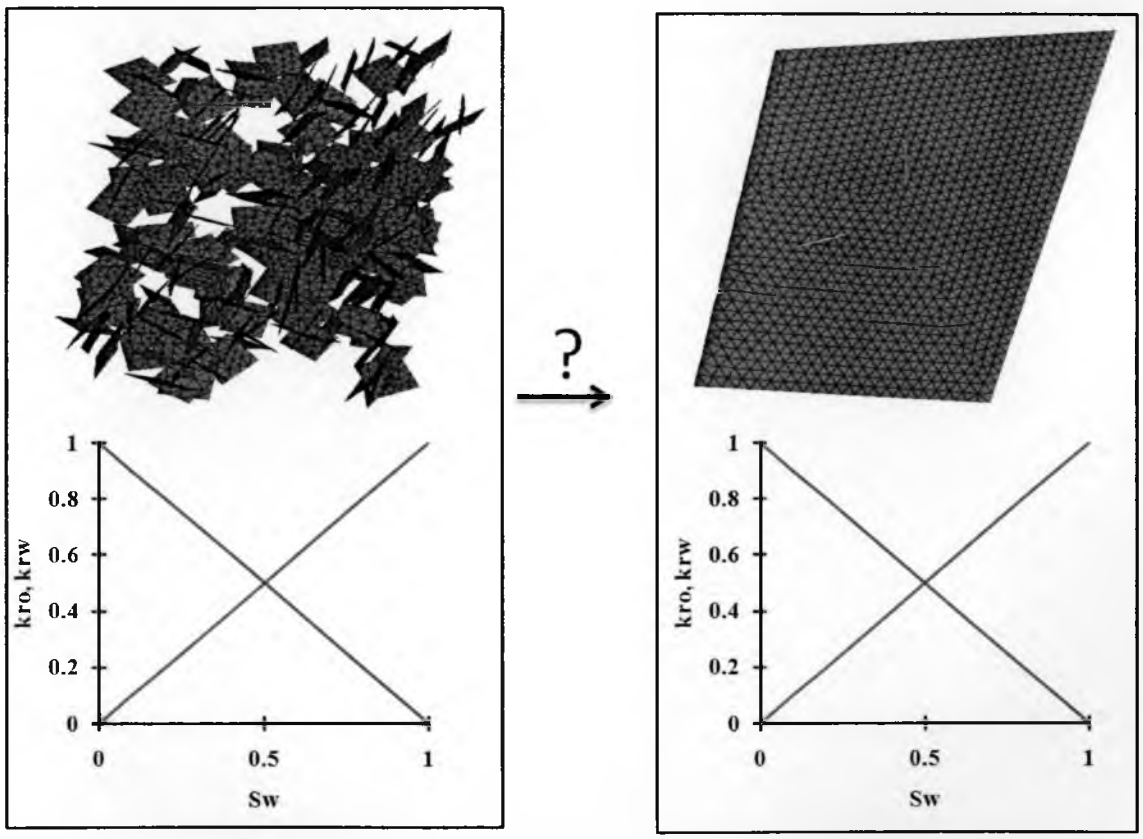

Figure 6.2 Can embedded fault zone fractured network be represented by single seismic feature in flow simulation?

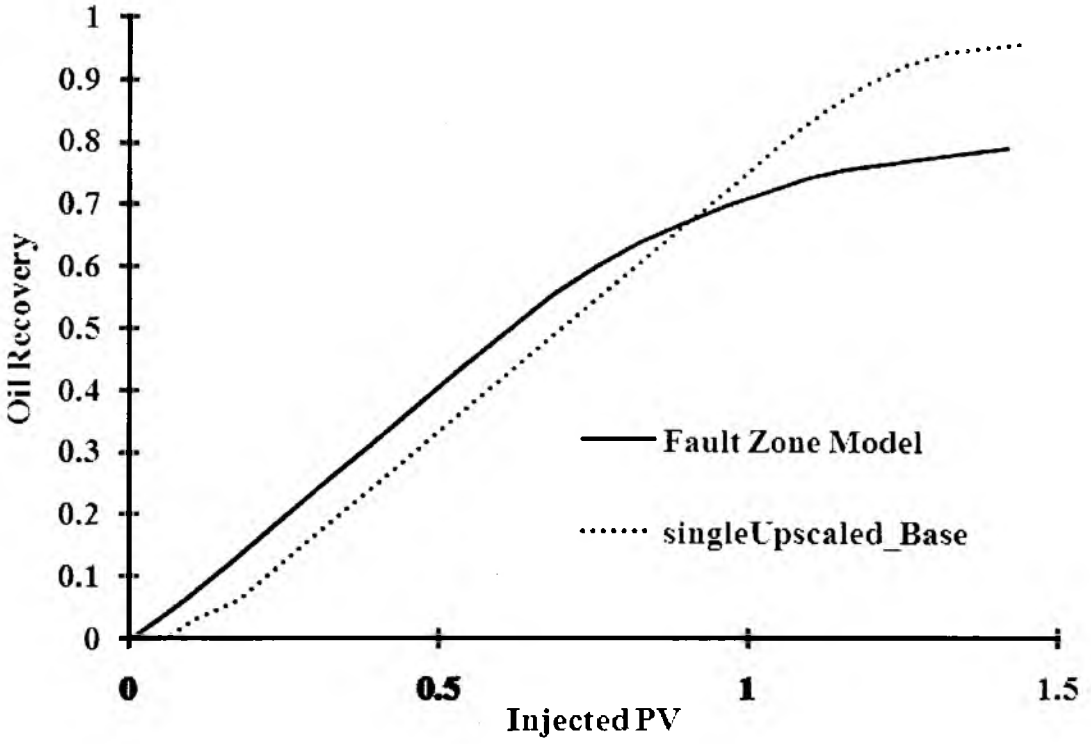

Figure 6.3 Comparisons of oil recovery between embedded zone model and single feature model with straight-line relative permeability.

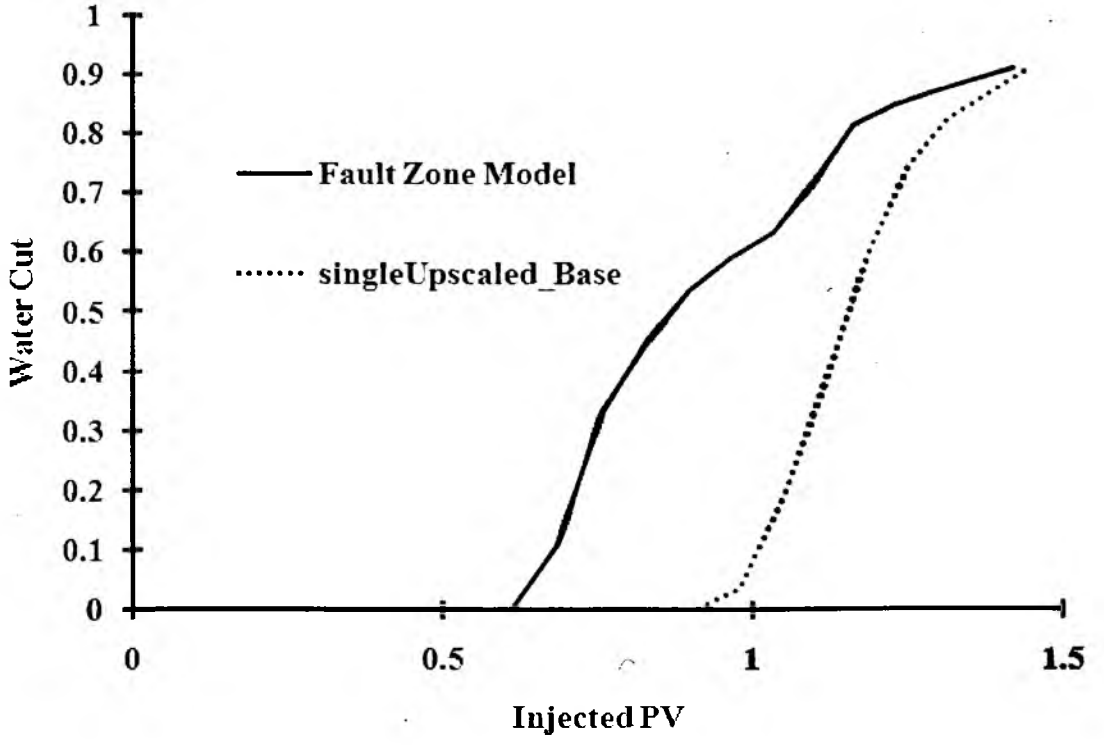

Figure 6.4 Comparisons of water cut between embedded zone model and single feature model with straight-line relative permeability.

Instead of correlating with the simulation time, both oil recovery and water cut are correlated with injected pore volume (PV) which gives the dimensionless analysis in order to remove the effects of OOIP difference from two models. This method of analysis will be applied through this study and will not be mentioned again. The above two comparisons clearly show that a single feature cannot represent the embedded zone model with the same straight-line relative permeability curve. For example, the water breakthrough from the single feature is 0.905 of injected PV but the fault zone gives 0.613 injected PV. There are 0.292 injected PV differences which yields about 47.6% error from the embedded zone studies. Therefore, the conclusion from this case is that the embedded fault zone cannot be simply represented by a single feature with the same relative permeability curve. Then the following question is whether it is possible to use a polynomial relative permeability curve in the single feature as the upscaled embedded zone model?

6.5.2 Can Embedded Fault Zone Be Represented by Upscaled Single Seismic Feature?

Following case study 1, if the embedded fault zone model still had the straight-line relative permeability with the end points of 0 and 1, could this single feature be upscaled to achieve the same result from the embedded zone model by changing the relative permeability on the single feature? (Figure 6.5)

The Corey-exponent representations (Equation (6-3) and (6-4)) are a well-known model of the water and oil relative permeability functions.

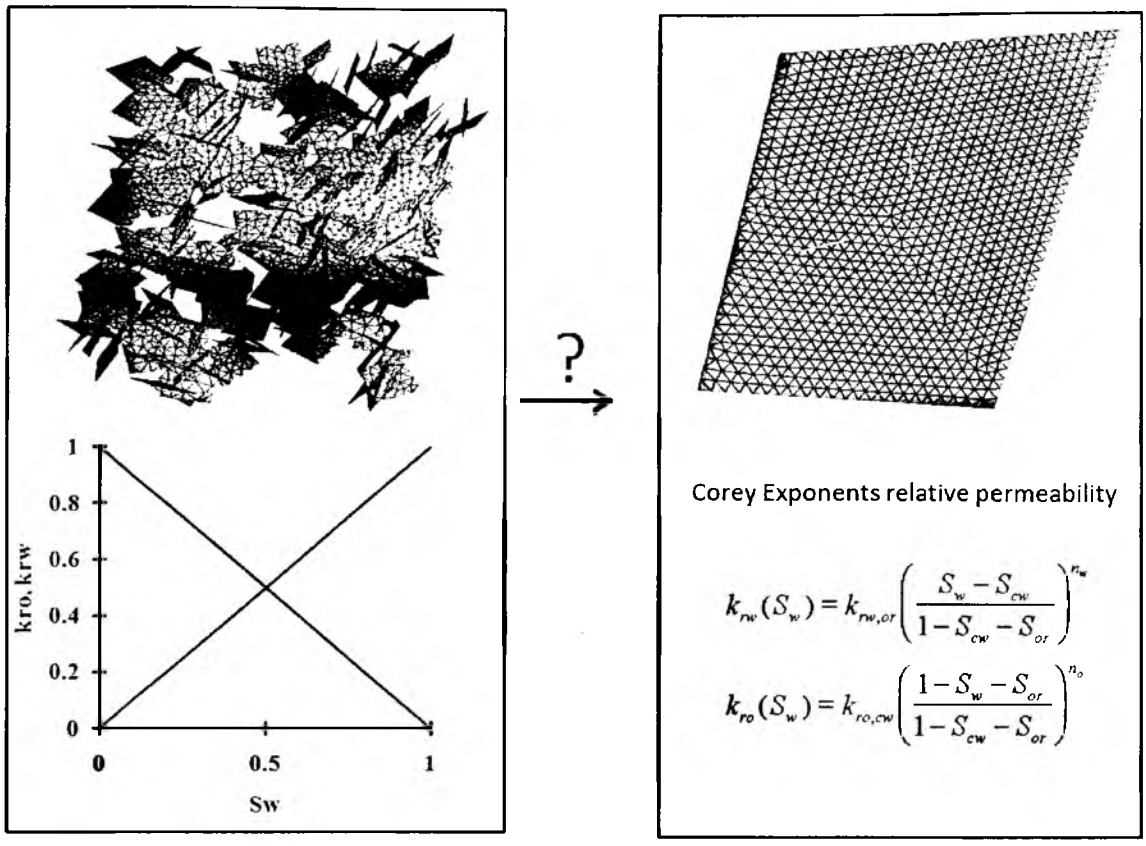

Figure 6.5 Can the embedded fault zone model be represented by a single seismic feature model with different relative permeability?

$$k_{rw}(S_w) = k_{rw,or}\left(\frac{S_w - S_{cw}}{1 - S_{cw} - S_{or}}\right)^{n_w} \tag{6-3}$$

$$k_{ro}(S_w) = k_{ro,cw}\left(\frac{1 - S_w - S_{or}}{1 - S_{cw} - S_{or}}\right)^{n_o} \tag{6-4}$$

with $k_{rw,or}$ and $k_{ro,cw}$ being the end-point relative permeability, S_{cw} the connate water saturation, S_{or} the residual saturation, and n_w and n_o the so called Corey exponents for water and oil, respectively.

By Corey-exponent formulations, a series of relative permeability curve were generated and applied on the single feature simulations. One good example of this type of upscaling is shown in Figure 6.6.

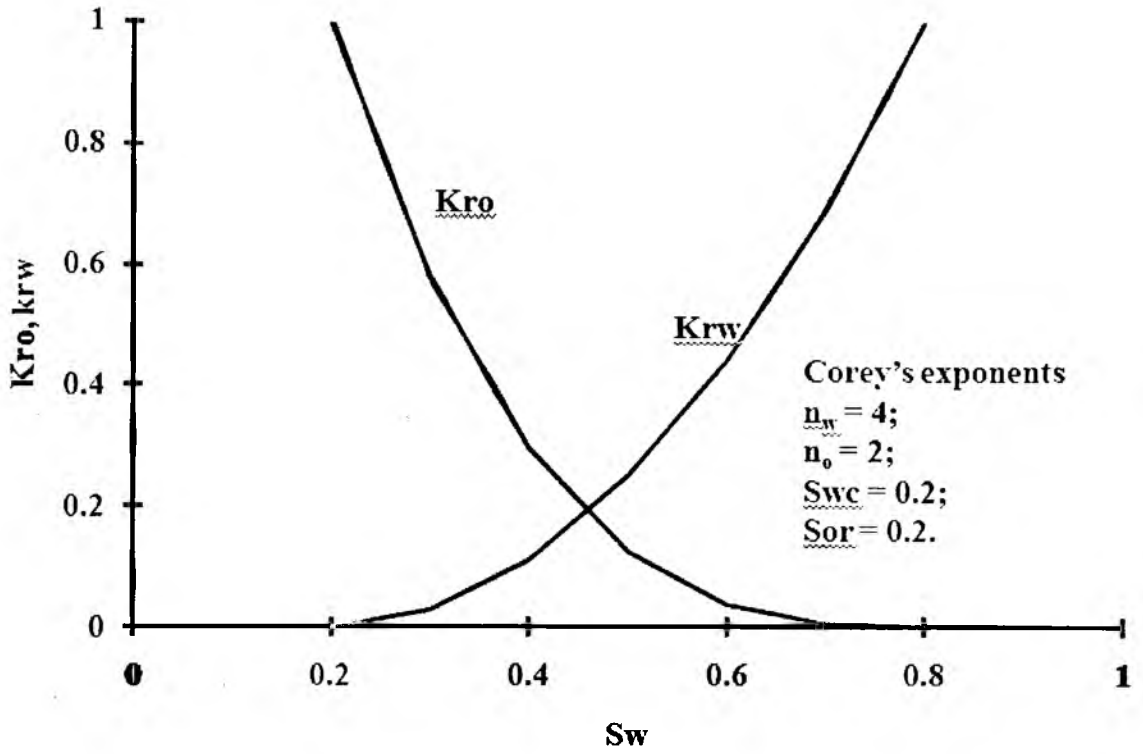

Figure 6.6 One example of Corey-exponent relative permeability curves

As shown in Figure 6.7 and 6.8, the water breakthrough from the embedded zone study has been perfectly matched by this upscaled single feature model. The water cut values at the end of simulation have been roughly matched too. The water cut curve between breakthrough and end are not matched and the shapes are different. The embedded fault zone water cut curve has two inflexions but not from the upscaled single feature study. This is due to the effects of the side supporting water and flow pathway from the embedded zone model. If production wells on the top are controlled by constant rate, water coming from the reservoir side will face the competition of gravity and viscous force: part of the water will be sucked directly to the producers instead of flowing to the bottom and evenly building up from the bottom. This phenomenon will be discussed later in the rate sensitivity study section. Oil recoveries in the above figures are

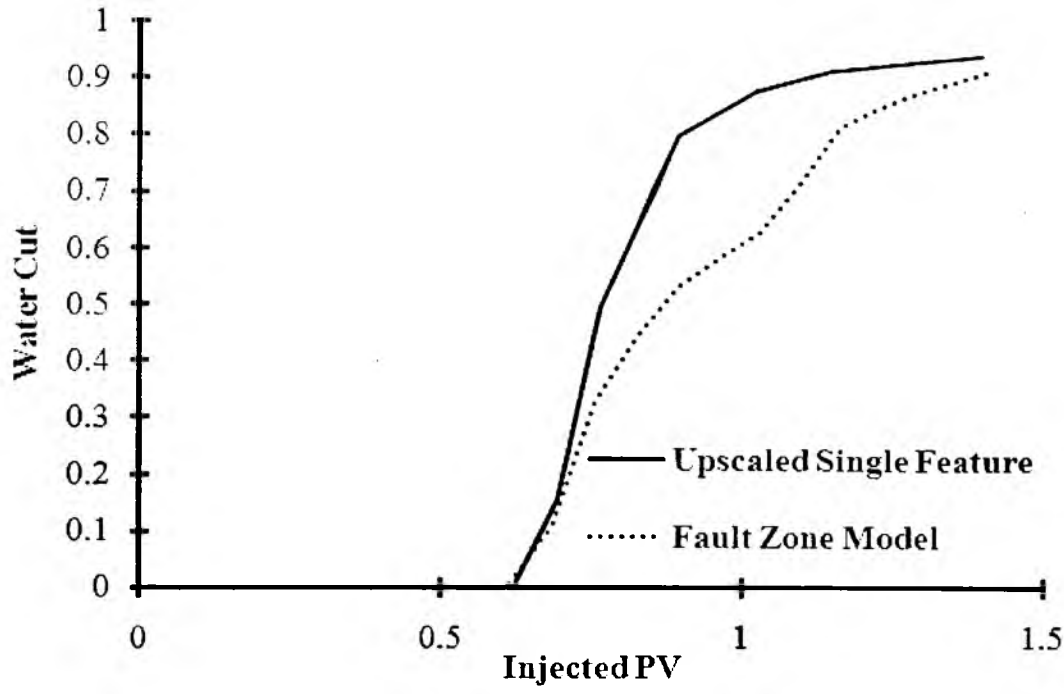

Figure 6.7 Comparisons of water cut between the embedded fault zone model and the Corey-exponent relative permeability represented single feature

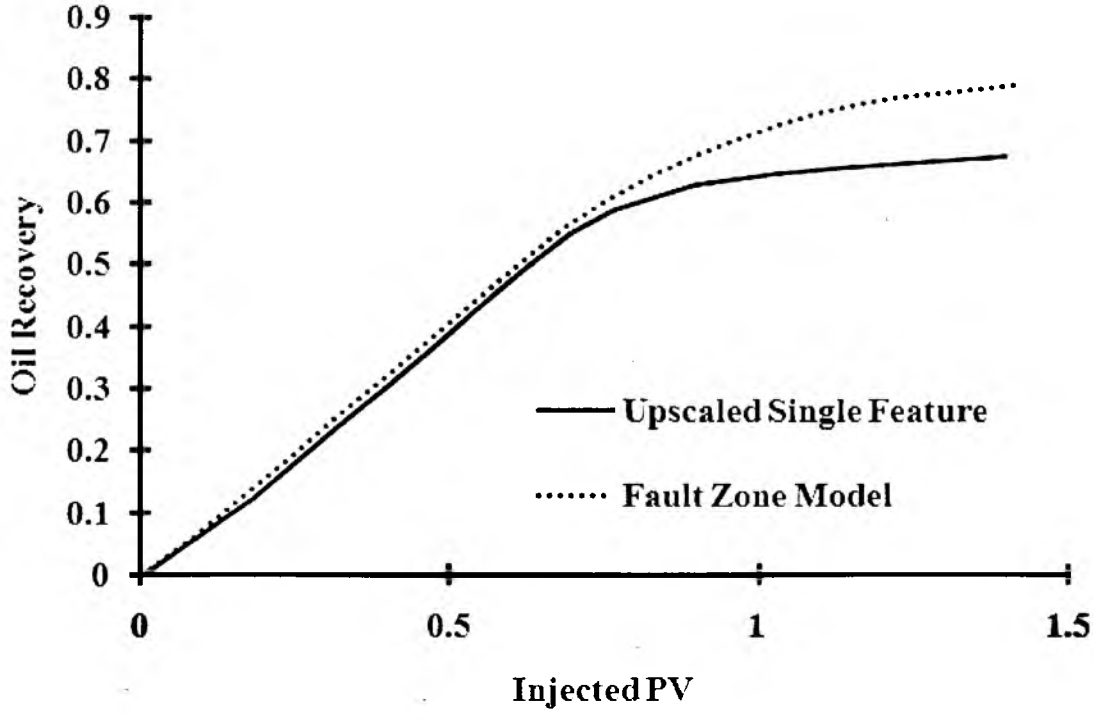

Figure 6.8 Comparisons of oil recovery between the embedded fault zone model and the Corey-exponent relative permeability represented single feature

well matched till about 0.7 PV injected (close to water breakthrough); then the upscaled single feature presents lower oil recovery due to the higher water cut.

The conclusion from this case study is that it is possible to upscale the embedded zone model to single feature using polynomial relative permeabilities such as the Corey-exponent representation. However, this type of upscale might not offer an exact solution from the embedded zone model due to too many uncertainties such as flow path, connectivity, etc. One example from the embedded fault zone model study in Figure 6.9 shows some stranded oil due to the geometric trap, which might not be presented by the single feature relative permeability upscaling.

Figure 6.9 An embedded fault zone simulation shows geometric trapping of the oil.

6.5.3 Impacts from Depth-Dependent Reservoir Properties

Both case studies discussed above have the basic assumptions of constant porosity and permeabilities in all features. It is reported that the basement fracture/microfracture porosity changes very strongly with depth (Chan et al., 2006). A more realistic depth-dependent porosity and permeability distribution models presented below will be applied on embedded fault zone study. This is to learn impacts from depth-dependent reservoir properties.

As shown in Figure 6.10, the porosity depth-dependent model offers the range from 0.1 to 0.9 on the embedded fault zone model from the bottom to the top with the total depth of 5300 ft. Permeability will be directly correlated with the porosity ranging

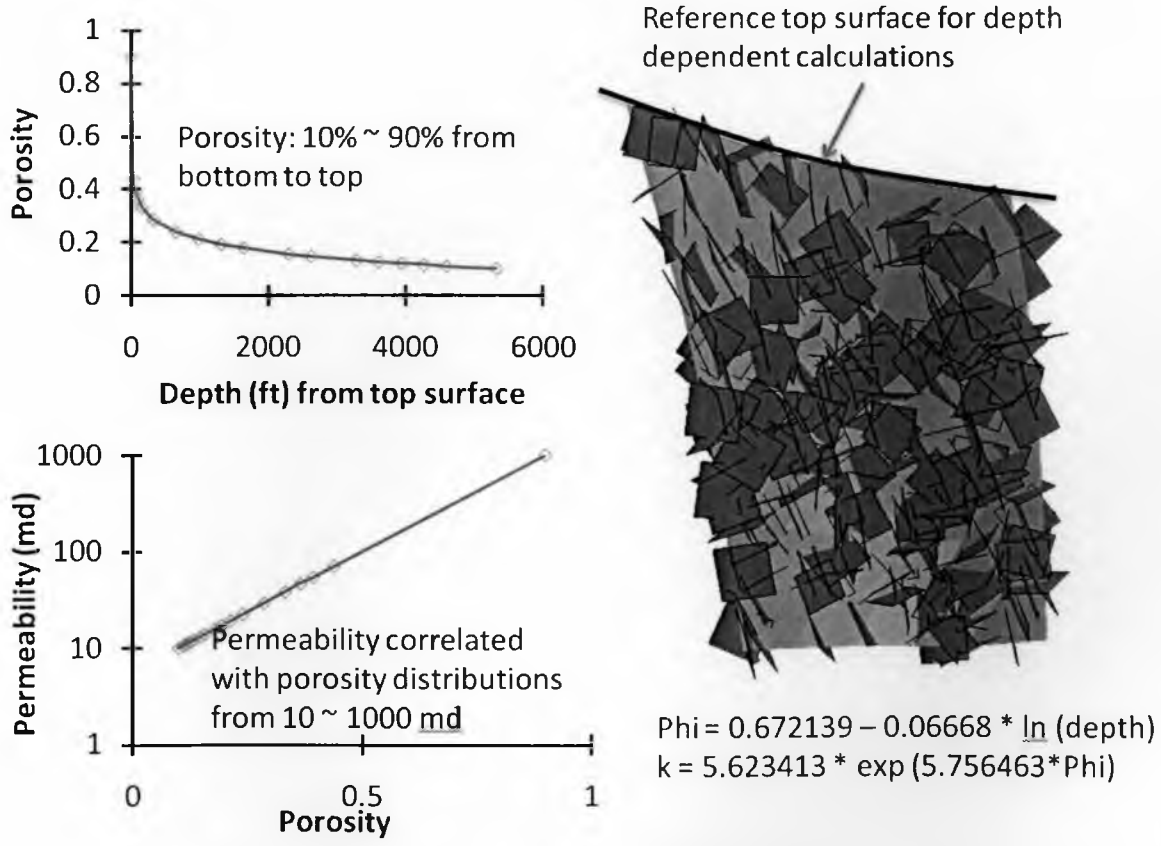

Figure 6.10 Illustration of depth-dependent porosity and permeability models and their reference surface in the embedded fault zone model

from 10 md to 1000 md and indirectly dependent on depth from the top. The reference top surface is as shown above on the top of the embedded fault zone model. This reference top surface was used to compute the faults porosities and permeabilities.

In this section, three depth-dependent simulations were introduced: heterogeneous porosity, heterogeneous permeability, and both heterogeneous porosity and permeability. These simulation results are drawn with the uniform property simulation (no depth dependence) result from case study 1.

Oil recovery comparisons in Figure 6.11 show that the nondepth-dependent embedded zone model offered the highest oil recoveries at the end of simulation with 1.4 injected PV. The depth-dependent porosity model gave the lowest oil recovery for both uniform permeability and heterogeneous permeability cases. The oil recovery from

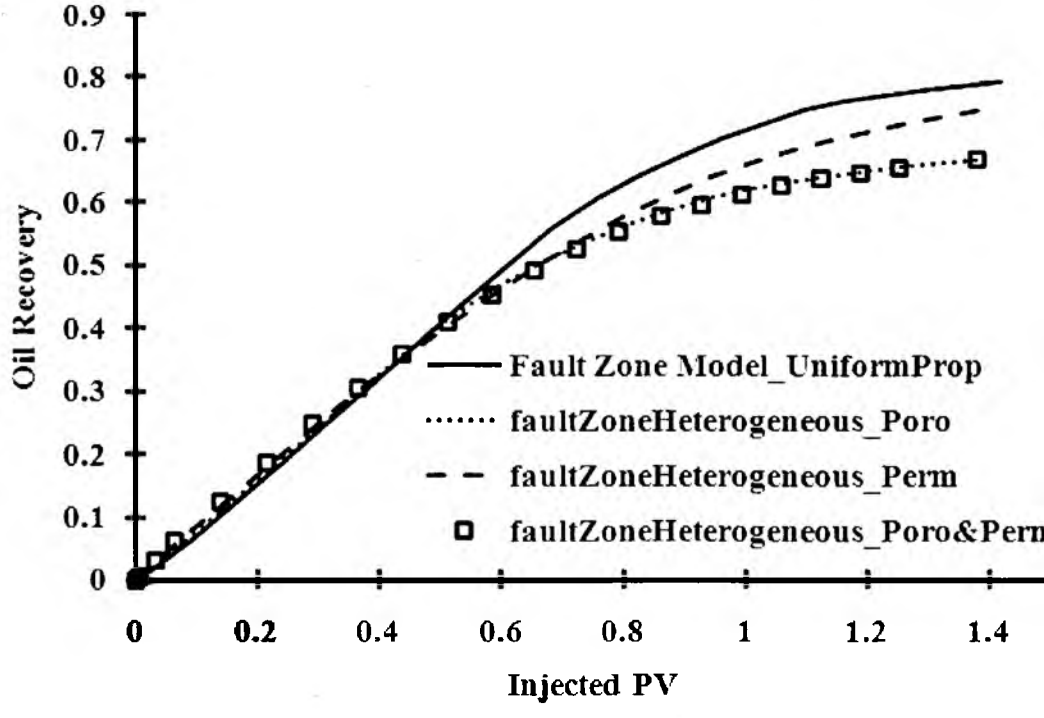

Figure 6.11 Comparisons of oil recovery among depth-dependent reservoir property models and nondepth-dependent reservoir property model in the embedded fault zone study.

depth-dependent permeability with nondepth-dependent porosity model is between the the oil recoveries for the other two cases.

In general, as depth dependence is introduced, water breakthrough occurs earlier. As shown in Figure 6.12, with only permeability variation, the water cut rises more gradually after breakthrough due to the fact the porosity is evenly distributed. When porosity is constrained in the bottom, the water level rises more rapidly, breakthrough occurs earlier and water cut rises more rapidly.

The figures of residual oil saturation distributions in Figure 6.13 show that with less pore volume in the bottom, the porosity depth-dependent modeled fault zone (bottom two figures) fills faster to give quicker breakthrough. The permeability heterogeneity modeled embedded fault zone shows that a certain level of tortuosity is introduced because of the equal distribution of pore volume, and thus the fault-zone fills up slowly.

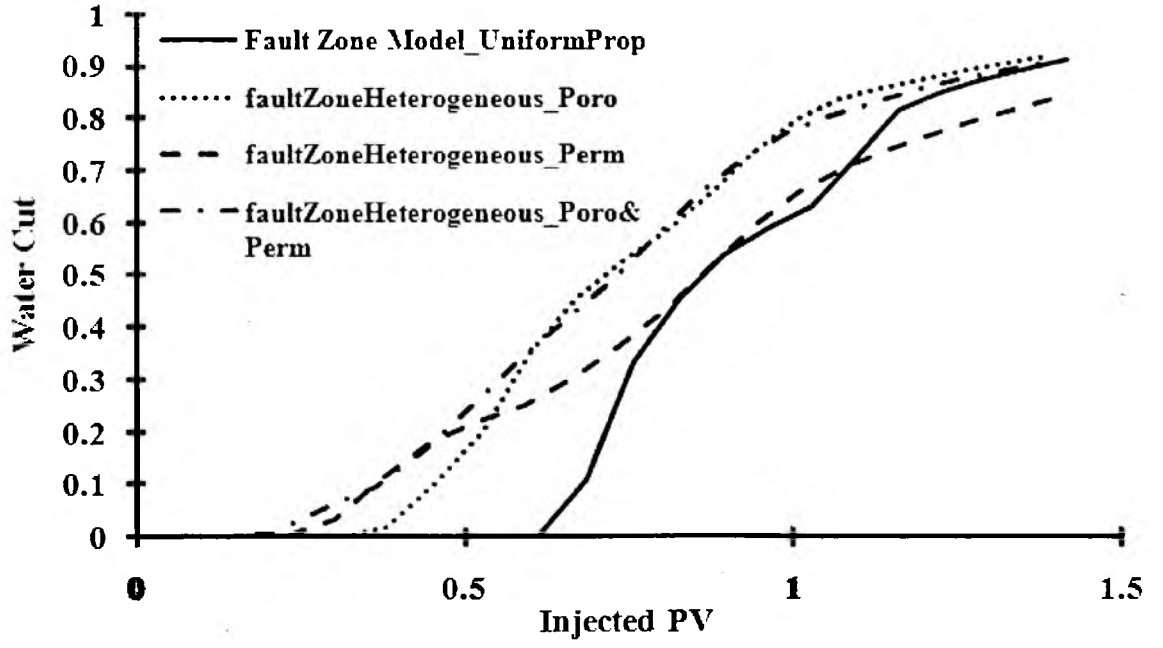

Figure 6.12 Comparisons of water cut among depth-dependent reservoir property models and nondepth-dependent reservoir property model in the embedded fault zone study.

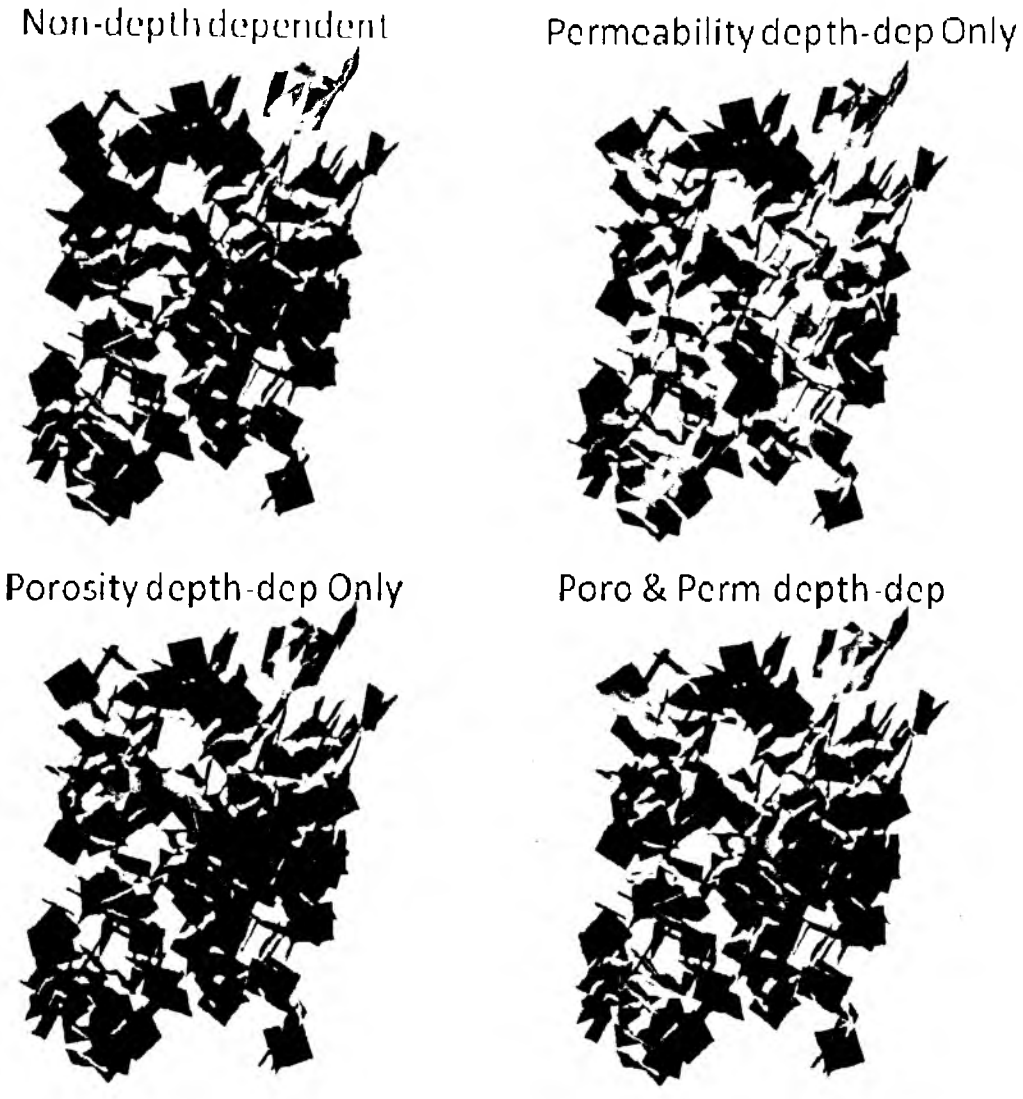

Figure 6.13 Residual oil saturations in the embedded fault zone depth-dependent studies

Similar to case study 2, some efforts have been made to upscale this embedded fault zone model by a single seismic scale feature with the same depth-dependent property distributions. Corey-exponent formulations were applied again in this upscaling study. The water cut curve is very sensitive with the end point adjustment. Two of the closest water cut matches between depth-dependent embedded fault zone and single feature model are presented in Figure 6.14.

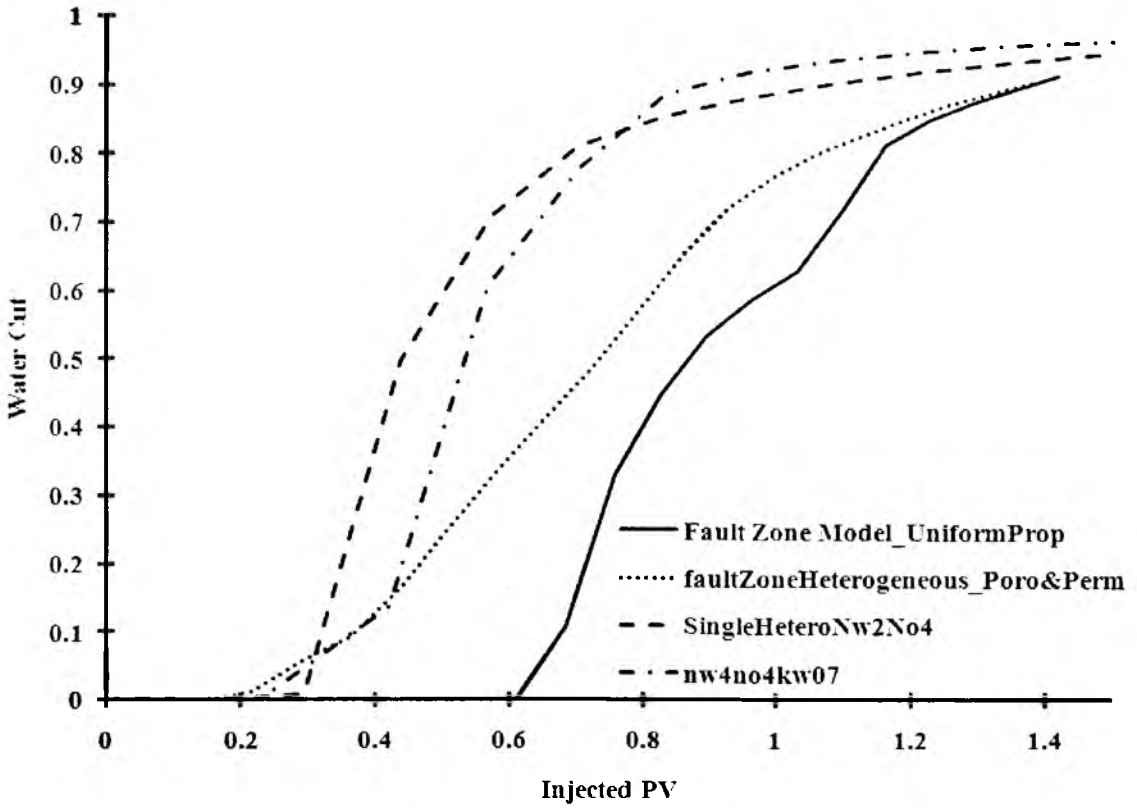

Figure 6.14 Comparisons of water cut between the embedded fault zone model and Corey-exponent relative permeability represented single feature with depth-dependent properties.

Figure 6.14 shows that by adjusting the end points and the Corey's exponents, the water breakthrough from an upscaled single feature could be roughly matched on this highly heterogeneous depth-dependent embedded fault zone model. Obviously the full water cut curve cannot be reached by this effort. This is probably coming from the flow pathway on the embedded zone model by the local cluster densities. In order to precisely match the embedded zone model, instead of using a simple property distribution function, some local fracture network density characterization might be required on the single feature model. Integrating a DFN modeled basement reservoir into a conventional finite-

difference simulator (such as ECLIPSE) for multiphase simulations was discussed in Chapter 4. It is believed that this kind of integrating work plus the relative permeability adjustment will have the water cut curve matched well for embedded fault zone upscaling.

6.5.4 Production Rate Impact on the Single Feature Represent Embedded Fault Zone Through a Conventional Finite-Difference Simulator (ECLIPSE)

Excessive water production is a popular phenomenon observed from some fractured basement reservoirs (Chan et al., 2006). Excess water not only reduces the artificial lift efficiency, but also imposes various types of damage to the oil zones. The postproduction treatment of water is also very costly due to environmental considerations. Understanding of how production rate affects the displacement of oil by water in a basement reservoir system becomes essential.

In this section, production rate sensitivity on a single basement feature model was studied by the conventional ECLIPSE simulator. This single feature could be treated as the "upscaled" embedded zone model even though it does not have any relationship to the embedded zone mentioned before other than similarity in size.

As shown in Figure 6.15, this single feature ECLIPSE model has the size of 4500 by 0.4 by 5300 ft. There are 9540 grid cells (106 by 1 by 90) with equal cell size (50 by 0.4 by 50). The connectivity (kh value) on each cell is the equaled (100,000 md-ft). Constant bottom water pressure support (6,000 psi) has been applied as the bottom boundary conditions and nonflow conditions on the rest of boundaries. Four production wells are set on the top of single feature as shown on the figure with different total fluid

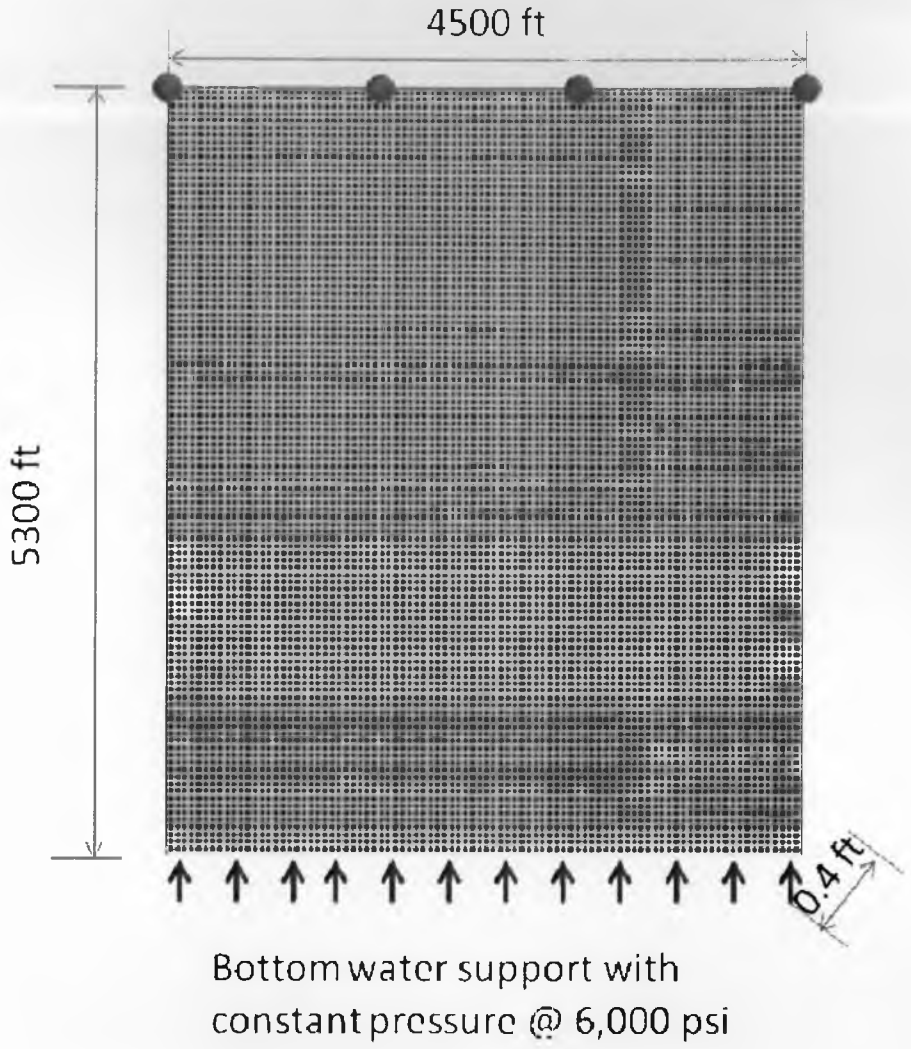

Figure 6.15 Illustrations of ECLIPSE single feature model for rate sensitivity study

rate control. Straight-line relative permeability (with the end points of 0 and 1) is adopted in this rate sensitivity study. By adjusting the production rates, this study will answer three primary questions:

1) Does the oil recovery factor relate to production rate?
2) Does water cut relate to the production rate?
3) Does produced water relate to oil recovery?

Three different production rates (200, 100 and 50 STB/day per well) were applied to this single feature ECLIPSE model. The results are shown in Figure 6.16.

The recovery factors from three simulations are the same as in Figure 6.16. In other words, the production rate will not affect the recovery factor on this single feature model. The slowest rate (50 STB/day) simulation has reached its ultimate recovery with the smallest amount of water being injected. The highest rate (200 STB/day) simulation requires the largest amount of water injected in order to reach its ultimate recoveries. Looking at the curvature from three simulations, the difference between "rate 50" and "rate 100" is very small. However, "rate 200" presents more significant curvature than the other two simulations.

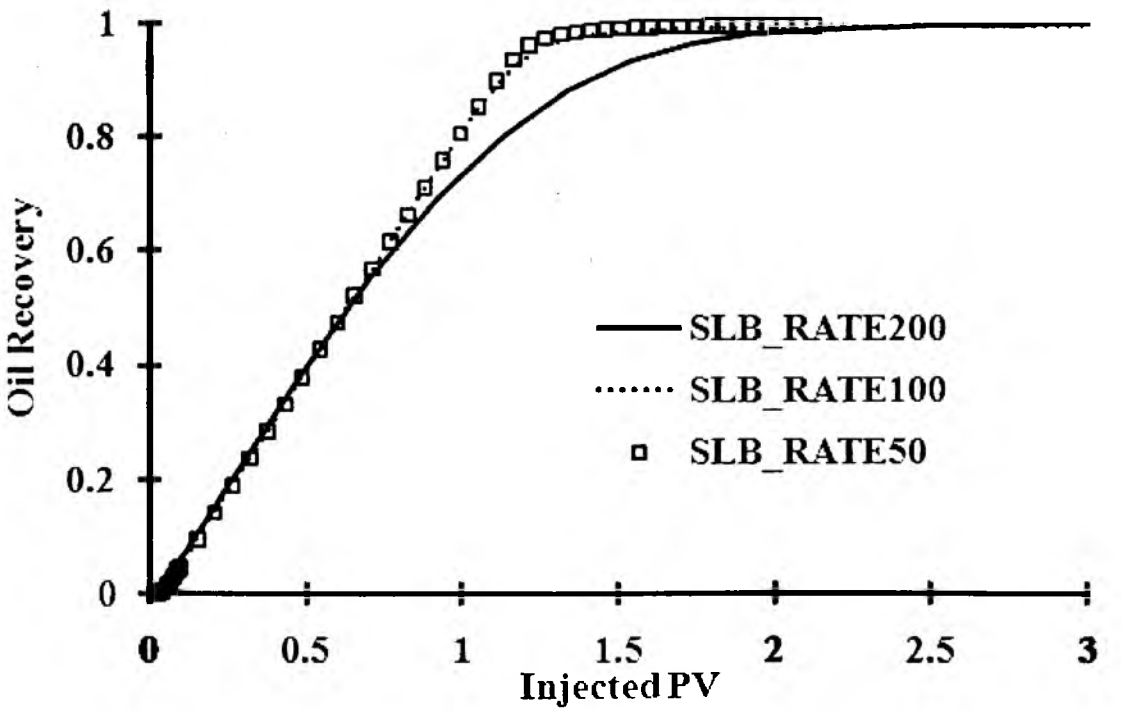

Figure 6.16 Comparisons of oil recovery with different production rates

Water cut results in Figure 6.17 show that high production rate deserves earlier water breakthrough than low rate cases. Similar to the oil recovery figure, the water breakthrough is not linearly relative to the production rate. For example, water breakthroughs for three rate cases are: "rate 200" (0.476 PV), "rate 100" (0.934 PV), and "rate 50" (1.05 PV). The breakthrough difference between "rate 200" and "rate 100" simulations is almost doubled. However, the breakthrough difference between "rate 100" and "rate 50" simulations is only about 10%. Phenomena observed from this water cut figure are that the higher the rate, the earlier the breakthrough and the larger amount of supporting water required. These differences explained higher rates could get bigger water conning during the production.

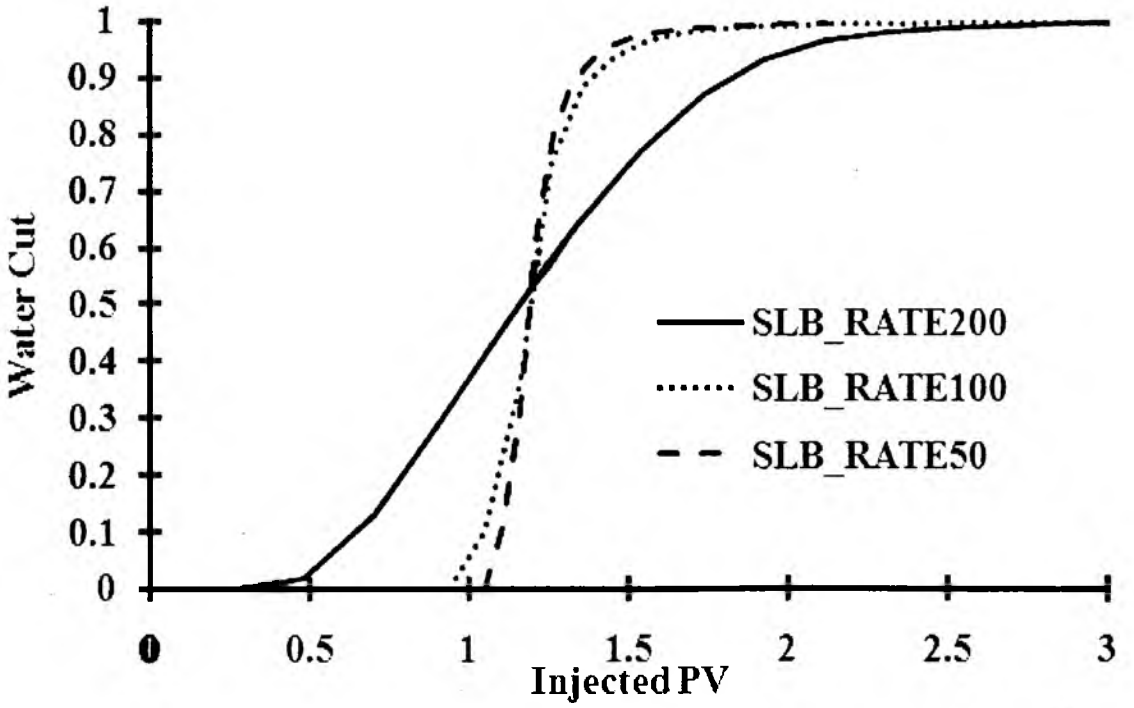

Figure 6.17 Comparisons of water cut with different production rates

Since a higher operating rate could get the water conning phenomena, to reach the same oil recovery, a larger amount of water will be produced with higher rate operations as shown in Figure 6.18, quantitatively, if 95% oil recovery is the goal of production, the amounts of water being produced from various rates are: rate 200" (0.487 PV), "rate 100" (0.0624 PV), and "rate 50" (0.0238 PV). The ratios of produced water with various production rates are: 20.5: 2.61:1.

The conclusion from this case study could be summarized as the following: for a single feature basement model, production rates will not affect the ultimate oil recovery but they will definitely affect the water cut and water productions.

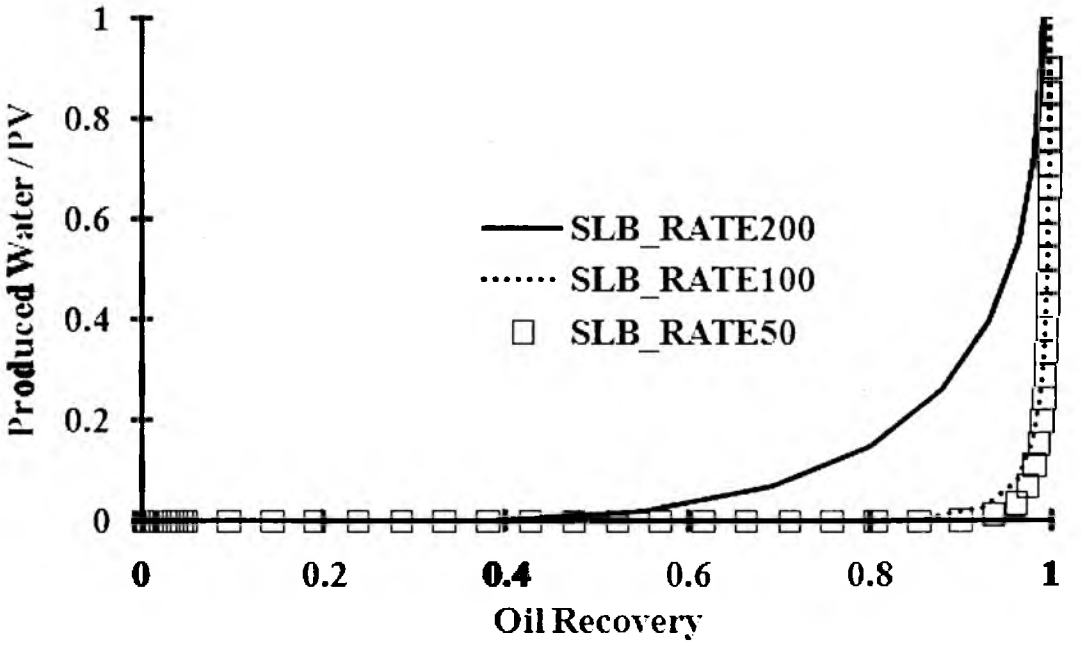

Figure 6.18 Comparisons of produced water correlated with oil recovery for various rates operations

6.5.5 Production Rate Impact on the Single ECLIPSE Feature with Different Boundary Conditions

Bottom water support and side water support are the two most popular basement reservoir driving forces. In this section, as shown in Figure 6.19, with these two types of boundary conditions, the impact of production rate will be studied using the single ECLIPSE feature model. In this model, only one well is set at the top of the single feature. Bottom aquifer support is characterized with the constant pressure of 6,000 psi control from the bottom of the single feature. Side aquifer support is mimicked by two injectors from the middle of two sides in the single feature model with constant pressure of 4,800 psi control. Three various operating rates (400, 200, 100 STB/day) are given for each of the boundary conditioned models.

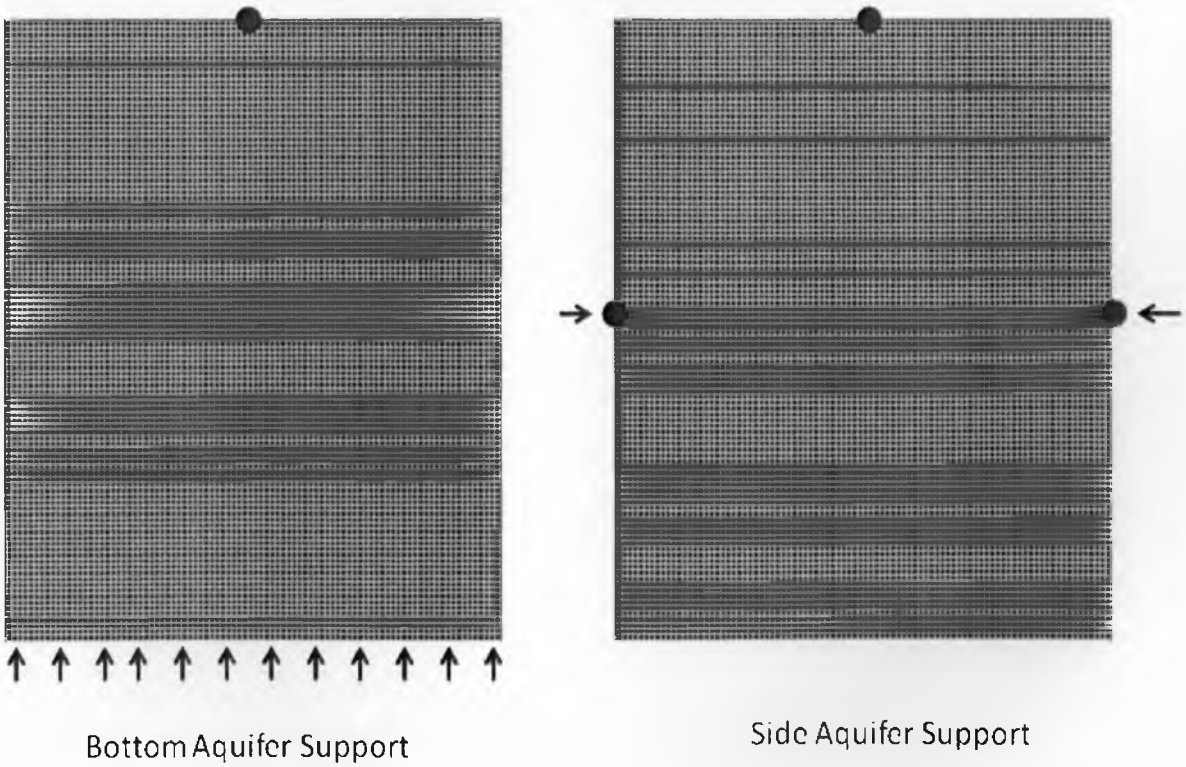

Figure 6.19 Illustrations of bottom aquifer support and side aquifer support single feature models

Similar to the last case study, Figure 6.20 shows that the ultimate oil recovery will not be affected by various production rates on the single basement feature. To reach all simulations' ultimate recoveries, higher production rates require more water to be injected than lower operating rates. With the same highest operating rate, the side aquifer supporting system has a significantly different oil recovery curve than the bottom supporting system.

Water cut results in Figure 6.21 show the significant difference on the highest rate of the side water supporting system (*SideRate400*). Instead of a monoincreasing shape, simulation of *SideRate400* has two inflexions on its water cut curve as shown above. The earlier breakthrough and inflexion could be explained from its oil/water saturation distribution snapshots. Three oil saturation distribution snapshots are listed in Figure 6.22. The simulations listed from left to right are *BottomRate400*, *SideRate400*,

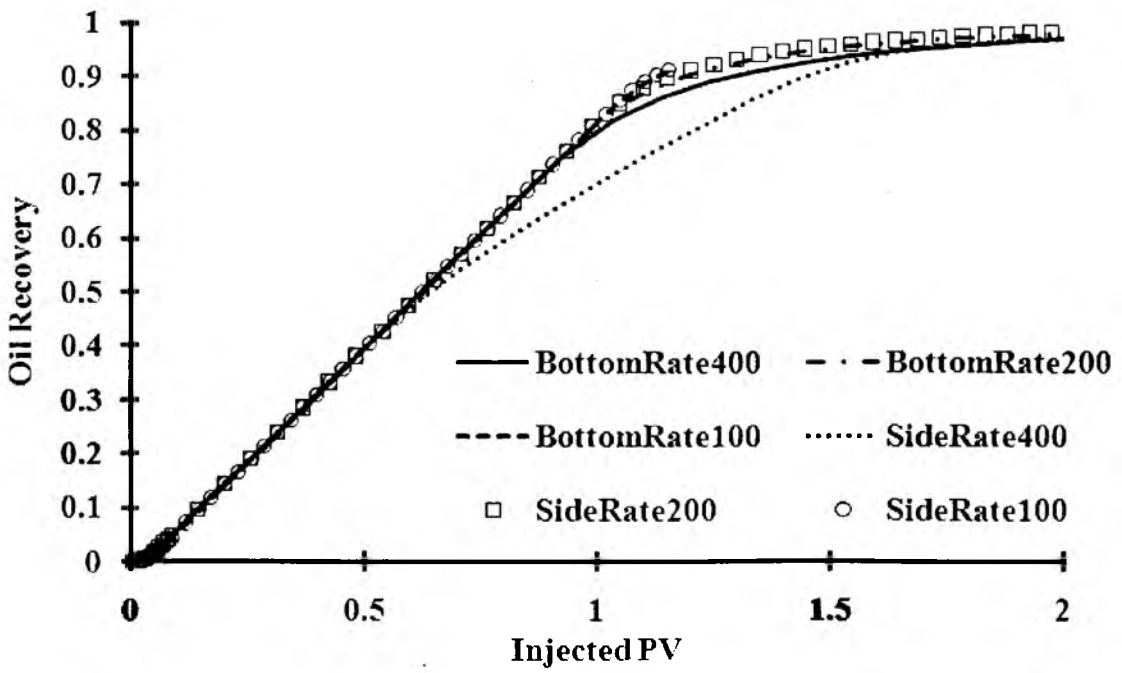

Figure 6.20 Comparisons of oil recovery between different boundaries with various rates

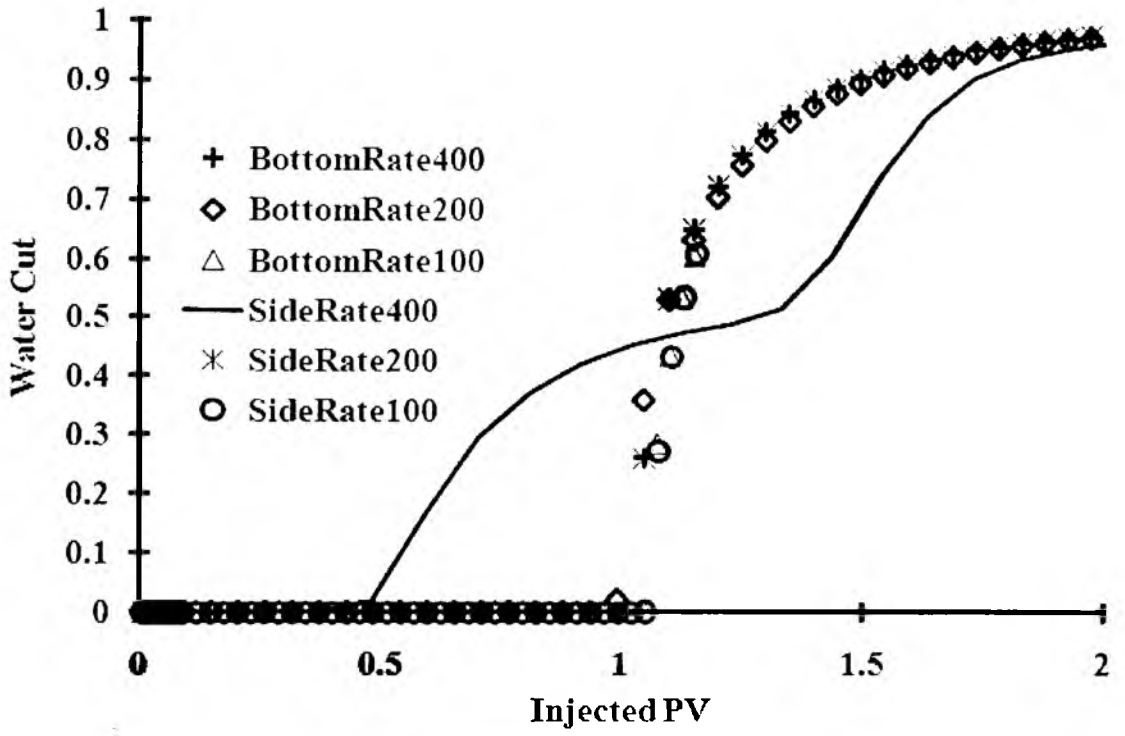

Figure 6.21 Comparisons of water cut between different boundaries with various rates

and *SideRate200*. Pictures on each row are outputted from the same time frame. *BottomRate400* shows that water was evenly built from the feature's bottom and has a conning to the production well at the top middle of the single feature domain. *SideRate400* shows that supporting water comes from two sides, and most of the water will flow to the bottom but part of the water will be sucked into the producer directly through the water conning. Compared to *SideRate400*, all side supporting water in simulation of *SideRate200* will flow to the bottom from the middle and will be built up from bottom.

Simulation of *SideRate400* is a good example of side water intruding flow path by the competition of gravity force and viscous force. Tracing the water saturation distribution figures, inflexion on *SideRate400* water cut curve happened around day

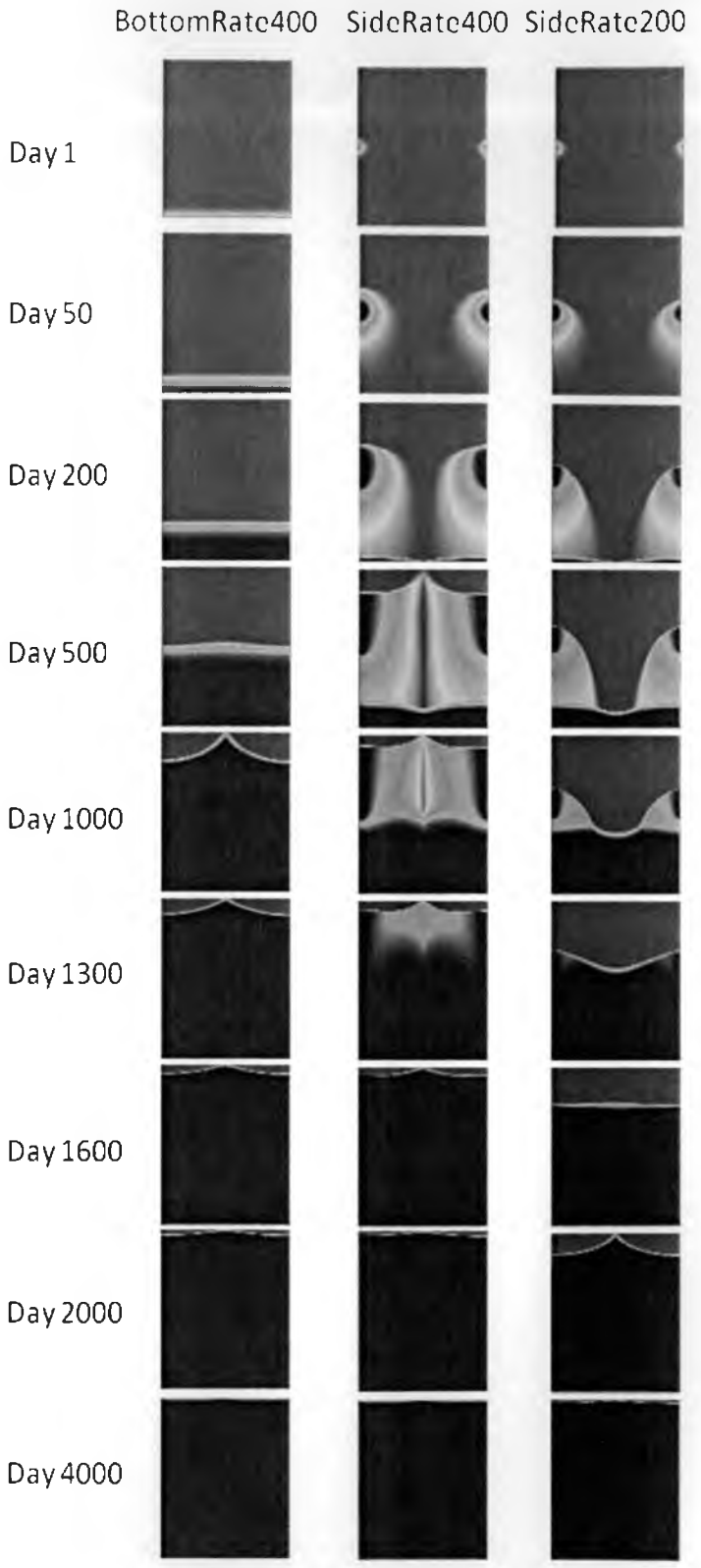

Figure 6.22 Snapshots of oil saturation distributions from various production rates and boundary conditions

1,850 where the side supporting water totally mixed with the bottom buildup waters. With side supporting water, operators should be extremely careful in paying attention to the production rate in order to reduce excessive water productions.

6.5.6 Gravity Number Effects of Single ECLIPSE Feature with Side Supporting

Large vertical single basement feature is easily dominated by the gravity force. However, if the feature had side water intrusion and oil being produced on top of the feature, the operating rate might become essential to have excess water produced. This is due to the fact that the various operational speeds will lead the viscous force changes. Once viscous forces overcome gravity force, side intruding water will be directly sucked into the producers. On a large single vertical basement feature, studying its oil-water displacement mechanism between the gravity force and the viscous force will be meaningful to the reservoir management.

For multiphase fluid flow in porous media, the gravity number (Shook et al., 1992; Kulkarni et al., 2006) was defined as a dimensionless group of the ratio of gravity forces and viscous forces. As an operational parameter dependent group, gravity number helped us understand the dominant reservoir forces on a single sidesupported basement feature, namely gravity force and viscous force. Gravity number is defined as Equation (6-5).

$$N_G = \frac{\Delta\rho.g.\mathbf{k}/\emptyset}{\mu_o.v} \tag{6-5}$$

where, $\Delta\rho$ is the density difference between the displacing and displaced phases, g is the gravity, **k** is the permeability, μ_o is the oil viscosity.

Figure 6.23 and 6.24 show water cut and oil recovery results from various production rates (100, 200, 300, 400, 600 STB/day). Obviously, higher production rates resulted in earlier water breakthroughs and lower oil recoveries under certain injected pore volumes. Figure 6.25 shows that with certain pore volume being injected, the relationships between the oil recovery and the gravity number are quite sensitive. In this study, as the only variable parameter, production rate is in reverse ratio with the gravity number. Lower operating rate resulted in higher gravity number. Figure 6.25 depicts that lower gravity number resulted in lower oil recovery. While the gravity number reached a certain value, recovery will be kept constant. This turning point becomes steeper with the injected PV increasing. In other words, the reservoir being operated around the turning point resulted in the most efficient recovery schema.

This gravity number analysis could explain the phenomena observed on the rate sensitivity study at Chapter 5.

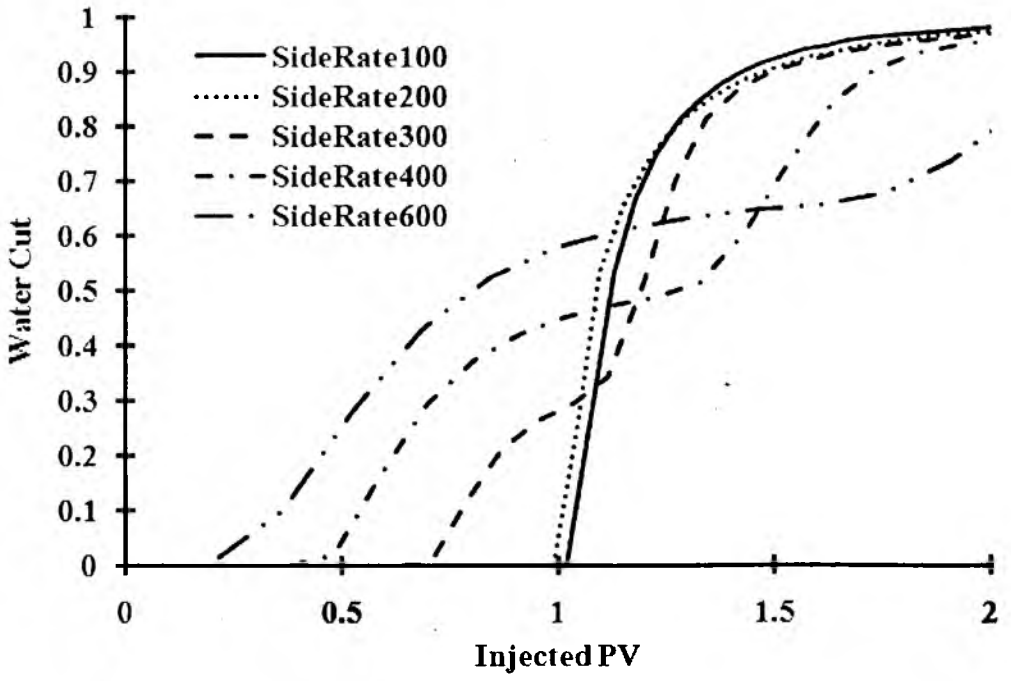

Figure 6.23 Water cut comparisons of rate sensitivity test with side water support

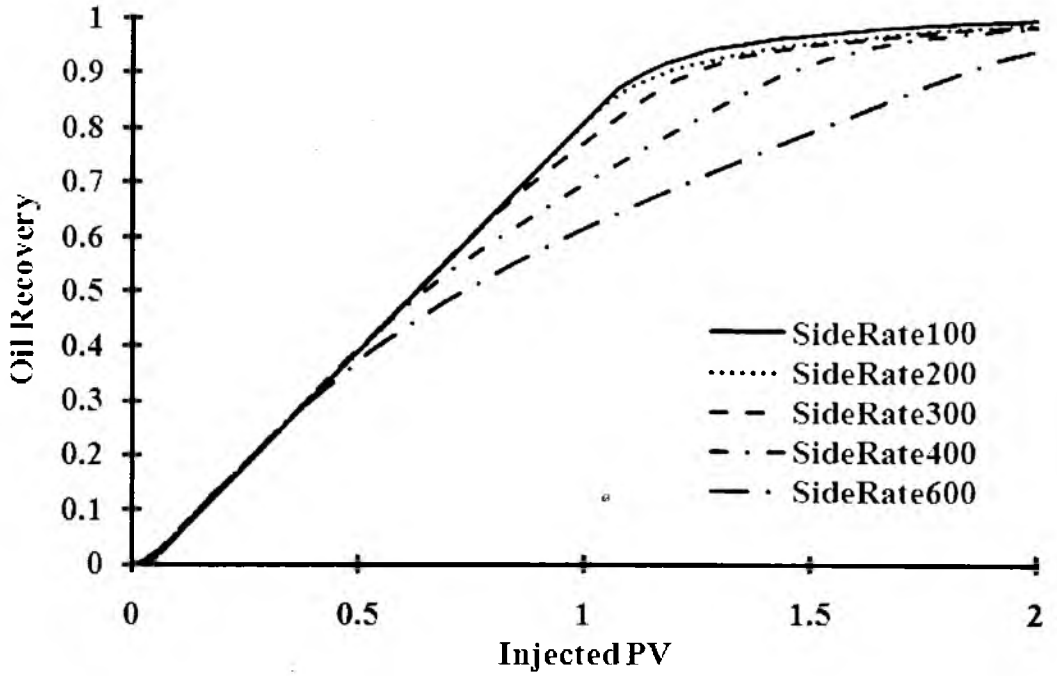

Figure 6.24 Oil recovery comparisons of rate sensitivity test with side water support

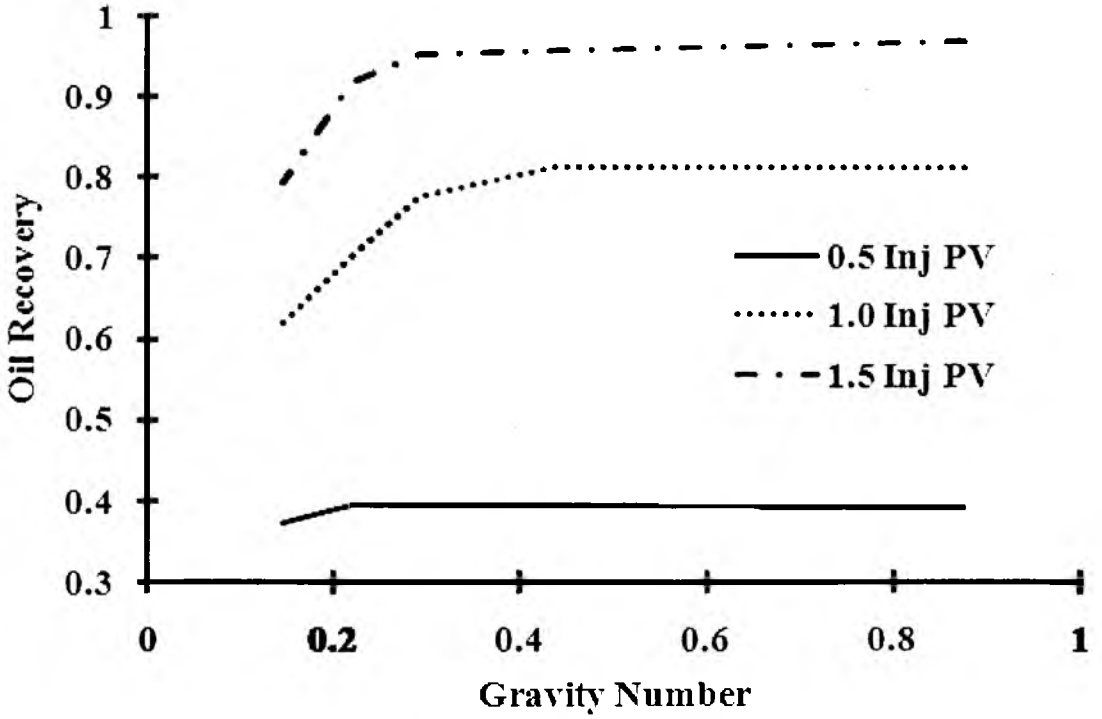

Figure 6.25 Comparison of oil recovery versus flood gravity number by operating rate variations (Rate from left to right are: 600, 400, 300, 200, and 100 STB/day)

6.6 Chapter Summary

This work quantitatively demonstrates the multiphase behavior of one type of DFN characterized embedded fault zone model and its upscaling study. The embedded fracture model tests the influence of the fracture network within major seismic features. Some conclusions that could be drawn from this work are listed below:

1) The DFN characterized embedded fault zone model can represent the single fault from a 3-D seismic reflecting survey in a more realistic way. This model reflects the reality that fracture zones and faults are themselves made up of conducting fracture networks. Multiphase direct simulation of this embedded DFN model is meaningful but might be computing intensive.
2) The approach to the upscaled embedded fault zone model with the single feature model could provide upscaled properties to either DFN based simulators or conventional ECLIPSE simulators. Stranded oil in an embedded zone model simulation cannot be reflected by this type of single upscaling. In order to precisely match the embedded zone model's behavior, this work suggests more local fracture network analysis is needed.
3) Depth-dependent basement fracture properties require more efforts during the upscaling process and this type of depth-dependent relationship does have an impact on the water-oil displacement mechanism.
4) Operating rates cannot affect ultimate oil recovery from a single feature study but do have significant impact on water production. This water-rate relation might be essential with the side water supporting boundary conditions.

5) Gravity number analysis was performed on the side water supporting single feature system. The optimum operating rate could be achieved by correlating the recovery and gravity number.

6.7 Nomenclature

$\boldsymbol{B}$	=	formation volume factor
B_r	=	formation volume factor at the reference pressure
C	=	compressibility, 1/psi
$C_{B,}\boldsymbol{\mu}$	=	compressibility of formation factor and viscosity, 1/psi
$\boldsymbol{g}$	=	acceleration of gravity, ft/sec^2
$\mathbf{k}$	=	permeability tensor, md
k_r	=	relative permeability
$k_{rw,or}$, $k_{ro,cw}$	=	end-point relative permeability for oil and water
N_G	=	gravity number
n_w, n_o	=	Corey exponents for water and oil respectively
$\boldsymbol{o}$	=	oil phase
$\boldsymbol{P}$	=	fluid pressure, psi
$\boldsymbol{S}$	=	phase saturation
S_{cw}	=	connate water saturation
S_{or}	=	residual oil saturation
$\boldsymbol{u}$	=	velocity, ft/day
$\boldsymbol{w}$	=	water phase
WC	=	water cut
WP	=	water production, pore volume

$\emptyset$	=	porosity
ρ	=	density, lbm/ft^3
μ	=	viscosity, cp

6.8 Bibliography

Cao, H., Aziz, K.: "Evaluation of Pseudo Functions," paper SPE 54589 (May 1999)

Chan, K., Lam D.D., Ivanov, A., Apisitsareekul, K., Hai, L.V., Nghi, N.C., Hung, V.Q., and Lang. L.D, "Production Improvement Water Shutoff for White Tiger Field," SPE 103329 (2006)

Coats, K.H., Dempsey, J.R., and Henderson, J.H.: "The Use of Vertical Equilibrium in Two-Dimensional Simulation of Three-Dimensional Reservoir Performance," SPEJ (1971) 63-71.

Christie, M.A., and Blunt M.J.: "Tenth SPE Comparative Solution Project: A Comparison of Upscaling Technique," paper SPE 66599, (2001)

Ding, Y., Basquet, R., Bourblaux, B., "Upscaling Fracture Networks for Simulation of Horizontal Wells Using a Dual-Porosity Reservoir Simulator," paper SPE 92774 (2006)
Dean, R.H., and Lo, L.L.: "Simulations of Naturally Fractured Reservoirs," SPERE (May, 1988) 638-648

Durlofsky, L.J., Jones, R.C., and Milliken, W.J., "A New Method for the Scale Up of Displacement Processes in Heterogeneous Reservoirs," paper presented at 1994 European Conference on the Mathematics of Oil Recovery (1994)

Fu, Yao, "Multiphase Control Volume Finite Element Simulations of Fractured Reservoirs," Ph.D Dissertation, University of Utah, Salt Lake City (2007)

Fu, Y., Yang, Y-K., and Deo, M., "Three-Dimensional, Three-Phase Discrete-Fracture Reservoir Simulator Based on Control Volume Finite Element (CVFE) Formulation", paper SPE 93292, (2005)

Pooladi-Darvish, M. and Firoozabadi, A., "Experiments and Modelling of Water Injection in Water-wet Fractured Porous Media", J. Can. Pet. Tech., vol. 39, no. 3 (2000)

Hewett, H.A. and Archer, R.A.: "Scale-Averaged Effective Flow Properties for Coarse-Grid Reservoir Simulation," paper SPE 37988, June 1997

Jacks, H.H., Smith, O.J.E., and Mattax, C.C.: "The modeling of a Three-Dimensional Reservoir with a Two-Dimensional Reservoir Simulator – The Use of Dynamic Pseudo Functions," SPEJ (1973) 175-185.

Kyte, J.R. and Berry, D.W.: "New Pseudo Functions to Control Numerical Dispersion," SPEJ (1975) 269-276.

Kulkarni, M.M., and Rao, D.N., "Characterization of Operative Mechanisms in Gravity Drainage Field Projects Through Dimensional Analysis", SPE 103230 (2006)

Muggeridge, A.H., "Generation of Effective Relative Permeabilities from Detailed Simulation of Flow in Heterogeneous Porous Media," *Reservoir Characterization II*, L.W. Lake, H.B. Carroll, and T.C. Wesson, 197-225 (1991)

Okano, H., Christie, M.A., Subbey, S., Sambridge, M., Monfared, H., "Quantification of Uncertainty in Relative Permeability for Coarse-Scale Reservoir Simulation," paper SPE 94140 (2005)

Romm, E.S., "Fluid Flow in Fractured Rocks" (English translation) W.R. Blake (transl.), Philips Petroleum Co., Bartlesville, Okla. (1972)

Rossen, R.H., and Shen, E.I.C.: "Simulation of Gas/Oil Drainage and Water/Oil Imbibition in Naturally Fractured Reservoirs," SPERE (November, 1989) 464-470.

Shook, M., Li, Dachang and Lake L., "Scaling immiscible Flow through Permeable Porous Media by Inspectional Analysis," in Situ, 16(4), 311-349 (1992)

Talukdar, M.S., Banu, H.A., Torsater, O., Kleppe, J., "Applicability and Rate Sensitivity of Several Up Scaling Techniques in Fractured Reservoir Simulation" paper SPE 59048 (2000)

Warren, J.E. and Root, P.J.: "The Behevior of Naturally Fractured Reservoir," SPEJ (September 1963).

Yang, Yi-kun, Finite-element Multiphase Flow Simulation, Ph.D Dissertation, University of Utah, Salt Lake City, UT (2003)

CHAPTER 7

MULTIPHASE FLOW STUDIES ON FRACTURED/FAULTED TYPE II RESERVOIRS WITH DISCRETE FRACTURE NETWORK APPROACHES

(A paper in preparation)

Huabing Wang[1], Craig Forster[1], Chung-Kan Huang[1], and Milind Deo[1]

1. Department of Chemical Engineering

University of Utah

Salt Lake City, UT 84112

7.1 Abstract

A new fully-implicit, three-dimensional (3-D), three-phase, discrete fault/fracture with matrix, black-oil simulator provides new insight and understanding of oil production from reservoirs in fractured, medium-permeability sandstone or carbonate formation. Results obtained with a controlled volume finite element (CVFE) method compare favorably to the lab scale core experiment. One quarter of a lab core experimental sample (18.75 by 18.75 by 121.92 cm) with five orthogonal fractures was modeled by discrete fracture network (DFN) in this study. At the beginning of this chapter, this model was used to verify the new simulator. The results on this core scale modeling are highly matched lab results at low flow rate. In the high flow rate region, the simulation results reflected a slightly delayed water breakthrough but predicted excellent final recovery fraction with the experiment. Then, dip-slip fault and strike-slip fault geological models were constructed and studied for various purposes of fracture network impact on Type II reservoirs. By these studies, the following aspects of Type II reservoirs were quantitatively evaluated: understanding the importance of a fault that separates and connects two lobes of a fractured reservoir, line drive scenarios on a heterogeneous matrix with fractures, and existence of ultrahigh permeability faults between injector and producer on a heterogeneous system. This work demonstrated that the CVFE method provides a much-improved ability to represent complex fracture/fault geometries in porous formations underground and that it has a strong capability to handle the multiphase fluid flow problems. These advantages are important in helping understand the uncertainties caused by fracture network existence when attempting to develop innovative approaches to reservoir management.

7.2 Introduction

Naturally fractured reservoirs make up a large and increasing percentage of the world's oil/gas reserves. Generally, naturally fractured reservoirs could be classified in four types (Nelson, 2001) from the fractures' positive contributions to the overall reservoir quality. Type II fractured system is the largest fractured reservoir type worldwide. In this reservoir type fractures provide the essential reservoir permeability and matrix supplies any significant porosity or storage. An early knowledge of fracture/matrix interaction is extremely important to determine whether the matrix porosity can be drained by the fracture system. The recovery from reservoirs where fractures dominate permeability is often a fraction of the resource recovered from conventional reservoirs in which matrix permeability dominates. The lower recovery and higher risks relate to the difficulty of forecasting how various completion placements, water flood patterns, and tertiary recovery processes will actually perform in fractured reservoirs. A reduction in risk and an improvement in understanding of reservoir behavior will lead to enhanced profitability from under-exploited fractured fields. Fractures do more than simply increase reservoir permeability. Fundamentally, fractures alter reservoir connectivity and heterogeneity. A precise characterized fracture network model will be the key to improving oil and gas recovery in naturally fractured reservoirs. Identifying, characterizing, and mapping the fracture network in terms of the dominant flow paths, aperture, length, height, connectivity, conductivity, and frequency distribution are crucial for optimal reservoir management. However, it is well known that the accurate simulation of multiphase fluid flow in this reservoir type remains a significant challenge.

Dual-porosity modeling is the most popular simulation technique for Type II fractured reservoir flow predictions. This model was first introduced to the petroleum industry by Warren and Root (1963), and methods for simulating dual-porosity systems have been proposed by several authors (Kleppe and Morse, 1974; Yamamoto et al., 1971; Kazemi et al., 1976; Rossen, 1977; Dean and Lo, 1988; Fung et al., 1991; and others). If the matrix blocks are linked only through the fracture system, this could be treated conventionally as a dual porosity single-permeability system, since fluid flow though the reservoir takes place only in the fracture network with the matrix blocks acting as sources. If there is the possibility of flow directly between neighboring matrix blocks, this is conventionally considered to be a dual porosity dual permeability system. The dual porosity system is represented by two different continua, one representing the porous matrix and the other representing the fractures. Fluid flow is primarily through the high permeability, low porosity fractures surrounding individual matrix elements. The matrix blocks contain the majority of the reservoir volume and act as sources or sinks to the fractures. A transfer function describes the mass transfer between the matrix and fracture continua. This core part of transfer function is represented by a shape factor. The whole picture of the dual-porosity model is that the geological and flow complexity are reduced to a single parameter – the shape factor and the shape factor might be too ideal to represent fluid flow in such a heterogeneous environment (Gong et al., 2006). The model is also limited to the sugar cube representation of fractured media. The transfer function between the fracture and the matrix may not be properly described when gravity and viscous effects are involved. This approach also assumes that the media have dense

closely connected fractured networks and may not be very accurate when treating only a few fractures.

The DFN (Dershowitz et al., 1979; Basquet et al., 2005; Araujo, et al., 2004) approach models the geometry of the fracture network explicitly and provides a realistic way of modeling fractured reservoir performance. However, these DFN descriptions are generally too detailed to be simulated by conventional reservoir simulators. Some research has been done by connecting DFN with the dual-porosity model for the case of single-phase flow by Dershowitz (1998). This approach is limited with single-phase flow, but no accurate multiphase flow study has been reported.

In this study, a flux-based upstream-weighted three-dimensional, two-phase (oil, water) black-oil CVFE simulator was developed and employed (Yang, 2003; Fu et al., 2005). This CVFE formulation was validated and numerically verified through the indexing method (Chapter 3) and the manufactured solution method (Yang, 2003; Fu, 2007). This CVFE formulation's rotatable permeability is good at tensor handling and makes possible the direct accurate simulation of the DFN modeled fractured reservoir.

At the beginning of the study, the simulator was verified with the core scale lab experiment on high/low velocity scenarios. Then several large-scale Type II fractured reservoir models were studied by this simulator. The impact of the fractured network's existence on the Type II fractured reservoir with multiphase (two-phase or three-phase with compressibility, capillary pressure and gravity considered) flow were studied with this new technique. It showed that this is a powerful tool in helping to understand the role of fractures for multiphase flows.

7.3 Type II Fractured Reservoir Modeling

The explicit treatment of fractures and faults is detailed in Kim and Deo (2000) and Yang (2003). The fluid potential and saturation values are defined on the vertices of the tetrahedron for the rock matrix calculations. The tetrahedron and the associated control volumes are shown in Figure 7.1.

For type II fractured reservoir simulations, the fluid potential value in the tetrahedron is interpolated using the interpolation functions. The fluid saturation value is calculated for each control volume from the solution of the residual equations, which are the fully discretized partial differential equations. For detailed numerical methods refer to Fu et al. (2005).

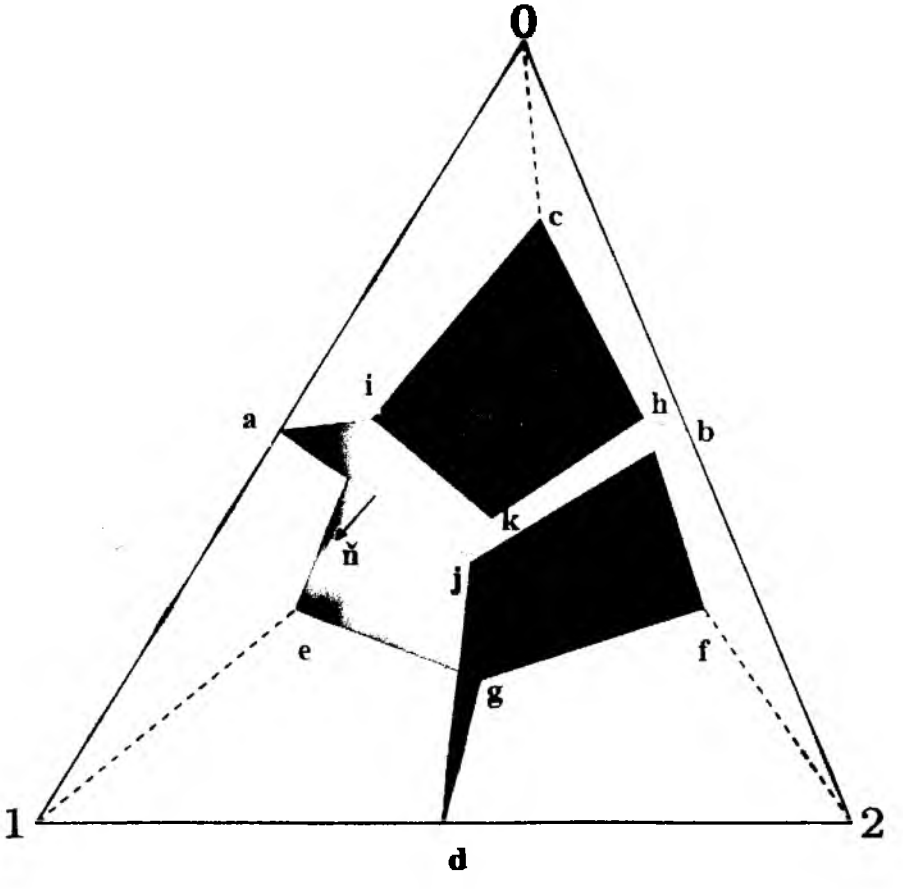

Figure 7.1 A tetrahedral element with associated control volumes

7.4 CVFE Simulator Verification with Pooladi-Davish and Firoozabadi's Fracture Water Level (FWL) Experiment

A reported experiment by Pooladi-Davish and Firoozabadi (2000) was used to verify the Type II CVFE simulator. Montegudo et al. (2004) verified this experiment through the simulation approach with good agreement. Their experiment consisted of flooding water over a type II matrix-fracture apparatus. The apparatus is made by assembling 12 matrix blocks as shown in Figure 7.2.

Water was injected with different rates from the bottom of the apparatus to expel the nC10 which initially filled in all the fractures and matrix blocks. They reported the oil recovery versus the pore volume injected at different rates.

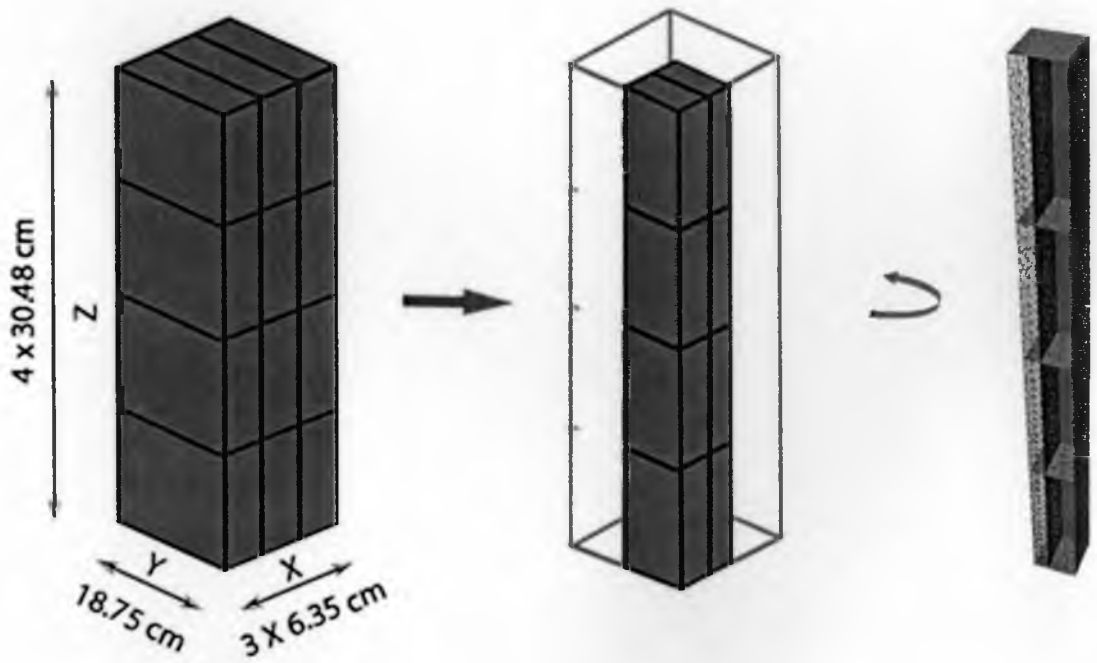

Figure 7.2 Rock assemblies of the stacked blocks and the domain used in the modeling

Considering the symmetry feature of the problem, only a quarter of the domain was adopted to be simulated (as shown above) in this CVFE simulator verification. The domain was meshed by CUBIT, a finite-element mesh generator developed by Sandia National Laboratories. An isothermal black-oil model was used and the critical input parameters for this modeling are summarized in Table 7.1:

The analytical curves are used to calculate relative permeabilities Equations (7-1) and (7-2).

Table 7.1 Summary of critical data for modeling Pooladi-Davish and Firoozabadi's fracture water level experiment

Simulator	**CVFE**	
Grid information		
N_t	2374, 6741, 9488	
Fluid property	Water	oil
μ (cP)	1.0	0.94
γ (lbf/ft^3)	59.28	49.92
Rock property		
Φ (m, f)	0.315, 1.0	
k (m, f) (md)	2.48, 846.37	
Rock-fluid data		
S_{or}	0.35	
Fracture		
Pc_{wo} (psi)	0.0	
Kr_{wo}, n_w	1.0, 1.0	
Kr_{no}, n_o	1.0, 1.0	
Matrix		
Pc_{wo} (psi)	-0.1156 ln(S_o)	
Kr_{wo}, n_w	0.2, 4.0	
Kr_{no}, n_o	0.8, 2.0	
Initial conditions		
P (psi)	14.7	
S_w	0.0	
Boundary conditions	Nonflow boundary conditions	
Well conditions		
Injection	Water rate (PV/hr)	0.011, 0.160
Production	Total liquid rate (PV/hr)	0.011, 0.160

$$kr_w = kr_{wo} S_o^{n_w} \tag{7-1}$$

$$kr_o = kr_{no}(1 - S_o)^{n_o} \tag{7-2}$$

where

$$S_o = \frac{S_w}{1 - S_{or}} \tag{7-3}$$

The oil recovery results from numerical simulation and experiment are compared with the water injection rate of 0.011 and 0.160 PV/hr as shown in Figure 7.3.

The numerical model simulated by the CVFE simulator predicted slightly lower ultimate oil recovery with both high and low injection rates. At a low injection rate, the CVFE simulator almost predicted the exact the same water breakthrough as the Pooladi-Davish and Firoozabadi (2004) experiment. However, with a high injection rate, water

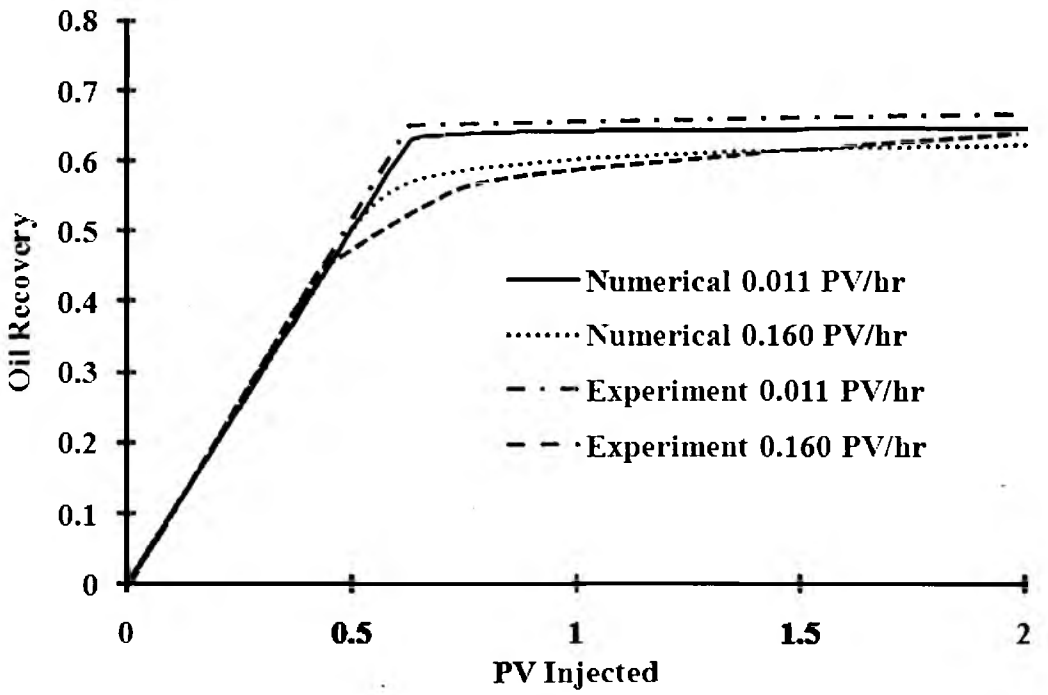

Figure 7.3 Oil recovery comparisons between experiment results and simulation results on low water flooding rate (0.011 PV/hr) and high water flooding rate (0.160 PV/hr)

breakthrough was delayed in the numerical simulation. This effect might be caused by the unit relative permeability assigned for the fluid flow with fractures. The capillary force effects might need to be considered in the main fractures during the modeling of this process. Another possible reason for this effect is the fracture permeability set up in DFN modeling. This model was very small and thin compared with the reservoir scale system; also, it was hard to check how many of the system errors might have been generated from the experiment. The fracture permeability might be set slightly lower in the numerical model. Then the permeability becomes essential in the high rate case. At a high injection rate, the breakthrough was dominated by the displacement in the fractures; the process of water imbibitions to drain the oil out of the matrix was comparably slower than the process acting on the fractures. Therefore, an earlier breakthrough compared with the low injection rate case was expected and shown from both numerical simulations and the experiments.

To check if the numerical model converged on the grid sizes, this domain had been meshed into three different finite volume resolutions. The meshed elements numbers were 2374, 6741 and 9488. At the injection rate of 0.160 PV/hr, these three discretized domains were simulated and the oil recoveries are shown in Figure 7.4.

The results showed that a very small discrepancy could be observed at these three grid resolutions. These simulation results indicate that the CVFE simulator can achieve good convergence at different resolution scales and can match experiment results. This suggested that the CVFE simulator could be numerically applied to study complex Type II system.

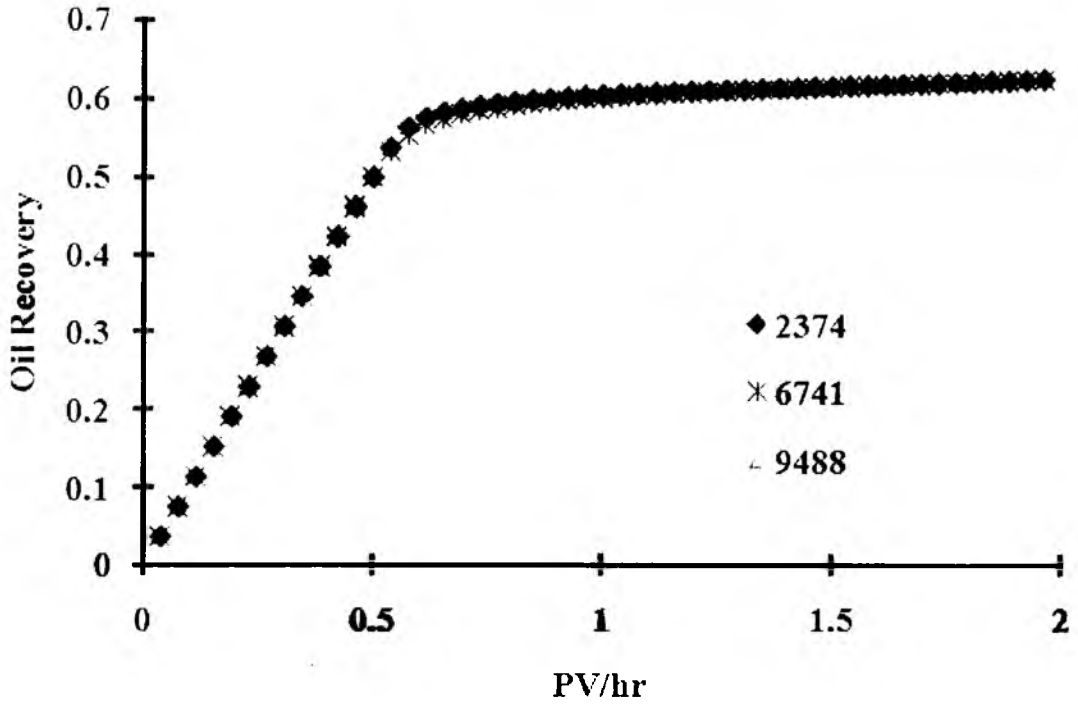

Figure 7.4 Oil recovery comparisons on different finite volume refinement with 0.160 PV/hr water injection rate

7.5 Applications

7.5.1 "Dip-Slip Faults" Model: a Dip-Slip Fault Separates and Connects Two Lobes of a Fractured Reservoir

A dip-slip fault is a fault whose main sense of movement (or slip) on the fault plane is vertical. Geologically, dip-slip faults can be classified as "reverse" and "normal." A normal fault occurs when the crust is extended. Alternatively such a fault can be called an extensional fault. The hanging wall moves downward, relative to the footwall. A reverse fault is the opposite of a normal fault–the hanging wall moves up relative to the footwall. Reverse faults are indicate shortening of the crust. The dip of a reverse fault is relatively steep. The angle might be greater than 45°. Normal and reverse dip-slip faults are shown in Figure 7.5.

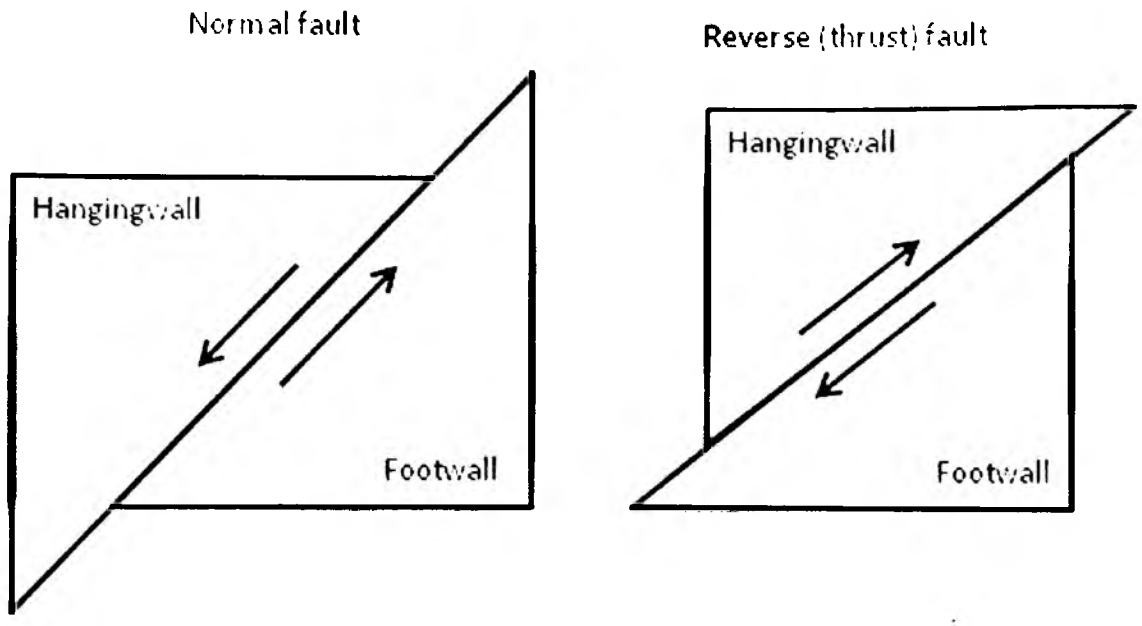

Figure 7.5 Cross-sectional illustrations of normal and reverse dip-slip faults

In this section, a conceptual model of two type II fractured reservoirs connected by a normal fault was constructed and studied. The basic assumption in this model was that in approaching to the normal fault, the intensity of small fractures in the matrix increases, and the matrix porosity and permeability increases as well. Two scenarios were studied in order to compare the normal fault impact on the oil productions in this type of reservoir: very permeable "tunnel" (assigned 10,000 md) and not very permeable "barrier" (assigned 100 md). There were six wells: two wells on the bottom corners of the upper reservoirs (refer to Figure 7.6); two producers on the bottom corners of the dip-slip fault and two producers on the bottom corners of the lower reservoir. The phase model was initially set as three-phase: oil, water and solution gas. For more details regarding reservoir model properties, refer to the data summary table in Figure 7.6 and Figure 7.7.

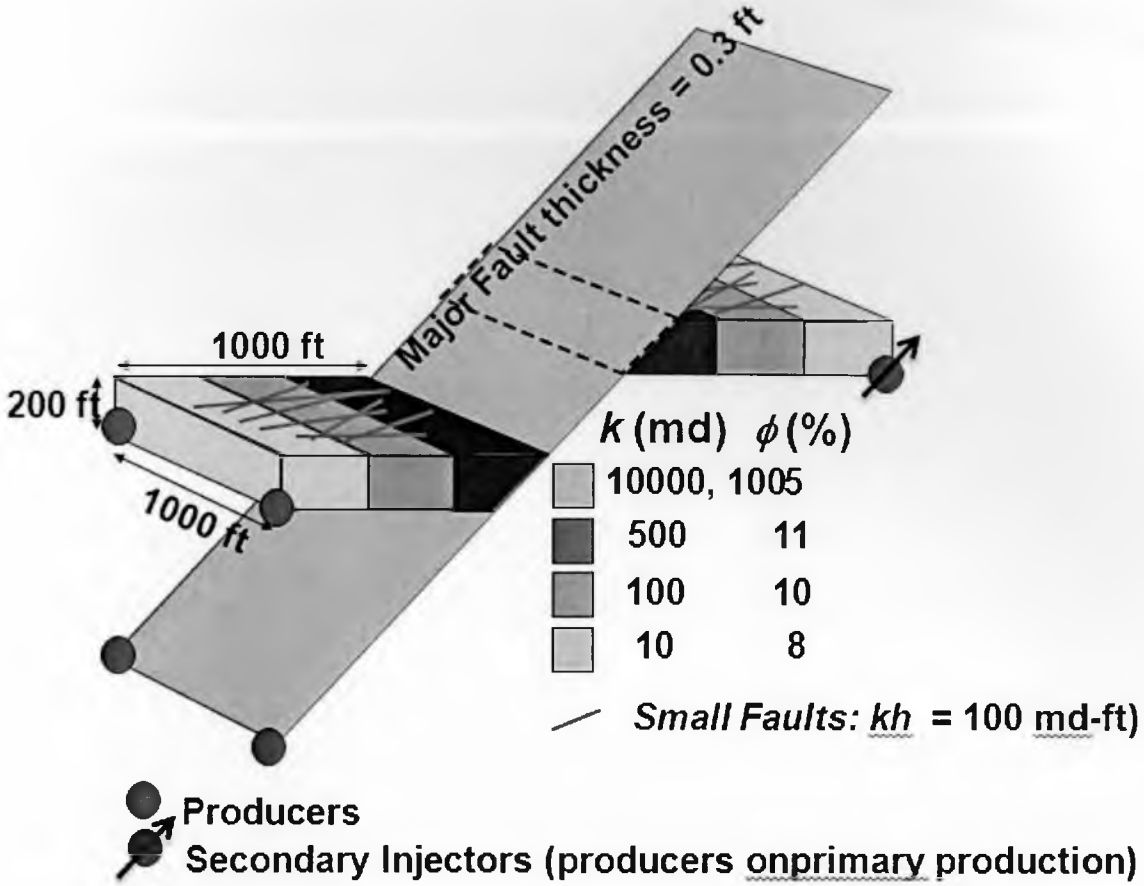

Figure 7.6 Illustration of three-dimensional heterogeneous type II fractured reservoir connected by normal fault

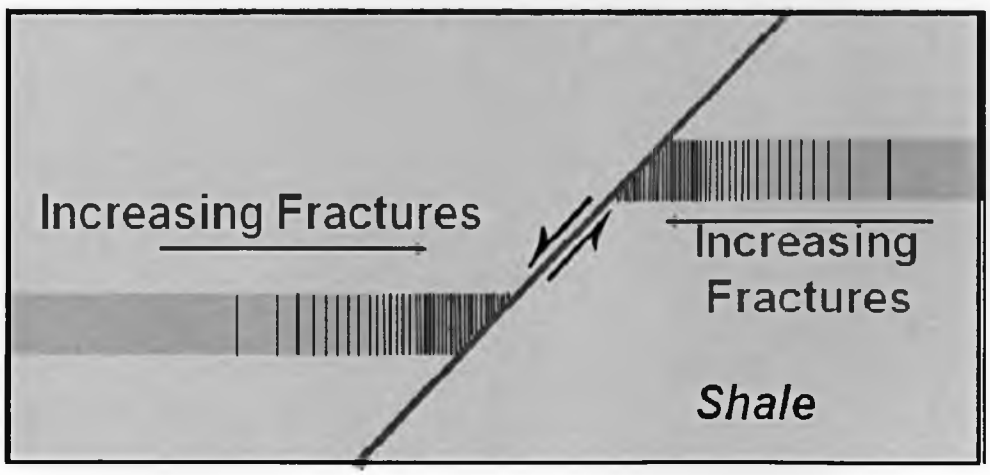

Figure 7.7 Cross-section of type II reservoirs connected by normal dip-slip fault

The dimensions of the two connected reservoirs are the same (1000 by 1000 by 200 ft). The fractures inside of each reservoir have different orientation and size. The connecting fault is 1000 by 2642 by 0.3 ft with dip angle of 45^{o}.

As described in Table 7.2, two simulations were performed on this conceptual model: normal fault with 10000 md permeability case and 100 md permeability case. Other than the normal fault permeabilities, all of the simulation conditions are exactly the same between these two simulations. The total simulation time was 6000 days with the first 600 days as the primary production time and the secondary production thereafter. During the primary production period, all six wells were operated as the producer with bottom hole pressure (BHP) control at 2200 psi.

In the primary production stage, the reservoir driving force was combined of the solution gas driving and the gravity driving. As the pressure dropped, more and more solution gas was released from the oil phase to keep the reservoir pressure. Starting from day 601, two wells on the bottom corner at the upper reservoir were turned into the injector and began injecting water. These two converted water injector are operated by BHP control which pressure is 1000 psi higher than the operating conditions of the rest producers. This reservoir production stage was called secondary production period. The secondary productions were kept until the end of the simulation. Some results (such as oil recovery percentage, oil production rate, water cut) of these simulations are compared in the rest of this section.

Table 7.2 Summary of data for modeling type II reservoirs connected by normal fault

Simulator				**CVFE**			
Grid information							
Node number				4321			
Fracture triangle elements				3131			
Matrix tetrahedron elements				16960			
Fluid property			Water		oil	gas	
Density (lbf/ft^3)			62.0		45.0	0.062428	
Hydrocarbon properties (pressure related)				Oil			Gas
Pressure (psi)	Rs (Mscf/stb)	Bo (rb/stb)	C_{Bo} (1/psi)	μ_o (cp)	$C_{\mu o}$ (1/psi)	Bg (rb/Mscf)	μ_g (cp)
400	0.165	1.0120	1e-5	1.17	0.0	5.90	0.0130
800	0.335	1.0255	1e-5	1.14	0.0	2.95	0.0135
1200	0.500	1.0380	1e-5	1.11	0.0	1.96	0.0140
1600	0.665	1.0510	1e-5	1.08	0.0	1.47	0.0145
2000	0.828	1.0630	1e-5	1.06	0.0	1.18	0.0150
2400	0.985	1.0750	1e-5	1.03	0.0	0.98	0.0155
2800	1.130	1.0870	1e-5	1.00	0.0	0.84	0.0160
3200	1.270	1.0985	1e-5	0.98	0.0	0.74	0.0165
3600	1.390	1.1100	1e-5	0.95	0.0	06.5	0.0170
4000	1.500	1.1200	1e-5	0.94	0.0	0.59	0.0175
4800	1.676	1.1400	1e-5	0.91	0.0	0.49	0.0185
5200	1.750	1.1480	1e-5	0.90	0.0	0.45	0.0190
5600	1.810	1.1550	1e-5	0.89	0.0	0.42	0.0195
Water properties*							
Reference pressure ($p_{ref.}$ psi)					14.7		
Water formation factor B_{wr} @ reference pressure (rb/stb)					0.0142		
B_{wr}'s compressibility (1/psi)					1.0e-6		
Water viscosity (μ_{wr}) @ reference pressure (cp)					0.96		
μ_{wr}'s compressibility (1/psi)					0.0		
Rock property							
Φ (matrix)					0.11		
Φ (fracture)					0.0		
Φ (fault)					0.05		
k (matrix) (md)					10, 100, 500		
k (fracture) (md-ft)					100		
k (fault)					10000, 100		

Table 7.2 Continued

Rock-fluid data *(Oil-water system)*					
	S_w	k_{row}	K_{ro}	p_{cow} (psi) (matrix)	p_{cow} (psi) (fracture)
	0.20	0.00	1.00	7.0	0.0
	0.30	0.07	0.40	4.0	0.0
	0.40	0.15	0.125	3.0	0.0
	0.50	0.24	0.0649	2.5	0.0
	0.60	0.33	0.0048	2.0	0.0
	0.80	0.65	0.00	1.0	0.0
	0.90	0.83	0.00	0.5	0.0
	1.00	1.00	0.00	0.0	0.0
Gas-water system					
	S_w	k_{rgw}	K_{rw}	p_{cgw} (psi) (matrix)	p_{cgw} (psi) (fracture)
	0.00	0.00	1.00	0.0	0.0
	0.04	0.00	0.60	0.2	0.0
	0.10	0.022	0.33	0.5	0.0
	0.20	0.10	0.10	1.0	0.0
	0.30	0.24	0.02	1.5	0.0
	0.40	0.34	0.00	2.0	0.0
	0.50	0.42	0.00	2.5	0.0
	0.60	0.50	0.00	3.0	0.0
	0.70	0.8125	0.00	3.5	0.0
	0.78	1.00	0.00	3.9	0.0

Initial conditions	
P (psi)	3200
S_w	0.22
Rs	1.27

Boundary conditions	Non-flow boundary conditions

Well conditions (BHP controlled)	Primary production	Secondary production
Well 1 (upper reservoir)	2200 psi (producer)	3200 psi (injector)
Well 2 (upper reservoir)	2200 psi (producer)	3200 psi (injector)
Well 3 (lower reservoir)	2200 psi (producer)	2200 psi (producer)
Well 4 (lower reservoir)	2200 psi (producer)	2200 psi (producer)
Well 5 (fault)	2200 psi (producer)	2200 psi (producer)
Well 6 (fault)	2200 psi (producer)	2200 psi (producer)

* Water properties (pressure related) were calculated with the Equations (7-4) and (7-5).

$$B = B_r \exp\left[-C_B(P - P_{ref})\right] \tag{7-4}$$

$$\mu = \mu_r \exp\left[-C_\mu(P - P_{ref})\right] \tag{7-5}$$

Oil recovery results are shown in Figure 7.8. As was observed, the recovery rate in the higher fault permeability case was much greater than in the lower fault permeability case. For both studies, oil recovery rates slowed when they entered the secondary recovery stage. This was due to the reduction of production wells (all six wells produced at the primary production and two wells at the upper reservoir were turned into injectors). Quantitatively, at the end of the primary production period, oil recovery in the higher fault permeability case was 13% compared with 7% with the lower fault permeability case. This represents an approximately 6% difference based on total reservoir capacity. At the end of simulation (day 6000), the higher fault permeability case gave 32% total recovery and the lower fault permeability case offered 14% total recovery. The difference between the two cases was about 18% of total oil in place.

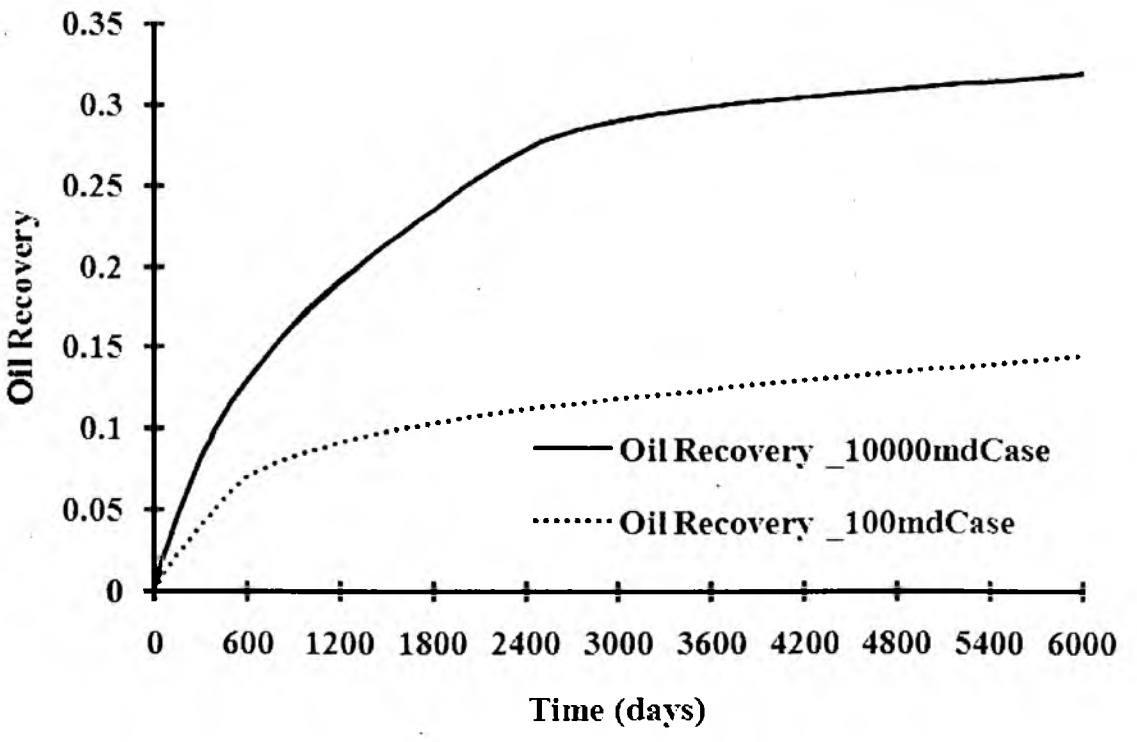

Figure 7.8 Oil recovery comparisons between two case studies (10000 md and 100 md fault permeabilities)

Meanwhile, the higher fault permeability case offered double the amount of oil recovery than the other case. For the higher fault permeability case the oil recovery curve could be cut into three stages: day 1 to 600 (primary production), day 601 to about 2250, and after day 2250. The slopes of oil recovery fractions declined with time. The first rate reduction has been explained (well number reductions). The second slope turning point (around day 2250) could be explained by the water breakthrough on the two wells located at the bottom of the normal fault. There was no clear oil recovery curve slope change (on the secondary production period) in the lower fault permeability case. After day 2250, both curves showed close slopes which means they had a similar oil production rate. This can be observed in Figure 7.9. Since behaviors of production wells on the lower reservoir and fault were different in each case study, oil produced from the reservoir and the fault are presented separately.

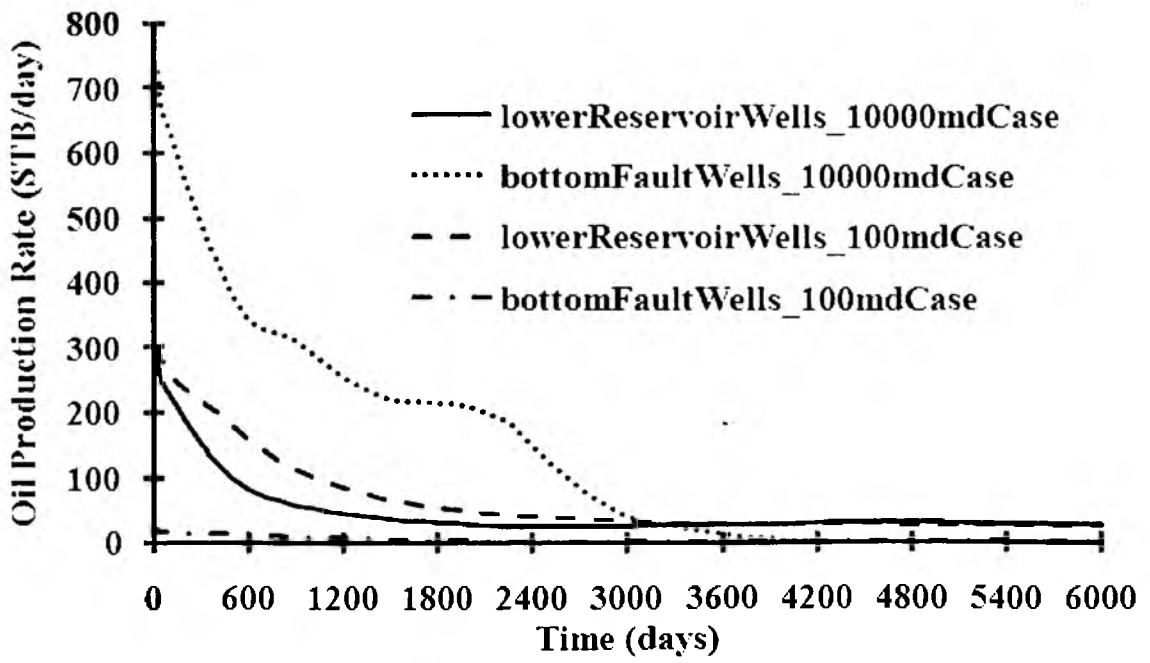

Figure 7.9 Oil production rate comparisons between two case studies (10000 md and 100 md fault permeabilities)

The oil production rate and water cut results shown in Figures 7.9 and 7.10 clearly depict the well behaviors with normal fault permeability differences and the well locations. In the first simulation with 10000 md fault permeability, the production wells on the bottom faults contributed most of the oil production until their water cuts reached very high points. This curve could be divided into five stages: from day 1 to 600, the production rate sharply declined due to the reservoir pressure decrease; from day 601 to day 1400, the production rate decreased due to reduced producers and water injection; from day 1401 to day 2250, a stable production stage, water injections pushed oil from upper reservoir to producers on the bottom of the fault; from day 2250 to 4000, more and more water was produced by these wells due to the breakthrough (at day 3250, oil produced from fault producers was equal to the oil produced from lower reservoir

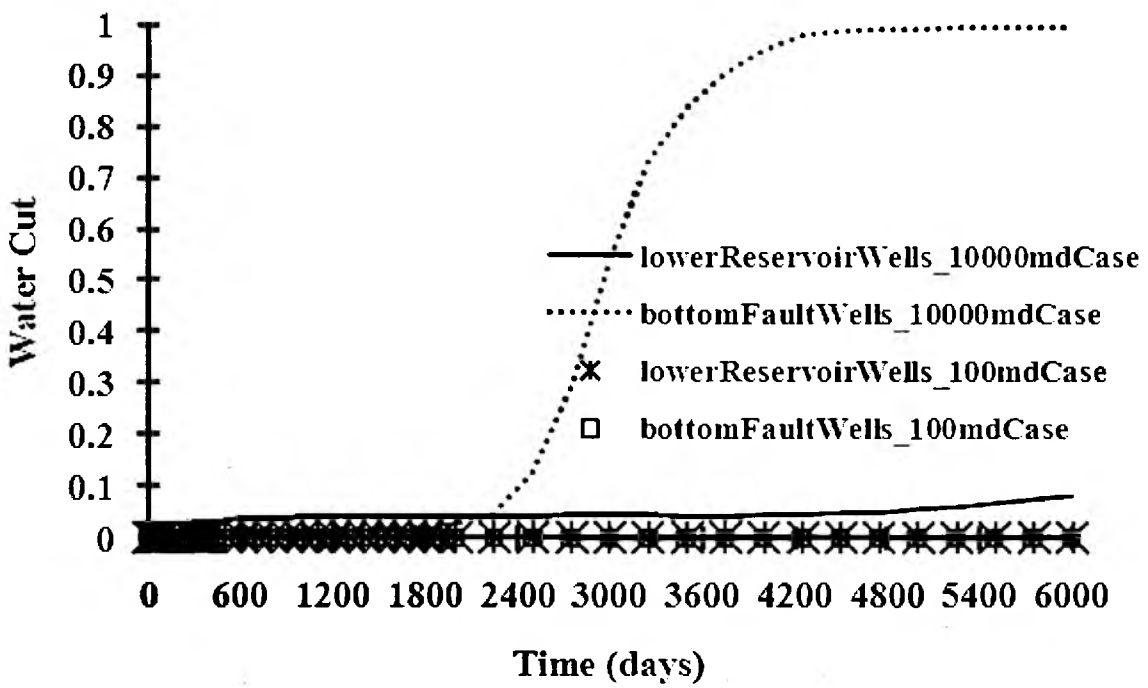

Figure 7.10 Water cut comparisons between two case studies (10000 md and 100 md fault permeabilities)

producers, and at day 4000, the water cut from fault producers was over 96%); from day 4000 to the end of simulation, oil production on the fault producers dropped from 5.35 stb/day to 0.64 stb/day with the highest water cut of 99.7%. However, for the fault producers on the simulation with 100 md fault permeability, the water breakthrough never happened due to the lower fault permeability. The oil production rate on those wells changed only mildly during the whole simulation period. The oil production rate figure suggests an interesting phenomenon in the behavior of lower reservoir producers in these two case studies. The lower reservoir producers with 100 md fault permeability case produced more oil than the higher fault permeability case; this might be due to a combination of higher near-fault matrix permeability effects and the gravity effect. Since the near-fault matrix has 500 md permeability and the fault has only 100 md, part of the oil flow from the top reservoir or upper fault might have gone into the lower matrix instead of flowing directly down to the bottom fault producers. Furthermore, the water cut figure shows that the lower reservoir producers in the 10000 md fault permeability case had a certain amount of water produced during the simulation but not in the other case with 100 md fault permeability. Some snapshots of oil saturations might help to understand these physical behaviors.

The snapshots of oil saturations below present the fault permeability impact on oil production (Figure 7.11 and Figure 7.12). Two pictures in each row represent the same case on the same time oil saturations but from different viewing angles. For example, on the first row of the 10000 md fault permeability case, two pictures represent the same oil saturation distributions at day 600 (just after the primary productions). The picture on the left gives the west-east view, which is good for watching the front side of the normal

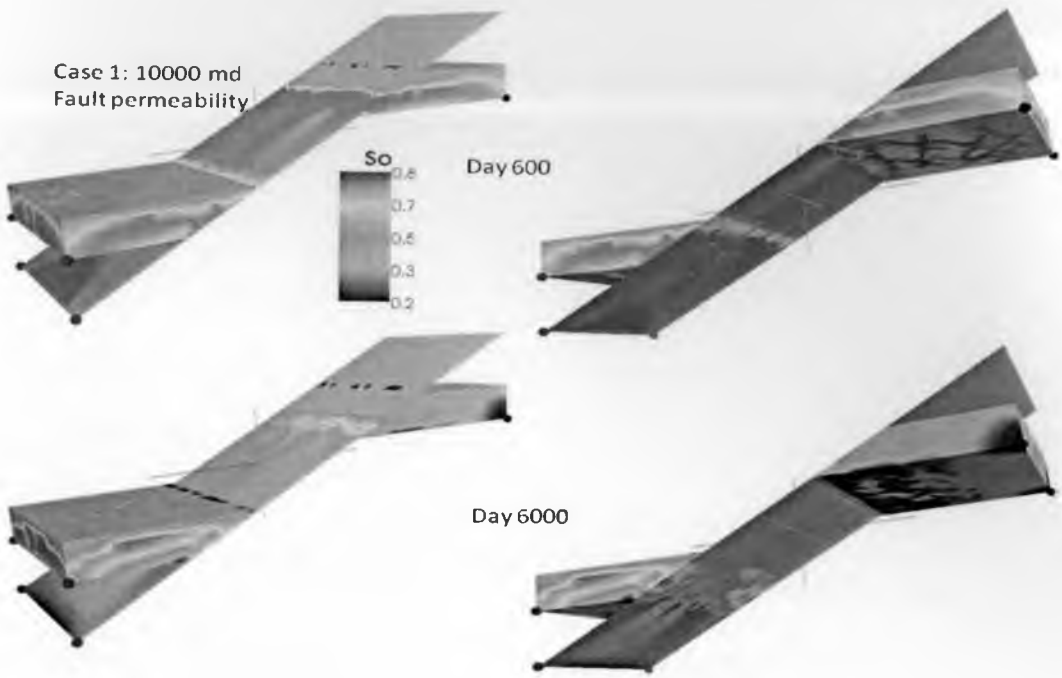

Figure 7.11 Snapshots of oil saturations in 10000 md fault permeability case with day 600 (upper) and 6000 (lower)

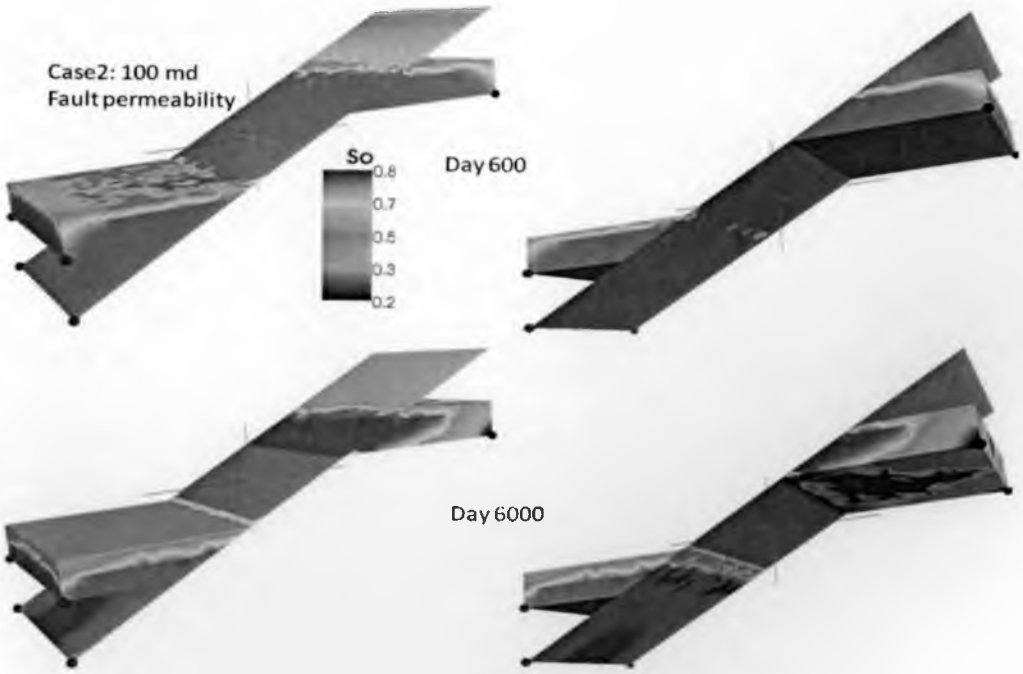

Figure 7.12 Snapshots of oil saturations in 100 md fault permeability case with day 600 (upper) and 6000 (lower)

fault and the top side of the lower reservoir; the picture on the right was taken from another angle and obtained a clear view point of the rear side of the normal fault and the lower side of the upper reservoir. Comparing the two case studies at the end of primary production (day 600), the 10000 md case clearly had more oil drained from both reservoirs and the upper fault to the bottom of the normal fault then the other case. On the pictures of the simulation end, water clearly shows up on the bottom of both reservoirs and the fault in first case with 10000 md fault permeability. For the 100 md fault permeability case, the injecting water front had not yet even reached the normal fault. At day 6000, the oil saturation profile on the lower reservoir in the 10000 md case showed a strap distributed from bottom producers to the top of lower reservoir and the fault. This effect may have been generated for two reasons: 1) the upper oil saturation vacancy (above the lower matrix producers) was generated by gravity, and 2) the lower oil saturation vacancy was from the water injection from upper reservoir transferred by the normal fault and invading from the fault side to the bottom of the lower reservoir.

This study showed the great capability of the CVFE multiphase reservoir simulator in handling complex type II fractured reservoirs. The reservoir's observed behavior agreed well with the common sense expectations of the designed reservoir. Surely there was still room to play around with this conceptual model for different recovery plans, but it was outside of the scope of this study. The fractures in the reservoir certainly formed some fluid flow paths and geometric traps for the hydrocarbons. The normal fault played a key role in the process of oil productions for this kind of hydrocarbon recovery. Practically, if the normal fault had been used in the production, it would have essentially impacted the oil recovery, and brought many uncertainties. The

fault has to be carefully characterized in the flow model and the simulation tool has to be carefully selected as well.

7.5.2 Outcrop to Simulation: "Teasdale Fault" Line Drive Scenario: Heterogeneous Matrix with Small Fracture

This was another multiphase type II reservoir study. In this section, the Teasdale fault, as shown in Figure 7.13, a major left-lateral strike-slip fault zone in southern Utah was chosen to model another important type II fractured reservoir. Distinguished from the dip-slip fault in the last application, the strike-slip fault is usually nearly vertical and

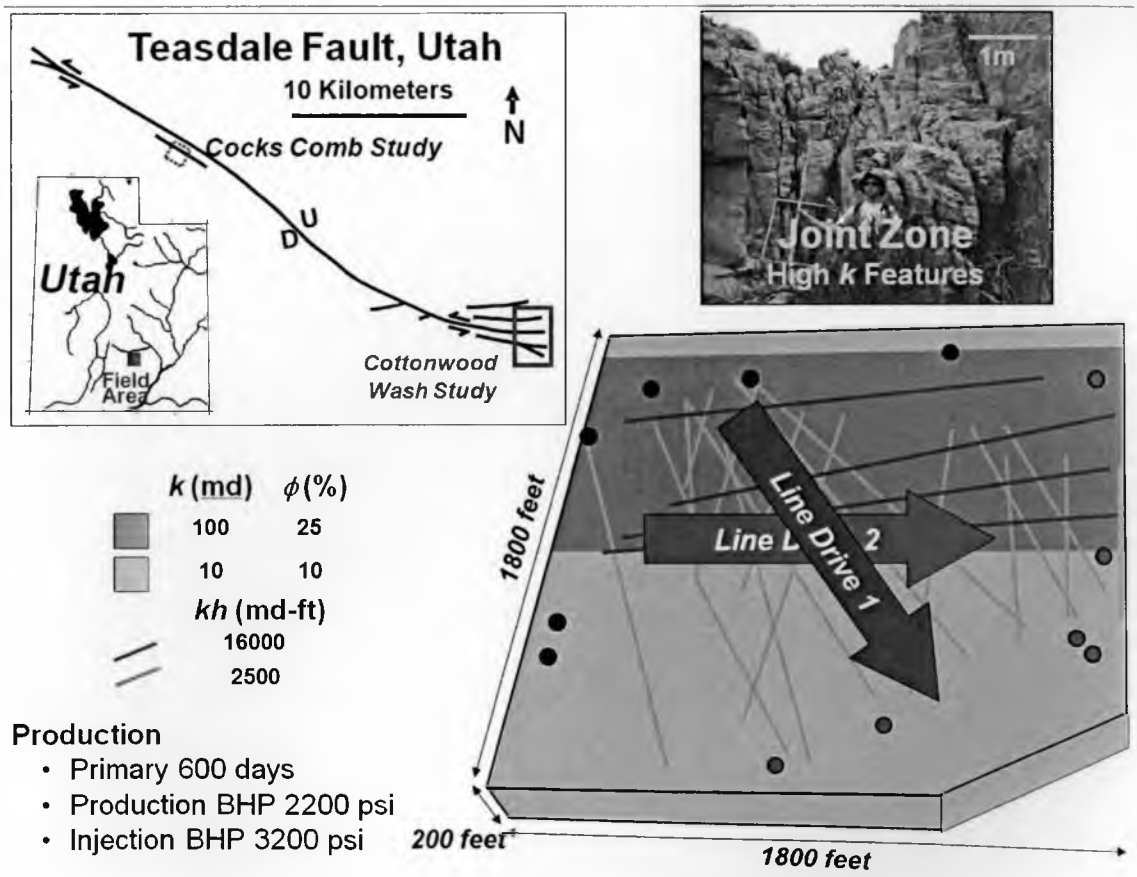

Figure 7.13 Illustration of modeled area, outcrop of joint zone with high permeability features and heterogeneous type II flow model

the foot wall moves either left or right or laterally with very little vertical motion.

Outcrop analogs found along the 40-km Teasdale Fault (cutting Aeolian Navajo Sandstone) helped to construct the reservoir model for the multiphase flow purpose. The reservoir model was built with the dimension of 1800 by 1800 by 200 ft. There were two sets of faults inside the simulation domain: relative low permeability (2500 md-ft conductivity) set in the direction of NE-SW and high permeability (16000 md-ft conductivity) set in W-E direction. The matrix had two different zones: a high permeability matrix zone (with 100 md permeability and 25% porosity) and a low permeability matrix zone (with 10 md permeability and 10% porosity). All high permeability set faults (four in total) were located in the high permeability matrix zone. The low permeability set faults crossed both matrix zones. All of the faults were DFN modeled with two-dimensional planes and discretized as finite-element triangles. The reservoir matrix was discretized as finite-element tetrahedrons by conforming to fault triangles. Since most of the fluid properties (density, viscosity, PVT characteristics) in this application were the same as those of the dip-slip fault model (refer to Table 7.2), in this section, only the differences of the critical reservoir data are summarized in Table 7.3.

As shown in the model illustration and critical data summary, two line drive studies were designed based on two distinguished fault sets. Both studies were three-phase based and hydrocarbon was recovered in two stages—primary pressure recovery and secondary water flooding recovery. There were six wells in each simulation. In the primary recovery stage, all of six wells were producers with 2200 psi BHP control. In the secondary production, three wells on either the north or the west side were turned into injectors with 3200 psi injecting pressure control; the other three wells had the same

operating conditions as before. This study was designed to observe the physical impact of the strike-slip fault on the hydrocarbon recoveries.

Figure 7.14 shows that there was no significant difference in the primary production stage. The line drive 2 case study presented a little bit more oil recovery than the line drive 1 case study (7.8% : 7.1%). However, the line drive 2 simulation showed stronger oil recovery fractions than the line drive 1 simulation after the water injection.

Table 7.3 Summary of critical data for modeling Teasdale Fault type II reservoir

Simulator	**CVFE**	
Grid information		
Node number	5765	
Fracture triangle elements	3356	
Matrix tetrahedron elements	27994	
Rock property		
Φ (matrix)	0.25, 0.10	
Φ (fault)	0.0	
k (matrix) (md)	10, 100	
kh (fault) (md-ft)	2500, 16000	
Initial conditions		
P (psi)	3200	
S_w	0.22	
Rs	1.27	
Boundary conditions	Non-flow boundary conditions	
Well conditions (BHP controlled)		
Line drive study 1	Primary production (day 0 ~ 600)	Secondary production (day 601 ~ 6000)
Well 1 (N-left)	2200 psi (producer)	3200 psi (injector)
Well 2 (N-middle)	2200 psi (producer)	3200 psi (injector)
Well 3 (N-right)	2200 psi (producer)	3200 psi (injector)
Well 4 (SW-left)	2200 psi (producer)	2200 psi (producer)
Well 5 (SW-middle)	2200 psi (producer)	2200 psi (producer)
Well 6 (SW-right)	2200 psi (producer)	2200 (producer)
Line drive study 2	Primary production (day 0 ~ 600)	Secondary production (day 601 ~ 6000)
Well 1 (W-upper)	2200 psi (producer)	3200 psi (injector)
Well 2 (W-middle)	2200 psi (producer)	3200 psi (injector)
Well 3 (W-lower)	2200 psi (producer)	3200 psi (injector)
Well 4 (E-upper)	2200 psi (producer)	2200 psi (producer)
Well 5 (E-middle)	2200 psi (producer)	2200 psi (producer)
Well 6 (E-lower)	(producer)	2200 psi (producer)

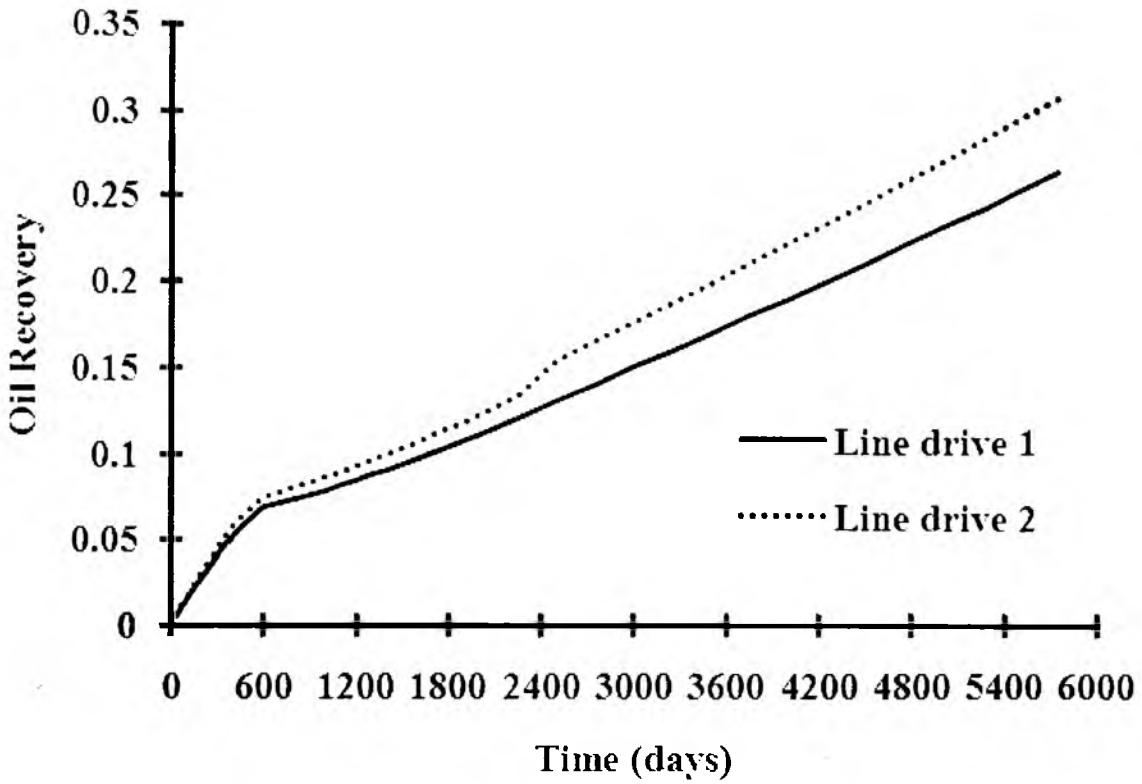

Figure 7.14 Comparisons of oil recoveries between line drive 1 and line drive 2

At the end of simulation, the line drive 1 simulation resulted in 26% total recovery and the line drive 2 resulted in a 30% total oil recovery fraction. There was 4% difference between the two case studies based on original oil in place. These results were consistent with the designed Teasdale type II model. The line drive 2 simulation was designed to flush the reservoir from W – E by that high permeability fault set (four faults in total). The line drive 1 simulation was designed to use a relatively low permeability fault set (16 faults in total) flush reservoir in N – SW direction. Some oil saturation distribution snapshots are listed later. Two dates were selected for both simulations: day 600 at the end of primary production and day 6000 at the end of simulation.

Figure 7.15 shows the faults' effects on the primary production stage. Significantly lower residual oil saturation could be seen on the bottom of the high permeability fault set from the bottom view of line drive 2 simulation (right bottom picture). Since there were more faults in the lower permeability fault set than in the high permeability fault set (17:4), line drive 1 shows more even residual oil distributions than line drive 2 at the end of primary production (pictures in left column). There were more oil concentrations in the upper middle region of the line drive 2 study than there were in the other case. This region had high permeability in both matrix and faults. Since all of the wells in line drive 2 were distributed at either the east of west side of the domain,

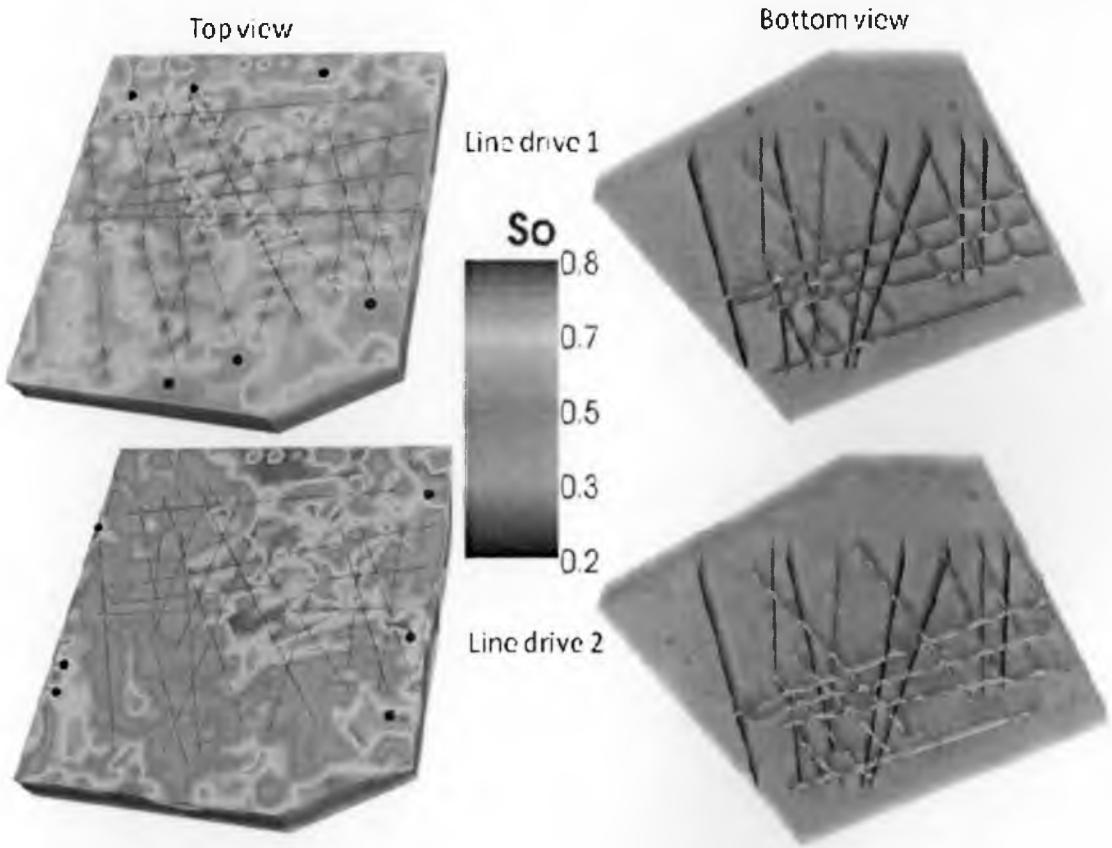

Figure 7.15 Oil saturation comparisons between line drive 1 and line drive 2 at the end of primary production (day 600)

lower operating pressure (2200 psi) made hydrocarbons migrate from other high pressure regions. Faults had a very important role in collecting oils from nearby places through their "highway" network to transport them to the lower pressure gradient region. It was observed that even though the oil recovery figure showed similar recovery fractions at the end of primary production, the residual oil saturation was distributed very differently for the two recovery scenarios. Practically, this observation could aid in understanding production in a highly heterogeneous type II fractured reservoir in three ways:

- Could help to set up well networks based on fault properties such as orientation and permeability.
- Could help to trace hydrocarbon migrations in the primary production by simulation.
- Could help to make decisions for setting up the injection wells in the secondary recovery stage.

The oil saturation distribution snapshots at the end of simulation (day 6000) are shown in Figure 7.16. Figure 7.17 shows that there was no significant difference in the secondary production stage.

Water flooding patterns are visible for both line drive studies at the end of simulation in Figure 7.16. Especially from the bottom view of both cases, the higher permeability fault set trapped significant water (blue) than the other fault set. Even though two injectors and two producers were set up on the low permeability matrix zone in the case study of line drive 2, the water front in the higher matrix permeability zone was still far beyond that of the low matrix zone from the bottom view pictures. It was

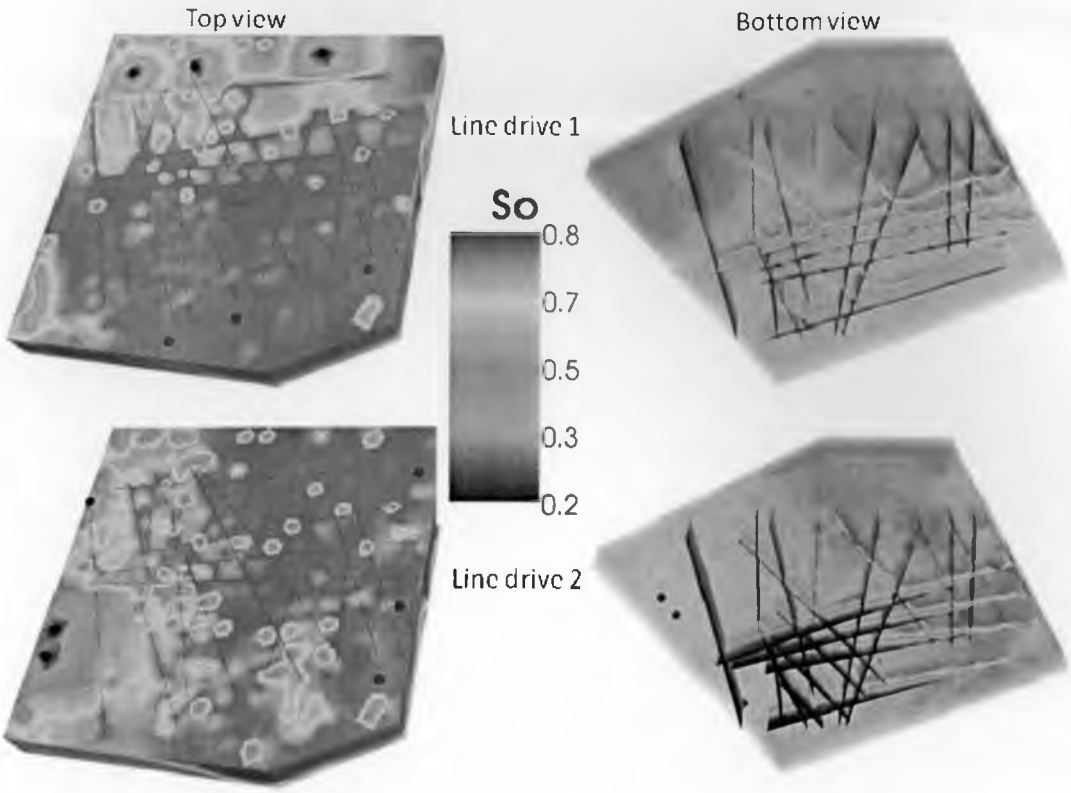

Figure 7.16 Oil saturation comparisons between line drive 1 and line drive 2 at the end of simulation (day 6000)

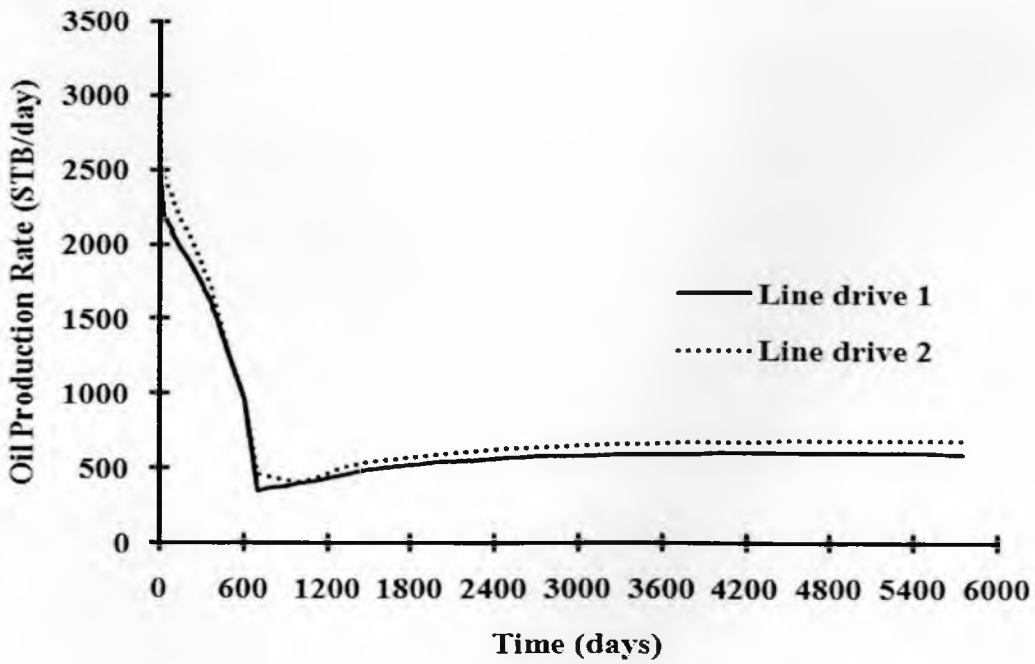

Figure 7.17 Oil production rate comparisons between two line drive case studies

also possible to observe from both case studies that the oil saturation at the bottom was much lower than at the top. This was especially true near the injection wells. Physically, this was due to the gravity effect: water is much denser than oil (62:45). As shown in the domain description at the beginning of this application, the thickness of this reservoir model was 200 ft and the gravity effects happened very soon after flooding water was injected. Compared to the results at the end of primary production, the top view of the oil saturation snapshot at the end of simulation showed that higher oil concentration was pushed from injection wells to the production wells.

Figure 7.18 shows that line drive 2 case study had a higher oil production rate than the other case all through the simulation. At the primary stage, the difference was about 0.6% to 11.2%. There was a sharp increase for the rate difference right after water injection (up to 34.2%). Then it quickly declined to 4.4%. This observation could be explained by one injector on line drive 1 being located on the corner of a fault. The injecting pressure could be quickly transferred through the fault network to push more oil out of the producers. The location of this specific well could also be used to explain the production rate difference between the two case studies. After the big jump and decline at the beginning of secondary recovery, the oil production rate difference in the line drive 2 case study had a couple more relatively sharp climbs which were also counted as the fault network effect and eventually showed smooth and slow increase through the simulations. The rate difference between the two case studies was about 10% ~ 15%. This could give the conclusion that in the type II fractured reservoir the water flooding pattern should be carefully selected based on the fracture/fault characteristics.

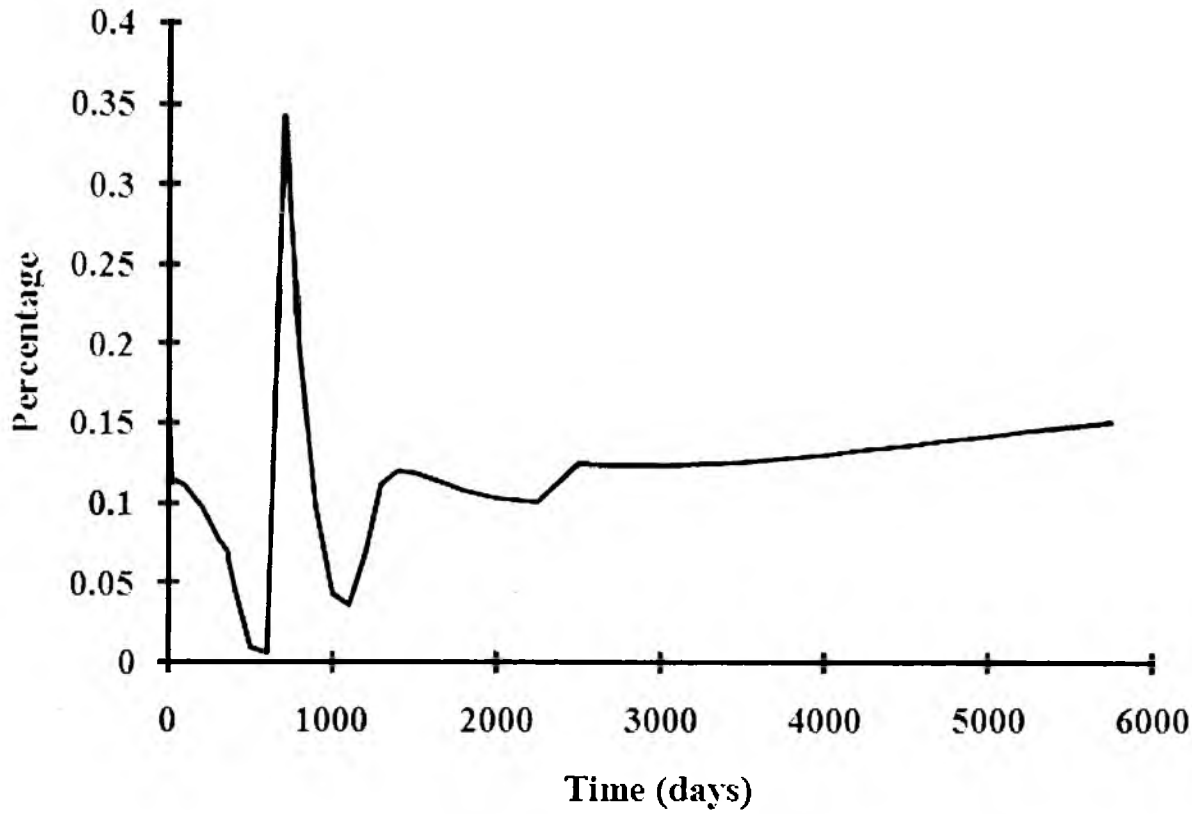

Figure 7.18 (Line drive 2 oil rate - Line drive 1 oil rate)/ Line drive 1 oil rate

7.5.3 "Preferred Pathway" on Type II Reservoir

Some "preferred pathway" case studies have been performed on the type I reservoirs and described previously (Chapter 3). For type II fractured reservoir, if injection and production wells happened to be located on the connected high permeability fracture/fault network, the short-circuit flow path will be formed and will lower oil recovery efficiency dramatically. In this application, the Teasdale Fault domain was being simplified to study this type of physical phenomena. Instead of a highly heterogeneous type II reservoir model used in last application, the matrix in this study

was assigned homogeneous porosity (12.7%) and permeability (0.5 md). There are three simulations in this study:

1) Base case (with 500 md-ft fault transmissivity);
2) Preferred pathway case (500,000 md-ft on preferred pathway and 500 md-ft on rest faults);
3) Preferred pathway with cut-off zones (500,000 md-ft on preferred pathway, 0.5 md-ft on cut-off pathway zones and 500 md-ft on the rest of faults).

This case study was confined as two phases (oil and water). There were two wells in total and they were located at the two ends of preferred pathway (as shown in domain description below). The critical data are summarized in Table 7.4.

The circled faults (four in total) in the above domain (Figure 7.19) were assigned with high permeability (500000 md-ft) in the simulation of preferred pathway. The fault circled in black at the middle was treated as the "cut-off" fault zone which was assigned to 0.5 md-ft permeability in the simulation of preferred pathway with cut-off zone studies. The injection well was marked as a blue dot on the end of the southwest fault and the production well was marked as a red dot on the corner of the northeast fault as shown in the domain description. In this application, water was injected from day 1 and total simulation time was 10,000 days. The oil saturation snapshots of different times are shown in Figure 7.20.

Figure 7.20 shows that the water flooding patterns are totally different due to the existence of high permeability fault short-circuit in the type II fractured reservoirs. The first row of pictures in the figure above represents the simulation results of day 100; the

Table 7.4 Summary of critical data for modeling type II reservoirs connected by normal fault

Simulator			**CVFE**	
Grid information				
Node number			5765	
Fracture triangle elements			3356	
Matrix tetrahedron elements			27994	
Fluid property			Water	oil
μ (cP)			1.0	0.94
γ (lbf/ft^3)			59.28	49.92
Rock property				
Φ (m, f)			0.127, 1.0	
k (matrix) (md)			0.5	
k (fracture) (md-ft)			500, 500000, 0.5	
Fluid data				
			Water properties*	***Oil properties****
Reference pressure (p_{ref}, psi)			14.7	14.7
Water formation factor B_r @ reference pressure (rb/stb)			**1.0**	1.0
B_r's compressibility (1/psi)			1.0e-6	1.0e-5
Water viscosity (μ_r) @ reference pressure (cp)			0.96	0.9725
μ_r's compressibility (1/psi)			0.0	0.0
Rock-fluid data				
Oil-water system				
	S_w	k_{row}	K_{rw}	p_{cow} (psi) (matrix)	p_{cow} (psi) (fracture & fault)
	0.20	0.00	1.00	**7.0**	0.0
	0.30	0.07	0.40	**4.0**	0.0
	0.40	0.15	0.125	**3.0**	0.0
	0.50	0.24	0.0649	**2.5**	0.0
	0.60	0.33	0.0048	**2.0**	0.0
	0.80	0.65	0.00	**1.0**	0.0
	0.90	0.81	0.00	**0.5**	0.0
	1.00	1.00	0.00	**0.0**	0.0
Initial conditions				
P (psi)			3300	
S_w			0.2	
Boundary conditions				
			Non-flow boundary conditions	
Well conditions				
Injection (BHP, psia)			5500	
Production (BHP, psia)			50	

Figure 7.19 Illustration of preferred pathway characterization in type II fractured reservoir and preferred pathway with cut-off zone (circled).

base case study showed much shorter water injection trajectories than the other two cases due to the difference of fault permeabilities. When comparing the preferred pathway case in the middle column with the preferred pathway with cut-off zone case in the last column, it is clear that the injecting water was flowing through the highest permeability fault to the producer. The following observations can be made from the three case studies over the entire simulation:

1) The base case showed a relatively even water saturation front from the injector to the producer. Injecting water could push oil out of the matrix to nearby faults and then use the fault as its transportation tool sending reservoir fluid into the producer.

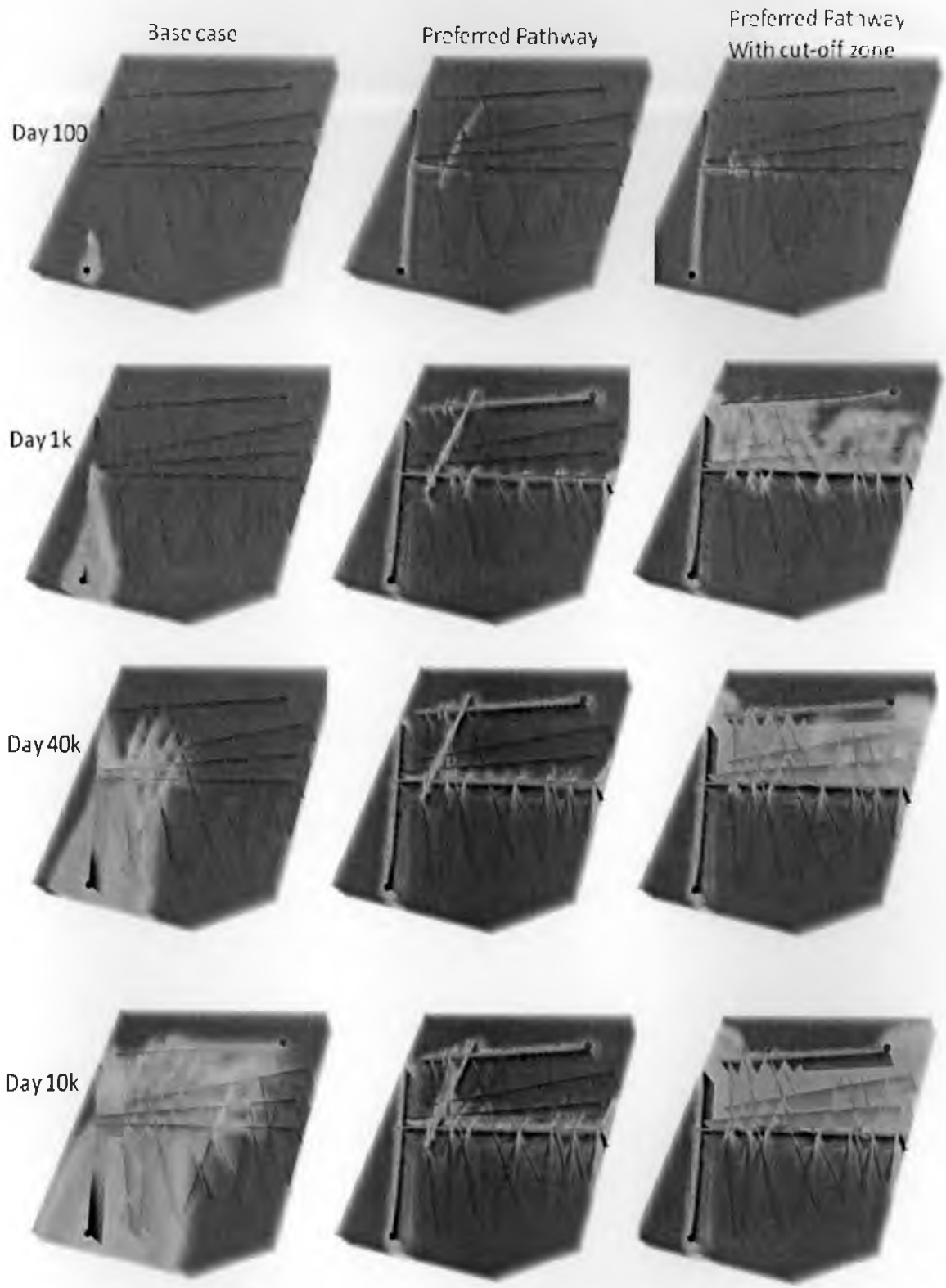

Figure 7.20 Oil saturation distribution comparisons among different fault permeabilities on different time scales

2) The preferred pathway case showed that only oil near high permeability faults would flood out. Most oil in the relatively low permeability faults did not get the chance to flood out.

3) The preferred pathway with cut-off zone case study showed that most of oil between two high permeability faults was flooded out at the end of simulation.

Figure 7.21 shows that at the beginning of the simulation, for a very short period both preferred pathway and cut-off zone cases had identical oil recovery rate, which was higher than the base case. This was due to the existence of a higher permeability fracture/fault near the injector. After a while, the trend of oil recoveries in the recovery figure displayed the recovery rate with the order from high to low: the cut-off zone case, the base case and the preferred pathway case. This was very encouraging in regard to the

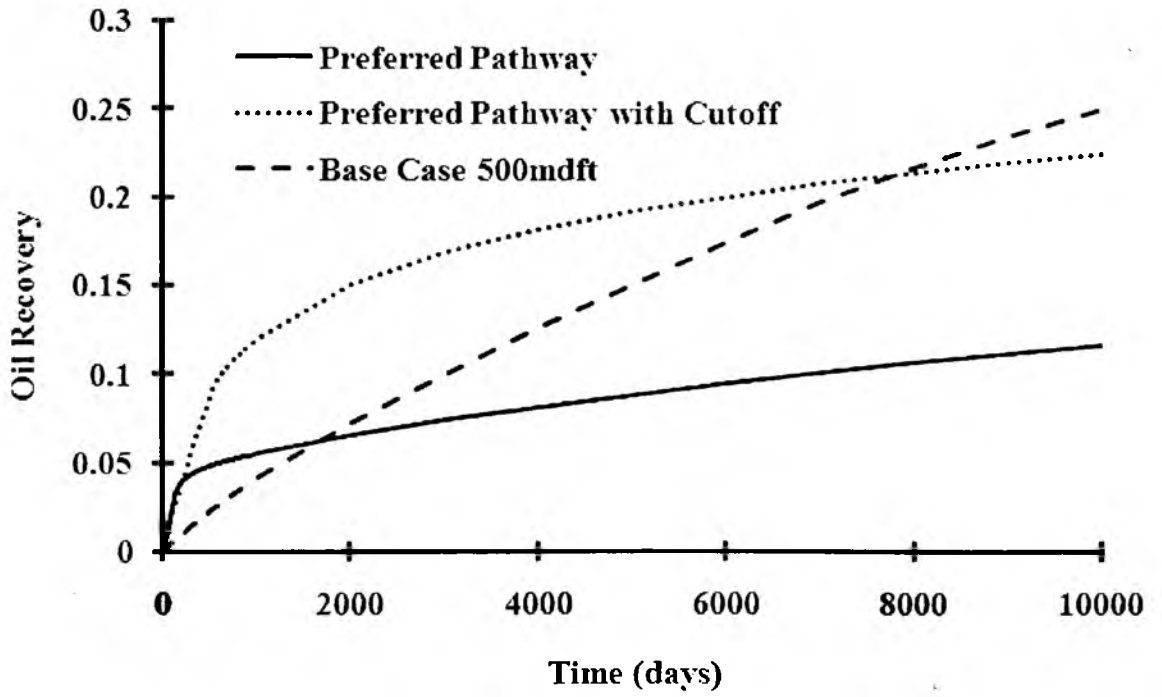

Figure 7.21 Oil recovery fraction comparisons for preferred pathway type II fractured reservoir studies

idea of treating higher permeability fractures/faults with special techniques such as gels in order to reduce or block the water flow. Such treatment can dramatically increase oil production.

Figure 7.22 showed that the existence of ultrahigh permeability short-circuits could be either an enemy or friend during oil recovery. Geologically, those ultrahigh permeability faults exist externally. However, the negative effects from high permeability fault existence could also be converted into a preponderant element if the correct production strategies were designed or the right treatments were applied. In this application, the base case showed more consistent production behavior than the other two cases. The ratios of initial and end-day oil production rates were 5.12 (base case), 58.47 (preferred pathway case) and 54.48 (cut-off zone case). The oil recoveries at the end of

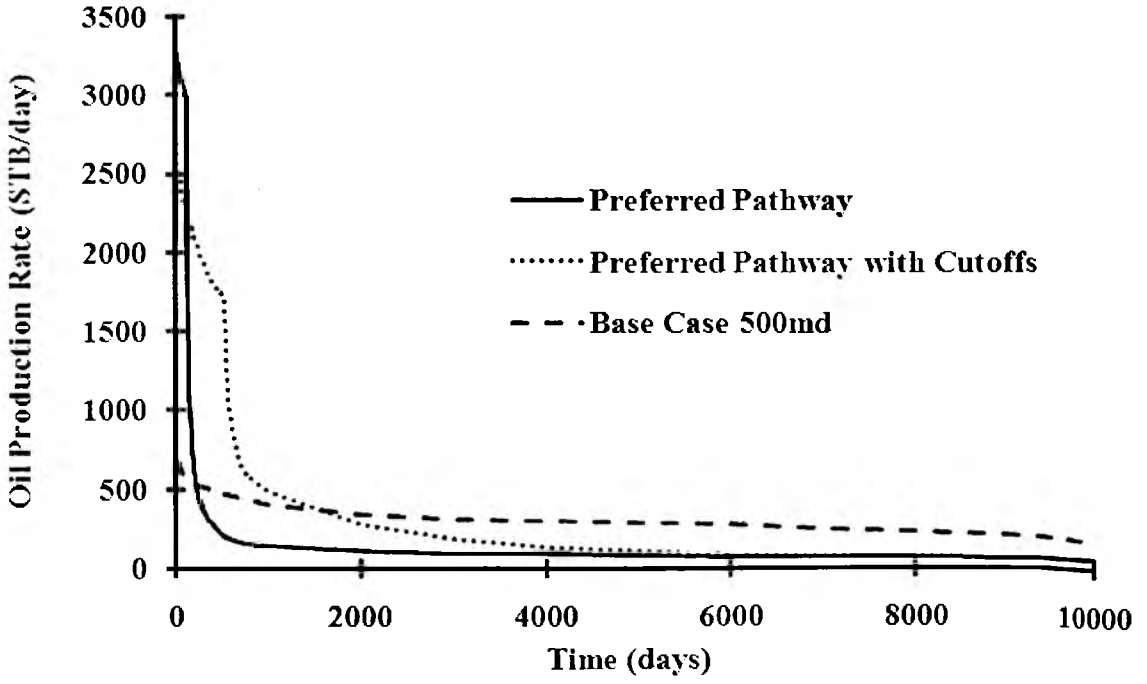

Figure 7.22 Oil production rate comparisons for preferred pathway type II fractured reservoir studies

simulation (day 10000) were 25% (base case), 11% (preferred pathway case) and 22% (cut-off zone case).

The plot of oil recovery with injection pore volume (PV) in Figure 7.23 explains the cost-effectiveness ratio for production oil from these type II fractured reservoirs. To achieve 10% oil recoveries, the base case required 0.07 PV injections; the preferred pathway case needs 0.84 PV water injections; and the cut-off zone case needs 0.10 PV injections. However, to get the same oil recovery, the time spent on each case is 3000, 7000 and 610 days. Obviously the cut-off zone model offered the best production plan to reach this goal by combining these two analyses. Being distinguished from the type I basement reservoir, type II fractured reservoir had much higher original oil in place but might have a much lower recovery rate than the basement reservoir.

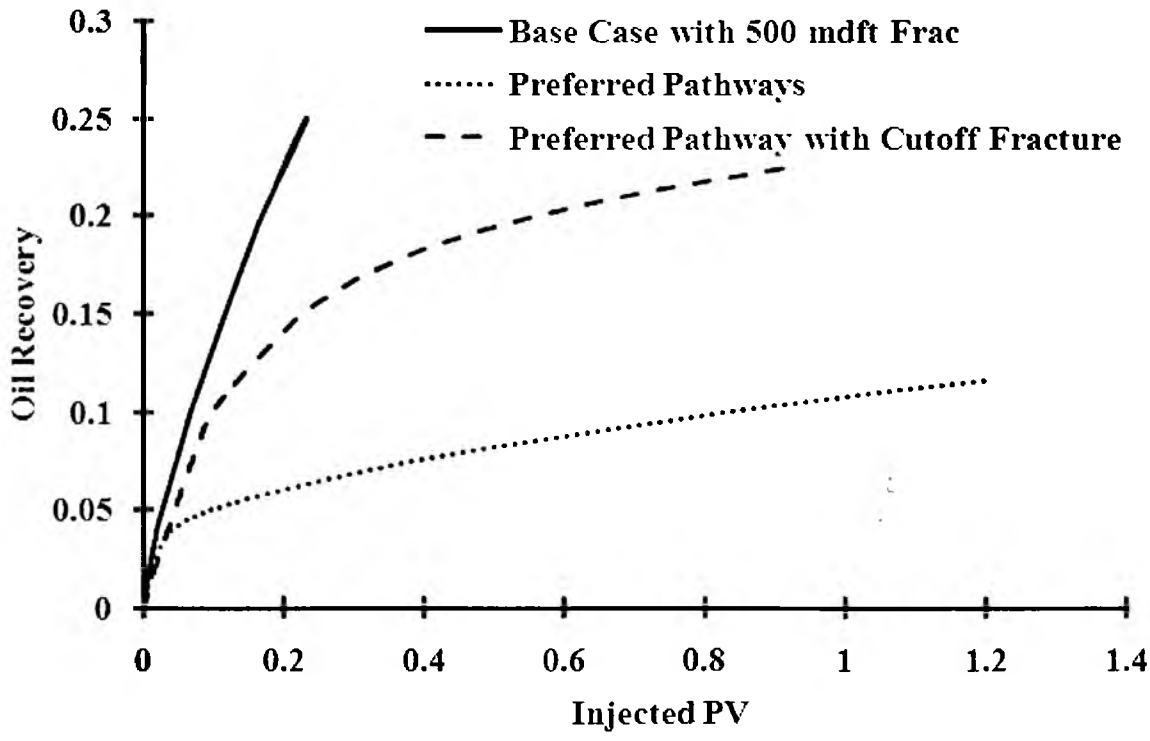

Figure 7.23 Dimensionless analysis of oil recovery vs. injection water

Some points could be highlighted from the study of this application:

- In type II fractured reservoirs, if injection and production wells were linked by ultrahigh permeability fracture networks, the water flooding might get difficulty for sweeping most of the reservoir's hydrocarbons. This situation had to be seriously treated during the reservoir management.
- The method to gel or block the main preferred pathway fracture/faults could dramatically eliminate the negative effects caused by ultrahigh preferred pathway. The advantages might include higher recovery rate, lower injection water demands, lower produced water treatment cost (can reach two-magnitude difference or more), etc.
- This preferred pathway type of study and especially the treatment idea such as the cut-off zones theory were still directly related to the topic of fracture network connectivity. In practical, precise reservoir characterization, it becomes essential to study this type of problem.

7.6 Chapter Summary

In this chapter, a new three-dimensional, three-phase, unstructured-grid black-oil simulator was introduced for a highly heterogeneous type II fractured reservoir study. A series of simulations with Type II reservoirs (reservoirs featuring both the matrix and the fractures) was performed primarily to demonstrate the capability of this in-house CVFE simulator. This simulator was good at directly calculating fluid flow through DFN modeled fractures/faults. At the beginning of the chapter, this CVFE Type II simulator was quantitatively verified with the reported core-flood data. The results were in good agreement in various conditions. The usefulness of using discrete-fracture models was

discussed by looking at production from faulted-fractured systems. It was shown that given a certain reservoir and fracture description the simulator could be employed to optimize oil recovery.

7.7 Nomenclature

a ~ k	=	point identifying the tetrahedral control volume
B	=	formation volume factor
		(Subscripts g, o and w refer to gas, oil and water respectively)
B_r	=	formation volume factor at the reference pressure
C	=	compressibility
$C_{B,\mu}$	=	compressibility of formation factor and viscosity, 1/psi
e	=	fracture/fault storage aperture, ft
g	=	gas phase
k	=	absolute permeability, md
k_r	=	relative permeability
o	=	oil phase
p	=	fluid pressure, psi
q	=	flux vector
R_s	=	gas-oil ratio, MSCF/STB
S	=	phase saturation
		(Subscripts g, o and w refer to gas, oil and water respectively)
S_{or}	=	residual oil saturation
u	=	velocity, ft/day
w	=	water phase

$\emptyset$	=	porosity
ρ	=	density, lbm/ft^3
μ	=	viscosity, cp

7.8 Bibliography

Aavatsmark, I., Barkve, T. and Mannseth, T.: "Control Volume Discretization Methods for 3D Quadrilateral Grids in Inhomogeneous, Anisotropic Reservoirs", paper SPE 38000, (1997)
Araujo, H., Lacentre, P., Zapata, T., Del Monte, A., Dzelalija, F., Repsol-YPF; Gilman, J., Meng, H., Kazemi, H., Ozkan, E., "Dynamic Behavoir of Discrete Fracture Network (DFN) Models," paper SPE 91940 (2004)

Basquet, R., Cohen, C.E. and Bourbiaux, B., "Fracture Flow Property Identification: An Optimized Implementation of Discrete Fracture Network Models," paper SPE 93748 (2005)

Dean, R.H., and Lo, L.L.: "Simulations of Naturally Fractured Reservoirs," SPERE (May, 1988) 638-648

Dershowitz, B., LaPointe, P., Eiben, T., Wei, L., "Integration of Discrete Feature Network Methods with Conventional Simulator Approaches," paper SPE 49069 (1998)

Dershowitz, W. S., "A Probablistic Model for the Deformability of Jointed Rock Masses" M.S. Thesis, Massachusetts Institute of Technology, Cambridge, MA (1979)

FRED User's Mannual, Golder Associate (2007)

Fu, Y., Yang, Y-K., and Deo, M., "Three-Dimensional, Three-Phase Discrete-Fracture Reservoir Simulator Based on Control Volume Finite Element (CVFE) Formulation", paper SPE 93292, (2005)

Fung, L.S., Hiebert, A.D., and Nghiem, L.X., "Reservoir Simulation With a Control Volume Finite Element Method", paper SPE 21224 (1991)

Gong, B., Karimi-Frad, M., and Durlofsky, L.J., "An Upscaling Procedure for Constructing Generalized Dual-Porosity/Dual-Permeability Models from Discrete Fracture Characterizations", paper SPE 102491, (2006)
Kazemi, H. et al.: "Numerical Simulation of Water-Oil Flow in Naturally Fractured Reservoirs," SPEJ (Dec. 1976) 317-26.

Kim, J. and Deo, M.D., A Finite Element Discrete Fracture Model for Multiphase Flow in Porous Media, AIChE J. Vol 46, #6, 1120 (2000)

Kleppe, J. and Morse, R. A., "Oil production from fractured reservoirs by water displacement", paper SPE 5084 (1974)

Monteagudo, J.E.P. and Firoozabadi, A., Control Volume Method for the Numerical Simulation of Two-Phase Immiscible Flow in Two- and Three-dimensional Discrete Fracture Media, Water Resource Research, Vol. 40. (2004)

Pooladi-Darvish, M. and Firoozabadi, A., "Experiments and Modelling of Water Injection in Water-wet Fractured Porous Media", J. Can. Pet. Tech., vol. 39, no. 3 (2000)

Ronald A. Nelson, "Geologic Analysis of Naturally Fractured Reservoirs", Gulf Professional Publishing, second edition (2001)

Rossen, R.H.: "Simulation of Naturally Fractured Reservoirs with Semi-Implicit Source Terms," paper SPEJ (Dec. 1977) 201-10.

Verma, S. and Aziz, K.: "A Control Volume Scheme for Flexible Grids in Reservoir Simulation", paper SPE 37999, (1997)

Warren, J.E. and Root, P.J.: "The Behevior of Naturally Fractured Reservoir," SPEJ (September 1963).

Yamamoto, R. H., Ford, W.T., Padgett, J. B. and Boubeguira, A. "Compositional reservoir simulator for fissured systems – The single block model", Petrol. Eng. J., 11, No.2, pp. 113-28 (1971)

Y. K. Yang, "Finite-Element Multiphase Flow Simulation". PhD thesis, University of Utah, Salt Lake City, UT, (2003)

CHAPTER 8

THE RESERVOIR SIMULATOR REMOTE COMPUTING INTERFACE DEVELOPMENT

Reservoir simulation is an important tool in modern-day reservoir management. Calculation of accurate pressure and saturation distributions requires solutions of coupled partial differential equations. When the system of interest is a highly heterogeneous, anisotropic porous medium, accurate representation and simulation requires the use of high performance computing. High performance computing know-how and infrastructure are not easily available to independent producers who might benefit from the technology. The objective of this chapter was to make this technology accessible to independent operators through remote access via the internet. The idea was to have the simulator reside in a remote site (server) and provide the user with a client interface to interact with the server and perform the calculations. Since the client-side computer requirements are minimal, this approach would provide wider access to sophisticated computing.

Some of the considerations that went into planning this interface were:

- Robustness of the server-side simulator
- Ease of use on the client side
- Platform independence on the client side
- Speed of computing
- Quick and easy transfer of results to the client

8.1 Overview

The Utah Finite-Element Simulation (UFES) Reservoir Simulator Interface consists of two separate service packages: the UFES Reservoir Simulator Interface Server package, and the UFES Reservoir Simulator Interface Client package.

The interface server package is located on the computer which is supposed to handle all of the detailed computations within reservoir simulation. The mesh generator and the finite element simulator should also be on the same computer as the server package. The interface client package should be installed on the end-user's computers.

Both programs are written in JAVA and operate on any computer with JAVA Runtime Environments (JRE) available. Since the current simulator is compiled in LINUX/UNIX environments, the Interface server package should be executed under LINUX/UNIX operating systems. The interface client package can be installed on any computer on which JRE is installed. IBM RS/6000, Silicon Graphics, SUN, Pentium-based PCs, AMD-based PCs etc with more than 256 Mb of RAM would all be appropriate to run these applications.

8.2 Design

With the needs identified at the beginning of the chapter, Java was chosen as the language of implementation. Platform independence and compatibility of client and server protocols were the overriding factors in this decision. Use of Java meant that, as long as a Java Running Environment (JRE) was installed on the client side, simulations could be performed remotely. The interface was designed to be modular: there were two layers in the implementation process, the server side interface and the client side interface.

The Java Socket was chosen as the data transfer channel. A full set of communication protocol was defined for these two layers.

The server side interface directory should include the following items:

- The server side interface Java classes for client side commands waiting, commands accepting, commands translating, commands sorting, detail job order submitting on local server, job results detecting on local server and transferring back to the client etc.
- The finite element meshing software packages for the meshing of reservoir domain with its fractures, wells information, etc.
- The reservoir simulator.

The client side interface has the following functions:

- The main frame module which is written by Java Swing. The title bar, file menu, tool bar and drawing canvas should be listed in this frame.
- A drawing module is designed for reservoir drawing by Java 2D Graphics technique: closed domain boundary is in polygon mode; fractures are in 2D line mode; injection wells are in circle mode; production well is in square mode. End-user can use the mouse functions, like click and drag, to draw rough reservoir domain. For every action on the domain drawing, the relative coordinate information will be recorded into the XML format data input file automatically. Also, this class can handle a saved file instead of drawing from the very beginning.
- A communicating module was planned for communicating with the server to finish the reservoir mesh. This module was designed to pick up the current

domain information from the drawing canvas (basically the coordinates of all vertices such as boundaries, fractures and wells) and send it to the server through Java Sockets with its meshing order by specific protocol, then accepting the meshed results from the server and transferring the meshed info into the client frame. At the same time, it will combine the mesh info with the reservoir description file to form final simulation data input XML file automatically.

- Another communicating module was used to communicate with the server to complete the final simulation. It was built to send the final simulation data input XML file into the server with its simulating order, then wait and accept the simulation results in real time. Furthermore, after accepting every image file from the server, this class would call another class to display the image results.
- A displaying module is required to display the results, either mesh results or final simulation results.
- A monitoring/debugging module was needed to generate another window as Java input/output monitor. This is called the Java Input/Output Console. By this module, the end-user can easily see the process, the simulation status and error messages. Also, this function was very helpful in debugging the code.
- Multithreading implementation was necessary to run multiple jobs on the server without having to wait for jobs to finish.

8.3 Developments

8.3.1 Interface Workflow

An example of 2-dimensional interface workflow is as follows.

- Open the client side interface executive file (UFESSimulator.jar). The default domain information of the interface is to create a new reservoir domain.
- Draw the closed domain boundaries first.
- Draw the fractures, injection wells, and production wells within the reservoir domain boundaries.
- Save all of the coordinates information mentioned above into "*_ori.xml" file. "*" which is the file name. "ori" means original file which is not meshed yet. XML is the file format.
- Connect the client side interface with the server and send the domain information mentioned above to the server for meshing
- Receive the meshed information from the server and automatically generate a final data input XML file as "*_fin.xml" format. "fin" represents "final" which is distinguished from "ori".
- Use a file editor find and open "*_ fin.xml" file and make related modifications such as the wells information, simulation time, etc. The details will be discussed in later sections.
- Connect the client interface with the server, send the modified "*_fin.xml" file to the server and ask the server side simulator to run the simulation.
- Interface server detects the simulation results in real time and sends the results back to clients.

- Receive the simulation results from the server and display them on the client side local machines (either by slide show or animation).

With a previously saved simulation domain, the only difference of simulation workflow is items 2 and 3 from the new reservoir domain simulations. On the second step: use "open a saved *_ori.xml" file action instead of "Draw the closed domain boundaries first". The user can make modifications to geometrical features. Well information, etc. is modified by opening the xml input file and modifying it directly.

8.3.2 Features

All of the interface code is written in Java. The codes are compiled and zipped into an executable file by Java. The interface runs on JRE 5.0 and above under any operating systems. This makes the interface accessible to users across all computing platforms.

The data files in the interface and in the simulator are in XML format. XML is a standardized markup language for documents containing structured information. Structured information contains both content (words, pictures, etc.) and some indication of what role that content plays. Almost all documents have some structure. Reservoir simulation data files, include complicated data information about boundaries, fractures, wells, simulation period, etc. and are highly structured documents. The XML specification defines a standard way to add markup to documents. The client side interface centralized almost all of the reservoir simulation tools which include tools from drawing the domain to viewing simulation results.

By using the socket technique, a robust data communicating protocol has been established between the server and the client. Through specific port channels, the server

can identify the working orders from the clients and run jobs in specified high performance computers. Furthermore, the server side interface has the capability of detecting and transferring the newest simulation results back to the client in "real-time." The source code is modularized, which makes it easy to maintain. Other new functions can be plugged into the interface potentially. An example of the client-side interface is shown in Figure 8.1.

8.3.3 Ancillary Module

In this developed reservoir simulation interface package, some ancillary programs are provided. All of them are written by using the independent Java module. During the

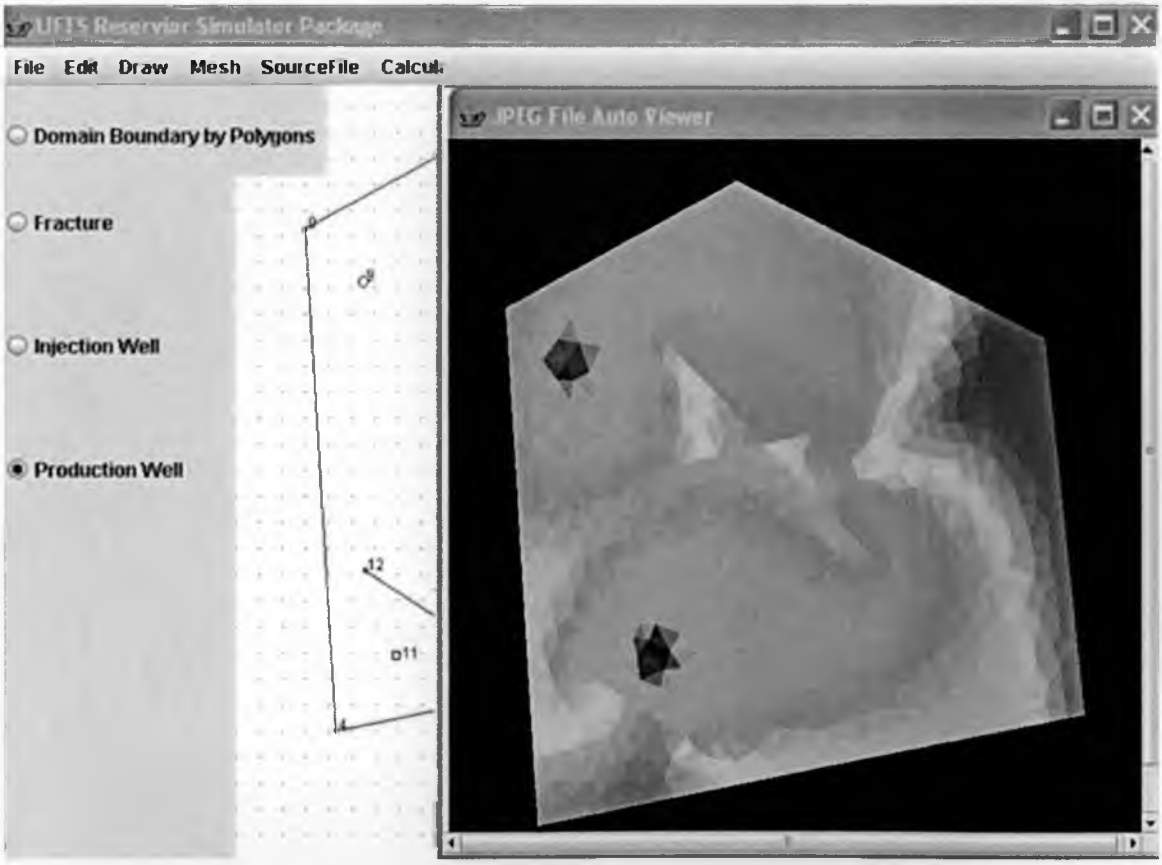

Figure 8.1 A snapshot of client-side remote fractured reservoir computing interface.

processes such as domain generating, meshing, simulating, some of these functions are called by the interface automatically, some are not. They can always open these programs anytime.

Figure 8.2 demonstrates the modular client-server interfaces concept discussed in this section. This is a very flexible modular reservoir simulation platform which can be expended with more functionality.

8.3.3.1 Mesh Visualization Module

This program is designed for the purpose of triangle mesh element viewing. The name of "Triangle Mesh Shower V1.0" is given to this program. This window will be opened right after the domain action. This is mostly used for the cases where the domain is repeatedly modified and meshed. If the end user closes the last mesh map accidentally, he/she can retrieve it by clicking the sub menu of the Mesh menu bar.

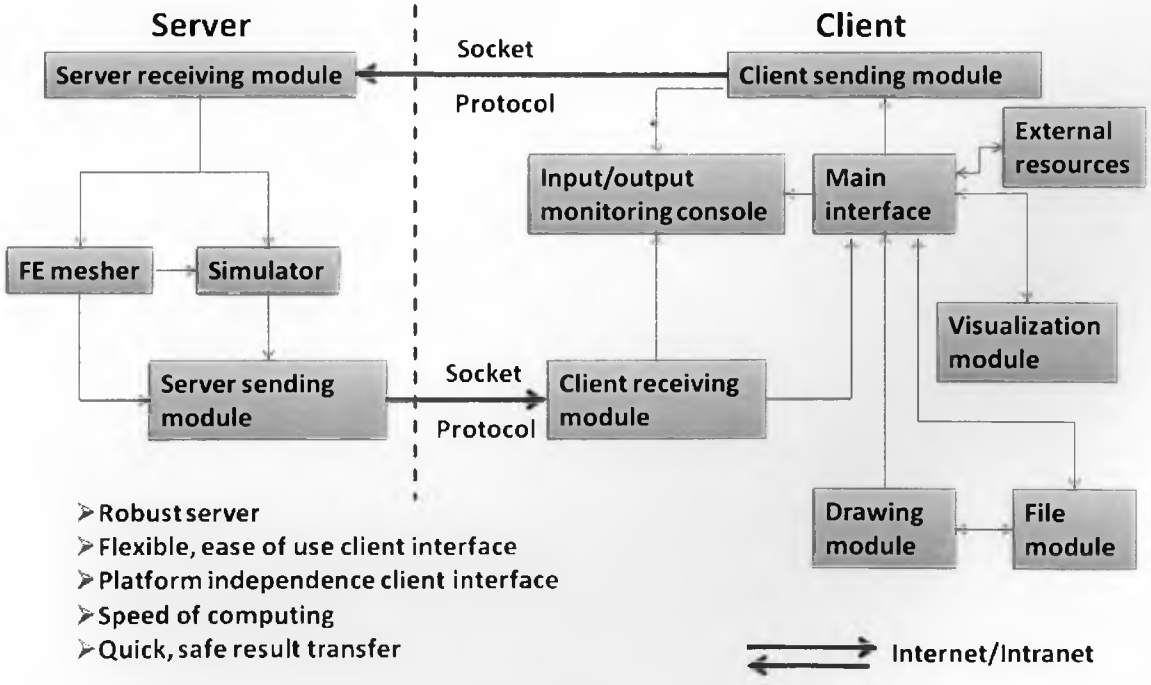

Figure 8.2 Modular client-server interfaces for "real time on-line" reservoir simulations

8.3.3.2 Results Visualization Module

User can either view the simulation results dynamically by using the animation window or by using this "Result Images Viewer." This is a picture view program used to visualize the result image separately. This function is located at the sub menu button of the Simulation results under the Calculation menu bar.

8.3.3.3 File Editor Module

This program was written to view the XML input file. In the middle of the simulation, if the end user wanted to view the input XML data file, the file editors provided by the system or this program could be used. This is a read only file editor, and cannot be used to modify or edit the input XML file. For this reason, this is only for quick viewing of the input file and serves as a backup to other system editors.

8.3.3.4 Interface Input/Output Console

The purpose of this console is to serve as a monitor for this client-server mode reservoir simulation interface. By using this program, the user and the programmer can check the status of the simulation. All of the input/output actions between the user and the interface, the client interface and the server, are displayed by this control console. Since the whole interface package is based and executed on the Java Running Machine, if there is something wrong in the compiler, the error information is also displayed in this window. Furthermore, some prequalification conditions were built into the original Java code, so that if the user's input file had mistakes or did not follow the right processes, the system will provide the coded error information to the end user through this console.

8.4 Definitions

Server: The high performance computing resource which is used for accepting work orders from the end user (client) to complete computing jobs. In this work, the server package is included in the executable Java server side interface class, triangle mesh software package and the finite element simulators. The whole server package is included in one directory located on the specified Linux/Unix machines.

Client: The end user. In this work, the client package is composed by a series of Java source code and its executable file which is located on the end user's local machines.

Java: A web based objective oriented computer language developed by Sun Inc. This computer language is running under Java Running Environments (JRE) instead of directly under the operating systems. In this reservoir simulator interface work, all of the computer code was written by Java language.

XML: A markup language for documents containing structured information. In this reservoir simulator work, all of the data are default saved as XML format.

Java Socket: A network Input/Output communicating technique in Java. From the standpoint of clients: programs that open a socket to a server that is listening for connections. However, client sockets themselves are not enough; clients are not much use unless they can talk to a server. There should be a server side socket opened to host the client socket by the same port number specified in both sockets. Here in this interface package, the server side socket is kept opened all the time to listen for the client sockets requests. The client side socket will only be opened while the end user wants to submit jobs on the server through specified socket communicating protocol.

Java Swing: A graphic user interface (GUI) toolkit of Java. The main reservoir simulator interface frame is written by Java Swing such as all the panels, buttons, text fields, and so on.

Java 2-D Graphics: A two-dimensional graphic drawing toolkit of Java. In the current reservoir simulator interface, the reservoir domain drawing canvas was written by this technique. The closed reservoir domain is drawn by its polygon shape, fractures by its line shape, and injection wells by its round shape and the production well by its square shape.

Java Threads: A very important topic for Java programming. For the current reservoir simulator interface developing, thread concepts are hired for the end user to run separate tasks at the same time within the same interface.

8.5 Chapter Summary

A complete fractured reservoir simulation package (2-D) with interactive client-server communicating interface has been designed and developed from this work. This modular package includes fractured reservoir domain drawing, meshing, input file generation, remote computing, image viewing, etc. The concept of remote fractured reservoir online computing has been successfully proven through this work. Potentially, the package can be extended to be a platform of integrating the multidimensional, multiphase, multiscale fractured reservoir study from characterization to simulation.

CHAPTER 9

DEVELOPING AND INTEGRATING FRACTURED RESERVOIR SIMULATION WORKFLOW

Simulating fractured reservoirs and predicting oil recovery requires integration work. The integration work should include geologic knowledge, petrophysical properties representation, well modeling and well history input. Most times, data required for this integration are scattered in various models and programs. One of the main objectives of this research program is to bring about the integration of the geologic fracture network model and reservoir simulation input file.

9.1 Overview

A workflow tool was created in this project with the following features:

- Treatment of fracture only reservoir or reservoirs with fractures and matrix.
- Meshing the domain created. Meshing was discussed in detail later in this chapter.
- Assigning properties to the control volumes and/or elements created during the meshing exercise.
- Creating a simulation input file.
- Assigning wells and well operational parameters.
- Describing well production histories.
- Executing the simulator with the given input file.

- Generating output data for production analysis and for visualization.
- Visualizing the results.

A schematic of this workflow is demonstrated in Figure 9.1.

9.2 Fractured Network Characterization Packages

"FracMan Reservoir Edition" (FRED) is a sophisticated general program for importing a number of geologic inputs into a geologic model to create fracture sets characteristic of all of the measured data. FRED was used in this project as the primary fracture generation tool. These fracture sets may be operational in a Type I reservoir environment or a Type II reservoir situation, where the fracture sets are embedded into a

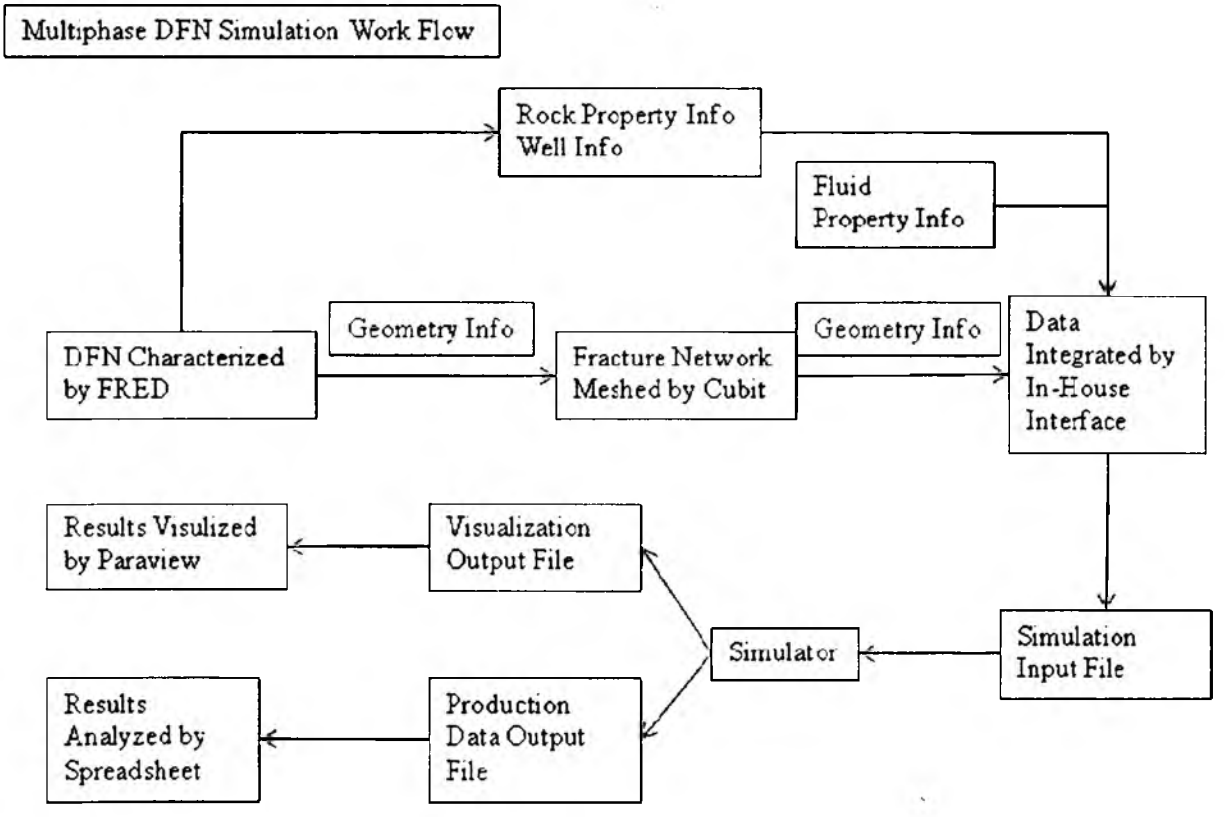

Figure 9.1 An example of multiphase DFN simulation workflow

reservoir matrix. When creating reservoir simulation input files using the sophisticated fracture network, both these aspects need consideration.

PETREL is another powerful petroleum reservoir characterization package. Since the 2007 version, some FRED functions are integrated into the PETREL package. The PETREL package is used in this workflow to characterize the structural fault and to generate corner point grid blocks. These grid blocks could be combined with FRED generated DFN models for the purpose of permeability and intensity upscaling. The upscaled model could be simulated by conventional finite-difference simulators such as ECLIPSE and IMAX.

9.3 Mesh Software Packages

Domain meshing is a big concept for reservoir simulation. In order to calculate the fluid flow through the porous media, modeled reservoir domain must be meshed based on numerical discretization method adopted. Today, the trend in simulator development is to separate the meshing part from the flow calculation (simulator) part, and use the output from the meshing part as input for the simulator. The meshing part is normally done by meshing software. Through this approach, one simulator should be able to couple with different meshing programs.

As mentioned in the last section, in this fractured reservoir integrating workflow, the PETREL package is adopted for conventional finite-difference meshing with an upscaled DFN model inside of grid blocks,

The control volume finite-element discretization method (CVFE) applied in this research has the advantage of easy handling unstructured geometry and a higher order of accuracy. The finite-element mesh software packages include CUBIT from Sandia

National Lab, HyperMesh from Altair Co., RoseMesh from Golder Associate, and MeshMaster from Golder Associate.

9.4 Assembling Simulation Input File

PETREL has a very mature package to put production/injection history and petrol-physical data into the ECLIPSE input file. For the workflow of simulating upscaled DFN modeled fractured reservoir by conventional finite-difference simulator, PETREL can have the work done.

For unstructured grid CVFE simulation, there is not any commercial software that could be directly applied in assembling the simulation input file. In this work, an interface (different from Chapter 8) has been developed to assemble the meshed unstructured DFN geometry with wells and other petro-physical information to form the input data file. This interface package is designed as modulated too. It has the very flexible capability to assemble different CVFE simulation input files, such as: type I and type II fractured reservoir, 2-dimensional or 3-dimensional, 2-phase or 3-phase, and so on.

9.5 Simulators

The simulators integrated in this fractured reservoir study include both conventional finite-difference simulators such as ECLIPSE and the finite-element based unstructured simulator of CVFE. The finite-difference simulator is used for upscaled DFN modeled fracture reservoir studies. The single porosity models were applied on type I fractured reservoir and the dual porosity models were used on type II fractured reservoir upscaling calculations through this finite-difference simulator.

For unstructured DFN modeled fractured reservoir, the CVFE simulator is adopted for direct DFN characterization simulations.

9.6 Data Analysis

A postprocessing code has been developed through this integrating workflow for the CVFE simulator. These postprocessing efforts include the pressure or saturation distributions; injection or production analysis by phases, by independent wells or by total reservoir performance. The postprocessed data could be directly imported by a coded spreadsheet file and all kinds of analyzing curves and figures are generated by that coded spread sheet file automatically.

9.7 Visualization

Other than the in-house visualization tool in Chapter 8, ParaView is adopted as the standard visualization package for this fractured reservoir integrating workflow. ParaView is an open source, multiplatform application designed to visualize data sets of sizes varying from small to very large. ParaView runs on distributed and shared memory parallel as well as single processor systems and the successful testing has been reported. Today, ParaView development continues as a collaboration between Kitware, Sandia National Labs, CsimSoft, Los Alamos National Lab, Army Research Lab and others.

9.8 Chapter Summary

As shown in Figure 9.2, a multiphase, multidimensional fractured reservoir simulation workflow has been developed through this work. This workflow includes accurate simulating of finite-element based unstructured DFN modeled type I and type II fractured reservoir and their upscaled studying through conventional finite-difference

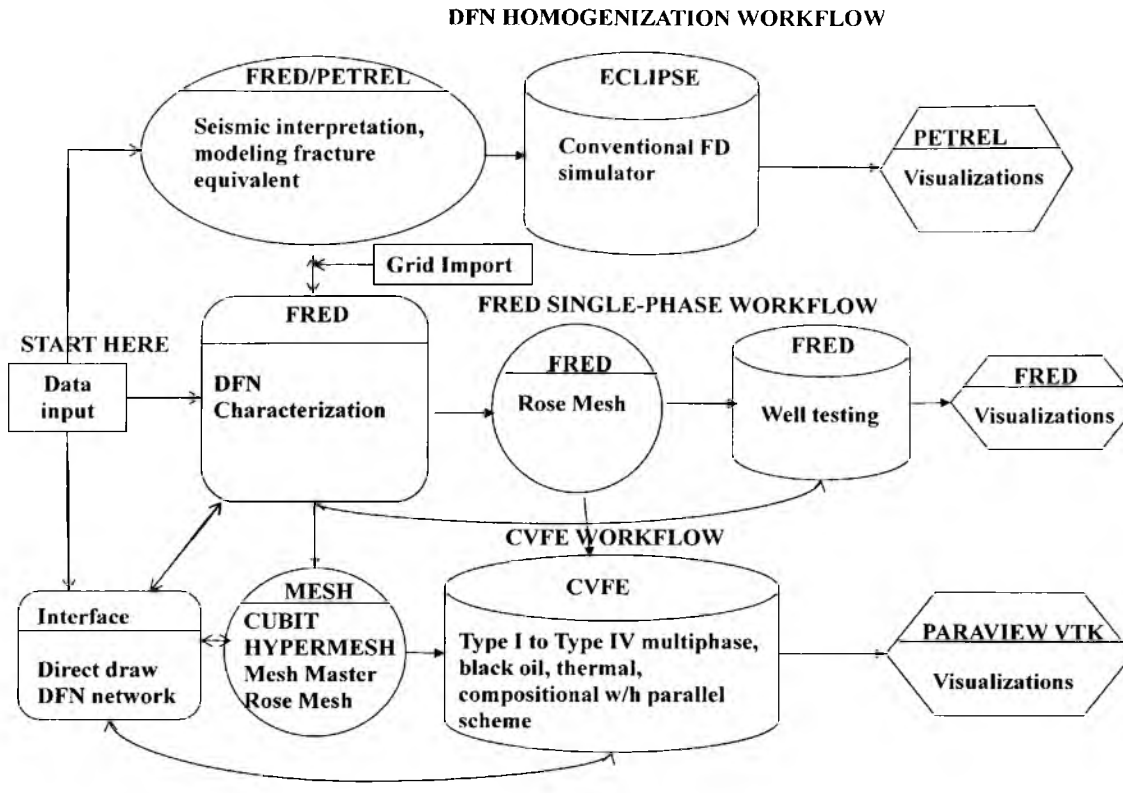

Figure 9.2 Illustration of workflow on fractured reservoir simulation

based simulator. To assure this fractured reservoir integrated workflow to be seamless, lots of work has been accomplished from the characterization through the postprocessing analysis such as the visualization. Developing and integrating an accurate, efficient workflow to model and simulate the multidimensional, multiphase, multiscale fractured reservoir was a significant contribution.

CHAPTER 10

SUMMARY

The viability of using discrete-fracture network (DFN) models in a variety of applications was explored in this dissertation. The dissertation was organized into a series of papers from Chapter 3 to Chapter 7, each examining different aspects of DFN modeling.

In Chapter 3, we first compared the results from a regular fracture network discretized using ECLIPSE (a commercial reservoir simulator) with DFN equivalents, and showed that the results were in close agreement, even under three-phase flow conditions. Then we looked at the effect of different fracture properties on multiphase flow performance in reservoirs. When a random distribution of permeability was used for the network, the flow performance was dominated by the presence of the low permeability features. The way in which this permeability is distributed also impacts recovery and water cut. The DFN protocol allows us to cut off main connections in the flood pathway (between injector and producer) and evaluate its impact. It is shown that primary production is not impacted significantly from the disturbance in connectivity, but water flood performance is. Changing orientations of fractures results in different rates of recovery, but does not impact the overall recovery. When the fracture height is reduced in one of the two intersecting networks recovery is significantly lowered. The DFN approach also allowed us to evaluate "what-if" scenarios. If one of the main pathways between the injector and producer has inherently higher permeability (or an induced high

permeability) then water channels through this pathway lower recovery by as much as 10-15%. By blocking the preferred pathway, water can be diverted into other parts of the reservoir, increasing oil recovery.

In the second paper, as the fracture network was made more irregular, results from the real DFN simulations differed considerably from the regularized ECLIPSE simulations. (It should be recognized that it is difficult to simulate highly irregular networks using ECLIPSE). However, the irregular networks can be homogenized using a variety of approaches and we looked at using the Oda method, and a simple geometric upscaling approach. As the homogenized ECLIPSE grids were made finer using the ODA method, surprisingly, convergence was not achieved. This is because the Oda method of upscaling and homogenization is more accurate when the fracture penetrates the entire block diagonally. The simple geometric homogenization scheme involved using a fine mesh and assigning the permeability of the fracture to the block that it penetrated. This approach led to the homogenized results matching the DFN simulation results to certain extent.

The next paper in Chapter 5 dealt with the examination of recovery from fractured basements. Typically, seismic data are used to map out the large fault features which form the basis of the basement oil reservoir. It is hypothesized, however, that oil also exists in smaller "subseismic" features. This paper dealt with figuring out recovery mechanisms in reservoirs with varying amounts of distribution in the seismic and subseismic features, using a hypothetical conceptual model. In the first set of models where the feature permeabilities were homogeneous, it was observed that lower subseismic zone permeabilities led to lower recoveries and quicker water breakthrough.

Recovery analyses of reservoirs with different amounts of oil in the subseismic features revealed that distributing more of the oil in the subseismic (smaller) features resulted in lower recoveries. This trend was exacerbated when the subseimic features had lower permeabilities on top of having higher amount of oil. Lower recovery was usually accompanied by earlier breakthrough. When depth dependent properties were used, the steeper, nonlinear case exhibited lower recoveries, but later breakthroughs. The later beakthrough trends were believed to be due to lower rates of injection in the lower permeability zones of the reservoir. These ideas were reinforced when cases of different distributions in seismic and subseismic zones were studied along with depth-dependent property variations. Thus the challenges of recovering oil from basements with large oil distributions in subseismic features became evident in this study, especially when these features were of low permeability or heterogeneous. The most important conclusion from this paper was the effect of rate on recovery at the given pore volume injection. The first conclusion in this regard was that the displacements were rate dependent no matter what the oil distribution was in the seismic and subseismic features, with higher recovery obtained at lower rates. The second conclusion was that more oil was associated with subseimic (smaller) features, the differences in recoveries were larger. The consequence of this is that at higher rates the breakthroughs were quicker and oil was produced at consistently higher water cuts compared to lower rates. The recovery analysis is consistent when viewed from the point of view of recovery as a function of gravity number.

In Chapter 6, a set of Corey-type relative permeability curves was used to create a reasonable match of recovery and water-cut performance of a complicated three-

dimensional embedded zone model. The embedded zone model is a hypothetical depiction of the make-up of a large seismic zone. This was represented using three sets of fractures. The idea was to use straight-line relative permeabilities for the embedded zone and match it using curved relative permeabilities for the single feature. This type of analysis provides insight on types of relative permeabilities to use, if a bunch of single features were used to describe all of the seismic zones in a field scale model. Implementation of depth-dependent properties in the embedded zone showed that adding heterogeneity at this scale produced results similar to those observed with seismic/subseismic models – namely, lower recoveries and quicker breakthroughs. The rate effect was also observed in single-feature Eclipse simulations with side-water injection. A critical gravity number was shown to be operative.

In Chapter 7, a series of simulations with Type II reservoirs (reservoirs featuring both the matrix and the fractures) were performed primarily to demonstrate the capability of the in-house CVFE simulator. In the first part of this paper, we validated the simulator using experimental core-flooding data. The results were in good agreement except at the highest rate. The usefulness of using discrete-fracture models was discussed by looking at production from faulted-fractured systems. It was shown that given a certain reservoir and fracture description the simulator could be employed to optimize oil recovery.

Reservoir simulation of fractured reservoirs, particularly in the DFN mode is challenging because of requirements of data integration, manipulation, transformation and visualization. Hence, a set of tools was developed to facilitate generation and handling of a large number of files. This included generating input files suitable for meshing, generating simulator input files from meshing output and managing simulator

files for data analysis and visualization. In addition, a JAVA-based interface was built for generating/drawing two-dimensional fracture maps, with automated mesh generation and simulation.